SLAC-R-519
UC-404

ATOMIC AND ELECTRONIC STRUCTURES OF NOVEL SILICON SURFACE STRUCTURES

Jeffrey Harve Terry, Jr.

Stanford Linear Accelerator Center
Stanford Synchrotron Radiation Laboratory
Stanford University, Stanford, California 94309

March 1997

Prepared for the Department of Energy under contract number DE-AC03-76SF00515

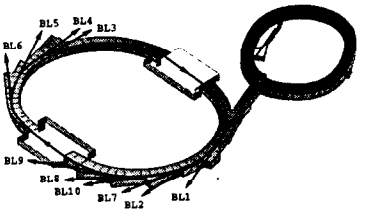

Printed in the United States of America. Available from the National Technical Information Service, U.S. Department of Commerce, 5285 Port Royal Road, Springfield, Virginia 22161

* Ph.D. thesis

ATOMIC AND ELECTRONIC STRUCTURES OF NOVEL SILICON SURFACE STRUCTURES

A DISSERTION
SUBMITTED TO THE DEPARTMENT OF CHEMISTRY
AND THE COMMITTEE ON GRADUATE STUDIES
OF STANFORD UNIVERSITY
IN PARTIAL FULFILLMENT OF THE REQUIREMENTS
FOR THE DEGREE OF
DOCTOR OF PHILOSOPHY

JEFFREY HARVE TERRY, JR.

MARCH 1997

To my wife, Julie, for her continuous support
and to my son, Casey Jeffrey, for making it all worthwhile.

ABSTRACT

The modification of silicon surfaces is presently of great interest to the semiconductor device community. Three distinct areas are the subject of inquiry: first, modification of the silicon electronic structure; second, passivation of the silicon surface; and third, functionalization of the silicon surface. It is believed that surface modification of these types will lead to useful electronic devices by pairing these modified surfaces with traditional silicon device technology. Therefore, silicon wafers with modified electronic structure (light–emitting porous silicon), passivated surfaces (H–Si(111), Cl–Si(111), Alkyl–Si(111)), and functionalized surfaces (Alkyl–Si(111) have been studied in order to determine the fundamental properties of surface geometry and electronic structure using synchrotron radiation–based techniques.

First, light–emitting porous silicon was studied using photoluminescence, photoemission (PES) and near–edge x–ray absorption fine structure spectroscopy (NEXAFS). Changes in the valence band and in the Si 2p core level spectra of electrochemically–etched light–emitting porous silicon prepared with different etching parameters and upon thermal annealing were studied. Broadening of the Si 2p core level as chemical etching time increased was observed. Upon annealing the core level linewidth decreased and the valence band progressed from a large featureless spectrum to a spectrum with three main features. PES also showed that no impurity species were present in large concentrations. Finally, the NEXAFS spectra showed that the surface of light–emitting porous silicon was crystalline. Therefore, luminescence from amorphous silicon and from impurity based molecular species on electrochemically etched porous silicon was ruled out. The luminescence mechanism that best described all available experimental data was based upon a silicon species that degrades upon annealing and strongly resembles crystalline silicon such as a system of bulk-like terminated quantum confinement regions.

Second, the passivated surfaces were studied using photoemission spectroscopy and extended x–ray absorption fine structure spectroscopy (EXAFS). The H–Si(111) surface was found to react with an evaporated metal, Au. Photoemission spectra showed that as Au

was first deposited a uniform layer of atomic–like Au formed on the surface. At intermediate Au coverages, a Au–silicide layer approximately 2–3 ML thick formed. The composition of the silicide was not uniform. The remaining Au formed a metallic layer between the silicide and the silicon surface. Finally, at high coverages, the silicide and metallic Au layers attenuated the bulk signal. The Si 2p core level emission still observed was predominately from the silicide layers which remained above the metallic Au film. Thus, this system was observed to consist of 2–3 ML layers of Au–silicide above a thick film of Au that sat directly on top of the bulk silicon. Au deposition on the H–Si(111) surface was nearly identical to that observed from Au deposition on the Si(111) 7x7 surface. As Ge was deposited uniform, amorphous layers formed on top of the H–Si(111) surface. The Si–H bonds were not significantly affected by Ge deposition. Moderate annealing led to the formation of ordered Ge islands on top of 1–2 uniform layers of Ge above the Si surface. Again, this was not very different from direct deposition of Ge on a Si(111) 7x7 surface. No oxidation of the ideal H–terminated surface was observed after exposures as high as 100,000 L O_2. However, surface oxidation was observed when the H–Si(111) surface was exposed to molecular and atomic halogens. The Si 2p core level spectra from the halogen–exposed surfaces showed two components, from bulk silicon and from silicon bonded to a single halogen atom. This result was unlike halogen exposure of the Si(111) 7x7 surface where halogen exposure results in mono–, di–, and trihalogenated Si atoms. EXAFS spectroscopy showed that the Si–Cl bond length of the Cl–Si(111) surface was 2.03 ± 0.02 Å.

Finally, the Si(111) surface could be functionalized because the H on the H–Si(111) surface and the Cl on the Cl–Si(111) surface could be replaced by alkyl groups. To provide direct evidence of surface bonding, the alkyl–terminated silicon surfaces were characterized using both valence band and core level photoemission to determine the electronic structure of the interface. Scanned–energy, chemical–shift photoelectron diffraction (PED) on the C 1s core level and near–edge x–ray absorption fine structure spectroscopy (NEXAFS) were used to determine the local bonding geometry at the monolayer–substrate interface. Valence band spectra were used to identify the alkyl groups present as the C 2s–based molecular orbitals provided a fingerprint region in the spectra. Si 2p and C 1s core level both contained chemically–shifted components providing direct evidence of Si–C

bond formation. Scanned–energy, chemical shift PED was used to determine that the alkyl chains sat in atop sites with a Si–C bond length of 1.85 ± 0.05 Å. NEXAFS spectroscopy showed that the alkyl chains were oriented on the surface. Thereby, showing that synthetic chemistry methodology can in fact reliably produce alkyl–terminated silicon surfaces.

ACKNOWLEDGEMENTS

Many people at SSRL deserve my profound thanks for the help that they have offered. Piero Pianetta, my adviser, provided continuous trust, support and guidance. He has created a unique environment where cross–discipline collaboration has always been the norm. This environment has fostered the creativity entailed in this work.

I am also grateful to the members of my thesis committee. I sincerely thank Professor Edward Solomon for agreeing to be my co–adviser. Professor Christopher E. D. Chidsey has been a collaborator who has consistently provided ideas and was a participant in many helpful technical discussions. I thank Professor John Griffin for serving on my committee. I am indebted to Professor Walter Harrison for chairing the thesis committee and for providing technical insight to many problems through my tenure at Stanford.

Two co–workers must be singled out above all other. Dr. Renyu Cao and Dr. Christer Wigren provided help, friendship, and discussions through the difficult times of experimental apparatus design and construction. Without their help, this work could not have been completed. Finally, I would like to thank the members of the research group of Professor Pianetta, who have provided their assistance. I extend my gratitude to Renee Mo, Eric Nelson, Changyoung Kim, Matt Richter, Paul King, Stephanie Yoshikawa, Jin Wu, and Xiaoyu Yang. Matt Linford of Professor Chidsey's group has been an excellent collaborator during my time at Stanford.

I would also like to acknowledge the many staff members of Stanford and SSRL for their support and friendship. My thanks go to George Husek, Ron Morris, Stan Wanner, Al Armes, Gloria Barnes, Lisa Dunn, Todd Slater, and Peter Boyd. Dr. Louis J. Terminello provided free synchrotron time out of his personal allotment so that I could carry out specific experiments. I am forever in his debt. Dr. David Shuh and Dr. Britt Hedman provided helpful advice during my stay. I deeply appreciate the help offered by all other not mentioned by name.

Finally, I would like to acknowledge the support of my family and friends. My wife, Julie

has been at my side throughout my graduate career and my son, Casey Jeffrey, has really livened up the end. My parents, in–laws, and grandparents have provided support when the going got tough. I appreciate the help that was provided by my brothers and sister. I was greatly helped by the friendship of Ed Hanson and Matt Linford.

TABLE OF CONTENTS

ABSTRACT v

ACKNOWLEDGEMENTS viii

TABLE OF CONTENTS x

LIST OF TABLES xiv

LIST OF FIGURES xv

CHAPTER I. INTRODUCTION 1

I.1.MOTIVATION 1

I.2.TECHNIQUES 2

I.2.1.Photoemission 2

I.2.2.Photoelectron Diffraction 5

I.2.3.Spectral Decomposition 12

I.3.THESIS ORGANIZATION 12

I.4.REFERENCES 13

CHAPTER II. LIGHT-EMITTING POROUS SILICON 22

II.1.ABSTRACT 22

II.2.INTRODUCTION 22

II.3.EXPERIMENTAL 25

II.3.1.Sample Preparation and Transportation 25

II.3.2.Photoluminescence Measurements 25

II.3.3.Photoemission Measurements 26

II.3.4.Near–Edge X–Ray Absorption Spectroscopy 27

II.3.5.Thermal Annealing 27

II.4.RESULTS 28

II.4.1.Photoluminescence 28

II.4.2.Wide–Scan Photoemission Spectroscopy (XPS) 29

II.4.3.Si 2p Core Level and Valence Band Photoemission 29

II.4.4.NEXAFS 33

II.5.DISCUSSION 34

II.5.1.Photoluminescence 34

II.5.2.Amorphous Silicon Mechanism 34

II.5.3.Impurity Mechanism 35

II.5.4.Quantum Confinement Mechanism 36

II.5.5.Surface Termination Mechanism 37

II.6.CONCLUSION 39

II.7.ACKNOWLEDGEMENTS 39

II.8.REFERENCES 40

CHAPTER III. HYDROGEN–TERMINATED Si(111) 54

III.1.ABSTRACT 54

III.2.INTRODUCTION 55

III.3.EXPERIMENTAL 58

III.3.1.H–Si(111) Preparation 58

III.3.2.Surface Reactions 60

III.3.3.Photoemission Measurements 61

III.3.4.Thermal Annealing 63

III.4.RESULTS 64

III.4.1.Hydrogen–Terminated Si(111) 64

III.4.2.Gold Deposition on H–Si(111) 65

III.4.3.Germanium Deposition on H–Si(111) 71

III.4.4.Oxygen Deposition on H–Si(111) 73

III.4.5.Halogenation of the H–Si(111) Surface 73

III.4.6.Alkylation of the H–Si(111) Surface 75

III.5.DISCUSSION 78

III.5.1.H–Si(111) as Passivation Layer in Device Processing 78

III.6.CONCLUSION 78

III.7.ACKNOWLEDGEMENTS 80

III.8.REFERENCES 80

CHAPTER IV. ALKYL–TERMINATED Si(111) SURFACES 99

IV.1.ABSTRACT 99

IV.2.INTRODUCTION 100

IV.3.EXPERIMENTAL 103

IV.3.1.Sample Preparation and Transportation 103

IV.3.2.Photoemission Measurements 105

IV.3.3.Chemical–Shift, Scanned–Energy Photoelectron Diffraction 106

IV.3.4.Near–Edge X–Ray Absorption Spectroscopy 107

IV.3.5.Thermal Annealing 107

IV.4.RESULTS 108

IV.4.1.Valence Band 108

IV.4.2.Si 2p Core Level Photoemission 113

IV.4.3.C 1s Core Level Photoemission 118

IV.4.4.Chemical–Shift, Scanned–Energy Photoelectron Diffraction 121

IV.4.5.Near–Edge X–Ray Absorption Spectroscopy 127

IV.4.6.Thermal Annealing 131

IV.5.DISCUSSION 134

IV.5.1.Alkyl Monolayers 134

IV.5.2.Applications of Chemical–Shift Photoelectron Diffraction 136

IV.6.CONCLUSION 137

IV.7.ACKNOWLEDGEMENTS 137

IV.8.REFERENCES 138

CHAPTER V. ZINC OXIDE 171

V.1.ABSTRACT 171

V.2.INTRODUCTION 171

V.3.EXPERIMENTAL 173

V.4.RESULTS 173

V.5.DISCUSSION 174

V.6.CONCLUSION 174

V.7.ACKNOWLEDGEMENTS 175

V.8.REFERENCES 175

CHAPTER VI. CONCLUSION 181

LIST OF TABLES

Table I.1:	The fitting parameters from the narrowest Si 2p and C 1s core level spectra as described in the text are given.	16
Table II.1:	The electrochemical etching parameters and labels used in this experiment are shown.	42
Table IV.1:	Si 2p core level peak positions from the spectra in Figure IV.7 taken at a photon energy of 130 eV.	142
Table IV.2:	Si 2p core level intensities from the spectra in Figure IV.7 taken at a photon energy of 130 eV.	143

LIST OF FIGURES

Figure I.1:	An idealized version of a photoemission experiment is shown.	17
Figure I.2:	A typical C 1s core level spectra taken at a photon energy of 350 eV from an alkyl terminated Si(111) sample is shown decomposed into two singlet components. The components are attributed to emission from the bulk–like C atoms in the alkyl chain (C–C) and to emission from the C atom bound to the Si surface (C–Si).	18
Figure I.3:	The three–step model of the photoemission process is depicted.	19
Figure I.4:	A single–scattering photoelectron diffraction event is shown.	20
Figure I.5:	The angles used in the calculation of PED spectra are shown.	21
Figure II.1:	A detectable photoemission event is shown. Any electron that is emitted or scattered elastically into the acceptance cone of the analyzer is measured.	43
Figure II.2:	The experimental electrochemical etching apparatus is pictured below in a cross sectional view.	44
Figure II.3:	Photoluminescence spectra of the different light emitting samples excited with an Ar ion laser (525 nm) are shown. Labels correspond to those	45

in Table 1. Labels F - A indicate the relative intensity of the peaks that cannot be resolved, indicated in the figure by the arrow.

Figure II.4: Photoluminescence from a G–type sample before and after annealing to approximately 600 C are shown. 46

Figure II.5: Si 2p core level spectra taken with photon energy of 150 eV for samples with preparations in Table 1 are illustrated. The large feature shifted to higher binding energy in A is due to the presence of an oxide layer. 47

Figure II.6: Si 2p core level spectra taken with photon energy of 140 eV for samples with preparations in Table 1 are illustrated. 48

Figure II.7: The progression of the valence band ($h\nu = 40$ eV) from a sample with preparation G as a function of annealing temperature is shown. Spectra from a Si (100) wafer dipped in HF, and from Si (100) 2x1, ($h\nu = 60$ eV), are also shown. 49

Figure II.8: Si K-edge adsorption spectra from amorphous Si, crystalline Si, Total yield from LES, and Auger yield from LES are shown. 50

Figure II.9: Background subtracted Total yield Si K-edge data are shown from amorphous, crystalline, and LES. 51

Figure II.10: The Corresponding Fourier Transforms of the 52

data shown in Figure II.9.

Figure II.11: Auger yield NEXAFS of the Si K-edge after annealing are shown. 53

Figure III.1: Comparison of valence band spectra from the H–Si(111) and Si(111) 7x7 surfaces shows that the two surface states S1 and S2 were removed by etching indicating that surface dangling bond were saturated. 83

Figure III.2: Silicon 2p core level spectra taken with a photon energy of 130 eV with different Au coverages on H–Si(111) are shown. Some spectra have been taken at different pass energies and scaled to fit in the figure. The labeled features are discussed in the text. 84

Figure III.3: As in Figure III.2 except the spectra were taken with a photon energy of 110 eV. 85

Figure III.4: As in Figure III.2 except the substrate was p–type H–Si(111). 86

Figure III.5: Au 4f core level spectra from p–type Au/H–Si(111) taken with a photon energy of 130 eV. 87

Figure III.6: Valence Band spectra taken at normal emission with a photon energy of 27 eV with different Au coverages are shown. 88

Figure III.7: Silicon 2p core level spectra taken at a photon energy of 130 eV with different Ge coverages are 89

shown.

Figure III.8: Silicon 2p core level spectra taken at a photon energy of 110 eV with different Ge coverages are shown. 90

Figure III.9: Germanium 3d core level spectrum from Ge/H–Si(111) before and after annealing is shown. A reference spectrum from a 3 ML Ge film after surfactant growth with antimony on a Si(111) substrate. 91

Figure III.10: Silicon 2p core level spectra from HF etched Si(111) exposed to O_2 in vacuum are shown. These spectra were taken at a photon energy of 130 eV. 92

Figure III.11: Same as Figure III.10 except the samples were etched with NH_4F instead of HF. 93

Figure III.12: Si 2p core level spectra for H–Si(111), Cl_2 exposed H–Si(111), and Br_2 exposed H–Si(111) taken at a photon energy of 130 eV. These spectra have been decomposed into two spin–orbit doublets. Clearly, replacement of H by the halogens was observed. 94

Figure III.13: Comparison of the Si 2p core level from a H–Si(111) surface exposed to Cl_2 in vacuum in total darkness and from one exposed to Cl_2 under UV illumination and transferred through air into the vacuum chamber. 95

Figure III.14: A valence band spectrum from H–Si(111) exposed to 1–pentene is shown. Note that the C 2s region (-12 to -22 eV) provides a means of identifying the surface species because the number of components observed is equal to the number of C atoms in the chain. The solid vertical lines are referenced gas phase binding energies of the C 2s based molecular orbitals in n–pentane(Potts and Streets 1974) See text for an explanation of the referencing procedure. 96

Figure III.15: Surface sensitive Si 2p core level spectra from methyl–terminated Si(111) and H–Si(111) surfaces exposed to 1–pentene and 1–decene taken at a photon energy of 130 eV. **The spectrum from a H–Si(111) sample exposed to 1–octadecene was taken with a photon energy of 120 eV because a larger electron escape depth was necessary in order to increase the signal strength of the Si 2p core level. This spectrum was then aligned with those of the short chains. 97

Figure III.16: The C 1s core level spectra taken at a photon energy of 350 eV from a H–Si(111) sample exposed to 1–pentene is shown decomposed into two singlet components. The components are attributed to emission from the bulk–like C atoms in the alkyl chain (C–C) and to emission from the C atom bound to the Si surface (C–Si). 98

Figure IV.1: Valence band spectra from methyl–, pentyl–, decyl–, and octadecyl–terminated Si(111) surfaces 144

are shown. These spectra were collected at a photon energy of 55 eV. A valence band spectrum from a Si(111) 7x7 surface is shown as a reference.

Figure IV.2: The valence band spectra from the alkyl–terminated surfaces are shown along with spectra from the corresponding alkane. It is evident that alkyl chains are present on the silicon surfaces and that the valence band can be used a fingerprint to identify the alkyl species. The alkane spectra(Pireaux et al. 1986) were collected with an XPS source and were aligned with the data from the present study. 145

Figure IV.3: A valence band spectrum from pentyl–terminated Si(111) is shown. Note that the C 2s region provides a means of identifying the surface species because the number of components observed is equal to the number of C atoms in the chain. The solid vertical lines are referenced gas phase binding energies of the C 2s based molecular orbitals in n–pentane(Potts and Streets 1974) See text for an explanation of the referencing procedure. 146

Figure IV.4: Valence band spectra from pentyl– and penteyl–terminated Si(111) are shown. Clearly evident is the sensitivity of the C 2s based molecular orbitals to chemical state, i.e. sp^3 vs. sp^2 hybridization in the chain. These spectra were taken with a photon energy of 55 eV. 147

Figure IV.5: Surface sensitive Si 2p core level spectra from methyl–, pentyl–, and decyl–terminated Si(111) samples taken at a photon energy of 130 eV. **The spectrum from an octadecyl–terminated sample was taken with a photon energy of 120 eV because a larger electron escape depth was necessary in order to increase the signal strength of the Si 2p core level. This spectrum was then aligned with those of the short chains. 148

Figure IV.6: Same as Figure IV.5 except the spectra were taken with a photon energy of 115 eV. These spectra are more bulk sensitive than those in Figure IV.5 due to a larger escape depth of the photoelectrons. 149

Figure IV.7: Shown are the Si 2p core level spectra from Figure IV.5 decomposed into multiple components. Three main features were observed and were attributed to emission from bulk–like Si, Si bound to C, and SiO_x species. 150

Figure IV.8: Si 2p core level spectra from hydrogen–, chlorine–, and methyl–terminated Si(111) surfaces are shown. These spectra have been decomposed into spin–orbit split doublets as described in the text. In each spectrum, a component is labeled as bulk silicon emission. The other component is attributed to the adsorbed species. 151

Figure IV.9: Carbon 1s core level spectra from methyl–, pentyl–, decyl–, and an octadecyl–terminated 152

Si(111) samples taken at a photon energy of 350 eV are shown. Two components were observed in all spectra. The intensity of the peak at a kinetic energy of 57.5 eV increased markedly from samples terminated with longer C chains. A corresponding decrease in intensity was observed for the higher kinetic energy component.

Figure IV.10: The C 1s core level spectra taken at a photon energy of 350 eV from the pentyl–terminated Si(111) sample of Figure IV.9 is shown decomposed into two singlet components. For reasons described in the text the components are attributed to emission from the bulk–like C atoms in the alkyl chain (C–C) and to emission from the C atom bound to the Si surface (C–Si). 153

Figure IV.11: A.) A C 1s spectra from a pentyl–terminated Si(111) surface taken with a photon energy of 350 eV is shown. It has been decomposed into two singlet components which for reasons described in the text have been labeled C–C and C–Si. B.) Same as in A.) except the photon energy was 370 eV. Note the difference in intensity of the C–Si component. C.) Experimental partial cross section determined by decomposing the C 1s core level as above is shown. The atomic partial cross section (0 order) was obtained by fitting a smooth function to the experimental data. 154

Figure IV.12: A.) A C 1s spectra from a methyl–terminated Si(111) surface taken with a photon energy of 155

350 eV is shown. It has been decomposed into two singlet components which for reasons described in the text have been labeled C–C and C–Si. B.) Same as in A.) except the photon energy was 370 eV. Note the difference in intensity of the C–Si component. C.) Experimental partial cross section determined by decomposing the C 1s core level as above is shown. The atomic partial cross section (0 order) was obtained by fitting a smooth function to the experimental data.

Figure IV.13: A.) The experimental modulation function, $\chi(k)$, and that from the best theoretical model is shown from the pentyl–terminated surface. The inset shows the R–factor analysis as a function of modeled Si–C bond length. The C–Si bond length was determined to be 1.85 ± 0.05 Å. B.) The experimental modulation function, $\chi(k)$, and that from the best theoretical model is shown from the methyl–terminated surface. The inset shows the R–factor analysis as a function of modeled Si–C bond length. The C–Si bond length was again determined to be 1.85 ± 0.05 Å. 156

Figure IV.14: The four layer slab used in the photoelectron diffraction calculations of both the methyl– and pentyl–terminated Si(111) surfaces. This slab depicts the alkyl group in an atop site which had the best fitting calculated χ function. In the case of the pentyl–terminated surface, this model includes scattering from the third layer silicon 157

atoms, but neglects scattering from the neighboring C atom.

Figure IV.15: The four layer slab used in the photoelectron diffraction calculations from the pentyl–terminated Si(111) surface. This slab depicts the alkyl group in an atop site which had the best fitting calculated χ function. This model includes scattering from the neighboring C atom, but neglects scattering from the third layer silicon atoms. 158

Figure IV.16: NEXAFS spectra from an octadecyl–terminated sample collected using the C KLL Auger line with the photon beam at glancing and grazing incidence are shown. The difference spectra which will be used to determine the orientation of alkyl chain is also shown. The main features are identified along with the position of the ionization potential. The C–C bond length in the chain was determined to be 1.53 Å by using the position of the σ^*(C–C) features as described in the text. 159

Figure IV.17: NEXAFS spectra collected as in Figure IV.16 from methyl–, pentyl–, decyl–, and octadecyl–terminated Si(111) samples are shown. Note that as the length of the alkyl chain decreased, the spectra show strong contribution from the absorption of the C atom bound to the Si substrate. This clearly shows up in the differences observed in the difference spectra from the different samples. 160

Figure IV.18: In order to obtain an accurate tilt angle of the alkyl chains with respect to the surface normal, the difference spectrum from the octadecyl–terminated sample (least contribution from the C atom bound to the surface) were compared to difference spectra from standard compounds with known tilt angles. This figure shows the NEXAFS spectra from Polyethylene (tilt angle 90°)(Stohr et al. 1987), Ca Arachidate (tilt angle 33°)(Outka et al. 1988; Outka et al. 1987), Cd Arachidate (tilt angle 0°)(Outka et al. 1988; Outka et al. 1987), and octadecyl–terminated Si(111). Note the similarity of the difference spectra of Ca Arachidate. 161

Figure IV.19: Valence band spectra taken from a pentyl–terminated Si(111) surface with a photon energy of 55 eV after annealing to the listed temperature are shown. Note that the pentyl chain did not break apart into smaller alkane units as was evidenced by the presence of only the 5 molecular orbitals on the pentyl–terminated surface. Silicon carbon alloying occurred at temperatures above 250° C (growth of peak at 44 eV). Above 600° C the surface reconstructed into the clean Si(111) 7x7 surface indicating that the alloy desorbed or diffused into the bulk. 162

Figure IV.20: Silicon 2p core level spectra from a pentyl–terminated Si(111) surface with a photon energy of 130 eV (surface sensitive) after annealing to the 163

listed temperature are shown. The transition from an alkyl–terminated surface to a clean Si(111) 7x7 surface is evident.

Figure IV.21: As in Figure IV.19 except the spectra are from a methyl–terminated surface. 164

Figure IV.22: As in Figure IV.20 except the spectra are from a methyl–terminated surface. 165

Figure IV.23: As in Figure IV.19 except the spectra are from a decyl–terminated surface. 166

Figure IV.24: As in Figure IV.20 except the spectra are from a decyl–terminated surface. 167

Figure IV.25: As in Figure IV.19 except the spectra are from an octadecyl–terminated surface. 168

Figure IV.26: As in Figure IV.20 except the spectra are from an octadecyl–terminated surface. 169

Figure IV.27: Representations of the surface structure consistent with the scanned–energy photoelectron measurements are shown. A.) The pentyl–terminated surface has a Si–C bond length of 1.85Å and the chain tilt angle must be less than 45° from the surface normal. B.) The methyl–terminated surface has a Si–C bond length of 1.85 Å and is directed along the surface normal. 170

Figure V.1: A Zn 3p core level spectrum taken at a photon energy of 350 eV and an O 1s core level spectrum 177

taken at a photon energy of 650 eV.

Figure V.2: Bulk terminated ZnO($10\bar{1}0$) surface used in calculations. 178

Figure V.3: LEED reconstructed ZnO($10\bar{1}0$) surface used in calculations. 179

Figure V.4: The experimental PED data is shown along with multiple–scattering calculations using both the Bulk and LEED clusters. 180

CHAPTER I.
INTRODUCTION

I.1. MOTIVATION

It is the goal of materials chemistry to create novel materials with physical properties tailored for a specific purpose. Presently, materials chemists are synthesizing new materials and structures in many areas, including: sensors(Petty 1996), light–emitting materials(Bradley 1995; Kowalsky et al. 1996; Park et al. 1996), photovoltaic materials(Paes, Pinho, and Losch 1989; Tiburcio-Silver and Joubert 1991; Unaogu and Okeke 1990), and semiconductors(Cao et al. 1992; Linford and Chidsey 1993; Linford et al. 1995; Terry et al. 1996; Yang et al. 1993; Yang et al. 1992). Often, these novel materials and structures are prepared using standard wet chemical methods(Linford and Chidsey 1993; Linford et al. 1995) rather than traditional methods performed under Ultra–high Vacuum Conditions (UHV), such as chemical vapor deposition and molecular beam epitaxy. It has also become difficult to characterize these novel materials as traditional surface science characterization techniques (Low Energy Electron Diffraction, Auger Spectroscopy, Photoelectron Spectroscopy) require UHV conditions and traditional synthetic chemistry characterization techniques (FTIR, Raman Spectroscopy) are hindered by low surface concentrations and surface attenuation. Therefore, it has become the job of physical chemists both to characterize these new materials and to provide characterization tools and methods for synthetic chemists. The main characterization tools utilized by these experiments where photoemission spectroscopy and photoelectron diffraction. Note that these are both methods that require the use of ultra–high vacuum conditions.

Since every novel silicon surface described in this work had at least one wet chemistry procedure performed outside of the UHV system, sample handling methods that minimized the risk of contamination by exposure to atmosphere were developed. The novel silicon surfaces were either prepared on–site using the wet chemical methods and then placed into the load–lock system of the vacuum chamber, immediately, or the samples were prepared off–site and transported to the Stanford Synchrotron Radiation Laboratory

in a vacuum compatible transfer chamber that could be backfilled with an inert gas or evacuated to pressures of less than 10^{-3} torr. In this way exposure to atmospheric conditions was limited. In most cases, this procedure was adequate to reduce contamination to acceptable levels. The exceptions were dealt with in manners described in the relevant chapter. This sample methodology coupled with the relative inertness of the samples studied here allowed the use of high–resolution photoemission spectroscopy and photoelectron diffraction to be used to study the interfacial structure of novel silicon surfaces. Brief introductions to these two main techniques, photoemission spectroscopy and photoelectron diffraction, used in this work will now follow.

I.2. TECHNIQUES

I.2.1. Photoemission

An excellent review of photoemission spectroscopy has been written by Hufner(Hufner 1995), therefore, only a brief summary will be given here. Photoemission Spectroscopy (PES), both angle–integrated and angle resolved photoemission, was used to determine the electronic structure of the novel Si surface structures studied in this work. PES is widely used in surface and interface studies because it is very sensitive to the electronic environment of the element under study. Therefore, both, the electronic structure of the interface and chemical reactions that occur at the interface can be studied. Furthermore, when combined with the variability of the photon energy at a Synchrotron radiation source, PES can be very surface sensitive, thereby insuring that only the interfacial region is studied. As the photon energy is varied the kinetic energy of the emitted photoelectrons also varies. Due to inelastic scattering in the sample, a maximum surface sensitivity (minimum escape depth) can be obtained. Typical escaped depths are on the order of approximately 5Å(Lindau et al. 1976). In this work, surface–sensitive PES was used to determine the electronic and geometric structures of the novel Si surfaces.

Figure I.1 shows an idealized photoemission experiment where an incident photon is absorbed by the sample with a photoelectron being emitted into the analyzer. The analyzer measures the kinetic energy of the photoemitted electron. The photoelectron kinetic

energy is related to the energy of the incoming photon by the basic Einstein relation of photoemission process shown in Eq. I.1.

$$E_{kin} = h\nu - E_b - \phi \tag{I.1}$$

where E_{kin} is the kinetic energy of the detected photoelectron, E_b is the binding energy of the electron in the final state (i.e. a state with a core hole), ϕ is the work function of the material, and $h\nu$ is the photon energy. Typically, photoemission experiments are carried out with an unbiased connection between the sample and the analyzer which causes the Fermi levels of the two systems to be aligned. Because the Fermi level of the sample and the electron detector are aligned, the measured kinetic energy of the photoelectron by an electron analyzer is given by Eq. I.2.

$$E_{kin} = h\nu - E_b - \phi_a \tag{I.2}$$

Here, ϕ_a is the work function of the analyzer which is constant for measurements performed with the same analyzer. Eq. I.2 allows one to determine the binding energy of an electron from the kinetic energy of the photoelectron, if and only if, the work function of the analyzer and the photon energy are accurately known. In this work, the photoemission spectra are typically shown as a function of the observed kinetic energy. Figure I.2 shows a typical photoemission spectrum.

One way to view the photoemission process is the three–step–model proposed by Spicer(Spicer 1958). Figure I.3 shows how the photoemission process can be broken up into three stages; excitation, transportation, and escape. In the excitation process, an electron absorbs the energy from a photon. If the photon energy is greater than the difference between the binding energy and the vacuum level, an electron can be excited into an

unbound final state. This photoelectron with a final state energy greater than the vacuum level is created in the interior of the sample under study. In the transportation process, the photoelectron migrates from the emitting atom to the surface of the sample. During the transportation process, an electron may undergo, either/both, elastic or inelastic scattering. Elastic scattering gives rise to diffraction effects measured as photoelectron diffraction or extended x–ray absorption fine structure spectroscopies. Inelastic scattering changes the energy of the photoelectron and results in, either, a loss of information or a loss of the electron. In general, the probability that an electron excited will reach the surface is $\exp(-x/\lambda)$, where λ is escape depth of the electron and x is the distance from the emitting atom to the surface. Finally, in the escape process, the photoelectron is refracted by the surface potential barrier during escape into the vacuum.

The measured photoemission electron intensity is proportional to

$$I \propto A \cdot \sigma(j,Z) \cdot C(Z) \cdot e^{-\frac{x}{\lambda}} \cdot f(\theta) \tag{I.3}$$

where A combines the photon flux, the area of the interaction region between the sample and photon beam, and the transmission function of the analyzer at the measured kinetic energy. I also depends upon the photoionization cross–section, $\sigma(j,Z)$, for the element Z at the energy of the incoming photons; the concentration of element Z, C(Z); the distance of the excited atom from the surface, x; the escape depth, λ; and the angular distribution function of the emitted photoelectron, $f(\theta)$.

In this work, the tunability of the synchrotron radiation excitation source was often utilized to set the escape depth, λ, which is a strong function of kinetic energy, to its minimum value for a particular surface. At the escape depth minimum which was typically below 5 Å for the energies used, it was possible to selectively highly the electronic structure of the near surface layers. As an example for C 1s photoemission from a thin enough overlayer such as the pentyl–terminated Si(111) surface (Figure I.2), it was possible to detect both the core level emission from the chain and the surface–reacted component.

However, as the alkyl chain length was increased, the surface component could no longer be observed. However, the C 1s core level photoemission spectra from the pentyl–terminated surface illustrates one of the most useful properties of photoemission spectroscopy, the chemical shift.

The measured kinetic energy of the photoelectrons are dependent upon Fermi level position, screening of the final state core hole, and chemical environment. A chemical shift occurs when the measured kinetic energy of the photoelectron is modified due to the chemical environment of the emitting atom. Most often chemical shifts are due to charge transfer. The chemical shift, ΔE_{nl}, of an orbital, nl, between an element in a bulk–like state, B, and the same element in a different chemical environment, C, in solid is(Eastman, Himpsel, and van der Veen 1982):

$$\Delta E_{n,l} = E_{n,l}(C) - E_{n,l}(B) \tag{I.4}$$

A simple way to look at chemical shifts is focus on the difference in the potential field that the core electrons are exposed to in the different chemical environments. One might expect from this simple model that as charge is transferred either to or away from the valence shell in different chemical environments that the core electrons will reorient themselves further from or closer to the nucleus of the emitting atom. Chemically–shifted components in core level photoemission measurements allows one to determine direct chemical bonding information. In this work, chemically–shifted components were used to determine chemical bond formation and interface structure.

I.2.2. Photoelectron Diffraction

Recently, photoelectron diffraction (PED) has been used to determine the geometric structure of many surface adsorbates(Fadley 1988; Fadley 1993; Fadley et al. 1994). In a PED measurement, the photoemission process creates a free electron from a core level that propagates away from the emitting atom as a spherical wave which undergoes scattering

from neighboring atoms. At the detector, the scattered waves interfere with the unscattered, primary wave. This interference is observed as variation in emitted electron intensity as a function of electron wave vector (**k**). As long as the initial state is localized in space, the photoelectron diffraction pattern is highly site specific. However, care must be taken to insure that the intensity modulations must be due to final–state scattering effects and not due to anisotropies from initial state chemical shifts. Since PED measurement are based upon the photoemission process, these measurements are both element–specific and chemical–state specific. Weiss, *et. al.*(Weiss et al. 1992; Weiss et al. 1993) have demonstrated the ability of chemical–shift, scanned–energy, photoelectron diffraction to determine the local geometric structure of adsorbate atoms in chemically different environments. This allows one to determine the surface geometry of a species where the same element exists in two or more chemically different sites.

The PED measurements are obtained by varying the momentum of the detected photoelectron. This can be done by varying the kinetic energy of the photoelectron, (scanned–energy), or by varying the detected electron, (scanned–angle). The azimuthal, scanned–angle photoelectron diffraction measurements have an advantage of having no instrument contribution to the measured intensity distribution, while the both scanned–energy and polar, scanned–angle measurements must be corrected for instrumental contributions. Scanned–energy PED measurements rely on the tunability of synchrotron radiation sources. Eq. I.2 shows how the kinetic energy of the photoelectron is dependent upon the photon energy, hν. The momentum of a free electron is related to its kinetic energy by Eq. I.5.

$$k = \sqrt{\frac{2m_e}{\hbar^2}E_K} \approx .512332 \cdot \sqrt{E_K} \qquad \text{(I.5)}$$

Thus, by varying the photon energy, the wave vector of the photoelectron is varied.

Scanned–angle, PED varies the wave vector of the detected photoelectron by varying the

detection angle. Scanned–angle, PED measurements are now typically made by rotating the sample rather than the analyzer, because it is now impractical to rotate the large hemispherical analyzers used in photoemission measurements. Figure I.1 defines the sample rotation angles. Azimuthal measurements are performed by scanning the angle, ϕ, while polar scans vary the angle, θ. Unfortunately, it can be difficult experimentally to vary the azimuthal angle, ϕ, due to heating, cooling, and temperature measurement leads that are usually attached to the sample because the leads often prevent full 360° rotation. The PED system utilized in this work was equipped with a sample manipulator (Thermionics) that did allow 360° rotation in azimuthal angle. It is also important that the reproducibility of the angular motion be approximately 0.1° to 0.5°. The angular reproducibility of the sample manipulator was better than 0.25° in both azimuthal and polar angle. Furthermore, the electron energy analyzer used for PED measurements should have an angular resolution of 1.0° to improve the fine structure of the data along with energy resolution of 0.1 eV to resolve small chemical shifts due to chemical bonding or surface differences relative to the bulk(Fadley 1988; Fadley 1993; Fadley et al. 1994). The hemispherical analyzer used in this work had angular resolution of ±1.5° and energy resolution of better than 50 meV.

Photoelectron diffraction relies upon the intensity modulations of the primary photoelectron wave due to interference from scattered waves. These intensity modulations for PED are easily measured because the anisotropy can be as high as:

$$\frac{I_{\max} - I_{min}}{I_{\max}} = 0.5 \; to \; 0.7 \qquad \text{(I.6)}$$

The peak intensity can very 30 to 50% with direction(Fadley 1993).

The elastic scattering factors for PED are strongly energy dependent. For electrons with kinetic energies below 200 eV, the scattering is isotropic. For 200–500 eV electrons, the scattering has two strong features. The strongest scattering is peaked at $\theta = 0°$ which corresponds to forward scattering. Weaker scattering occurs at $\theta = 180°$ which corresponds to

backscattering. Scanned–energy, PED measurements are typically performed in this range in order to determine the atomic positions of the near–neighbors below the emitting atom due to interference of the backscattered wave. Finally, for electrons with kinetic energy greater than 500 eV, forward scattering is dominant. This phenomenon is called forward focusing(Fadley 1993). In this case, it is trivial to determine bond angles, because the intensity modulations observed during scanned–angle measurements are due to the forward focusing through the near–neighbors. Since this is the case, the PED peaks are observed in the near–neighbor directions.

Unfortunately, it is not as simple to determine structural parameters over the other ranges. Therefore, all photoelectron diffraction spectra are compared with theoretical models. The simplest model which accurately characterizes the scattering process in the single–scattering cluster theory (SSC). The single–scattering model assumes that the photoemission process creates an outgoing photoelectron wave which can be scattered once by a neighboring atom. The primary wave and the scattered wave then interfere with each other at the detector which results in the intensity modulations as shown in Figure I.4. The angles used in the theoretical modeling are shown in Figure I.5.

Single scattering theory described below follows the description given by Barton. First, an incident X–ray with polarization, ε, ejects a core–level photoelectron(Barton 1985a; Barton 1985b; Barton, Robey, and Shirley 1986; Barton and Shirley 1985b; Barton and Shirley 1985a). The Transition Probability (TP) is given in the dipole approximation by Eq. I.7,

$$TP \propto \frac{(2\pi)}{\hbar} \cdot \left| \left\langle \psi_f \right| \varepsilon \cdot r \left| \psi_i \right\rangle \right|^2 \delta\left(E_f - E_i - \hbar\omega\right) \tag{I.7}$$

where ψ_i is the initial–state wavefunction and ψ_f is the final–state wavefunction with out-

[redacted]

$$\left\langle \psi_f \middle| \varepsilon \cdot r \middle| \psi_i \right\rangle = \left\langle \phi_{f,Ekin} \middle| \varepsilon \cdot r \middle| \phi_{i,k} \right\rangle \left\langle \psi^k_{f,R}(N-1) \middle| \psi^k_{i,R}(N-1) \right\rangle \tag{I.8}$$

The final–state wavefunction is a superposition of all outgoing states with wavevector **k**. Therefore, ψ_f can be written as:

$$\psi_f = \psi_0 + \sum_j \psi_j \tag{I.9}$$

where ψ_0 is the primary wave and the ψ_j are the scattered waves. Due to the small inter-atomic dimensions, the detector appears to be an infinite distance away in the direction of the wavevector k. Therefore, the photoelectron waves have the form of a spherical wave. The primary wave,ψ_0, will then be given by Eq. I.10,

$$\psi_0 = M(k) \cdot \cos(\gamma) \cdot \left(\frac{e^{ikr}}{kr} \right) \tag{I.10}$$

where M(k) is the matrix element described above, which acts as a scaling factor, and γ is the angle between the detector direction and the polarization vector of the incident radiation. The scattered waves are going to be spherical waves that originate at the near–neighbor atoms, $\mathbf{r_j}$, and are given by Eq. I.11.

$$\psi_j \propto \left(\frac{e^{ik\left|\vec{r}-\vec{r}_j\right|}}{k\left|\vec{r}-\vec{r}_j\right|} \right) \tag{I.11}$$

The scattered wave must be proportional to both the strength of the primary wave at the position of the scattering atom and, in the single–scattering approximation, to the scattering power, $k|f(\theta_j,k)|$ of the scattering atom in the direction of the analyzer. θ_j, then, is the angle between the bond vector, $\mathbf{r}_j$, and the analyzer direction. Therefore, ψ_j can be written as:

$$\psi_j = M(k) \cdot \cos(\beta_j) \cdot \left(\frac{e^{i(kr_j+\phi_j)}}{kr_j}\right) \cdot k\left|f(\theta_j)\right|\left(\frac{e^{ik|\vec{r}-\vec{r}_j|}}{k|\vec{r}-\vec{r}_j|}\right) \qquad \text{(I.12)}$$

The phase shift, ϕ_j, arises because of interactions between the primary wave and the core of the scattering atom. Notice that the amount of ψ_0 that is scattered from the jth atom decays as $1/r_j$. This allows for the conservation of flux. Because of this decay, PED is a short range probes.

However, since the detector is located in the far–field, i.e. a long distance from the emitter and scatterer, the exponential terms can be combined. The exponential terms can be combined because the only difference between the primary and scattered spherical waves at the detector position, **R**, is a phase difference of $-r_j \cos(\theta_j)$. Therefore, ψ_j can be written as:

$$\psi_j = M(k) \cdot \cos(\beta_j) \cdot \frac{\left|f(\theta_j)\right|}{r_j}\left(e^{i\left(kr_j - kr_j\cos(\theta_j)+\phi_j\right)}\right) \cdot \left(\frac{e^{ikR}}{kR}\right) \qquad \text{(I.13)}$$

The measured intensity, I, is given by $\psi_f^* \psi_f$. One can further define the intensity in the absence of diffraction, I_0, as $\psi_0^* \psi_0$. A normalized intensity function, χ, is then defined as $(I-I_0)/I_0$. To first order, χ given by Eq. I.14.

$$\chi = \sum_j \frac{\psi_0^* \psi_j + \psi_j^* \psi_0}{\psi_0^* \psi_0} \tag{I.14}$$

Substituting the values from Eq. I.10 and Eq. I.13 and performing algebraic manipulation allows χ to finally be defined as in Eq. I.15.

$$\chi(k) = 2\sum_j \frac{\cos(\beta_j)\left|f(\theta_j)\right|}{\cos(\gamma)} \frac{}{r_j} \cos\left(k\left(r_j - r_j \cos(\theta_j)\right) + \phi_j\right) \tag{I.15}$$

Note that the intensity oscillations depend strongly upon wave vector, k, and path–length difference, r_j-$r_j \cos(\theta_j)$.

The simplest method for describing the scattering power of the neighboring atoms uses the 'small atom approximation'(Fadley 1993). In the 'small atom approximation,' the assumption that the spherical wave, ψ_0, appears to the jth scatterer as a plane wave. Using this model, the scattering that produces the ψ_j can be described by a plane–wave scattering factor, $f(\theta_j)$,

$$f(\theta_j) = \left| (2ik)^{-1} \sum_{l=1}^{\infty} (2l+1)\{e^{2i\delta_l} - 1\} P_l(\cos\theta_j) \right| * e^{i\phi_j} \tag{I.16}$$

where the P_l are the Legendre polynomials, the δ_l are partial–wave phase shifts, and the ϕ_j are the scattering phase shifts described above.

Many improvements to the scattering theory described above can be made. First, the

scattering power can be described using the form of a spherical wave. Second, the effects of multiple scattering can be corrected for. The major correction made by multiple scattering cluster (MSC) theory is to reduce the predicted intensities of SSC theory. The intensity reduction occurs due to defocusing(Fadley 1993) of electrons. Defocusing occurs when two scatters are along the same line of sight. The first scatterer forward focuses the electron wave and the second scatterer defocuses the wave. This causes the detected intensity at that angle to be less than that predicted by SSC theory. These corrections have been described in detail elsewhere(Barton 1985a; Barton 1985b; Barton, Robey, and Shirley 1986; Barton and Shirley 1985b; Barton and Shirley 1985a; Fadley 1988; Fadley 1993; Fadley et al. 1994). In this work, the majority of the photoelectron diffraction calculations have been corrected for both spherical wave and multiple scattering.

I.2.3. Spectral Decomposition

All photoemission spectral decompositions were performed using a least–squares fitting routine. The fitting parameters were found by fitting the narrowest observed spectrum from each core level using Voight lineshapes. These fitting parameters were then used to decompose the core level spectra from other surface systems. The narrowest spectrum for the Si 2p core level was observed in the Cl–Si(111) system. The narrowest spectrum for the C 1s core level was observed in the octadecyl–Si(111) system. The fitting parameters from these two systems are given in Table I.1.

I.3. THESIS ORGANIZATION

Chapter II presents a study of the light–emitting porous silicon surface which utilized photoemission spectroscopy and near–edge x–ray absorption spectroscopy to determine the mechanism of the light–emission.

Chapter III presents a study of the H–Si(111) surface which utilized photoemission spectroscopy to study the reactivity of this surface. Reactions with Au, Ge, O_2, Cl_2, Br_2, and alkyl groups were investigated.

Chapter IV presents a study of alkyl–Si(111) surfaces which utilized photoemission

spectroscopy, chemical–shift, scanned–energy photoelectron diffraction, and near–edge x–ray absorption spectroscopy to examine the fundamental properties such as Si–C bond length and orientation. It must be noted that this was the first application of chemical–shift, scanned–energy photoelectron diffraction to an interface which was prepared *ex situ* using standard chemical synthesis techniques.

Chapter V presents a study of the ZnO($10\bar{1}0$) surface which utilized photoemission spectroscopy and scanned–angle photoelectron diffraction to determine the surface reconstruction of the ZnO dimers that are present at the surface. After the above success of photoelectron diffraction on the alkyl–terminated Si(111) surface, it was believed that photoelectron diffraction may be useful in determining the controversial surface reconstruction of the ZnO($10\bar{1}0$) surface.

I.4. REFERENCES

Barton, J. J. 1985a. Angle–resolved Photoemission Extended Fine Structure, Ph. D. Dissertation, University of California, Berkeley.

Barton, J. J. 1985b. Angle–Resolved Photoemission Extended Fine Structure: LBNL Report Number 19215, Lawrence Berkeley National Laboratory, University of California Berkeley, Berkeley.

Barton, J. J., S. W. Robey, and D. A. Shirley. 1986. *Physical Review B* 34:778.

Barton, J. J., and D. A. Shirley. 1985b. *Physical Review B* 32:1906.

Barton, J. J., and D. A. Shirley. 1985a. *Physical Review B* 32:1892.

Bradley, D.D.C. 1995. *Polymer electroluminescence: principles and prospects, IEEE Colloquium on 'Novel Display Technologies'(Digest No. 1995/138).* London, UK: IEEE.

Cao, R., X. Yang, J. Terry, and P. Pianetta. 1992. *Applied Physics Letters* 61:2347.

Eastman, D. E., F. J. Himpsel, and J. F. van der Veen. 1982. *Journal of Vacuum Science and Technology* 20:609.

Fadley, C.S. 1988. 'Recent developments in photoelectron diffraction,' in*Core-Level Spectroscopy in Condensed Systems. Proceedings of the Tenth Taniguchi International Symposium*, edited by J. Kanamori and A. Kotani, Berlin, West Germany: Springer-Verlag.

Fadley, C.S. 1993. *Surface Science Reports* 19:231.

Fadley, C.S., S. Thevuthasan, A.P. Kaduwela, C. Westphal, Y.J. Kim, R. Ynzunza, P. Len, E. Tober, F. Zhang, Z. Wang, S. Ruebush, A. Budge, and M.A. Van Hove. 1994. *Journal of Electron Spectroscopy and Related Phenomena* 68:19.

Hufner, Stefan. 1995. *Photoelectron Spectroscopy.* Edited by M. Cardona.Solid–State Sciences, vol. 82. Berlin: Springer–Verlag.

Kowalsky, W., D. Ammermann, A. Bohler, and S. Dirr. 1996. *Organic light emitting diodes, IPRM 1996.* Eighth International Conference on Indium Phosphide and Related Materials (Cat. No.96CH35930). New York, NY, USA: IEEE.

Lindau, I., P. Pianetta, K. Y. Yu, and W. E. Spicer. 1976. *Journal of Electron Spectroscopy and Related Phenomenon* 8:847.

Linford, M. R., and C. E. D. Chidsey. 1993. *Journal of the American Chemical Society* 115:12631.

Linford, M. R., P. Fenter, P. M. Eisenberger, and C. E. D. Chidsey. 1995. *Journal of the American Chemical Society* 117:3145.

Paes, H.R., Jr., L.M.O.C. Pinho, and W. Losch. 1989. In *Commission of the European Communities. Ninth E.C. Photovoltaic Solar Energy Conference. Proceedings of the International Conference*, edited by W. Palz, G. T. Wrixon, and P. Helm, Dordrecht, Netherlands: Kluwer Academic Publishers.

Park, J.Y., H.M. Le, G.T. Kim, H. Park, Y.W. Park, I.N. Kang, D.H. Hwang, and H.K. Shim. 1996. *Synthetic Metals* 7:177.

Petty, M. C. 1996. *Langmuir–Blodgett films: An Introduction.* Cambridge: Cambridge University Press.

Spicer, W. E. 1958. *Physical Review* 112:114.

Terry, J., M. R. Linford, C. Wigren, R. Cao, P. Pianetta, and C. E. D. Chidsey. 1996. *Applied Physics Letters* submitted.

Tiburcio-Silver, A., and J.C. Joubert. 1991. In *Tenth E.C. Photovoltaic Solar Energy Conference. Proceedings of the International Conference*, edited by A. Luque, G. Sala, W. Palz, G. Dos Santos, and P. Helm. Dordrecht, Netherlands: Kluwer Academic Publishers.

Unaogu, A.L., and C.E. Okeke. 1990. *Solar Energy Materials* 20:29.

Weiss, K.–U., R. Dippel, K.–M. Schindler, P. Gardner, V. Fritzsche, A. M. Bradshaw, A. L. D. Kilcoyne, and D. P. Woodruff. 1992. *Physical Review Letters* 69:3196.

Weiss, K.–U., R. Dippel, K.–M. Schindler, P. Gardner, V. Fritzsche, A. M. Bradshaw, D. P. Woodruff, M. C. Asensio, and A. R. Gonzalez–Elipe. 1993. *Physical Review Letters* 71:581.

Yang, X., R. Cao, J. Li, I. Terry, J. Wu, and P. Pianetta. 1993.in*Common Themes and Mechanisms of Epitaxial Growth Symposium*, Edited by P. Fuoss, J. Tsao, D. W. Kisker, A. Zangwill, and T. Kuech, Pittsburgh, PA, USA: Materials Research Society.

Yang, X., R. Cao, J. Terry, and P. Pianetta. 1992. in *Chemical Surface Preparation, Passivation and Cleaning for Semiconductor Growth and Processing Symposium*, Edited by R. J. Nemanich, C. R. Helms, M. Hirose, and G. W. Rubloff, Pittsburgh, PA, USA: Materials Research Society.

Table I.1: The fitting parameters from the narrowest Si 2p and C 1s core level spectra as described in the text are given.

Core Level	Kinetic Energy (eV)	Lorentzian HWHM (eV)	Gaussian HWHM (eV)	Spin–Orbit Splitting (eV)	Spin–Orbit Branching Ratio
Si 2p	25.94	0.0268	0.161	-0.605	0.5
C 1s	57.25	0.175	0.150	N/A	N/A

Figure I.1: An idealized version of a photoemission experiment is shown.

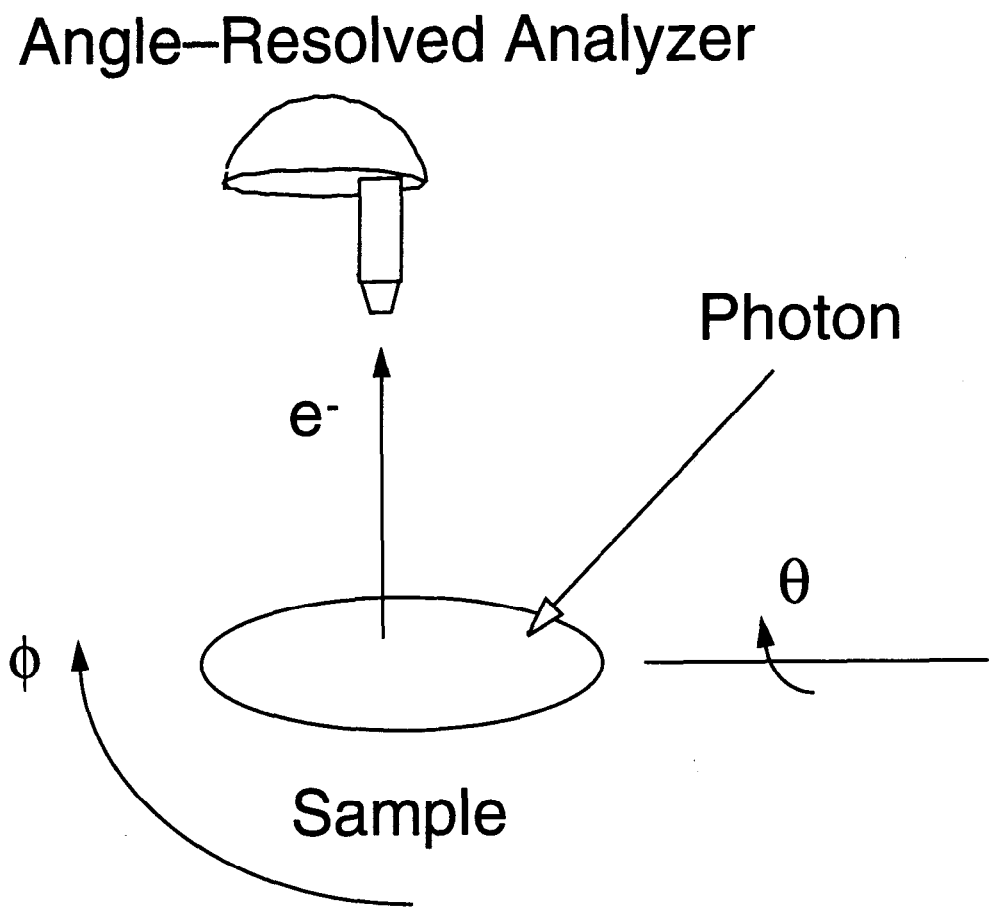

Figure I.2: A typical C 1s core level spectra taken at a photon energy of 350 eV from an alkyl terminated Si(111) sample is shown decomposed into two singlet components. The components are attributed to emission from the bulk–like C atoms in the alkyl chain (C–C) and to emission from the C atom bound to the Si surface (C–Si).

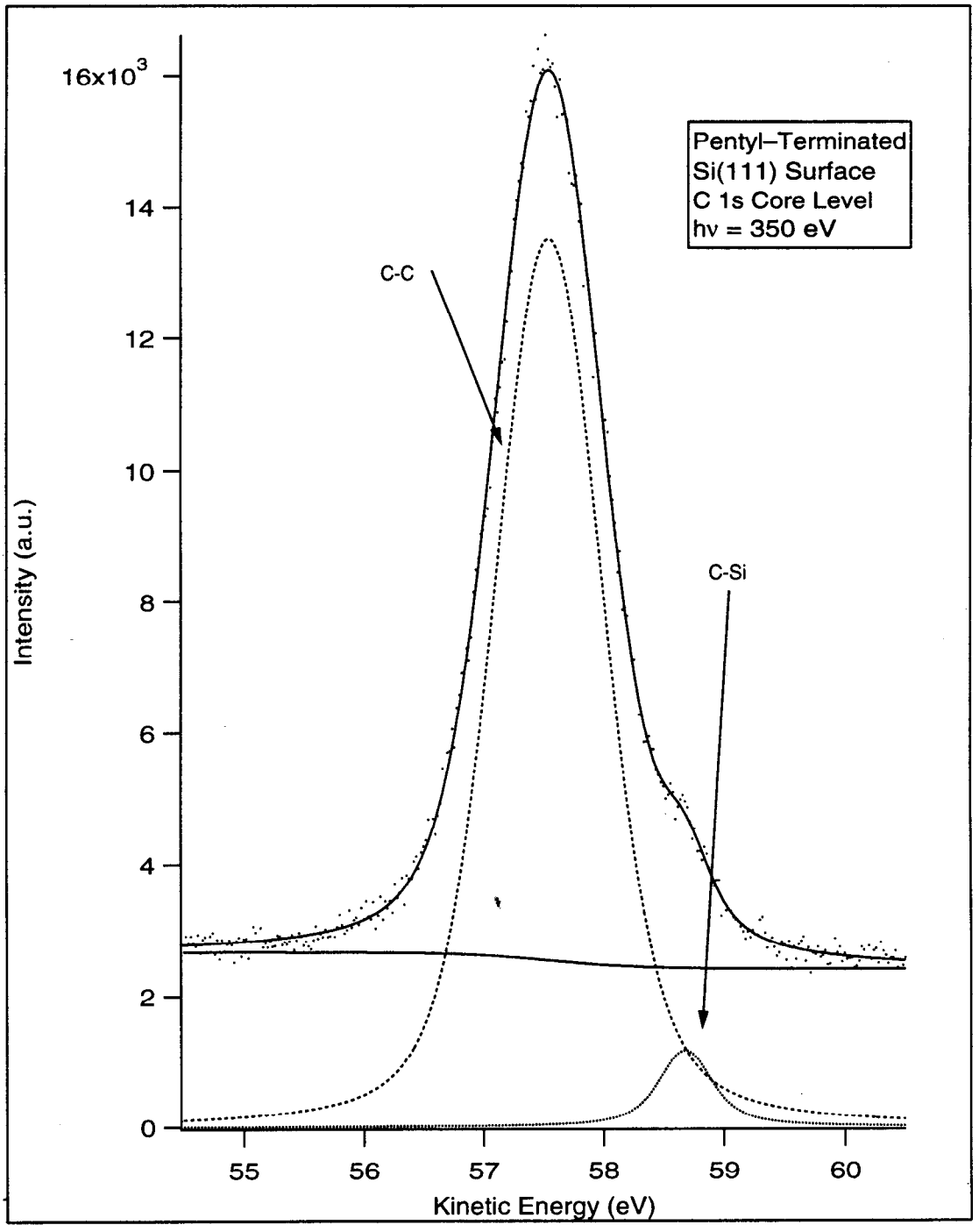

Figure I.3: The three–step model of the photoemission process is depicted.

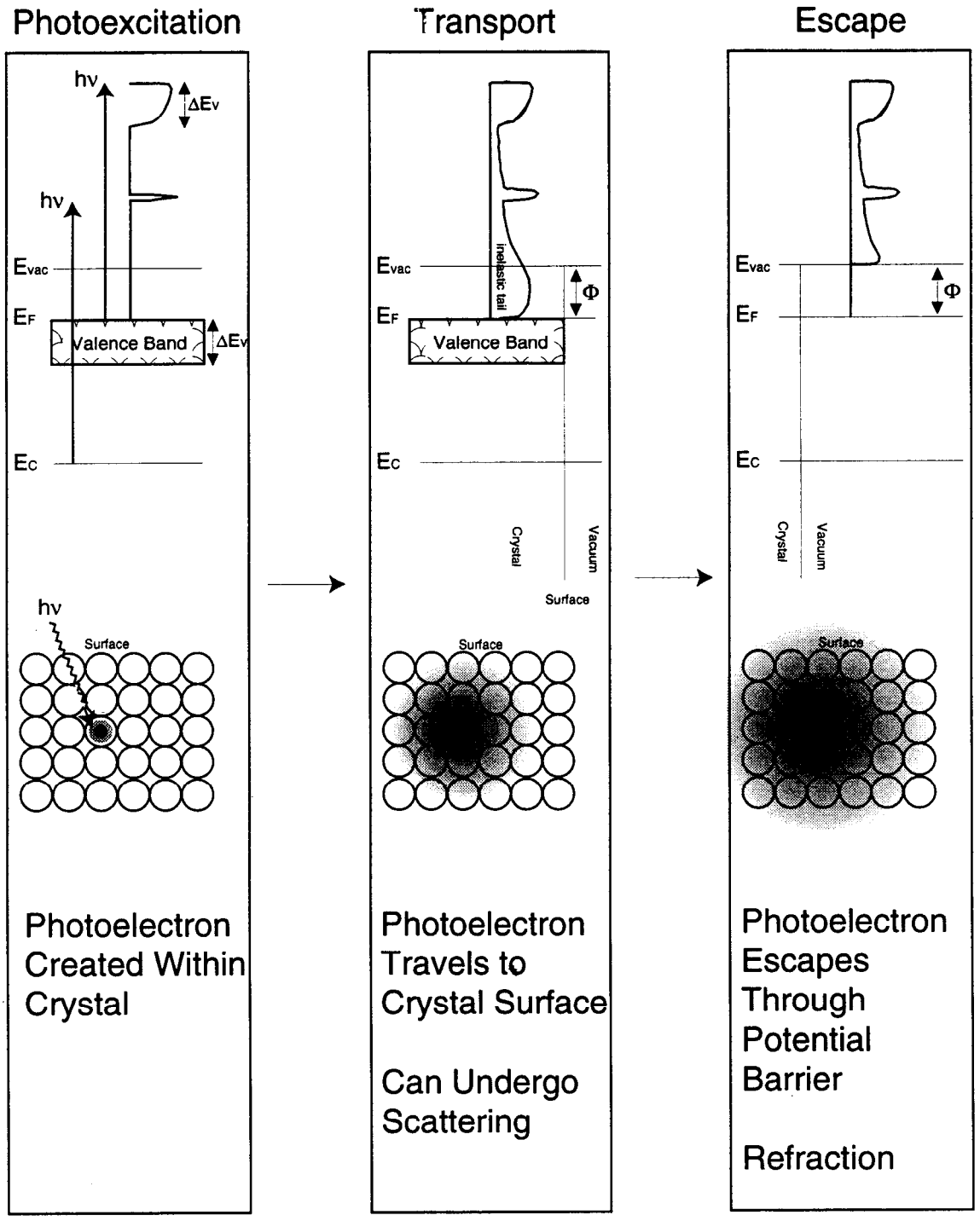

Figure I.4: A single–scattering photoelectron diffraction event is shown.

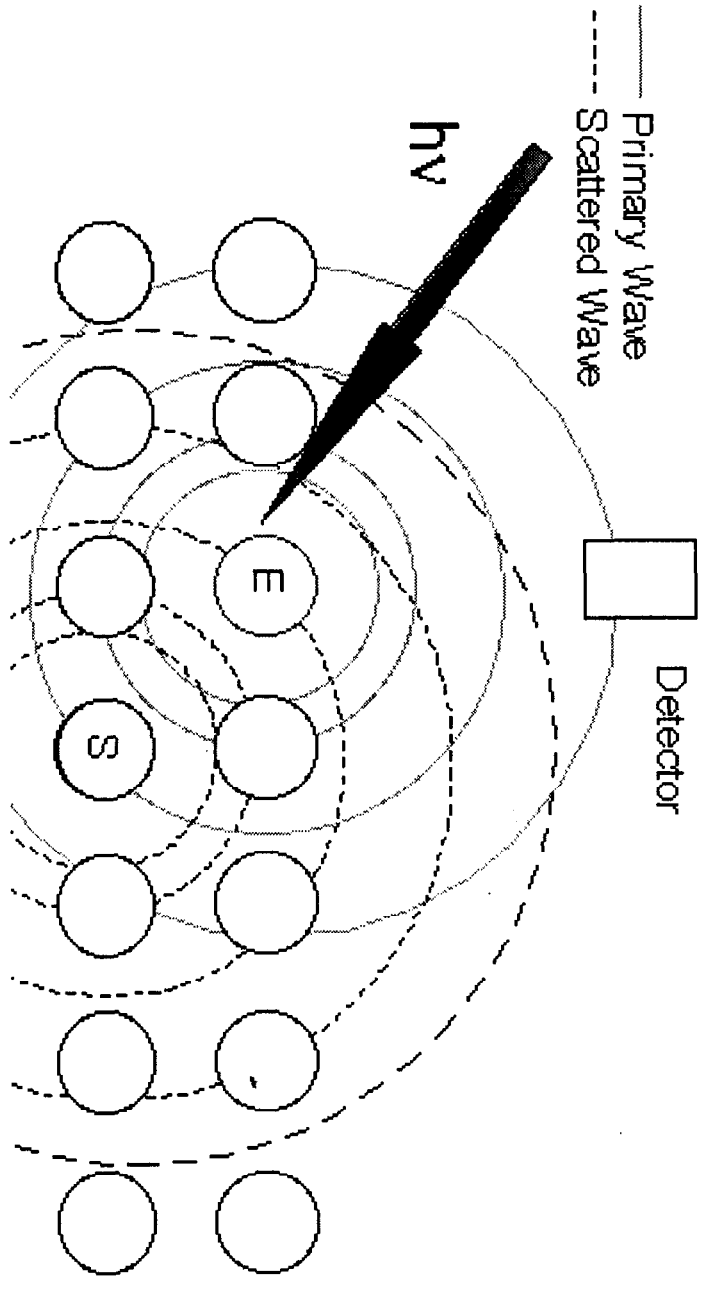

Figure I.5: The angles used in the calculation of PED spectra are shown.

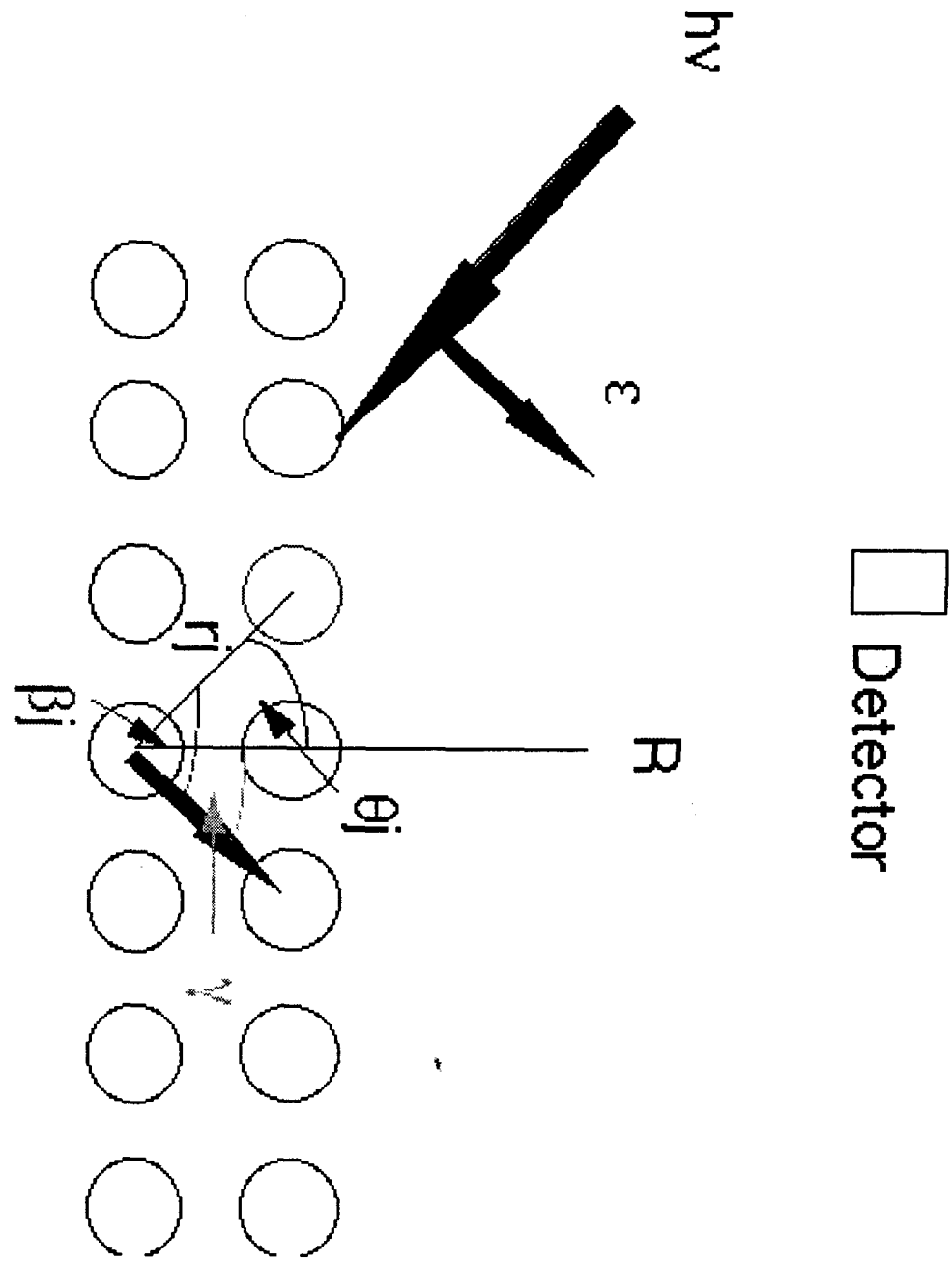

CHAPTER II.
LIGHT–EMITTING POROUS SILICON

II.1. ABSTRACT

Recently, it has been shown that silicon can be made to show appreciable luminescence above the band gap under optical excitation(Canham 1990). However, the mechanism for this unusual behavior is presently not well understood. In order to determine the mechanism for the observed light emission, photoluminescence, valence band photoemission, and Si 2p core level photoemission spectra were collected from electrochemically etched light emitting porous silicon (LEPS) samples prepared with different electrochemical and chemical etching exposures. The photoluminescence intensity was observed to increase and blue shift as the etching times were increased. Furthermore, the Si 2p core level broadened appreciably as the chemical etching time was increased. Impurity species were found to be present only in trace amounts, with carbon being the only species to be present on all samples. Valence band spectra were similar at all etching times with no strong features observed. Silicon K–edge x-ray absorption spectra (NEXAFS) were collected from a sample with the best photoluminescence and photoemission characteristics. The Si K-edge NEXAFS spectra clearly showed that the near surface region of the LEPS was crystalline. Annealing studies were carried out to determine how the sample decomposed. Upon annealing, the core level linewidth decreased, and the valence band developed well defined spectral features similar to those of the Si(100) 2x1 surface. The photoluminescence intensity decreased and was further blue shifted upon annealing(Terry et al. 1992). Finally, upon annealing only slight changes in the Si K-edge NEXAFS spectrum were observed. Our data was consistent with a photoluminescence mechanism involving a silicon species that degraded, decomposed, or desorbed upon annealing.

II.2. INTRODUCTION

Crystalline silicon does not, under normal conditions, emit light. This is because silicon is an indirect band gap material, as such it cannot obey the normal selection rules ($\Delta k = 0$)

for direct photon emission in crystalline solids. Therefore, it was remarkable when Canham discovered that electrochemically–etched silicon could be made to luminescence above the band gap under optical excitation(Canham 1990). This photoluminescence has been observed from silicon samples that have undergone electrochemical dissolution(Canham 1990) and anodic oxidation(Bsiesy et al. 1991). The anodization forms a porous layer with the pores propagating in [100] directions(Chuang, Collins, and Smith 1989). One theory postulates that when the pores become large the small unetched portions act as quantum wires(Canham 1990). This discovery may allow the production of silicon based optoelectronic devices. However, it will not be possible to effectively utilize light emitting porous silicon (LEPS) in optoelectronic devices until the luminescence mechanism is understood.

Many theories have been proposed to account for the photoluminescence: quantum confinement(Canham 1990), amorphous Si emission(Fathauer et al. 1992; Vasquez et al. 1992), SiH_2 on the surface acting as recombination centers(Tsai et al. 1992), and the presence of a high concentration of a luminescent species on the large surface area of the porous layers(Xu, Gal, and Gross 1992). Complicating the analysis, photoluminescence has also been observed from microcrystalline Si particles(Takagi et al. 1990) and from silicon subjected to a stain etch, which supposedly has structure similar to that of porous Si(Fathauer et al. 1992). In order to gain a better understanding of the mechanism of the luminescence, high-resolution core level spectroscopy, valence band spectroscopy, and near edge X-ray absorption fine structure (NEXAFS) was used to study the electronic structure of porous silicon formed by electrochemical dissolution and chemical etching similar to that of Canham(Canham 1990).

Surface–sensitive photoemission and surface–sensitive NEXAFS are excellent techniques with which to study light emitting porous silicon because both photoemission and Auger yield NEXAFS measure all elastically scattered electrons emitted by the sample into the acceptance cone of our analyzer. Figure II.1 depicts a direct photoemission event from a silicon atom on the side of a pillar on an idealized model of porous silicon. Because the pillars have aspect ratios of approximately 30 to 1, electrons from the base of the pillars

have vanishingly small probabilities of reaching the analyzer. Therefore, since the escape depths were less than 10 Å at the kinetic energies that were detected, only, a 10 Å layer around the top and upper sides of the pillars was studied. Most of the present theories of the photoluminescence mechanism can be differentiated by the presence of different surface species. In fact it is entirely possible that the surface plays a direct role in the photoluminescence mechanism of porous silicon, as it may hold a luminescent chemical species, or it may be terminated in a bulk-like manner which makes the luminescence possible. Therefore, in order to determine the photoluminescence mechanism, NEXAFS and photoemission spectra were collected from the porous silicon sample to study changes in the surface species as a function of sample preparation technique.

Photoluminesce spectra were recorded from samples that were prepared using different preparation techniques. Two features were obvious from the data. First, the photoluminescence intensity increased as the etching time increased. Second, the photoluminescence peak was blue–shifted as the etching time was increased. Finally, the samples were annealed, and photoluminesce spectra were again collected. A marked decrease in luminescence intensity was observed along with a large blue–shift in the luminescence wavelength. Surface sensitive photoelectron spectroscopy was performed on these samples to determine the role of the surface in photoluminescence.

The photoemission spectra showed broadening of the Si 2p core level as the wet chemical etching time was increased. The as–etched valence band spectra was featureless. Upon annealing, the core level linewidth decreased, and the valence band progressed from a large featureless spectrum to a spectrum with three main peaks. Unfortunately, it was not possible to decompose the photoemission spectra into identifiable components. Wide scan photoemission spectra showed that the only impurity present on all samples was C, although, F was present on the samples with longer etching times. Oxygen was often observed, but it was likely introduced during sample transfer through air rather than through the preparation technique.

Using surface sensitive NEXAFS spectroscopy, it was possible to show that the surface of electrochemically etched porous silicon was crystalline. As the silicon was not amorphous,

a luminescence mechanism based on amorphous silicon was not possible. Upon annealing, only minor changes in the Si K–edge absorption spectra were observed.

Unfortunately, it was impossible to definitively determine the photoluminescence mechanism of light–emitting porous silicon. However, it was possible to rule out a mechanism based on light emission from amorphous silicon, and it also appeared unlikely that an impurity species could account for the photoluminescence.

II.3. EXPERIMENTAL

II.3.1. Sample Preparation and Transportation

The samples were prepared by anodization of 0.1 to 0.9 Ω-cm, Boron doped, p-type Si (100) wafers in a solution of 1 part 48% HF to 1 part H_20 with a current density of 30 mA per cm^2. The etching apparatus is pictured in Figure II.2. The standard electrochemical etching time was 2 minutes. Most samples were further etched chemically in 48% HF for a standard time of 5 hours. In many experiments described below, these etching parameters were varied. The etching parameters and sample labels are listed in Table II.1. A G–type sample was most often used in experimental measurements due to its measured luminescence properties. After sample preparation, the samples were cleaved into two sections, one to be tested for photoluminescence and the other for the synchrotron radiation measurement. The samples were always transported in the dark both to and from the vacuum chamber at the synchrotron and the luminescence apparatus.

II.3.2. Photoluminescence Measurements

Photoluminescence was induced with 525 nm light from an Ar ion laser and detected with a cooled GaAs PIN Diode coupled to a photomultiplier. Because an *in situ* probe of photoluminescence was not available, the samples were tested prior to introduction into the vacuum chamber at the synchrotron and unmodified samples were retested in the photoluminescence apparatus to insure that the introduction of the samples into the vacuum system did not significantly affect photoluminescence intensity as was previously reported by Vasquez, et al(Vasquez et al. 1992).

II.3.3. Photoemission Measurements

The photoemission experiments were perfc rmed on three different experimental stations at the Stanford Synchrotron Radiation Laboratory (SSRL). Each beam line was optimized for a different photon energy range. Beam line III-1 used a Grasshopper monochromator that allowed study up to the C 1s core level ($h\nu$ = 50–300 eV). Beam line III-3 used a double crystal (InSb) monochromator for high energy ($h\nu$ = 1800–3000 eV) studies. Beam line I-2 used a Torroidal Grating Monochromator (TGM), which provided photons with energies from 6 to 150 eV. By using these multiple beam lines, it was possible to perform valence band, core level, and XPS experiments at a beam line directly optimized for each type of work.

Two experimental systems were also used for these experiments. The Beam line III experimental system consisted of a load–lock sample transfer system and two coupled experimental vacuum chambers. One chamber was used as a sample preparation chamber, where annealing and depositions could be performed. The second was used strictly as an analysis chamber. The analysis chamber housed a double pass cylindrical mirror analyzer. The overall instrumental resolution (monochromator and spectrometer) for the experiments carried out at BL III-1 using this analyzer was approximately 0.3 eV at a photon energy of 150 eV. When this system was used at BL III-3 to perform XPS measurements, the overall resolution at a photon energy of 2000 eV was approximately 2 eV. The Beam line I-2 experimental system consisted of a load–lock sample transfer system coupled to a vacuum chamber where both sample preparation and analysis occurred. This vacuum chamber was equipped with a VG ADES-400 angle–resolved spectrometer. At BL I-2, the overall resolution of the angle–resolved system was 0.6 eV at a photon energy of 150 eV. Both experimental systems had base pressures better than 6×10^{-10} Torr.

The angle–integrated photoemission data taken at BL III-1 and BL III-3 was taken without the use of an electron flood gun. These samples did show a certain amount of charging. The samples were then charge referenced using the C 1s impurity level. The angle–resolved photoemission system at BL I-2 was equipped with a flood gun, so the angle resolved photoemission data was taken with the use of a flood gun whenever charging was

observed.

II.3.4. Near–Edge X–Ray Absorption Spectroscopy

NEXAFS measurements were also performed at BL III–3 using the above described system. The absorption spectra of the Si K–edge were measured simultaneously in Total Yield Mode, by measuring the sample refresh current which is proportional to absorption(Stohr 1992), and in Auger Yield Mode, by measuring the intensity of the surface sensitive Si LVV Auger yield at 85 eV kinetic energy, again which is proportional to the absorption(Stohr 1992). The Auger electrons have an escape depth of approximately 5 Å(Cullis and Canham 1991). The sample refresh current was measured using a Keithley current amplifier placed between electrical ground and the sample. The Auger Yield was measured by setting the CMA at a kinetic energy of 85 eV with a pass energy of 200 V.

II.3.5. Thermal Annealing

Annealing studies were performed at BL 1-2 using the system described above. This system was equipped with a sample manipulator capable of electron bombardment heating. Annealing temperatures below 500° C were reached by radiant heating with a nude filament located behind the sample. Temperatures above 500° C were obtained by electron bombardment heating. E–beam heating entailed biasing the sample positively so that electrons emitted from the nude filament were accelerated into the sample. Once the desired temperature was reached, the sample was allowed to equilibrate and was then held at that temperature for 15 minutes. The sample was then cooled to room temperature before further analysis was performed.

One expected problem was observed in the spectra that should be noted. These experiments were not the typical surface science measurements where all sample preparation was performed under ultra–high vacuum conditions. Therefore, it was not possible to perform standard outgassing procedures. Normally, the sample holder would be outgassed prior to performing measurements of this nature to prevent possible cross–contamination of the sample. However, this was not possible as annealing the sample holder would necessarily entail heating the sample and thus would have destroyed the interface to be

studied.

II.4. RESULTS

II.4.1. Photoluminescence

In order to determine the effect of etching time on the photoluminescence behavior of porous silicon, photoluminescence spectra were obtained from samples prepared with the etching conditions given in Table II.1. Luminescence spectra from representative samples prepared with these etching condition are shown in Figure II.3. Obviously, the different etching parameters had an effect on the photoluminescence linewidth, intensity, and peak position. While longer etching times increased the luminescence intensity, the photoluminescence linewidth and wavelength decreased with longer etching times.

First, as shown in Figure II.2, the luminescence from samples A, B, C, E, and F, the samples with the lowest total etching times, had nearly constant emission over the range from 650 to 850 nm, so the linewidth was very broad. However, sample D, electrochemical etch only, started to show a distinct peak at 820 nm, although the linewidth was still very broad. The spectra from Samples G and H had the narrowest lineshapes with FWHM of 130 and 120 nm, respectively. The photoluminescence peak was also strongly blue–shifted as the etching time was increased between G and H, with the peak moving from 710 nm to 660 nm.

Only weak photoluminesce was observed from samples A, B, C, E, and F. Sample D, which underwent a 20 minute electrochemical etch, did emit light with enough intensity to possibly be useful in a device. It is important to note that the intensity increased by nearly an order of magnitude as the electrochemical etching time was increased from 10 minutes (C) to 20 minutes (D). An order of magnitude increase in luminescence intensity was also observed as the chemical etching time increased from two to five hours between preparations F and G. The intensity of an H–type sample was nearly 8 times that of the D–type sample. It was clear from the data that samples that underwent a short (two minute) electrochemical etch followed by immersion in a chemical bath (G and H) were much more luminescent that those that were just electrochemically etched (D).

Due to the strong photoluminesce measured from the G–type samples, some were annealed to determine what effect annealing would have on the photoluminescence spectrum. Figure II.4 shows the typical luminescence spectra both before and after annealing. After annealing, the photoluminescence intensity decreased by two orders of magnitude, indicating that the conditions responsible for the luminesce behavior were no longer present. Another curious feature was that the luminescence was further blue–shifted after annealing. This indicated that the luminescent species was modified upon annealing.

II.4.2. Wide–Scan Photoemission Spectroscopy (XPS)

XPS and Auger spectroscopy on these samples have shown the major impurities on the etched silicon surfaces to be C, O, and F. Carbon was the only impurity to be observed on all samples. These impurities were present in varying amounts, from trace levels up to approximately 5% of the observed silicon signal. This was in agreement with earlier studies on porous Si(Hardeman et al. 1985) and on stain etched silicon(Vasquez et al. 1992). This data suggested that electrochemically–etched porous silicon was not highly oxidized, in contrast to a previous report(Pickering et al. 1984). The Si 2p core level spectrum in Figure II.6 also implied that the porous silicon surface was not highly oxidized; a Si^{4+} peak at high binding energy was absent from the spectrum which suggested that SiO_2 was not present. This was in agreement with the data from stain etched porous silicon(Vasquez et al. 1992).

II.4.3. Si 2p Core Level and Valence Band Photoemission

Angle–integrated Si 2p core level photoemission spectra were obtained from samples prepared with the etching conditions given in Table II.1. These spectra are shown in Figure II.5. A Si 2p core level spectrum from a clean Si(100) 2x1 surface is also included as a reference. These Si 2p core level spectra were measured with a photon energy of 150 eV, at this photon energy, the kinetic energy of the emitted electrons was about 50 eV which corresponded to a mean free path of less than 7 Å. Therefore, these spectra probed the near surface region of the pores. Three features of these spectra were important: the presence or absence of oxidation, the peak position, and the core level linewidth.

The existence of surface oxidation was determined by the presence or absence of a peak at a position of 44 eV kinetic energy in the spectra in Figure II.5. A peak in this position would indicate that Si^{4+}, most likely due to SiO_2 formation, was present. Most samples did show some degree of surface oxidation. This was expected, as all sample were made *ex situ* and then transferred into the vacuum system. Therefore, these spectra, in effect, measure the rapidity of surface oxidation. The most oxidized samples were those with the lowest etching times and the weakest photoluminesce. This could clearly be seen, as a strong oxide peak existed in the Si 2p core level spectra from A–type samples. The spectra from B and C–type samples were nearly identical. The rapid oxidation in air of these samples could explain why electrochemically–etched porous silicon was previously reported to be highly oxidized(Pickering et al. 1984). Notice that samples that were etched for longer periods of time F and G showed no surface oxidation. This was likely due to the formation of an inert Si–H surface termination.

The core level spectra have not been aligned with the bulk Si 2p core level position as was done by Vasquez, *et al.*(Vasquez et al. 1992). Instead, they were charge–referenced using the C 1s core level(Swift 1982), which could also be observed on this beam line. In order to align the spectra at the bulk peak position, it would be necessary to either uniquely fit the observed spectra and assign one of the decomposed peaks to emission from bulk–like atoms or to assume that the centroid of the observed spectra corresponds to emission from bulk–like atoms. Due to the large linewidth of the observed Si 2p core level, it was not possible to uniquely decompose the spectra into spin–orbit split doublets. Therefore, the first method could not be used. Assuming that the peak centroid was due to bulk–like emission as was done by Vasquez, *et al.*(Vasquez et al. 1992), directly ruled out other possibilities. In fact, by charge–referencing with the C 1s core level position, one could see that the centroid of the Si 2p core level shifted to higher binding energy (lower kinetic energy) as the chemical etching time and the photoluminesce intensity increased. Vasquez, *et al.* could not have observed this shift because they made an assumption which removed this shift by referencing to the centroid(Vasquez et al. 1992).

Finally, the Si 2p core level was considerably broadened as the etching time was

increased. All spectra were significantly broader than the reference spectrum from a clean Si(100) 2x1 surface. Although, as discussed above, it was not possible to uniquely decompose these spectra, it was still possible to note qualitative changes in the spectral lineshape. The most noticeable change in lineshape occurred between F and G in the high resolution Si 2p core level spectra shown in Figure II.5. As the chemical etching time was increased from 2 hours (F) to 5 hours (G), the linewidth almost doubled. It must be noted that an order of magnitude increase in the photoluminescence intensity was also observed with this increase in chemical etching time(Terry et al. 1992). These observations implied that the surface underwent significant changes as the luminescence intensity increased.

It must be mentioned that another possible cause of the Si 2p core level broadening was nonuniform charging, but this was unlikely because of negligible charging of HF dipped samples. The charging was determined to be negligible by taking spectra with and without a flood gun and comparing them to determine lineshape changes. No significant effects were observed.

Annealing studies were performed on G–type samples because of their strong photoluminescence properties and relatively short preparation times. These samples, unlike those used in the sample preparation studies described above, were rapidly dipped in 48% HF immediately before introduction into the vacuum system. It has previously been shown that a rapid HF dip does not affect photoluminescence(Vasquez et al. 1992). Little charging was observed for this system. It appeared that HF dipped samples were more conducive to study using photoemission spectroscopy. The core level spectra, hν= 140 eV, (Figure II.6) were taken at temperatures from 25 to 550 °C. The spectra were collected after the sample had cooled back to room temperature after being annealed to the recorded temperature. The spectra have been shifted to account for band–bending effects. Upon annealing, the core level narrowed, the centroid shifted to lower binding energy, and the surface was oxidized. As described above, this oxidation was the result of outgassing of the sample holder, so only the linewidth decrease and centroid shift were critical to the understanding of the luminescence mechanism.

The narrowing and peak position progressed toward the spectrum from clean Si(100) 2x1

as the annealing temperature was increased. Above 550 °C, the Si 2p core level spectra were only slightly broader than those from the clean surface. Therefore, it was concluded that the bulk Si 2p core level was not at the centroid of the observed core level spectra, or alternatively, the moiety that was responsible for the observed core level shift had to have a larger binding energy than bulk silicon. As this moiety was destroyed or desorbed, the chemically shifted component decreased in intensity, accounting for both the linewidth narrowing and the peak position moving towards a more bulk–like position.

The core level valence band spectra, hν= 40 eV, (Figure II.7) showed a continuous change in their features with annealing. Reference spectra from both a clean Si(100) 2x1 surface and a hydrogen–terminated Si(100) surface are shown in Figure II.7. The spectra have been shifted to account for slight charging effects and band–bending. The valence band spectra from porous silicon was quite different than either reference spectra. It was a broad featureless spectrum. Upon annealing, several features appeared at higher binding energies. Even after annealing, the spectrum from G–type porous silicon did not resemble either reference surface.

Finally, it was important to note that these changes in the Si 2p core level were the converse of those observed as the sample etching time was increased. This data implied that the source of the Si 2p core level broadening and the source of the photoluminescence were related. Combining these results with those of the photoluminescence measurements, the following picture emerged: a decrease in luminescence intensity (Figure II.4), a decrease in core level linewidth (Figure II.6), and a change in the valence band features (Figure II.7) as the samples were annealed to 500 °C suggested that the surface played an important role in photoluminescence. These observations also affirmed the belief that surface sensitive photoemission could be used to study light–emitting porous silicon. This phenomenon led us to investigate the geometrical structure of the surface to determine if structural changes could be causing the observed changes in the photoemission spectra and in charging behavior.

II.4.4. NEXAFS

Surface sensitive NEXAFS of the Si K-edge was monitored to determine crystallinity of an undipped sample with preparation G. NEXAFS spectra from this sample (Total–yield and Auger–Yield), crystalline silicon, and amorphous silicon are shown in Figure II.8. Sharp features in the Auger–yield and Total–yield spectra were indicative of crystalline silicon. Amorphous silicon had broad peaks in these positions. Qualitatively, a comparison of the surface sensitive Auger–yield NEXAFS to the NEXAFS from crystalline silicon showed that the near surface layers of light emitting silicon were crystalline. The Total–yield data, with a probing depth of approximately 100 Å(Comin et al. 1985), was a deeper probe of the micron sized pillars. Qualitatively, the Auger–yield data was identical to the Total–yield data. Therefore, both the surface and near surface regions were crystalline.

In an attempt to quantify these measurements, a normalized intensity function (χ) was determined. It is shown in Figure II.9. This function was Fourier transformed to give a phase uncorrected radial distribution function shown in Figure II.10. It was clear that the spectra from light–emitting porous silicon had the higher shell structure from crystalline silicon which was lacking from the amorphous sample. Therefore, it must be concluded that the G–type light–emitting porous silicon was crystalline. This was in complete agreement with the interpretation of Cullis, *et al.*(Cullis and Canham 1991) for electrochemically–etched porous silicon but disagreed with the results of Vasquez, *et al.*(Fathauer et al. 1992; Vasquez et al. 1992), which state that stain–etched porous silicon was amorphous suggesting that electrochemically–etched porous silicon and stain–etched porous silicon were not as similar as had previously been thought.

Because the photoemission results showed that the surface structure changed upon annealing, a G–type light–emitting porous silicon sample was annealed to determine if structural changes in the pillars occurred. Figure II.11 shows the Auger yield NEXAFS spectra after annealing to the different temperatures. Only a slight smearing of the spectral features was observed. It was unlikely that these changes were caused by the loss of crystallinity upon annealing, as the sharp features typical of crystalline sample were still present. A more likely cause of the smearing of the spectral features was adsorption of gases that outgassed

from the sample holder during annealing.

II.5. DISCUSSION

II.5.1. Photoluminescence

It was evident from Figure II.5 that a large linewidth broadening of the Si 2p core level occurred as the pores were made larger by chemical etching. This broadening occurred between sample preparations F and G where there was also a corresponding order of magnitude increase in luminescence (Figure II.3). It appeared that the Si 2p core level was influenced by something that occurred during the chemical etching. Chemical etching had a much greater effect on photoluminescence and photoemission than electrochemical–etching. However, electrochemical–etching must take place to get pore formation started. Others have suggested that the etching process may result in the production of amorphous near surface layers(Fathauer et al. 1992; Vasquez et al. 1992), the deposition of hydrogen that cannot easily be detected using photoemission(Tsai et al. 1992), the production of a quantum confinement region(Canham 1990), or the deposition of an impurity species(Xu, Gal, and Gross 1992). Any of these possibilities could cause the observed core level broadening and the photoluminesce. Therefore, the possible mechanisms will be discussed in terms of their likely effect on the photoemission and NEXAFS data.

II.5.2. Amorphous Silicon Mechanism

If the surface layers of light emitting porous silicon were amorphous, the Si 2p core level would be broadened. However, the Auger yield K-edge spectra exhibited the same traits as crystalline silicon, indicating that the surface layers of light emitting silicon were crystalline. The escape depths of the Auger yield electrons and the photoemitted electrons were similar. Since the two techniques probed the same surface region and the NEXAFS spectra showed that the surface was crystalline, the linewidth broadening in the photoemission spectra cannot be caused by amorphous silicon layers.

However, this was not the case for the photoluminescence. Others have shown that it was possible for a surface to be crystalline but have underlying layers that were

amorphous(Comin et al. 1985). Total–yield NEXAFS spectra were collected concurrently to explore this possibility. As shown in the above NEXAFS data, the Auger–yield and Total–yield spectra were identical, indicating that both the surface and the near–surface region probed by Total–yield measurements were crystalline. These results were in complete agreement with the electron diffraction studies of Cullis, et *al.*(Cullis and Canham 1991) for electrochemically–etched porous silicon but differ drastically from the results by Vasquez, *et al.*(Fathauer et al. 1992; Vasquez et al. 1992) for stain etched porous silicon. However, the NEXAFS measurements prove unequivocally that the electrochemically–etched porous silicon was crystalline. Therefore, photoluminescence from amorphous silicon can then be ruled out as the luminescence mechanism.

II.5.3. Impurity Mechanism

XPS and Auger spectra were collected from the porous silicon to determine trace impurity species present at the surface of the pores. Carbon, oxygen, and fluorine were contaminants in light–emitting porous silicon. The presence of these contaminants and the high surface area of porous silicon together could provide a chemical species in high enough concentrations to give rise to luminescence. It was not possible to determine the exact concentrations of the impurity species without having a good model of the surface. As the surface was a varied network of interconnected pores, modeling the surface was impossible. It was only possible then to determine the relative amounts with respect to the intensity of the silicon peak. These relative impurity amounts varied from trace levels to approximately five percent of the silicon intensity for samples with the same luminescence intensity. Since the relative amounts varied on samples with the same luminescence intensity, it was unlikely that impurities caused the broadening in the silicon 2p core level. They may, however, play a role in photoluminescence because it would be possible for a photoluminescent chemical species to be present in areas deep in the pores from which little photoemission signal was measured. However, it would be unlikely that these species would have little effect on the surface structure, so some change from crystalline silicon would be observed in the NEXAFS data. Because the NEXAFS was so similar to the crystalline sample, it was unlikely that a chemical species chemisorbed to the pores could be responsible for the measured photoluminescence.

II.5.4. Quantum Confinement Mechanism

The photoluminescence data(Terry et al. 1992) showed the standard blue–shift and increase in luminescence intensity as the etching time was increased(Canham 1990). This behavior led Canham to postulate that a quantum confinement model best explained the luminescence in porous silicon(Canham 1990). Upon annealing, the luminescence intensity decreased and was blue–shifted. As our system had a slight oxidation problem from oxygen desorbing from the sample holder, it was possible that some pillars were oxidized and, thus, made smaller, blue shifting the luminescence. Otherwise, it was possible that silicon could migrate from the top of the pillars and fill in the space between the base of the pillars. This would leave behind smaller pillars which could luminesce at higher energy. The observed photoluminescence behavior was best described by the quantum confinement model, but could a quantum confinement model describe the observed Si 2p photoemission data and the Si K–edge NEXAFS data?

The features of the Si 2p core level spectra in Figure II.5 showed a progression from low binding energy to high binding energy upon annealing along, with significant linewidth broadening as the etching time was increased. Core level photoemission studies of metal clusters have shown that binding energy increases as the cluster size decreases(Egelhoff 1987). Since longer etching times increased the formation of small pillars, which would have a binding energy greater than that of crystalline silicon, one would expect the Si 2p centroid to progress to higher binding energy, as was observed. Furthermore, if pillars of many different sizes were present, the overlap of many peaks would cause the core level spectrum to be very broad, as was observed. Obviously, the quantum confinement region would need to be crystalline as the NEXAFS showed.

Annealing would not be expected to have any effect on a quantum confinement region until the silicon atoms gained enough energy to rearrange on the surface. If the smallest pillars with higher binding energy reconstructed before larger pillars, the photoemission spectra would show the above progression. However, the NEXAFS spectral features changed only slightly upon annealing. The photoluminescence would be expected to show a red–shift, but this was the opposite of what was observed. This type of pillar

reconstruction can be ruled out because it was contradicted by both the photoluminescence and NEXAFS data. A similar model, where silicon atoms could migrate from the top of the pillars and fill in the space between the base of the pillars forming wide crystalline areas with a few small pillars, could account for both the weak photoluminesce blue–shifted to higher energy and the reverse trend that occurred in the Si 2p photoemission, where the emission became more bulk–like as the annealing temperature was increased. Unfortunately, the quantum confinement model by itself did not completely describe all the observed experimental qualities of porous silicon, most notably, the decrease in luminescence intensity over time.

II.5.5. Surface Termination Mechanism

Two possible photoluminescence mechanisms can be based on silicon hydride formation. First, a Si_xH_y surface species may be photoluminescent. As this species desorbed or decomposed upon annealing, a change in photoemission features could occur, and according to this model the luminescence would also decrease. However, Si(100) wafers rapidly dipped in 48% HF have been studied. A core level spectra is shown in Figure II.5. The HF treated surfaces were hydrogen terminated and mono, di, and trihydride species were present(Chabal et al. 1989). The core level spectra from these samples showed only a small peak shifted 0.3 eV that can be attributed to the presence of hydrogen. Others have reported smaller shifts for the silicon hydride species on Si(111) and Si(100)(Karlsson et al. 1990; Larsson et al. 1987). Therefore, the large linewidth broadening that was observed cannot be explained only by using the core level shift of a SiH_x surface species. Any other Si based species, such as a silicon based polymer or siloxene, would have to satisfy the requirement that the Auger–yield Si K–edge absorption spectra be the same as that from crystalline silicon. Hence, it was unlikely that a molecular transition in a SiH_x species or siloxexe could be responsible for the luminescence observed in porous silicon.

The second mechanism would have the hydrogen providing a nearly ideal termination of the pillar structures, i.e. a terminated quantum confinement mechanism. The temperatures that were reached during annealing were well correlated with the desorption of mono and dihydride species from the porous silicon surface(Gupta, Colvin, and George 1988; Tsai et

al. 1992). Tsai, *et al.* have shown that luminescence intensity decreased as the dihydride species desorbed(Tsai et al. 1992). It was possible that hydrogen on a porous silicon pillar might have a different Si 2p core level shift than other SiH_x species. This was a difficult possibility to test, but it must be considered. Theoretical studies of a silicon hydride species on a small pillar must be performed. A more likely cause of the Si 2p core level behavior would involve the explanation given above based upon pillar size, with the small SiH core level shifts slightly contributing the observed broadening.

Further evidence for the terminated quantum confinement model can be found in ESR studies where a bulk-like surface termination was found to be important. V. Petrova-Koch, *et al.*(Petrova-Koch et al. 1992) have suggested that luminescence occurs only when the surface has an ideal termination. They have annealed porous silicon samples in oxygen and have observed photoluminescence after annealing to 800 °C. They postulated that at high temperature the oxygen ideally terminated the surface. Between room temperature and 800 °C, they observed a decrease in photoluminescence intensity that was related to the presence of dangling bonds; as the temperature was increased, the number of dangling bonds decreased, and luminescence increased.

The photoluminescence and photoemission behavior of this study also qualitatively suggested that surface termination was important. The post-anneal photoluminescence spectrum was blue shifted and severely attenuated(Terry et al. 1992). Figure II.6 shows that the surface did oxidize during the high temperature anneals. If, during annealing, a few small pillars were ideally terminated with an oxide layer, these oxide–terminated pillars would be made smaller and, so, the luminescence would be blue–shifted, if quantum confinement was responsible for luminescence. As only slight oxidation occurred, only a small number of pillars could be ideally terminated. The temperatures that were reached during annealing were well correlated with the desorption of mono and dihydride species from the porous silicon surface(Gupta, Colvin, and George 1988; Tsai et al. 1992). Above these temperatures then, the hydrogen was lost. As most pillars lose their H–termination and only a few become oxide–terminated, the luminescence intensity would be attenuated. Therefore, the model that best described all the experimental observation was based upon

an ideally–terminated quantum confinement region. It was likely that hydrogen played an important role in photoluminescence in a quantum confinement model by providing a bulk-like surface termination which prevented non–luminescent photocarrier–recombination at the surface.

II.6. CONCLUSION

The changes in the valence band and in the Si 2p core level spectra of electrochemically–etched light–emitting porous silicon prepared with different etching parameters and upon thermal annealing have been studied. Surface sensitive photoemission was a valid technique to use in the study of light emitting porous silicon. Broadening of the Si 2p core level as chemical etching time increased was observed. Upon annealing the core level linewidth decreased and the valence band progressed from a large featureless spectrum to a spectrum with three main features. However, luminescence from amorphous silicon and from impurity based molecular species on electrochemically etched porous silicon was ruled out. Photoluminescence was sensitive to surface structure. The luminescence mechanism that best described all available experimental data was based upon a silicon species that degrades upon annealing and strongly resembles crystalline silicon such as a system of bulk-like terminated quantum confinement regions.

II.7. ACKNOWLEDGEMENTS

Dr. W. A. Harrison and Dr. P. King are acknowledged for many helpful discussions. Dr. T. Kendelewicz provided help in analyzing the NEXAFS data. Dr. B. Street for allowed the use of his photoluminescence setup. H. Liu prepared and tested the luminescence from the porous silicon samples. This work was performed at the Stanford Synchrotron Radiation Laboratory, which is supported by the Department of Energy, Office of Basic Energy Science, Division of Chemical Sciences. The support of that Office's Division of Material Research for this research must also be acknowledged.

II.8. REFERENCES

Bsiesy, A., J. C. Vial, F. Gaspard, R. Herino, M. Ligeon, F. Muller, R. Romestain, A. Wasiela, A. Hamlimaoui, and G. Bomchil. 1991. *Surface Science* 254:195.

Canham, L. T. 1990. *Applied Physics Letters* 57:1046.

Chabal, Y. J., G. S. Higashi, K. Raghavachari, and V. A. Burrows. 1989. *Journal of Vacuum Science and Technology A* 7:2104.

Chuang, S.-F., S. D. Collins, and R. L. Smith. 1989. *Applied Physics Letters* 55:675.

Comin, F., L. Incoccia, P. Lagarde, G Rossi, and P. H. Citrin. 1985. *Physical Review Letters* 54:122.

Cullis, A. G., and L. T. Canham. 1991. *Nature* 353:335.

Egelhoff, W. F. 1987. *Surface Science Reports* 6:253.

Fathauer, R. W., T. George, A. Ksendzov, and R. P. Vasquez. 1992. *Applied Physics Letters* 60:995.

Gupta, P., V. L. Colvin, and S. M. George. 1988. *Physical Review B* 37:8234.

Hardeman, R. W., M. I. J. Beale, D. B. Gasson, J. M. Keen, C. Pickering, and D. J. Robbins. 1985. *Surface Science* 152/153:1051.

Karlsson, C. J., E. Landemark, L. S. O. Johansson, U. O. Karlsson, and R. I. G. Uhrberg. 1990. *Physical Review B* 41:1521.

Larsson, C. U. S., A. S. Flodstrom, R. Nyholm, L. Incoccia, and F. Senf. 1987. *Journal of Vacuum Science and Technology A* 5:3321.

Petrova-Koch, V., T. Muschik, A. Kux, B. K. Meyer, F. Koch, and V. Lehmann. 1992. *Applied Physics Letters* 61:943.

Pickering, C., M. I. J. Beale, D. J. Robbins, P. J. Pearson, and R. Greef. 1984. *Journal of Physics C* 17:6535.

Stohr, J. 1992. *NEXAFS Spectroscopy.* Edited by R. Gomer, *Springer Series in Surface Sciences*, vol. 25, Berlin: Springer–Verlag.

Swift, P. 1982. *Surface Interface Analysis* 4:47.

Takagi, H., H. Ogawa, Y. Yamazaki, A. Ishizaki, and T. Nakagiri. 1990. *Applied Physics Letters* 56:2379.

Terry, J., H. Liu, R. Cao, J. C. Woicik, P. Pianetta, X. Yang, J. Wu, M. Richter, N. Maluf, F.

Pease, A. Dillon, M. Robinson, and S. George. 1992. In*Chemical Surface Preparation, Passivation, and Cleaning for the Semiconductor Growth and Processing*. Edited by R. J. Nemanich, C. R. Helms, M. Hirose and G. W. Rubloff. vol. 259, San Francisco: Conference Proceedings of the Materials Research Society, 421.

Tsai, C., K.-H. Li, D. S. Kinosky, R.-Z. Qian, T.-C. Hsu, J. T. Irby, S. K. Banerjee, A. F. Tasch, J. C. Cambell, B. K. Hance, and J. M. White. 1992. *Applied Physics Letters* 60:1700.

Vasquez, R. P., R. W. Fathauer, T. George, A. Ksendzov, and T. L. Lin. 1992. *Applied Physics Letters* 60:1004.

Xu, Z. Y., M. Gal, and M. Gross. 1992. *Applied Physics Letters* 60:1375.

Table II.1: The electrochemical etching parameters and labels used in this experiment are shown.

Label	Electrochemical–Etch (minutes)	Chemical–Etch (hours)
A	2	0
B	5	0
C	10	0
D	20	0
E	2	1
F	2	2
G	2	5
H	2	20

Figure II.1: A detectable photoemission event is shown. Any electron that is emitted or scattered elastically into the acceptance cone of the analyzer is measured.

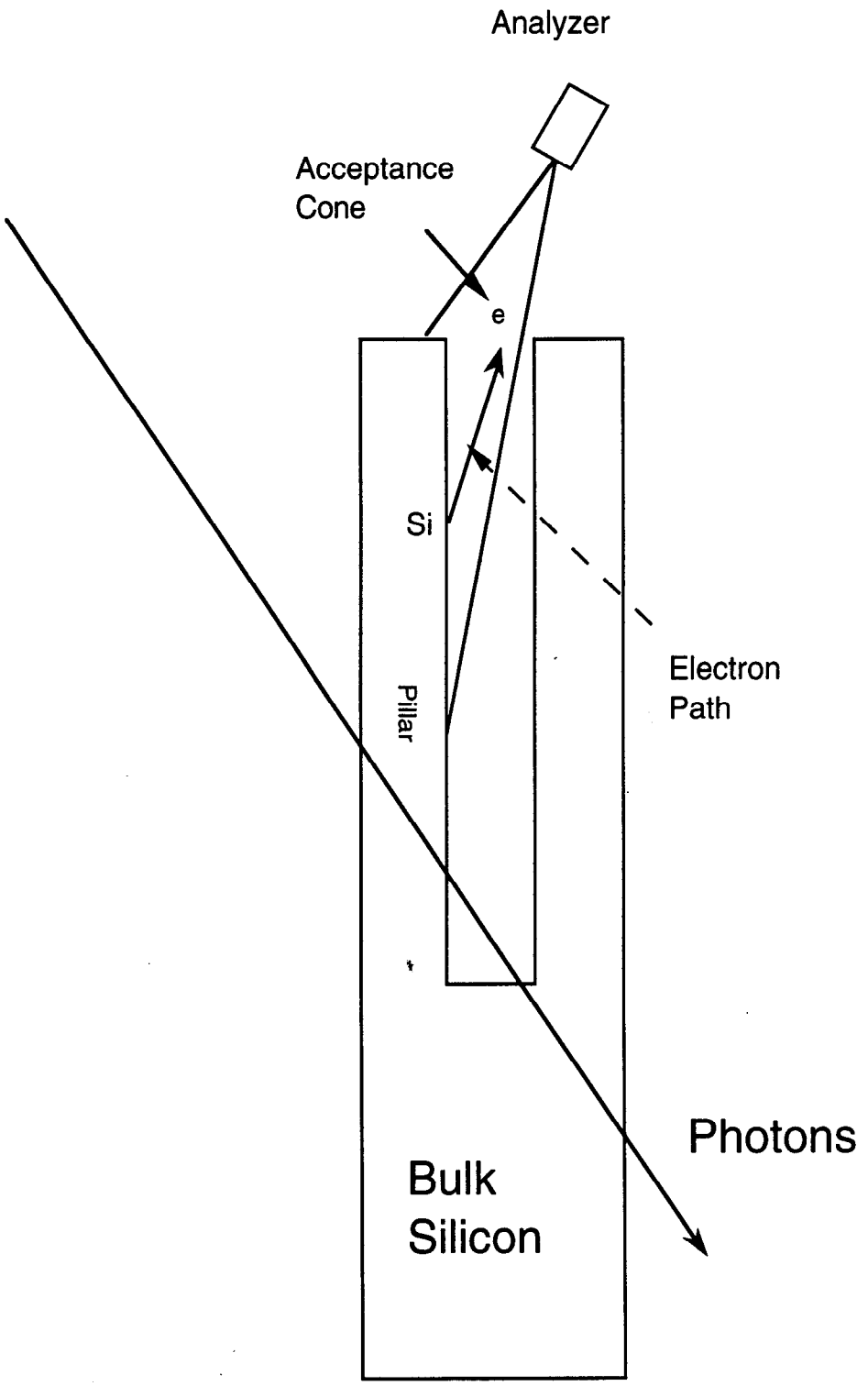

Figure II.2: The experimental electrochemical etching apparatus is pictured below in a cross sectional view.

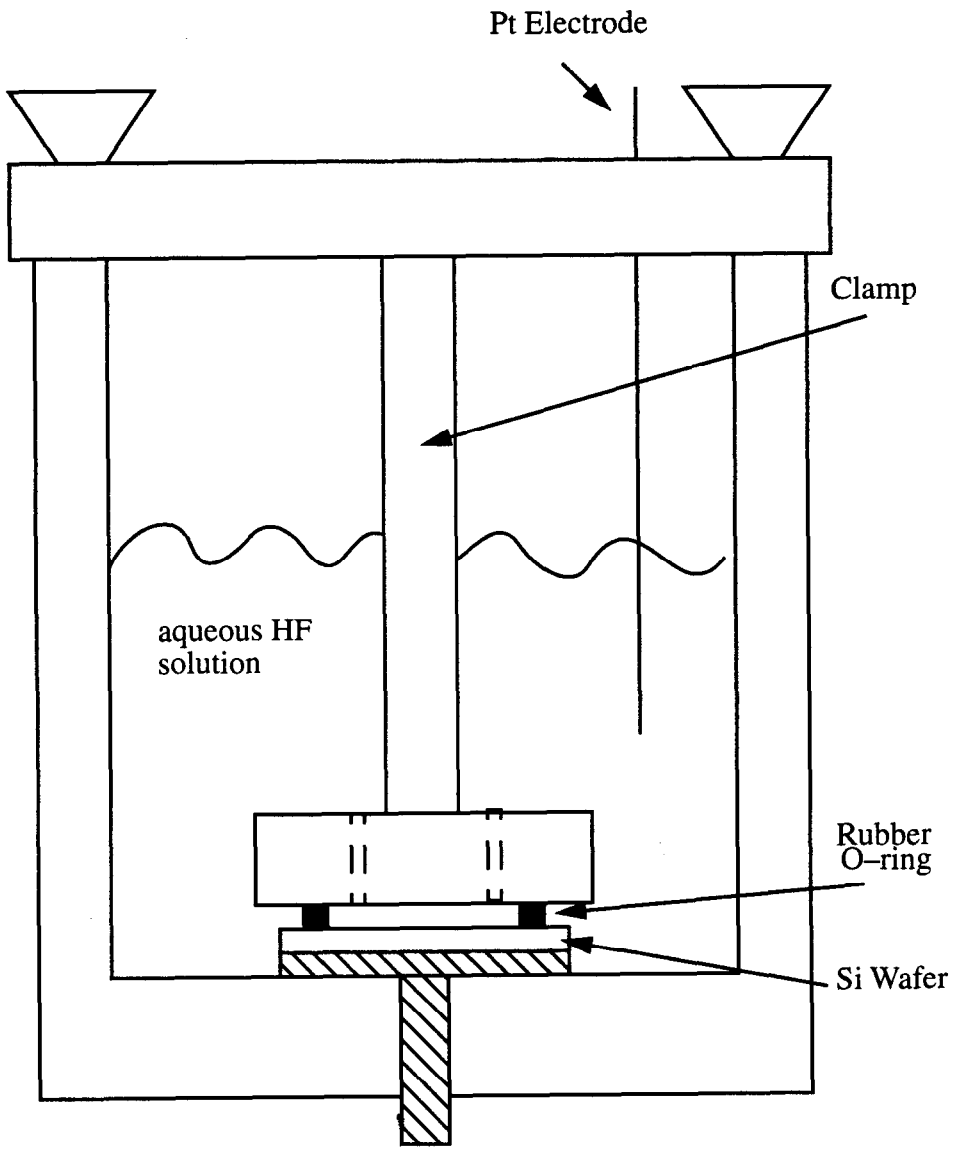

Figure II.3: Photoluminescence spectra of the different light emitting samples excited with an Ar ion laser (525 nm) are shown. Labels correspond to those in Table 1. Labels F - A indicate the relative intensity of the peaks that cannot be resolved, indicated in the figure by the arrow.

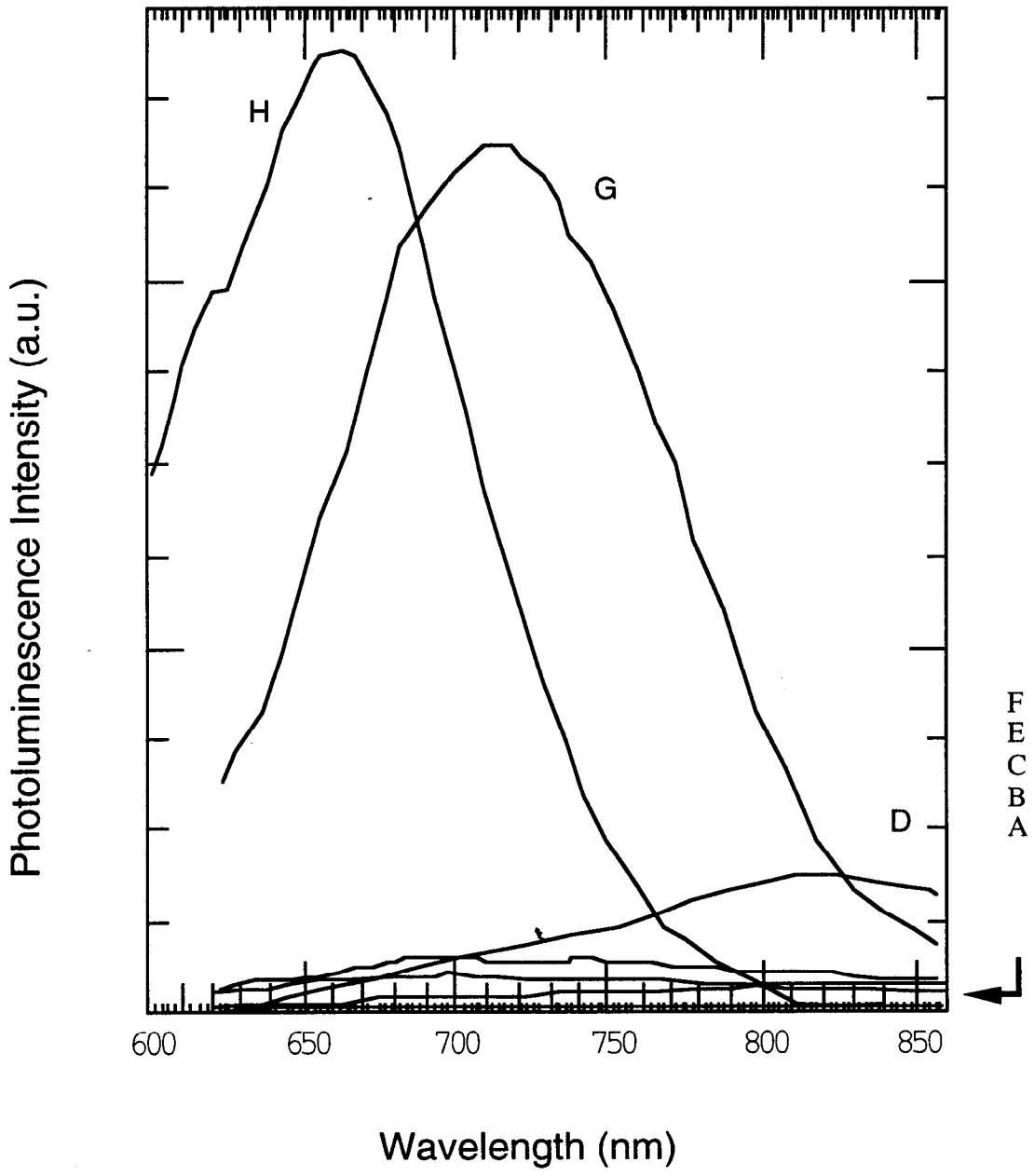

Figure II.4: Photoluminescence from a G–type sample before and after annealing to approximately 600 C are shown.

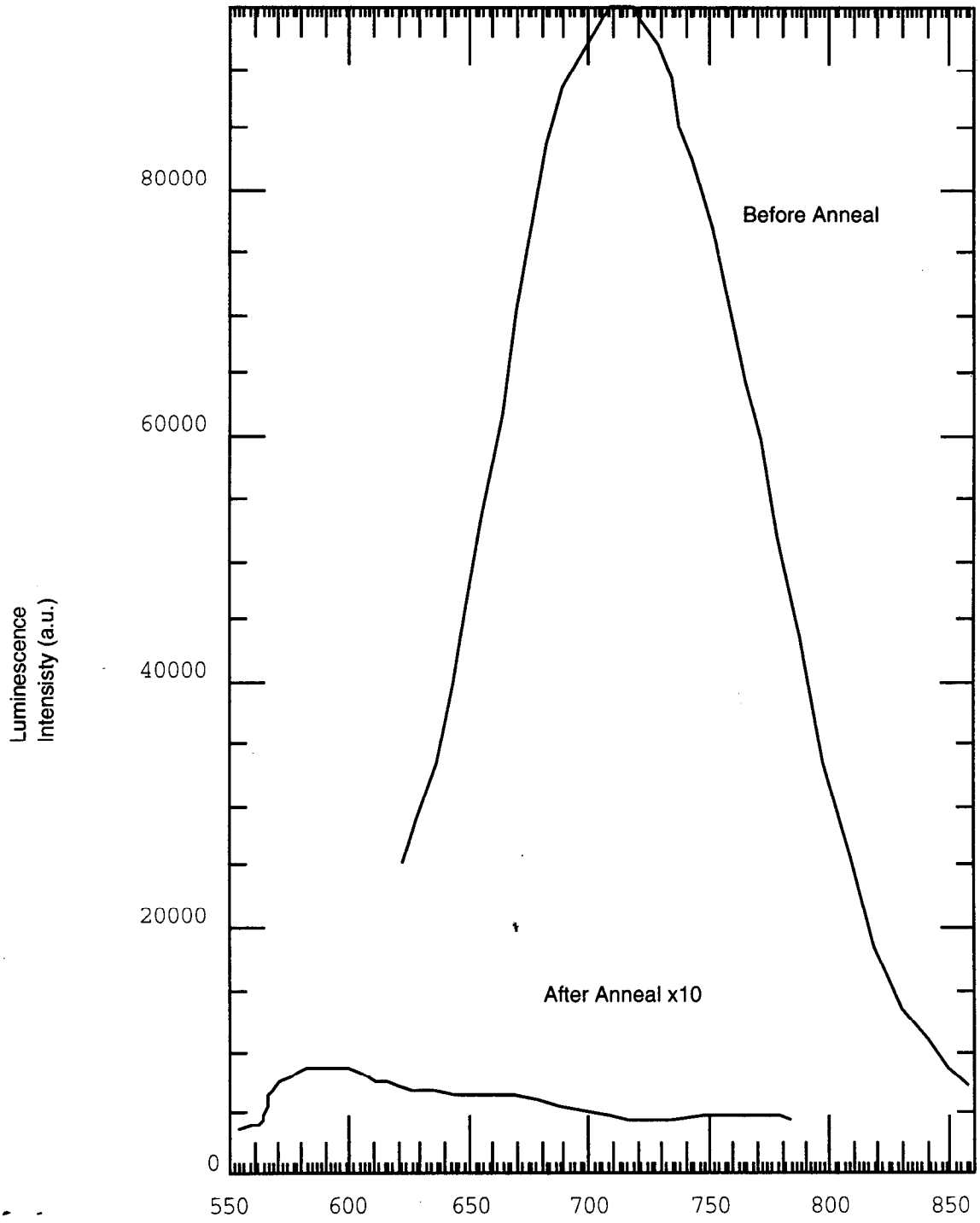

Figure II.5: Si 2p core level spectra taken with photon energy of 150 eV for samples with preparations in Table 1 are illustrated. The large feature shifted to higher binding energy in A is due to the presence of an oxide layer.

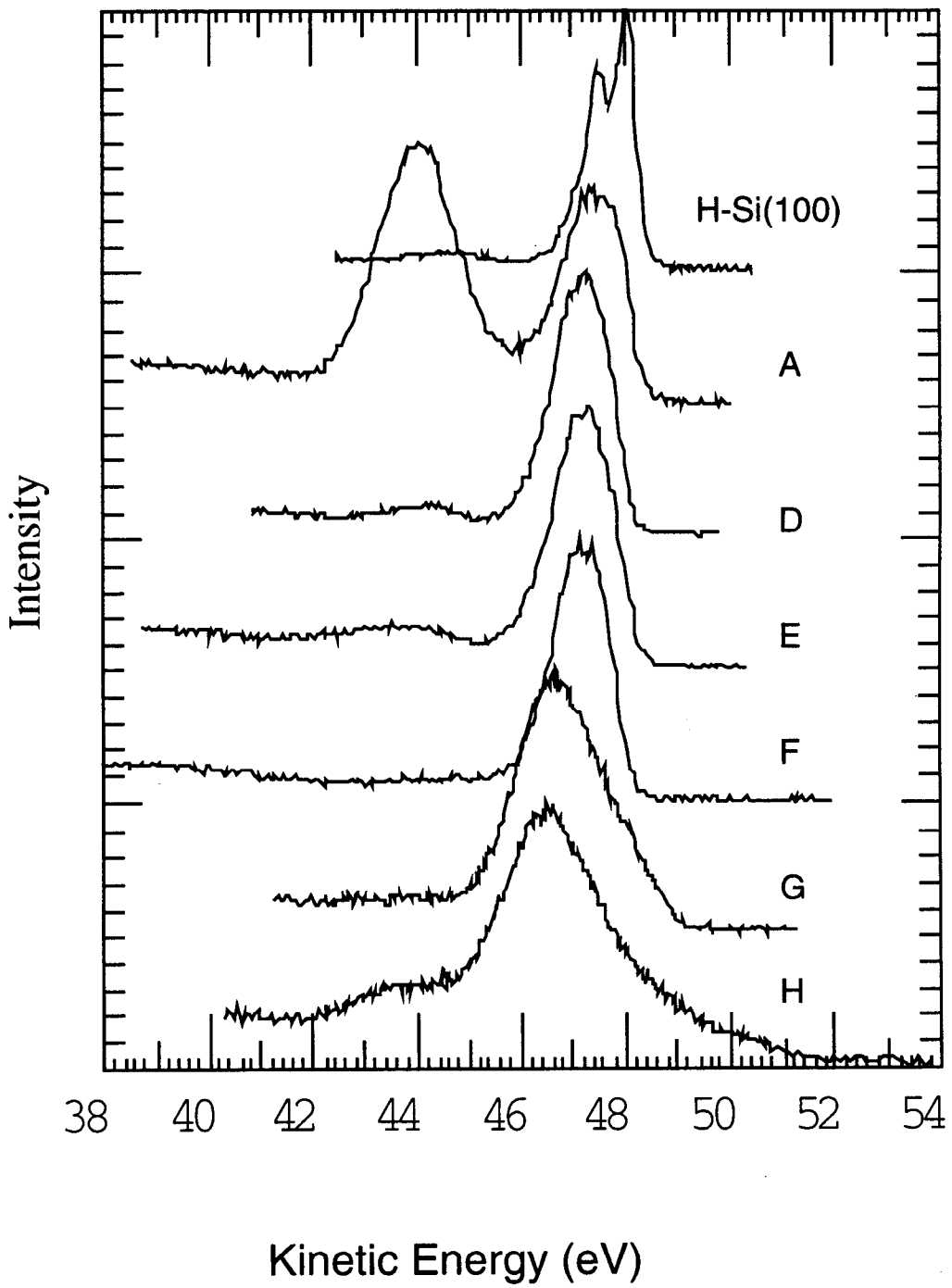

Figure II.6: Si 2p core level spectra taken with photon energy of 140 eV for samples with preparations in Table 1 are illustrated.

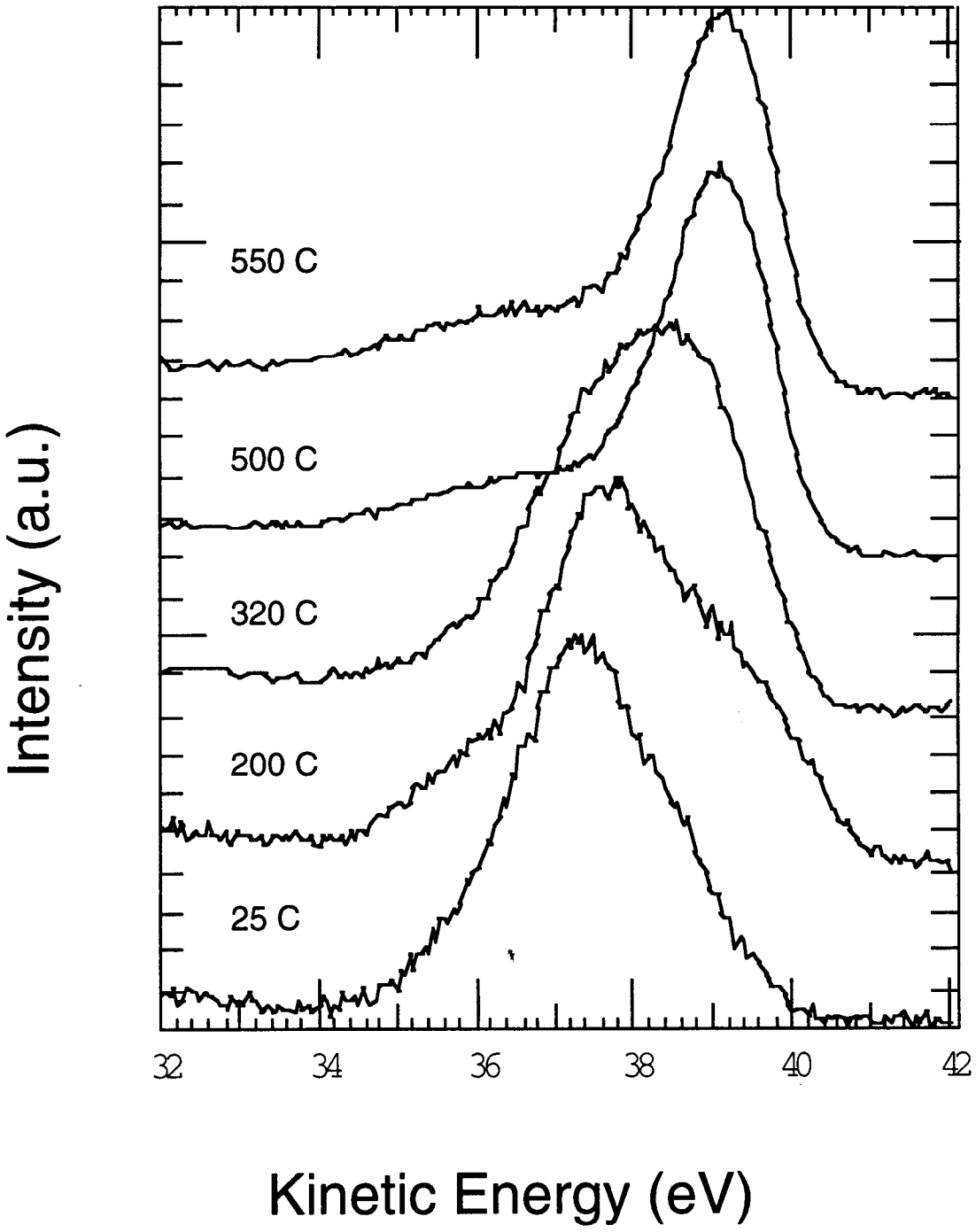

Figure II.7: The progression of the valence band (hν = 40 eV) from a sample with preparation G as a function of annealing temperature is shown. Spectra from a Si (100) wafer dipped in HF, and from Si (100) 2x1, (hν = 60 eV), are also shown.

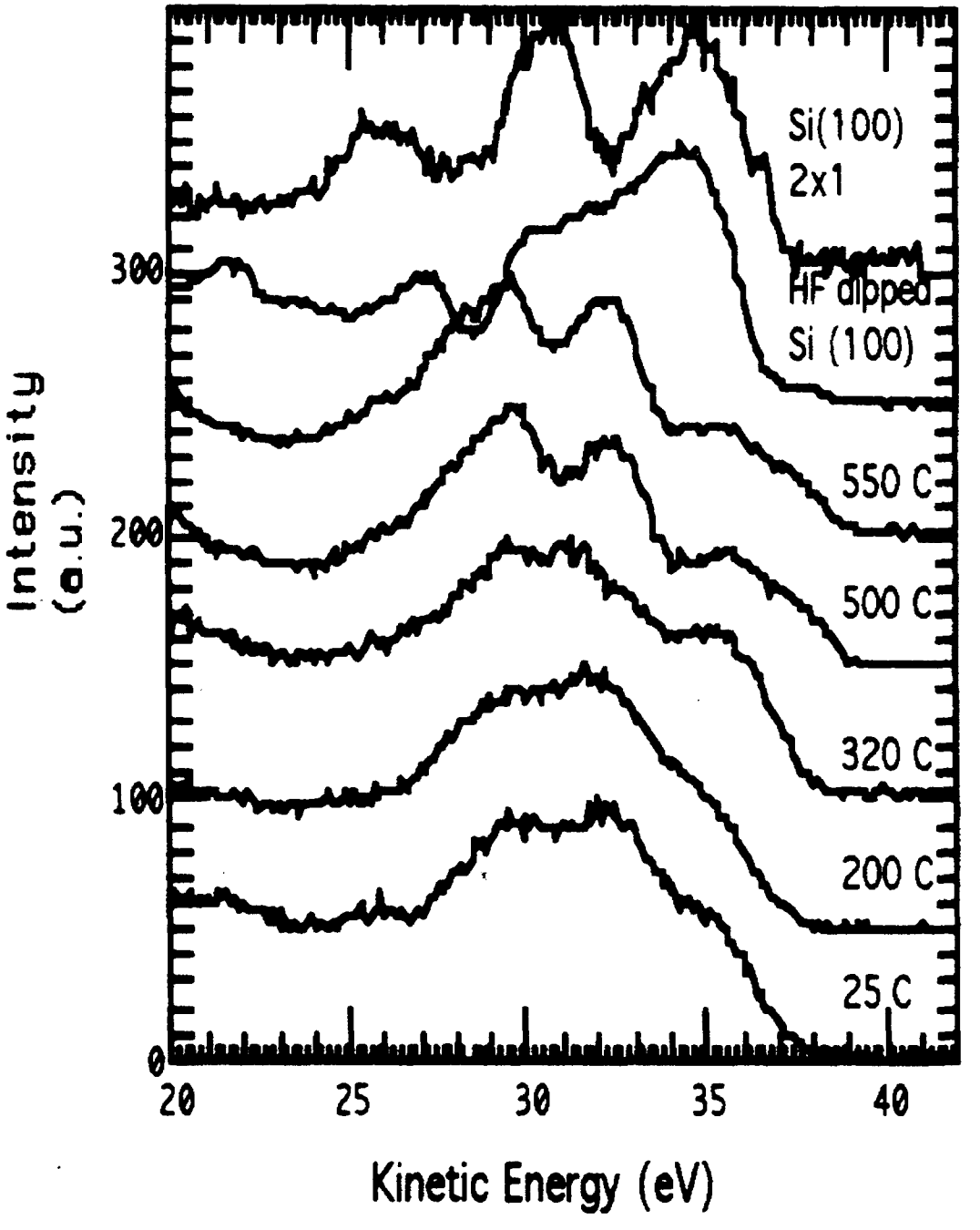

Figure II.8: Si K-edge adsorption spectra from amorphous Si, crystalline Si, Total yield from LES, and Auger yield from LES are shown.

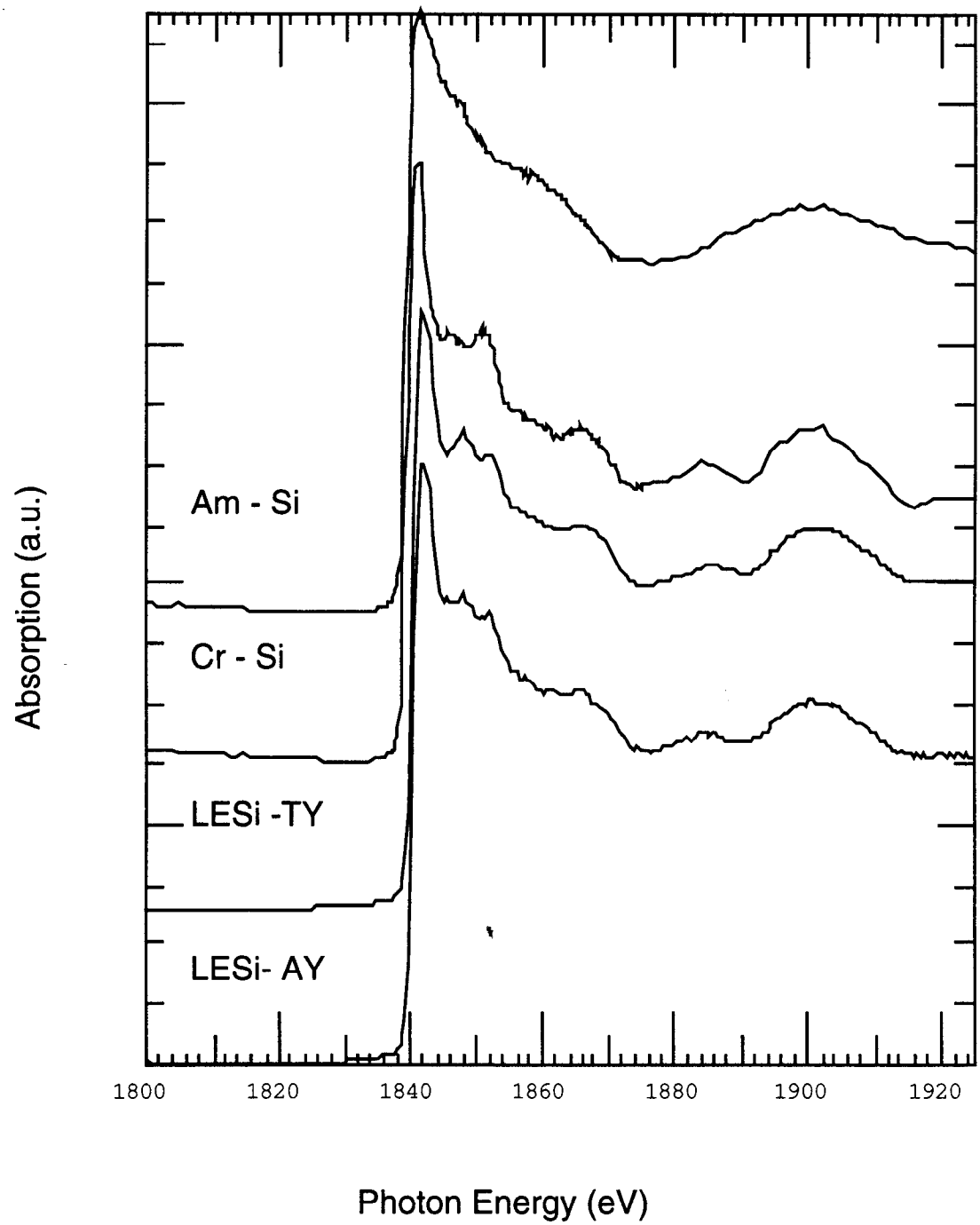

Figure II.9: Background subtracted Total yield Si K-edge data are shown from amorphous, crystalline, and LES.

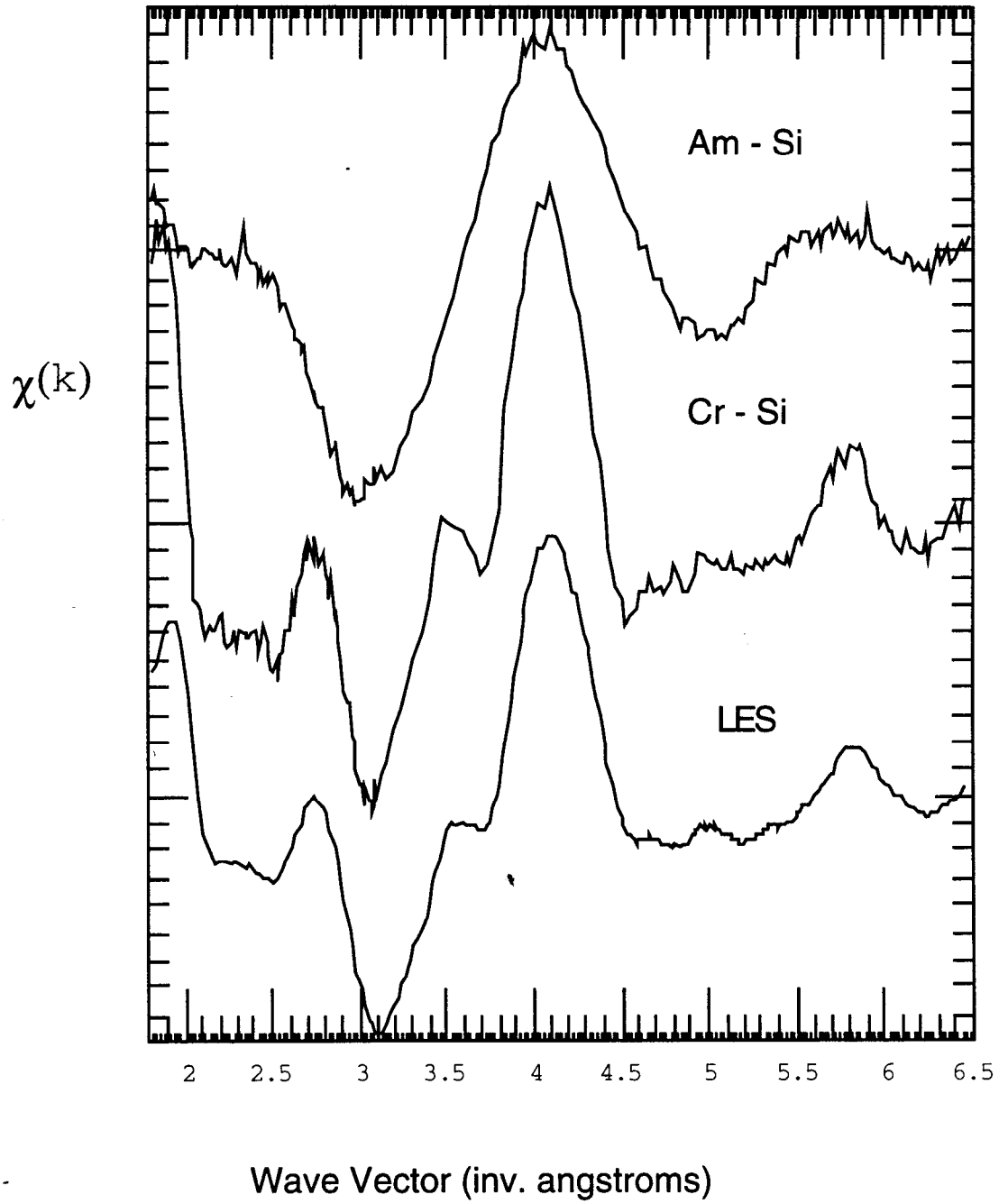

Figure II.10: The Corresponding Fourier Transforms of the data shown in Figure II.9.

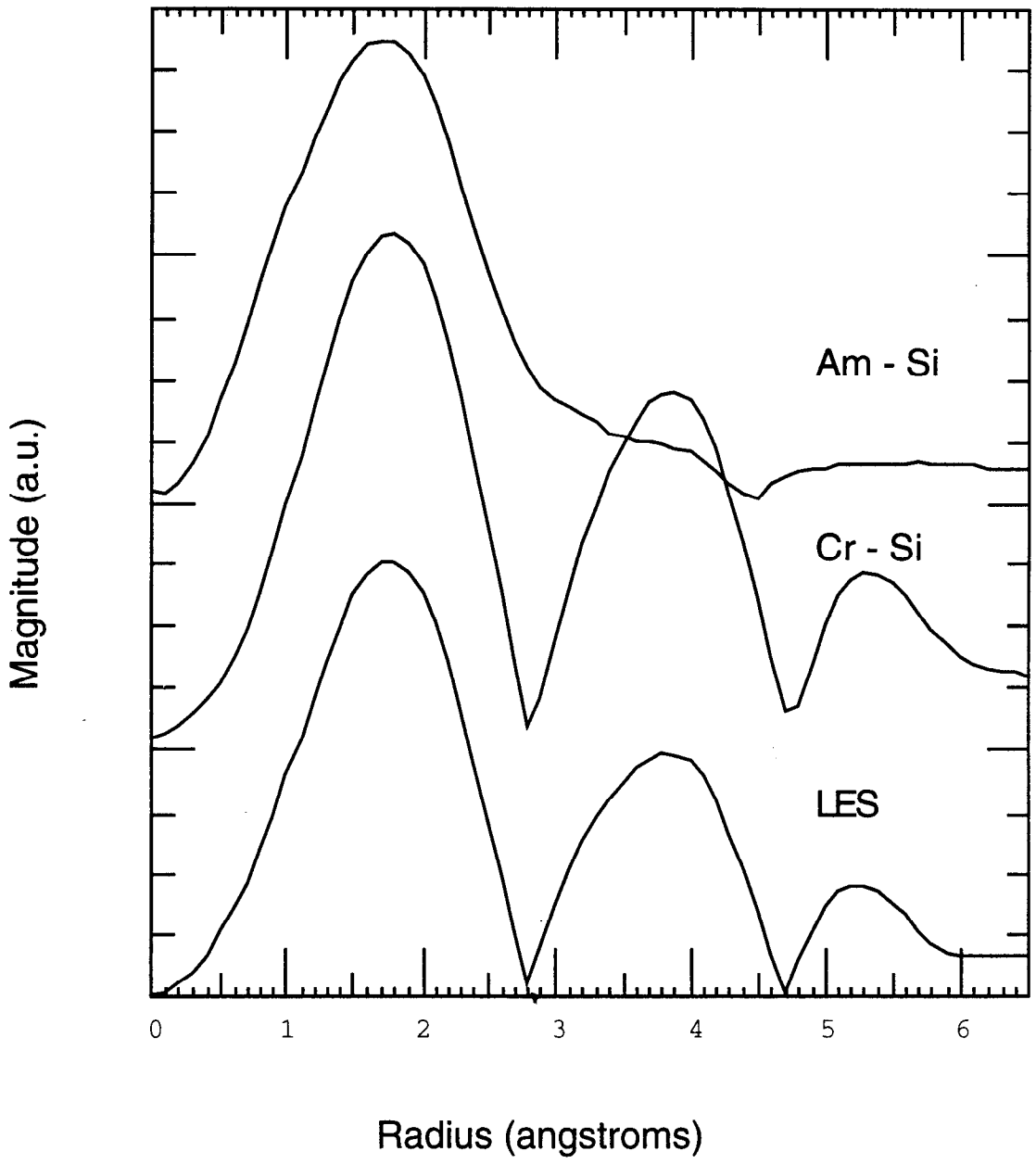

Figure II.11: Auger yield NEXAFS of the Si K-edge after annealing are shown.

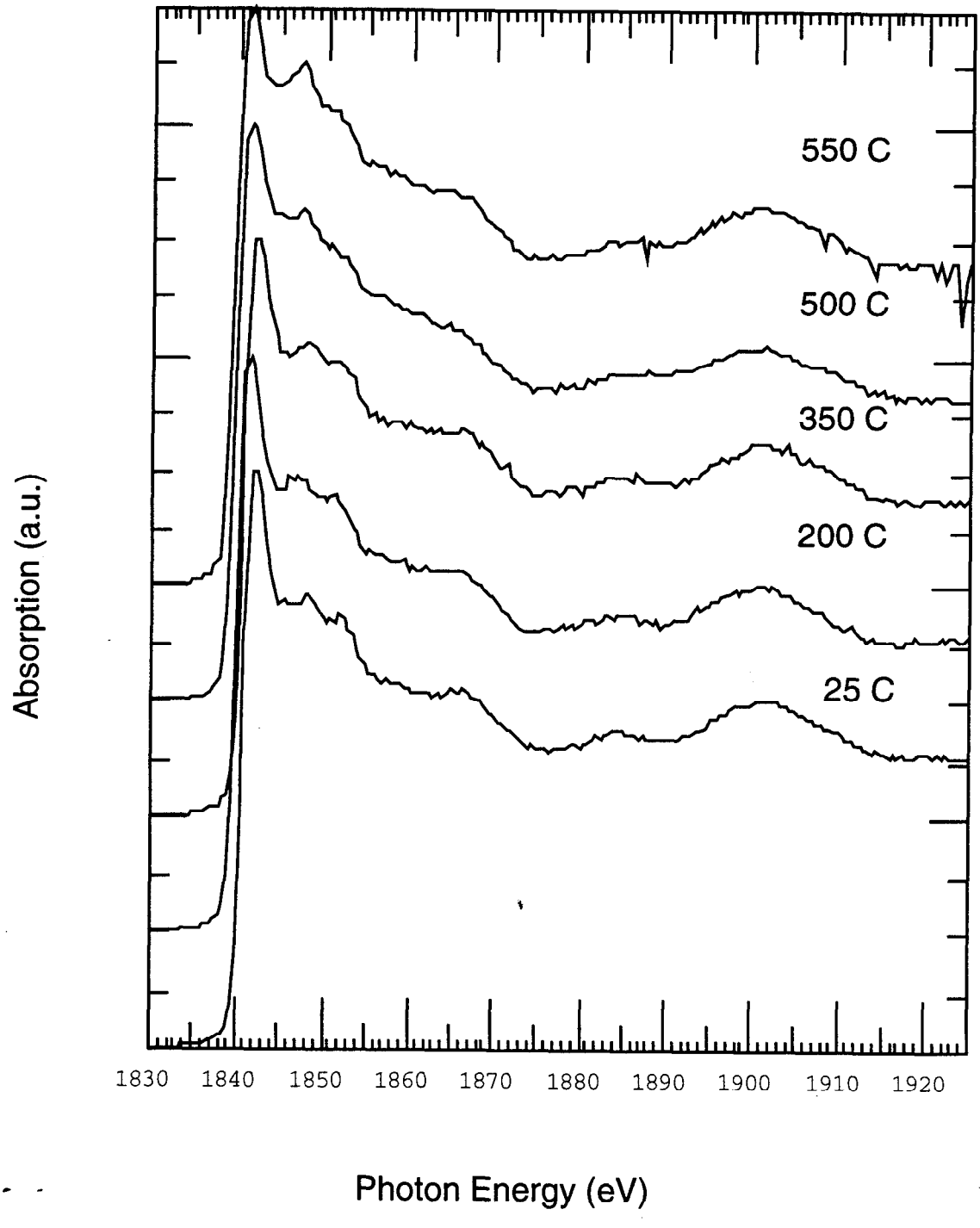

CHAPTER III.
HYDROGEN–TERMINATED Si(111)

III.1. ABSTRACT

The reactivity of H–Si(111) 1x1 prepared using wet chemical HF and NH_4F etching baths has been investigated. The clean H–Si(111) 1x1 surface and H–Si(111) surfaces exposed to Au, Ge, O_2, Cl_2, Br_2, and 1–alkenes were studied with photoemission spectroscopy. These particular compounds were chosen in order to test Schottky barrier formation (Au), heterogeneous surfactant growth (Ge), oxidation (O_2, Cl_2, Br_2), and surface functionalization (1–pentene). Two components were present in Si 2p core level spectra from the H–terminated surface. The H–Si(111) surface has been well characterized previously so the reactivity of this surface was studied(Hricovini et al. 1993). Stepwise depositions of Au were performed and the band bending was measured with photoemission spectroscopy. The Fermi level pinned near mid–gap as Au was deposited onto the as–etched surface. After the deposition of 1 ML of Au, a Au–silicide layer formed. This interfacial component indicated that the passivating H layer was compromised. As the Au coverage was increased, layers of pure Au formed between the bulk silicon and the Au–silicide layer. The observed behavior was nearly identical to that of Au deposition on the Si(111) 7x7 surface(Yeh et al. 1993). Next, the ability of the monohydride layer to sustain surfactant assisted growth of Ge was tested. Ge islanding was observed at 400°C indicating that good surfactant growth was not obtained. This was consistent with the recent results of A. Sakai and T. Tatsumi(Sakai and Tatsumi 1994) who report that the surface roughness was nearly the same with or without H at this temperature. Although the monohydride layer was not a good surfactant for the Si(111) surface at this temperature, further study at different temperatures is needed to determine the ability of the ideal monohydride layer to act as a surfactant. Both HF etched and NH_4F etched Si(111) samples were exposed to O_2 in vacuum. The HF etched samples showed oxidation at room temperature upon exposure to molecular oxygen while no oxidation was observed from the NH_4F etched samples. This indicated that the surface termination of the two samples was different as was observed by IR

spectroscopy(Higashi et al. 1990). These measurements suggested that fewer defect sites where oxidation was likely to occur were found on the NH_4F etched H–Si(111) surface. The H–terminated Si(111) surface was believed to be chemically inert as the O_2 exposures showed. However, it has recently been shown that this surface would react with halogens(Linford et al. 1997; Terry et al. 1996a) and 1–alkenes(Chidsey and Linford 1995; Linford 1996; Linford and Chidsey 1993; Linford and Chidsey 1997; Linford et al. 1995; Terry et al. 1997b). These reactions were studied using photoemission spectroscopy. Bromine and Chlorine reacted with the H–Si(111) surface upon exposure at 10 torr in the dark in a vacuum prep system attached to the main experimental chamber. These reactions were confirmed by observing the growth of a Si 2p component at high binding energy characteristic of halogen reactivity. Reactivity with 1–alkenes was confirmed by measuring both the Si 2p and the C 1s core level spectra. The identity of alkyl monolayer on the Si(111) surface was determined using the C 2s based molecular orbitals in the valence band. Therefore, it has been clearly demonstrated that the H–Si(111) surface under certain conditions was reactive. This has implications in device processing as the H–Si(111) surface is relied upon as a passivation layer.

III.2. INTRODUCTION

A standard method for preparing silicon surfaces has used HF etching to remove native oxide layers and to protect the surface from chemical attack. However, surfaces prepared in this manner are atomically rough. Due to the surface roughness, mono, di and trihydride species are present(Dumas, Chabal, and Jakob 1990; Higashi et al. 1990). Recently, a method for preparing ideal H–terminated Si(111) surfaces by chemically etching in aqueous NH_4F solutions was developed(Dumas, Chabal, and Jakob 1990; Higashi et al. 1990). Infra–red spectroscopy has shown this surface to be terminated entirely by the monohydride and to be flat on an atomic scale(Dumas, Chabal, and Jakob 1990; Higashi et al. 1990). A high–resolution photoemission study of this surface showed that the Si 2p core level was very narrow, with a total linewidth of 0.160 eV, and that narrow features related to Si–H existed in the valence band(Hricovini et al. 1993). These features in the core level and valence band spectra were much narrower than those previously reported

for H–Si(111) prepared by H exposure in vacuum(Karlsson et al. 1990). The discovery of this ideal H–terminated surface has opened up many possible avenues of study.

One area of study involves the interaction of metals with the passivated surface. Recent results of Hg deposition on this H–passivated surface have shown that the Hg/H–Si(111) interface behaved as an ideal Schottky diode(Wittmer and Freeouf 1992; Wittmer and Freeouf 1993). The explanation offered for this behavior had the H termination layer remaining between the Hg and Si. In this position, H prevented the formation of interface states responsible for the non–ideality of Schottky barrier heights. If Hg did not displace H, then it follows that H has the ability to prevent certain surface reactions. However, Wittmer and Freeouf(Wittmer and Freeouf 1992; Wittmer and Freeouf 1993) did not have a probe of surface reactions available to determine if a reaction occurred at the interface. They could only measure barrier height and so could not directly determine if Hg displaced H. Photoemission spectroscopy is an ideal probe of surface reactions and of the initial stage of Schottky barrier formation. Photoemission spectroscopy was used to investigate NH_4F etched surfaces that had been exposed to Au.

Three distinct coverage regions were observed in the Au/H–Si(111) system. For Au coverages, $\Theta < 0.7$ ML, the deposition of Au caused the Si 2p linewidth to become slightly broader than that from H/Si(111) so it was likely that Si–H bonds were still present at low Au coverages. The intensity of the bulk Si 2p component decreased exponentially as the Au was deposited suggesting that Au did not cluster on the surface. For Au coverages, 0.7 ML $\leq \Theta \leq$ 7 ML, a new component appeared in the surface sensitive Si 2p spectra. By comparing bulk and surface sensitive spectra, the new component was determined to originate from photoemission from silicon atoms that had reacted with Au to form a silicide. This indicated that the hydrogen–termination layer had been compromised. Furthermore, the intensity of the silicide peak saturated while the bulk peak continued to be attenuated. This suggested that a maximum silicide thickness existed. For Au coverages, $\Theta \geq 7$ ML, the bulk component was completely attenuated. Signal from the Si 2p core level indicated that the silicide segregated to the top of a thick Au film with a maximum silicide thickness of 2–3 ML. A third Si 2p component appeared at high coverages and was shifted to higher

binding energy than the silicide component. This component was attributed to Si from the silicide layer dissolving in the Au film. These results were nearly identical for Au deposition on the Si(111) 7x7 surface(Yeh et al. 1993).

The second area of study opened up by the discovery of an ideally H–terminated surface was in the area of surfactant assisted heterogeneous semiconductor growth. It has been shown that uniform Ge films can be grown on Si substrates when a third element (the surfactant) was first evaporated onto the Si substrate. Typical surfactants for Ge growth on Si are Sb, Te, and Se(Cao et al. 1992). One problem with surfactant assisted growth was that it was impossible to remove the surfactant once film growth was completed without destroying the film. These surfactants work by providing an ideal termination for the Si substrate. Therefore, at first glance, the H–terminated Si(111) surface should be an excellent choice for surfactant assisted growth. To test this hypothesis, Ge was evaporated onto the H–Si(111) surface and annealed to the typical growth temperature of 400°C.

The Ge growth on H–Si(111) was monitored using the Si 2p and Ge 3d core levels. The core level photoemission spectra showed that the Ge was first deposited in uniform, amorphous layers on top of the H–Si(111) surface. The Si–H bonds were not significantly affected by Ge deposition. Moderate annealing led to the formation of ordered Ge islands on top of 1–2 uniform layers of Ge above the Si surface. This was not very different from direct deposition of Ge on a clean silicon surface. Therefore, a monohydride layer did not behave as a surfactant on the Si(111) surface at temperatures above 400°C which was consistent with the results of Sakai and Tatsumi(Sakai and Tatsumi 1994).

The third and most important area of study was in the area of surface chemical reactions of the H–terminated Si(111) surface. Chemical reactions with O_2, Cl_2, Br_2, and 1–alkenes were investigated. Higashi, et al.(Higashi et al. 1990) have demonstrated that the H–Si(111) surface was inert with respect to oxidation by air and as such was an excellent passivation layer for semiconductor processing. In order to quantify this passivation property, controlled O_2 exposures were performed in the experimental vacuum system. Oxidation was monitored using the Si 2p core level. Both HF and NH_4F etched Si(111) surfaces

were tested. HF etched samples were found to oxidize while NH_4F etched samples did not oxidize under the same conditions. This indicated that the NH_4F etching provided a more uniform surface passivation layer. While O_2 did not react with the NH_4F etched Si(111) surface, halogens did react on the H–Si(111) surface(Linford et al. 1997; Terry et al. 1996a). Si 2p core level photoemission from silicon surfaces exposed to halogens (Cl_2, Br_2) showed that a monohalide terminated surface was formed. Under identical dosing conditions, Br_2 appeared to react to a greater extent than did Cl_2. Surface reactions with 1–alkenes have also been demonstrated to occur on the H–Si(111) surface(Chidsey and Linford 1995; Linford 1996; Linford and Chidsey 1993; Linford and Chidsey 1997; Linford et al. 1995; Terry et al. 1997b). Si 2p and C 1s core level photoemission has shown that these reactions left the surface alkyl–terminated. The alkyl group could be identified using the C 1s based molecular orbitals in the valence band.

The above described experiments well quantified the properties of the H–Si(111) surface. The H–Si(111) surface while originally thought to be very inert, in fact, was a reactive surface and will be used as a starting surface for functionalization of Si with organic compounds.

III.3. EXPERIMENTAL

III.3.1. H–Si(111) Preparation

Three methods were used to prepare the H–Si(111) surface: HF etching of a Si(111) wafer, NH_4F etching of a Si(111) wafer, and NH_4F etching of a pre–oxidized Si(111) wafer. The HF etched samples were used in only the oxidation studies. The NH_4F etched samples were used for the Au deposition, Ge deposition and oxidation studies. Finally, the pre–oxidized samples were used for the halogen and 1–alkene reactivity studies and the valence band mapping studies. The sample preparation procedures will be discussed in detail below.

In the HF etching procedure, n–type, Si wafers that were cut in a (111) orientation with less than 1° miscut were used as the substrate for HF etching. These wafers were etched in

a solution of concentrated HF for 10 minutes to produce a H–terminated surface. After etching, the surface was rinsed for 10 seconds in deionized H_2O to remove residual compounds from the etching process.

In the NH_4F etching procedure, n–type and p–type, Si wafers that were cut in a (111) orientation with less than 1° miscut were etched in a 40% solution of NH_4F by weight to produce the H–terminated surface. After etching, the surface was rinsed for 10 seconds in deionized H_2O to remove residual compounds from the etching process.

In the pre–oxidized NH_4F etching procedure, the Si(111) wafer was cleaned and a chemical oxide film was grown. The oxide film was grown using the following procedure(Linford et al. 1995): immersion in a 50/50 solution of conc. H_2SO_4 and 30% H_2O_2 at 100°C for 1 hour. The wafer was then removed from this solution and rinsed in deionized H_2O to remove all traces of the previous solution. After this step the H_20 was observed to spread out in a thin layer across the surface, indicative of the formation of a hydrophillic oxide layer. The wafer was then placed in a 50/50 mixture of 30% H_20_2 and conc. NH_4OH for 30 minutes, followed by another deionized H_2O rinse. The wafer was again immersed in a 50/50 solution of conc. H_2SO_4 and 30% H_2O_2 at 100°C for 1 hour. After which the surface was rinsed in deionized H_2O to remove all traces of the previous solution and then blown dry with dry nitrogen leaving a uniform oxide film on the silicon wafer.

Next, the oxide film was removed by etching in 40% aqueous NH_4F for 10 minutes producing a uniform H–terminated Si(111) surface. After etching, the surface was rinsed for 10 seconds in deionized H_2O to remove residual compounds from the etching process. This procedure was first described by Higashi, Chabal, and coworkers(Higashi et al. 1990). This preparation was chosen because the resultant surface has been shown to have a low step density along with large, uniform terraces, i.e. a nearly ideal starting surface for chemical synthesis.

III.3.2. Surface Reactions

In this study, all depositions and exposures were performed at room temperature. Au and Ge were evaporated from tungsten filament evaporators. These evaporators were outgassed prior to sample introduction until the chamber pressure while evaporating was below 1 x 10^{-9} torr. The depositions were monitored with a quartz crystal monitor that allowed us to determine coverages to an accuracy of 20%.

Oxygen exposures were performed by backfilling the experimental chamber with O_2 to the designated pressure as measured with an ion gauge. Note that by measuring with an ion gauge, atomic oxygen must have been produced in the chamber. O_2 exposures were measured in Langmuirs. After O_2 exposure, the chamber was re–evacuated to the base pressure of 1 x 10^{-10} torr before any measurements were performed. Chlorine exposures were performed using two procedures. In the first method, H–Si(111) was placed into a glass manifold vacuum system which was evacuated to <6x10^{-6} Torr, then 0.2 Torr Cl_2 (Matheson, 99.99%) was introduced and the system was illuminated for 15 seconds with a broadband 350–nm lamp (Spectronics, MB–100, fluorescent flood). In the second method, a gas manifold was attached to the sample transfer arm to protect the chamber from large doses of Cl_2 and dosing was performed in the transfer arm. This system held the sample in total darkness during dosing. Chlorine gas (Matheson, 99.999%) was introduced to the dosing system through a leak valve until the dosing pressure was 8.00 torr as measured by a Baratron gauge (Capacitance). The sample was held at this pressure for 30 minutes. The residual Cl_2 was pumped away and the sample was directly introduced into the analysis chamber. Multiple Cl_2 exposures were necessary to chlorinate the sample. Bromine exposures were performed with the same gas manifold system as the Chlorine exposures. Liquid Bromine was purified by multiple freeze–pump–thaw cycles. Utilizing the high vapor pressure of Br_2, Br_2 vapor was introduced to the dosing system through a leak valve until the dosing pressure was 9.00 torr as measured by a Baratron gauge (Capacitance). The sample was held at this pressure for 15 minutes. The residual Br_2 was pumped away and the sample was directly introduced into the analysis chamber.

The chemical reactions(Linford 1996; Linford and Chidsey 1993; Linford and Chidsey 1997; Linford et al. 1995; Terry et al. 1997b) with 1–alkenes were performed *ex situ* as follows: a fused silica cuvette was filled with five to six grams of the corresponding 1–alkene, $H_{2n}C_n$, (Aldrich, 99%) and a shard of freshly prepared H–Si(111) (Higashi et al. 1990; Linford et al. 1995). The cuvette was sparged with argon until half of the pentene had evaporated. Next, either, the silicon surface was illuminated for 2 hours with a mercury arc lamp (185 and 253.7 nm, Jelight 80–2049–2 pen lamp), or it was allowed to sit in the solution for 12-24 hours under normal room lighting, then removed, rinsed with ethanol, then water, and finally, dried. After preparation the alkyl–terminated silicon samples were transported to the Stanford Synchrotron Radiation Laboratory for analysis. The wafers were placed in vials sealed with a viton septum. The septum was puncture with two needles, one used as an Ar inlet and the other acted as a purge. After the vial was filled with Ar, the sample was transported to the Synchrotron, mounted on a sample holder, and placed into the analysis chamber. Exposure to atmosphere was limited in order to reduce the risk of sample contamination.

III.3.3. Photoemission Measurements

The Au, Ge, and O_2 experiments were performed with the 6 m Toroidal grating monochromator on Beam Line I–2 at the Stanford Synchrotron Radiation Laboratory. The useful energy range of this beam line was between 10 and 200 eV. The experimental chamber was equipped with a VG ADES 400 angle resolved hemispherical analyzer with a combined resolution (analyzer and monochromator) of 0.37 eV at a photon energy of 130 eV. This analysis chamber used a load–lock sample transfer system and housed a low energy electron diffraction analyzer (LEED) for surface ordering studies. The base pressure of this system was $1x10^{-10}$ torr.

The VB and Si 2p core level photoemission spectra from the halogen and 1–alkene reaction studies were collected at BL 8–1 at the Stanford Synchrotron Radiation Laboratory. BL 8–1 uses a Toroidal Grating Monochromator (TGM). At this beam line, photons with energies between 10 and 200 eV were available for use, therefore, only valence band and low binding energy core levels could be studied. It was not possible to observe the C 1s

core level (binding energy of 290 eV) at this beam line, necessitating the use of different samples for the respective studies. The analysis chamber used for these measurements consisted of a load–lock sample transfer system, a low energy electron diffraction analyzer (LEED), and a double pass Cylindrical Mirror Analyzer (CMA). Valence band spectra were typically obtained using a photon energy of 55 eV and an analyzer pass energy of 10 eV. Silicon 2p core level spectra were obtained using photon energies of 130 eV, 115 eV and 110 eV to observe relative intensity changes as the electron escape depth varied(Eastman, Himpsel, and van der Veen 1982; Hricovini et al. 1993). Varying the escape depth of the photoelectrons aided in the assignment of the observed components. The total energy resolution (monochromator and analyzer) was determined to be 200 meV at a photon energy of 130 eV.

The C 1s core level photoemission spectra from the samples reacted with 1–alkenes were collected at BL 10–1 at the Stanford Synchrotron Radiation Laboratory. BL 10–1 uses a Spherical Grating Monochromator (SGM). This beam line has photons selectable within the energy range of 180 eV to 1000 eV. However, the usable energy range had an upper limit of 650 eV because of the use of a Ni refocusing mirror. This beam line was well suited for the study of the C 1s core level, but was not acceptable for either valence band studies due to low cross sections at these energies or Si 2p core level studies due to large electron escape depths. The analysis chamber for the C 1s core level measurements consisted of a load–lock sample transfer system, a reverse–view LEED, and a 100 mm VSW hemispherical electron energy analyzer. The photon beam and the analyzer were fixed at an angle of 30°. Carbon 1s spectra were collected at a photon energy of 350 eV. The total energy resolution (monochromator and analyzer) was determined to be 150 meV at a photon energy of 350 eV. Carbon 1s core level spectra were collected from pentyl–, decyl–, and octadecyl–terminated Si(111) surfaces.

All core level spectra were decomposed using the least–squared fitting procedure described in Chapter I. The Si 2p core level spectra were fit using spin–orbit split doublets with Voight lineshapes with a branching ration of 0.5 and spin–orbit splitting of 0.605 eV. Si 2p Spectra taken at Beam line I-2 were fit with a Lorentzian linewidth of 0.07 eV

FWHM, while those taken at Beam line 8–1 used a Lorentzian linewidth of 0.053 eV FWHM. The C 1s spectra taken at Beam line 10–1 were fit using singlet Voight lineshapes with a Lorentzian linewidth of 0.342 eV FWHM.

III.3.4. Thermal Annealing

Annealing studies were performed with sample manipulators capable of electron bombardment heating. Annealing temperatures below 500° C were reached by radiant heating by a nude filament located behind the sample. Temperatures above 500° C were obtained by electron bombardment heating. E–beam heating entails biasing the sample positively so that electrons emitted from the nude filament are accelerated into the sample. Samples were slowly brought up to the desired temperature to minimize contamination from the sample holder which could not be outgassed prior to data collection. The pressure was held below 5×10^{-9} torr during all temperature ramping. The sample was held at the desired temperature for 10 minutes and then cooled to room temperature before any measurements were taken. The temperature was measured with a Chromel–Alumel thermocouple welded to the sample holder. The sample temperature had previously been calibrated to the thermocouple reading to within 25°C with an optical pyrometer. The sample was then cooled to room temperature before further analysis was performed.

One expected problem was observed in the spectra that should be noted. These experiments were not the typical surface science measurements where all sample preparation was performed under ultra–high vacuum conditions. Therefore, it was not possible to perform standard outgassing procedures. Normally, the sample holder would be outgassed prior to performing measurements of this nature to prevent possible cross–contamination of the sample. However, this was not possible as annealing the sample holder would necessarily entail heating the sample which would have destroyed the interface. However, it does not appear to significantly alter the results of the annealing studies.

III.4. RESULTS

III.4.1. Hydrogen–Terminated Si(111)

Figure III.1 shows the valence band spectra, taken with a photon energy of 21 eV, of both NH_4F etched silicon (H–Si(111)) and the clean Si(111) 7x7 surface. It was obvious that the NH_4F etching procedure saturated the dangling bonds normally present at the surface as the two typical dangling bond states labeled S1 and S2 were absent in the H–Si(111) valence band. This was consistent with the previous FTIR and photoemission results from H–Si(111)(Dumas, Chabal, and Jakob 1990; Higashi et al. 1990; Hricovini et al. 1993; Karlsson et al. 1990). By saturating the dangling bonds, NH_4F etching removed the most reactive sites and thus passivated the surface. A peak at binding energy of 6.6 eV that was not found in spectra from clean silicon was observed, therefore, it must have originated from a species formed during the etching process. Previous studies have observed features at 7 and 10 eV binding energies and assigned them to H–Si(Klug, Du, and Greenlief 1993). This precedent was followed and the observed feature at 6.6 eV was assigned to H–Si. This feature was used to determine the presence of hydrogen on the silicon surface in the Au and Ge depositions described below. The feature at 11 eV could not be positively identified as a H–Si state, so it is likely due to the overlap between a previously report H–Si peak(Klug, Du, and Greenlief 1993) and a normal Si valence band feature.

The lower spectrum in Figure III.2 shows a surface sensitive, hν = 130 eV, Si 2p core level spectrum from an NH_4F etched sample. The corresponding bulk sensitive spectra, hν = 110 eV, is displayed in Figure III.3. The surface sensitive spectrum in Figure III.2 was decomposed into multiple spin–orbit doublets, labeled B and H1 in Figure III.2, using a least squares fitting procedure with Voight lineshapes (convolution of a Gaussian and Lorentzian) as described in Chapter I. The spectra from these etched samples were very similar to those previously reported by Karlsson, *et al.* (Karlsson et al. 1990) for H–Si(111). They attributed the first component to bulk silicon and the second, higher binding energy component to Si bonded to H(Karlsson et al. 1990). Doubt was recently cast on this assignment by a high resolution study of NH_4F etched Si(111) by Hricovini, *et al.*(Hricovini et al. 1993). They observed three surface components, with very narrow

Lorentzian linewidths (35 meV) in their Si 2p core level spectra, and assigned a peak shifted 0.14 eV to higher binding energy with respect to the bulk component to Si bonded to H. It appeared that the resolution in this study was inadequate to resolve the H–Si component from bulk silicon component. This suggests that the low binding energy component (29.8 eV Kinetic Energy) was a combination of the bulk Silicon component and the H–Si component and that the high binding energy component (29.5 eV Kinetic Energy), referred to as H1, was a combination of the unassigned peaks of Hricovini, *et al* (Hricovini et al. 1993; Terry et al. 1994).

The component B of the Si 2p core level from H/Si(111) was shifted 0.50 eV to higher binding energy from the position of the bulk component of Si(111)7x7. This corresponds to the Fermi level moving 0.50 eV toward the conduction band minimum from its pinned position on the Si(111)7x7 surface. Using the Fermi level position of the Si(111)7x7 surface, previously determined by Himpsel, *et al.*(Himpsel, Hollinger, and Pollak 1983) to be $E_F - E_V = 0.63$ eV, the Fermi level position of the H–Si(111) was determined to be $E_F - E_V = 1.13$ eV for the n-type, NH_4F etched Si(111) surface. As the Fermi level position was resonant with the conduction band minimum for silicon ($E_C - E_V = 1.12$ eV), it was possible that the flat band condition was reached for NH_4F etched n–type Si. This would be expected if H quenched the surface states without adding any extrinsic states that could cause Fermi level pinning. However, the Fermi level position was identical for NH_4F etched p–type samples where the unpinned Fermi level position would be expected to be near the valence band maximum, $E_F - E_V = 0$ eV. This result indicated that the Fermi level was pinned near the conduction band minimum.

III.4.2. Gold Deposition on H–Si(111)

Au deposition on the NH_4F etched surface was studied because the Au/Si(111) interface had been well characterized(Molodtsov et al. 1991; Yeh et al. 1993). These previous studies had shown that Au was very reactive with the silicon substrate. With the initial Au deposition on the clean Si(111) surface, a silicide layer formed. As the amount of Au deposited was increased, it diffused through the silicide layer and formed metallic Au

layers between the silicide and the silicon substrate. The silicide was always observed to be at the vacuum interface. This well characterized system was invaluable for comparison purposes. Furthermore, a previous study(Iwami et al. 1984) had deposited Au on silicon surfaces previously exposed to atomic hydrogen. This study used electron energy loss spectroscopy (EELS) as a probe. EELS, unlike photoemission, is sensitive to hydrogen bonds. This study was also used for comparison purposes.

Figure III.2 (surface sensitive) and Figure III.3 (bulk sensitive) show Si 2p core level spectra from an n–type sample as a function of gold coverage. Figure III.4 is identical to Figure III.2 except the substrate was p–type. Au 4f core level spectra taken at a photon energy of 130 eV were also collected and are shown in Figure III.5. Valence band spectra are shown in Figure III.6. The coverages described in these figures define 1 ML as 7.8 x 10^{14} atoms/cm^2, i.e. the number of surface Si atoms. Spectral decompositions are shown for the surface sensitive Si 2p spectra (Figure III.2 and Figure III.4) and the Au 4f spectra, Figure III.5. The data was interpreted by noting three different coverage regimes, identical for both n– and p–type substrates. For Au coverages $\Theta < 0.7$ ML, the deposition of Au caused the Si 2p linewidth to become slightly broader than that from H/Si(111). Because the Si 2p lineshape was only slightly changed, it was likely that Si–H bonds were still present at low Au coverages. The intensity of the bulk component decreased exponentially as the Au was deposited. The exponential decrease of the Si 2p bulk component intensity was explained using a simple two layer model where the intensity would be expected to decrease as $\exp(-d/\lambda)$ where d is the distance from the surface and λ is the escape depth of the photoelectrons. The exponential attenuation of the core level strongly suggested that Au did not cluster on the surface.

The valence band spectrum was unchanged throughout this coverage region. The Si–H peak at 6.6 eV still showed strong emission. Using this information and the core level data described above, it can be inferred that at these low coverages of Au, Si–H bonds were present. The valence band spectra showed no emission near the Fermi level so at low coverage large metallic clusters did not occur on the surface.

The Au 4f spectra were collected to determine if they agreed with the above model. These

spectra were decomposed as described in Chapter I. As shown in Figure III.5, the spectra were dominated by photoemission from the silicide (Peak S). Even at these low coverages though, some metallic Au (Peak M) was present on the surface. Notice that the silicide peak was shifted to higher binding energy than the metallic component (bulk–like Au). This behavior was identical to that observed in the Si 2p component, where the silicide feature was also shifted to higher binding energy than the bulk Si component. Therefore, charge transfer cannot be used to describe the observed core level shifts. Final state effects were important in this system. This behavior can only be explained by screening in the Au 4f final state. The metallic Au rather then the Au–silicide better screens the core hole in the photoemission final state, thereby lowering its energy more that of the Au in the silicide. As this case demonstrates, one must always be cautious in assigning peaks in core level photoemission on the bases of charge transfer alone.

The bulk sensitive Si 2p core level shifted to lower binding energy (higher kinetic energy) as Au was deposited. The energy position of the bulk component centroid has been marked to make this progression easier to follow. This motion of the core level was entirely due to band bending. After the deposition of 0.1 ML Au, the bulk component shifted 0.5 eV. As discussed above, this signifies that the Fermi level moved 0.5 eV toward mid–gap. One possible explanation for the Fermi level movement could be formation of interface states causing Fermi level pinning. A second explanation could have the H remaining between the Au and the Si surface, where it might prevent the formation of interface states. In this case, the Fermi level motion would be caused by the formation of an ideal Schottky barrier where the shift is caused by the work function of Au. Wittmer and Freeouf(Wittmer and Freeouf 1992; Wittmer and Freeouf 1993) may have observed a Schottky barrier of this type. However, since Au was evaporated onto the surface, the effect of the heat of condensation on the passivation layer must be considered. This is an effect that Wittmer and Freeouf avoided by exposing their surface to liquid Hg. The energy imparted to the surface during condensation would be expected to destabilize the passivation layer. Also, the observed band bending was similar to that observed for low coverages of Au on the Si(111)7x7 surface(Yeh et al. 1993) where interface states cause Fermi level motion.The passivation layer was compromised during Au deposition and that interface states formed

which caused Fermi level pinning near mid–gap.

For Au coverages 0.7 ML $\leq \Theta \leq$ 7 ML, a new component appeared in the surface sensitive Si 2p spectra (Figure III.2). The two components in these spectra are labeled B and S. By comparing bulk and surface sensitive spectra, component B originated from photoemission from bulk silicon and component S from emission from silicon atoms that had reacted with Au to form a silicide. The composition of the Au silicide on the Si(111)7x7 surface has previously been determined to be Au3Si(Molodtsov et al. 1991; Yeh et al. 1993). The emission from the silicide layer was initially shifted 0.55 eV to higher binding energy relative to the bulk component. The shift to higher binding energy implies that charge was transferred from silicon to Au. However, the energy splitting between the silicide (S) and the bulk component (B) was not constant. It increased to a maximum observable splitting of 0.64 eV with increasing Au coverage. This indicated that the silicide composition was not uniform. The previously determined composition, Au_3Si, was a mean composition of the silicide layer.

The intensity of component (S) increased until the maximum intensity was reached after deposition of 7 ML Au. Intensity analysis showed that the silicide contained between 1 and 2 ML of reacted silicon. These results were consistent with those from the deposition of Au on the Si(111)7x7 surface(Yeh et al. 1993). In this previous study, the silicide was reported to stabilize after the deposition of 6 ML Au and to consist of 1 to 1.5 ML of reacted Si(Molodtsov et al. 1991; Yeh et al. 1993). The bulk component intensity continued to decrease exponentially as was observed at low coverages, which clearly indicates that Au was uniformly deposited on the surface. The bulk component (B) shifted further to lower binding energy due to increasing band bending. The band bending continued to increase up to a Au coverage of 7 ML when the bulk signal was last observed (Figure III.3). The data does show that the band bending was nearing saturation at this point. The fact that the band bending increased at high coverages is different from that of Au-deposition on the Si(111)7x7 surface where the band bending stabilized at a Au coverage of 2 ML(Molodtsov et al. 1991; Yeh et al. 1993). While the rate at which the band bending saturated was different, the final pinning positions were similar. It appeared that

the mechanism of Schottky barrier formation was the same for both surfaces because the final pinning positions were similar.

Figure III.6 shows the valence band taken with photon energy of 27 eV. Two interesting features were observed. First, photoemission intensity increased near the Fermi level which indicated the formation of metallic layers. Second, the spin–orbit splitting between the two peaks of the Au 5d doublet near 5 and 7 eV increased with the Au coverage. This progression has been marked in Figure III.6. This splitting began with a value of 1.4 eV which is near the value (1.5 eV) observed from atomic Au(Hiraki 1984). The increase of the Au 5d spin orbit splitting reflects evolution from atomic Au to metallic Au as coverage was increased. The final feature to notice in the valence band is at 6.6 eV, the H–Si peak described above. This feature overlapped with the Au $5d_{3/2}$ component so it could not be used to determine the presence of Si–H bonds. Because of this and the fact that the Si–H shift in the Si 2p core level spectra was unobservable due to the systems resolution, the results of an earlier study(Iwami et al. 1984) that used EELS, which is sensitive to H, and Auger spectroscopy to investigate Au deposition on a Si(111) surface that had been exposed to atomic hydrogen were used for comparison purposes. Iwami, *et al.* (Iwami et al. 1984) found that Si–H bonds were present until 5 ML of Au had been deposited. It appeared that some Si–H bonds remained at the Au–Si substrate interface, although, because a silicide was formed it was extremely unlikely that the uniform passivation layer remained intact.

These above described results were consisted with the behavior of the Au 4f core level. In this coverage region, the silicide peak of the Au 4f core level spectra saturated, while the metallic peak continued to grow in intensity. This was consistent with a thin silicide sitting on top of a growing layer of metallic gold.

For Au coverages $\Theta \geq 7$ ML, the bulk component of the Si 2p spectra was completely attenuated. A new component (S1) shifted 0.66 eV to higher binding energy relative to the silicide component (S) appeared in the surface sensitive spectra. This component was not observed for the Au/Si(111) system. As discussed earlier, the chemical shift of the silicide peak was due to charge transfer from silicon to gold atoms. Chemical shifts depend upon

the number of surrounding atoms. This implies that a new species with more Au surrounding the silicon atoms forms at high coverage. The silicide component (S) was attenuated as the S1 component increased. These findings strongly indicate that some Si atoms from the silicide dissolved in the Au layers. This is consistent with the higher binding energy of the S1 component.

Si 2p core level emission was observed after the deposition of 70 ML of Au, therefore the silicide layer did remain on the surface. The silicide which consisted of approximately 1 ML of silicon could then only account for 2–3 ML of reacted Au with composition Au_3Si. Therefore, the majority of deposited Au must have existed in metallic layers underneath the silicide. This is consistent with results from Au deposition on Si(111)7x7. In the valence band spectra, strong emission near the Fermi level indicated the existence of metallic layers. The Au 5d spin–orbit splitting reached a maximum value of 2.4 eV. This value was identical to the splitting observed from metallic Au(Hiraki 1984). Using the spin–orbit splitting data and the data on the amount of silicide present, it was natural for us to conclude that the majority of Au was deposited in a metallic state.

For Au coverages $\Theta < 0.7$ ML, a uniform layer of Au was formed on the surface. Silicon–hydrogen bonds were also detected. There was no evidence to suggest that a Au–Si reaction occurred at these low coverages. However, significant band bending, which was most likely the result of the formation of interface states causing the Fermi level to move toward mid–gap, was observed. In the coverage region, $0.7 \text{ ML} \leq \Theta \leq 7$ ML, a Au–silicide layer was formed. The Au was originally deposited onto the Si surface in an atomic–like manner. As more Au was deposited, metallic layers of Au were formed. The layers of silicide and metallic Au attenuated the bulk signal exponentially. The composition of the silicide was not uniform because the energy splitting between the silicide component and the bulk component was not constant. These results are consistent with those previously observed for Au/Si(111)(Iwami et al. 1984; Molodtsov et al. 1991; Yeh et al. 1993). However, the band bending continued to increase throughout this coverage range. This is different from Au deposition on Si(111)7x7 where the band bending saturated at lower coverage. It was clear that the band bending was nearing saturation at $\Theta = 7$ ML at a value similar to that of

the Au/Si(111) system. This implied that the mechanism for Schottky barrier formation was similar whether or not H was present. An earlier study(Iwami et al. 1984) observed Si–H bonds to Au coverages of 5 ML and no evidence to dispute this result was found. In the coverage region, $\Theta \geq 7$ ML, a thick metallic Au film formed. The silicide and metallic Au layers completely attenuated the bulk signal. However, Si 2p core level emission was still observed at high coverage. This emission must have originated from silicide atoms residing on top of the thick metallic Au film. Also, a Si 2p component never before observed was attributed to Si dissolved in the metallic Au. This component was attributed to dissolved silicon atoms that came from the silicide layer. This assignment was made because of the observed attenuation of the silicide component. This system consisted of 2–3 ML layers of Au–silicide above a thick film of Au that sat on top of the bulk silicon. It is likely that some hydrogen was still present at the interface between the metallic Au and Si. The presence of the original monohydride layer did not appear to inhibit the interaction between Au and Si.

III.4.3. Germanium Deposition on H–Si(111)

Studies (Cao et al. 1992) have shown that Sb and other species that saturate the dangling bonds on silicon surfaces act as surfactants. Surfactants minimize surface energy and provide a growth front for Ge on Si. The presence of a surfactant transforms the growth from Stranski–Krastanov (S–K) mode, 1–2 layers followed by island growth, to layer by layer growth. Since the monohydride saturates dangling bonds on the silicon surface and provides a uniform starting surface, it was possible that the monohydride layer would act as a surfactant on the Si(111) surface.

Figure III.7 shows surface sensitive Si 2p core level spectra. These spectra were taken with various coverages of Ge and were normalized to maximum intensity. No changes in Si 2p lineshape as Ge was deposited at room temperature were observed. The observed peak to valley ratio was constant within the experimental error. This was not surprising as no Ge–Si eomponent has previously been observed in the Si 2p core level from Ge–Si interfaces formed under different conditions(Cao et al. 1992; Carlisle, Miller, and Chiang 1992; Katnani et al. 1981; Lin, Miller, and Chiang 1991). However, since the lineshape after

deposition was identical to that from H–Si(111), it is likely that Si–H bonds still exist at the interface. As the sample was annealed to 400 °C, the Si 2p core level decreased in linewidth. Since the core level was a combination of Si–H and bulk Si, the decrease in linewidth implies that the Si–H bonds were destroyed. These bonds were destroyed well below the monohydride desorption temperature (530 °C) on the Si(111) surface(Greenlief, Gates, and Holbert 1989). The hydrogen would not be expected to remain on the Ge surface as the annealing temperature was above the monohydride desorption temperature (150 °C) on the Ge(111) surface(Steinmetz et al. 1990).

Figure III.8 shows the corresponding bulk sensitive Si 2p core level spectra. These spectra have had the bulk component aligned to compensate for band bending. The intensity of the Si 2p core level was attenuated as Ge was evaporated onto the surface. This indicated the presence of relatively uniform layers of Ge on the Si substrate. After annealing, the Si 2p core level decreased in linewidth and increased in intensity. Clearly seen in this figure was the fact that the Si 2p core level after annealing was much narrower than that from the H–terminated surface. Narrowing of the Si 2p core level has previously been determined to be caused by the formation of uniform Ge layers that force the Si atoms into a bulk–like environment(Cao et al. 1992; Carlisle, Miller, and Chiang 1992; Lin, Miller, and Chiang 1991). Again, this indicates that the H–Si bonds were broken during the annealing process. The Si 2p core level also showed a large increase in intensity after annealing. The only possible explanations for this increase in core level intensity are Ge islanding, Ge desorption, or Ge dissolution.

The Ge 3d core level, shown in Figure III.9, was initially very broad. After annealing it had narrowed enough that the spin–orbit splitting was observed (shoulder S in spectra appeared). This is indicative of ordering of the Ge layer as in the case of surfactant growth with Sb. The Ge 3d peak did not show much change in intensity after annealing. Therefore, annealing at 400 °C does not cause significant Ge desorption or dissolution, which indicated that the Ge formed islands. This would also cause the observed growth of the Si 2p intensity.

These results indicate that after annealing 1–2 uniform layers of Ge were formed on the

surface with Ge islands above these uniform layers. This is indicative of S–K growth so at these temperatures H did not act as a surfactant. These results are consistent with a recent high resolution transmission electron microscopy study of Ge growth on Si using atomic H as a surfactant(Sakai and Tatsumi 1994).

III.4.4. Oxygen Deposition on H–Si(111)

Both NH_4F and HF etched Si(111) surfaces were exposed to oxygen to determine how well the sample was passivated by the H layer. O_2 exposures of the clean Si(111)7x7 surface leads to significant surface oxidation with exposures as small as 0.1 L O_2(Schell-Sorokin and Demuth 1985). Note that the O_2 exposures described below were performed with an ion gauge filament turned on, thus some atomic oxygen must have been formed. Therefore, the below describe measurements measure the reactivity of both atomic and molecular oxygen.

The Si 2p core level spectra from HF etched Si(111) exposed to oxygen are shown in Figure III.10. Exposure to 100 L O_2 did not result in surface oxidation. However, further exposure to $3x10^5$ L O_2 did result in surface oxidation. This was in contrast to oxygen exposure to NH_4F etched Si(111). The Si 2p core level spectra from NH_4F etched Si(111) wafers exposed to O2 are shown in Figure III.11. As with the HF etched sample no oxidation was observed at exposures of 100 L O_2, but no evidence of oxidation was evident up to O_2 exposures of 100,000 L. Again, it must be noted that no evidence of oxidation was evident on the NH_4F etched Si(111) surface even with some exposure to atomic oxygen. This result was not surprising as NH_4F etching (monohydride termination) was known to give more ideal terminated surfaces than HF etching (mono, di, and trihydride termination)(Dumas, Chabal, and Jakob 1990; Higashi et al. 1990).

III.4.5. Halogenation of the H–Si(111) Surface

The chemisorption of molecular halogens on Si(111) 7x7 surfaces has been well studied(Chakarian et al. 1993; Whitman et al. 1990). They have been found to dissociatively chemisorb onto the Si(111) surface forming mono, di, and trihalide species on the surface.

In fact, a study by Thomas, *et al.*(Thomas, Rudder, and Markunas 1991) has studied chemisorption of Cl_2 and F_2 on the H–Si(111) surface. They have demonstrated that the H–Si(111) surface would not react with molecular halogens at low pressures (approximately 10^{-5} torr). However, they predicted that atomic halogen atoms would react by replacing the H atoms at the surface. H–Si(111) surfaces were exposed to molecular halogens at high pressures (approximately 10 torr) or under UV illumination to increase the amount of the atomic halogen present.

Figure III.12 shows Si 2p core level spectra taken at a photon energy of 130 eV from Halogen (Cl_2 and Br_2) exposed H–Si(111) surfaces. A reference spectra from the H–Si(111) surface was also included. These spectra were decomposed into spin–orbit doublets using Voight lineshapes (Gaussian and Lorentzian) as described above. Two components were observed in H–Si(111) surfaces exposed to both Cl_2 and Br_2. The lower binding energy component was attributed to photoemission from bulk Si atoms due to measurements made at more bulk sensitive photon energies. The other component had a large chemical shift (Cl_2 exposed — 0.8 eV; Br_2 exposed — 0.7 eV) to higher binding energy (lower kinetic energy) than the bulk component indicating that the Si was bonded to an element more electronegative than itself. Core level shifts of this magnitude are indicative of the presence of Si atoms in the Si^{1+} oxidation state(Chakarian et al. 1993; Himpsel et al. 1988; Whitman et al. 1990). Thus, this component was attributed to emission from a Si atom that had reacted with one halogen atom.

Figure III.13 shows Si 2p core level spectra from H–Si(111) exposed to Cl_2 in total darkness and under UV illumination. Two features are evident in these spectra. First, the Si $2p_{1/2}$ feature at 24.3 eV kinetic energy, from the silicon in the 1+ oxidation state due to bond formation with chlorine, was half the intensity in the dark sample as in the UV sample. Second, the spectra from the sample exposed in the dark was much broader than that from the UV exposed sample. Both the intensity decrease and the linewidth broadening occurred because the dark sample had both Cl– and H–terminated regions present. The incomplete reaction on the sample exposed to Cl_2 in darkness indicated that atomic

chlorine was the species that reacted with the H–Si(111) surface. Even in total darkness, some free chlorine atoms would be present which could account for the partial replacement of H in the dark exposed sample.

Obviously, the reaction of atomic halogens on the H–Si(111) surface did not proceed as far as the reaction of molecular halogens on the Si(111) 7x7 surface, where further oxidation of the Si surface atoms (Si^{2+}, Si^{3+}) was observed. This indicated that once the surface hydrogen had been replaced, forming the monohalide–terminated surface, etching of the silicon proceeded slowly or not at all. In fact, the monochloride–terminated surface has proven to be an excellent starting surface for substitution reactions with alkyl lithium reagents(Linford 1996; Terry et al. 1996b)

III.4.6. Alkylation of the H–Si(111) Surface

Si 2p, C 1s, and valence band photoemission spectra were collected from H–Si(111) surfaces exposed to 1–alkenes. The Si 2p and C 1s core level spectra showed multiple components indicative of chemical bond formation between the alkyl chain and the silicon substrate. The valence band spectra clearly showed that the respective alkane was present on the surface.

Figure III.14 shows the valence band spectrum of a H–Si(111) surface that was exposed to 1–pentene and the positions of the corresponding features in a photoemission spectra from gas phase pentane after adjusting for different reference levels (Fermi level in solids and Vacuum Level in gases) and screening differences(Potts and Streets 1974). This spectra were referenced to the position of the Fermi Level, so that peaks have negative binding energies. The region of binding energies between -12 to -21 eV, had five components that could clearly be resolved. Peaks in this region of the valence band are due to photoemission from the C 2s based molecular orbitals of alkyl groups. The observed binding energies of the five components in the spectrum from the H–Si(111) surface exposed to 1–pentene were -19.1 eV, -17.6 eV, -15.6 eV, -13.7 eV, and -12.8 eV. Potts *et al.* reported gas phase binding energies of the $1a_1$, $1b_2$, $2a_1$, $2b_2$, and $2b_u$ molecular orbitals of n-pentane with assumed C_{2v} symmetry to be -24.8 eV, -23.7 eV, -21.7 eV, -19.9 eV, and -18.74 eV,

respectively(Potts and Streets 1974). Shifting the gas phase data by 6 eV, to account for the different reference levels and screening due to the surface, brought the reported gas phase data (-18.8 eV, -17.7 eV, -15.7 eV, -13.9 eV, and -12.74 eV) from n–pentane(Pireaux et al. 1986; Potts and Streets 1974) into excellent agreement with the peak positions of the corresponding features in the spectra from the H–Si(111) surface exposed to 1–pentene. Therefore, it appeared that pentyl groups were present on the silicon surface. Corresponding features were also observed from H–Si(111) surfaces exposed to other 1–alkenes(Terry et al. 1997a).

The Si 2p core level spectra from H–Si(111) samples exposed to 1–pentene, 1–decene, and 1–octadecene are shown in Figure III.15. A reference spectrum from methyl–terminated Si(111) is also shown. As the number of carbon atoms in the alkene was increased, the intensity of the Si 2p photopeak decreased. The attenuation behavior of the Si 2p photopeak indicated that a thin film of alkyl groups was formed on top of the surface Si atoms. Only, two possible models could account for the observed attenuation behavior. First, the alkyl groups could be oriented nearly vertical to the surface, possibly with a chemical bond formed between the Si substrate and the terminal C atom of the alkyl group, so that by adding additional ($-CH_2-$) groups, i.e. increasing the number of C atoms in the alkene, the film thickness would be increased. Second, the alkyl groups could lie flat on the Si substrate, but then the attenuation behavior could only be explained, if the larger alkyl chains formed thicker films.

The Si 2p core level spectra also changed lineshape as the number of carbon atoms in the alkyl chain was increased. This suggested that the observed photopeak consisted of multiple spin–orbit doublets. These spectra have been decomposed into two spin–orbit doublets using a least squares fitting procedure with Voight lineshapes (convolution of a Gaussian and Lorentzian)(Terry et al. 1997a). The variation of lineshape occurred because the intensity ratios of the two components varied as the alkyl group increased in size. One component could be attributed to bulk Si. The other component was shifted 0.21 eV to higher binding energy than the bulk component. This indicated that charge was being transferred from the Si atoms to an element more electronegative than itself, i.e. a chemical bond was

formed at the interface. If the first model was correct, and the charge transfer occurred between the top layer Si atoms and the terminal C atom of the alkyl group, a component chemically–shifted to lower binding energy should be observed in the C 1s core level spectrum.

Figure III.16 shows a representative C 1s spectrum from a pentyl–terminated surface including a decomposition into two singlet components using Voight lineshapes. One component was attributed to emission from bulk–like Carbon atoms in the alkyl group, the other to the terminal C atom of the alkyl group bonded to the Si substrate. This assignment was made because two components were observed in the C 1s spectra until the chain length exceeded 10 carbon atoms, at which point, the low binding energy component, labeled C–Si in the figure, was no longer observed(Terry et al. 1997a). The observed behavior of the low binding energy component was consistent with an interfacial component, as one would expect an interfacial component to be significantly attenuated as the chain length increased. Furthermore, the direction of the chemical shift of the interfacial component, 1.1 eV to lower binding energy, was suggestive of C–Si bond formation. The observed charge transfer in the Si 2p and C 1s core levels both suggest that a bond was formed between the alkyl group and the Si substrate. This is in agreement with a previous study(Lapiano-Smith, Himpsel, and Terminello 1993) of ethyl–terminated surfaces formed by the decomposition of diethylsilane, where a broad C 1s spectrum approximately 2 eV wide was observed. In their study, the observed spectra were not decomposed, but it was likely that the 2 eV wide peak that they measured consisted of two components of approximately equal intensities, one C–C feature and one C–Si feature, as one would expect from that surface according to this model.

The observed intensity ratios of the two components in the C 1s core level spectrum were not in the expected 4 to 1 ratio from the chain length. The intensity ratio observed from the pentyl–terminated chain at a photon energy of 350 eV was approximately 20 to 1. The "incorrect" intensity ratios were attributed to photoelectron diffraction effects. In fact, the surface geometry of the alkyl groups has been determined to be best described by the first model, where the alkyl groups sat in atop sites with C–Si bond lengths of 1.85Å(Terry et

al. 1996b). Therefore, a chemical reaction occurred between the 1–alkenes and the H–Si(111) surfaces.

III.5. DISCUSSION

III.5.1. H–Si(111) as Passivation Layer in Device Processing

Semiconductor devices are moving to smaller dimensions where small regions of contamination can often cause device failure(Sze 1985). To minimize possible sources of contamination elaborate clean rooms have been devised to protect against dust particles(Sze 1985) and termination layers have been studied to determine if they prevent chemical reactions at the semiconductor surface(Nemanich et al. 1992). Because the H–Si(111) surface was remarkably resistant to chemical attack by oxygen, this surface has been used as a passivation layer in silicon device fabrication(Nemanich et al. 1992). However, as shown above, there are conditions where the ability of the H layer to act as a passivant breaks down. First, the hydrogen–termination was compromised when exposed to an evaporated metal (Au), and second, when exposed to molecular halogens and 1–alkenes.

In the first case, surface–termination was compromised due to Si–H bond breaking due to the excess energy from the heat of condensation of the deposited metal. Once the Si–H bonds were broken, the Au reacted with the silicon substrate to form a silicide layer. This is likely to occur whenever the heat of condensation of the deposited material is greater than the Si–H bond strength of 76 Kcal/mole(Thomas, Rudder, and Markunas 1991). In the second case, surface–termination was compromised due to a direct reaction of the Si–H surface species with the molecular compound. Clearly, the H–Si(111) surface is not inert. It was oxidized by reactive halogens and organic compounds. This study shows that the H–Si(111) surface is not a perfect passivation layer and indicates that caution must be exercised when using it as such. If care is not taken to prevent these known reactions, contamination may occur which could lead to device failure.

III.6. CONCLUSION

In summary, the flat band condition for NH_4F etched n–type Si was reached. As Au was

first deposited, a uniform layer of atomic–like Au formed on the surface. Silicon–hydrogen bonds were still present on the surface. The Fermi level pinned near mid–gap most likely as the result of the formation of interface states. At intermediate Au coverages, a Au–silicide layer approximately 2–3 ML thick formed. The composition of the silicide was not uniform. The remaining Au formed a metallic layer between the silicide and the silicon surface. Previous results(Iwami et al. 1984) suggested that silicon–hydride bonds could be found at the metallic Au –Si substrate interface. This interface then would be non–uniform. At high coverages, the silicide and metallic Au layers attenuated the bulk signal. The Si 2p core level emission still observed was predominately from the silicide layers which remained above the metallic Au film. The remaining Si 2p emission was attributed to Si atoms from the silicide that dissolved in the metallic Au. This system was observed to consist of 2–3 ML layers of Au–silicide above a thick film of Au that sat directly on top of the bulk silicon. As Ge was deposited, uniform, amorphous layers formed on top of the H–Si(111) surface. The Si–H bonds were not significantly affected by Ge deposition. Moderate annealing led to the formation of ordered Ge islands on top of 1–2 uniform layers of Ge above the Si surface. This was not very different from direct deposition of Ge on a clean silicon surface. There was no evidence of Ge–H formation. This was not unexpected as the annealing temperature was above the monohydride desorption temperature from Ge(111). A monohydride layer did not behave as a surfactant on the Si(111) surface at temperatures above 400°C which was consistent with the resent results of Sakai and Tatsumij(Sakai and Tatsumi 1994). No oxidation of the ideal H–terminated surface was observed after exposures as high as 100,000 L O_2. However, surface oxidation was observed when the H–Si(111) surface was exposed to molecular and atomic halogens. The Si 2p core level spectra from the halogen–exposed surfaces showed two components, from bulk silicon and from silicon bonded to a single halogen atom. This result was unlike halogen exposure to the Si(111) 7x7 surface where halogen exposure results in mono–, di–, and trihalogenated Si atoms(Chakarian et al. 1993; Whitman et al. 1990). Finally, the H on the H–Si(111) surface was replaced by alkyl groups when exposed to 1–alkenes. Valence band spectra were used to identify the alkyl groups present as the C 2s–based molecular orbitals provided a fingerprint region in the spectra. Si 2p and C 1s core level both contained chemically–shifted components providing direct evidence

of Si–C bond formation. These results clearly suggest that caution must be taken when using the H–Si(111) surface as a passivation layer as the surface is reactive under the conditions described above.

III.7. ACKNOWLEDGEMENTS

Julie A. Terry must be recognized for help with data collection. M. R. Linford prepared the UV exposed Cl surfaces and the alkyl–terminated Si surfaces. This work was performed at the Stanford Synchrotron Radiation Laboratory, which is supported by the Department of Energy, Office of Basic Energy Science, Division of Chemical Sciences. This work was also supported by that Office's Division of Material Research.

III.8. REFERENCES

Cao, R., X. Yang, J. Terry, and P. Pianetta. 1992. *Applied Physics Letters* 61:2347.

Carlisle, J. A., T. Miller, and T. C. Chiang. 1992. *Physical Review B* 45:3811.

Chakarian, V., D.K. Shuh, J.A. Yarmoff, M.C. Hakansson, and U.O. Karlsson. 1993. *Surface Science* 296:383.

Chidsey, C. E. D., and M. R. Linford. 1995. In the preceedings of the *Fourth International Symposium on Cleaning Technology in Semiconductor Device Manufacturing.*

Dumas, P., Y. J. Chabal, and P. Jakob. 1990. *Surface Science* 269/270:867.

Eastman, D. E., F. J. Himpsel, and J. F. van der Veen. 1982. *Journal of Vacuum Science and Technology* 20:609.

Greenlief, C. M., S. M. Gates, and P. A. Holbert. 1989. *Journal of Vacuum Science and Technology A* 7:1845.

Higashi, G. S., Y. J. Chabal, G. W. Trucks, and K. Raghuachari. 1990. *Applied Physics Letters* 56:656.

Himpsel, F. J., G. Hollinger, and R. A. Pollak. 1983. *Physical Review B* 28:7014.

Himpsel, F. J., F. R. McFeely, A. Taleb–Ibrahimi, J. A. Yarmoff, and G. Hollinger. 1988. *Physical Review B* 38:6084.

Hiraki, A. 1984. *Surface Science Reports* 3:357.

Hricovini, K., R. Gunther, P. Thiry, A. Taleb-Ibrahimi, G. Indlekofer, J.E. Bonnet, P.

Dumas, Y. Petroff, X. Blase, X. Zhu, S. G. Louie, Y. J. Chabal, and P. A. Thiry. 1993. *Physical Review Letters* 70:1992.

Iwami, M., M. Nishikuni, K. Okuno, and A. Hiraki. 1984. *Solid State Communications* 51:561.

Karlsson, C. J., E. Landemark, L. S. O. Johansson, U. O. Karlsson, and R. I. G. Uhrberg. 1990. *Physical Review B* 41:1521.

Katnani, A. D., N. G. Stoffel, H. S. Edelman, and G. Margaritondo. 1981. *Journal of Vacuum Science and Technology* 19:290.

Klug, D. A., W. Du, and C. M. Greenlief. 1993. *Journal of Vacuum Science and Technology A* 11:2067.

Lapiano-Smith, D. A., F. J. Himpsel, and L. J. Terminello. 1993. *Journal of Applied Physics* 74:5842.

Lin, D. S., T. Miller, and T. C. Chiang. 1991. *Physical Review Letters* 67:2187.

Linford, M. R. 1996. Chemical Functionalization of Hydrogen–Terminated Silicon Surfaces: The First Self–Assembled Monolayers on Silicon. Ph. D. Dissertaion, Stanford Universtity, Stanford, CA.

Linford, M. R., R. Cao, J. Terry, H. Luo, R. Mo, P. Pianetta, and C. E. D. Chidsey. 1997. *in* prep.

Linford, M. R., and C. E. D. Chidsey. 1993. *Journal of the American Chemical Society* 115:12631.

Linford, M. R., and C. E. D. Chidsey. 1997. in prep.

Linford, M. R., P. Fenter, P. M. Eisenberger, and C. E. D. Chidsey. 1995. *Journal of the American Chemical Society* 117:3145.

Molodtsov, S. L., C. Laubschat, G. Kaindl, A. M. Shikin, and V. K. Adamchuk. 1991. *Physical Review B* 44:8850.

Nemanich, R. J., C. R. Helms, M. Hirose, and G. W. Rubloff, eds. 1992. *Chemical Surface Preparation, Passivation, and Cleaning for the Semiconductor Growth and Processing.* Vol. 259. Pittsburg: Materials Research Society.

Pireaux, I. J., J. Riga, P. A. Thiry, R. Caudano, and J. J. Verbist. 1986. *Physica Scripta* T13:78.

Potts, A. W., and D. G. Streets. 1974. *Journal of the Chemical Society Faraday Transac-*

tions II 70:875.

Sakai, A., and T. Tatsumi. 1994. *Applied Physics Letters* 64:52.

Schell-Sorokin, A. J., and J. E. Demuth. 1985. *Journal of Vacuum Science and Technology A* 3:1475.

Steinmetz, D., F. Ringeisen, D. Bolmont, and J. J. Koulmann. 1990. *Surface Science* 237:135.

Sze, S. M. 1985. *Semiconductor Devices Physics and Technology.* New York: Wiley.

Terry, J., R. Cao, C. Wigren, and P. Pianetta. 1994. *Journal of Vacuum Science & Technology A* 12:1869.

Terry, J., M. R. Linford, R. Cao, J. Terry, P. Pianetta, and C. E. D. Chidsey. 1996a. In the proceedings of the *First International Conference on Synchrotron Radiation in Materials Science*, Chicago, IL., submitted.

Terry, J., M. R. Linford, C. Wigren, R. Cao, P. Pianetta, and C. E. D. Chidsey. 1996b. *Applied Physics Letters,* in press.

Terry, J., C. Wigren, R. Cao, P. Pianetta, M. R. Linford, and C. E. D. Chidsey. 1997a. in prep.

Terry, J., C. Wigren, R. Cao, P. Pianetta, M. R. Linford, and C. E. D. Chidsey. 1997b. in prep.

Thomas, R.E., R.A. Rudder, and R.J. Markunas. 1991. *Chemical Perspectives of Microelectronic Materials II Symposium* 204:327.

Whitman, L.J., S.A. Joyce, J.A. Yarmoff, F.R. McFeely, and L.J. Terminello. 1990. *Surface Science* 232:297.

Wittmer, M., and J. L. Freeouf. 1992. *Physical Review Letters* 69:2701.

Wittmer, M., and J. L. Freeouf. 1993. *Physics Letters A* 173:190.

Yeh, J. J., J. Hwang, K. Bertness, D. J. Friedman, R. Cao, and I. Lindau. 1993. *Physical Review Letters* 70:3768.

Figure III.1: Comparison of valence band spectra from the H–Si(111) and Si(111) 7x7 surfaces shows that the two surface states S1 and S2 were removed by etching indicating that surface dangling bond were saturated.

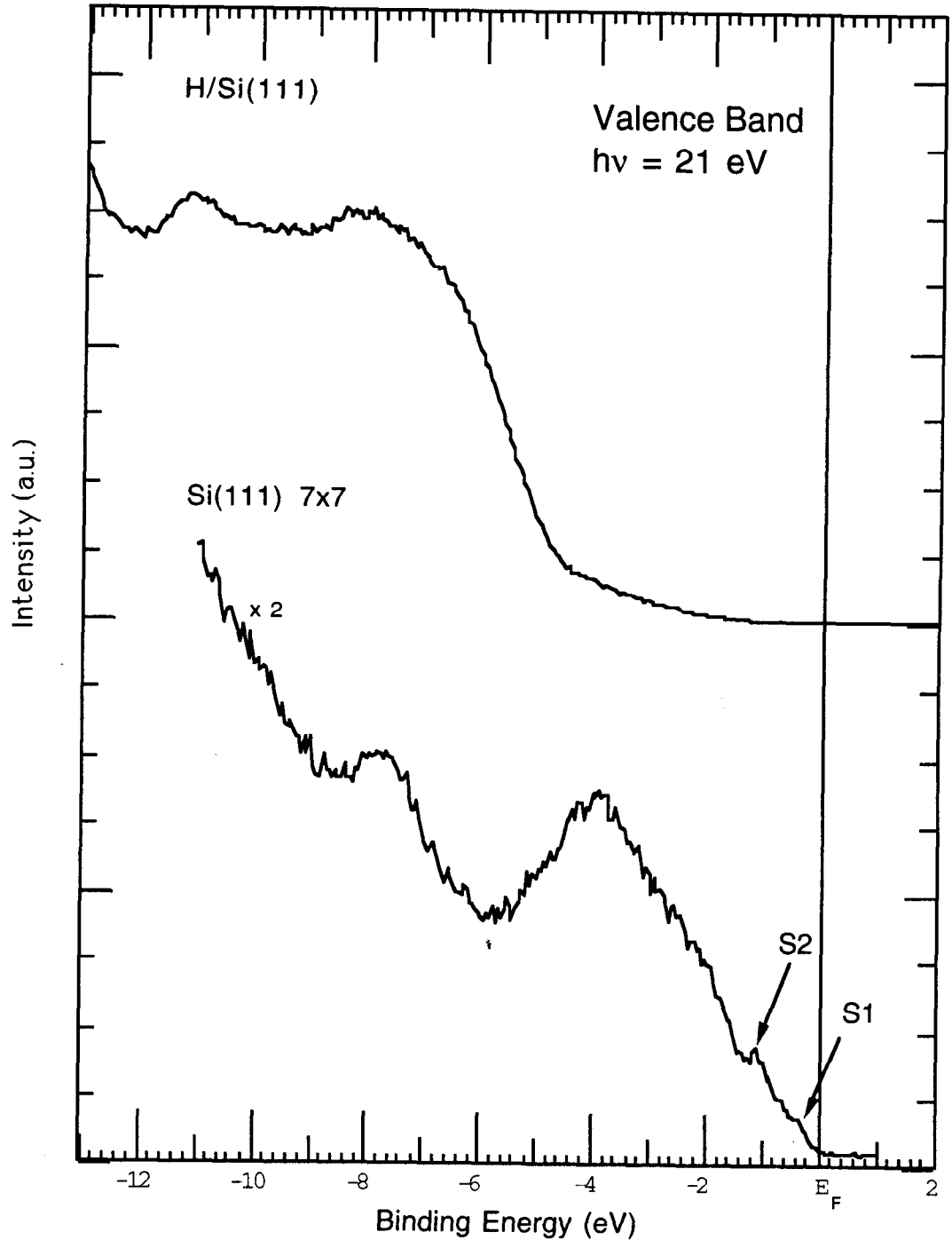

Figure III.2: Silicon 2p core level spectra taken with a photon energy of 130 eV with different Au coverages on H–Si(111) are shown. Some spectra have been taken at different pass energies and scaled to fit in the figure. The labeled features are discussed in the text.

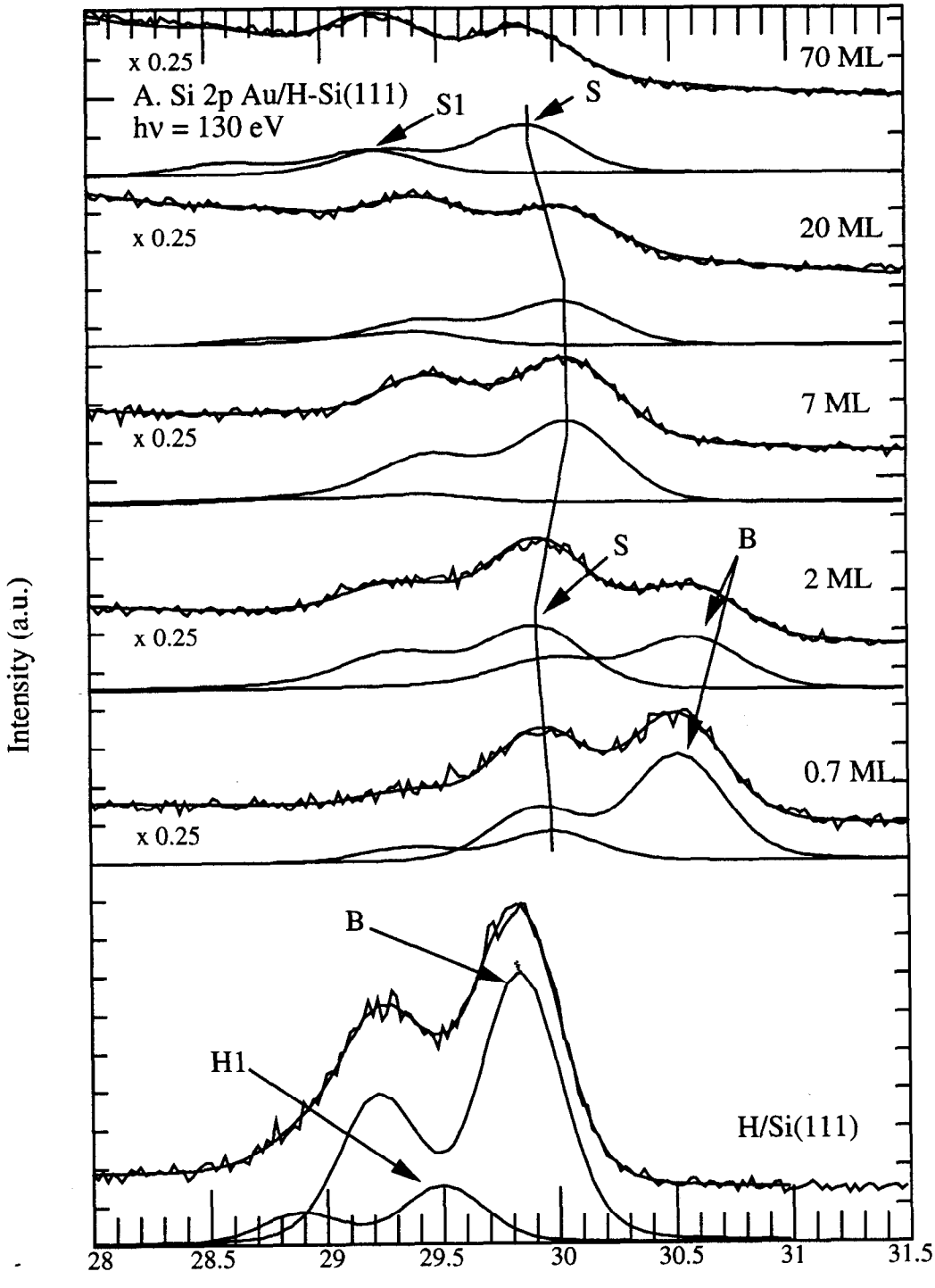

Figure 1A

Figure III.3: As in Figure III.2 except the spectra were taken with a photon energy of 110 eV.

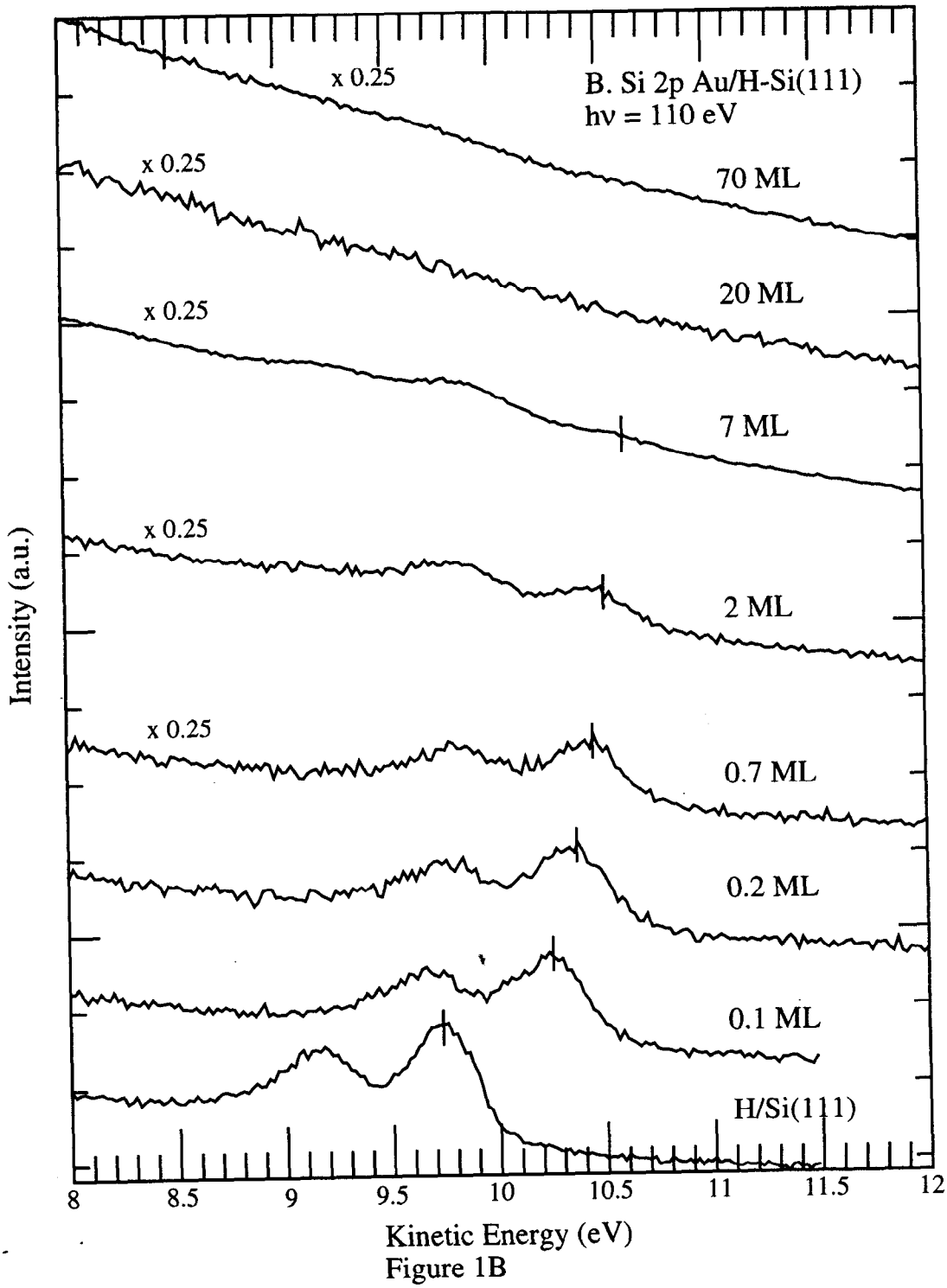

Figure 1B

Figure III.4: As in Figure III.2 except the substrate was p–type H–Si(111).

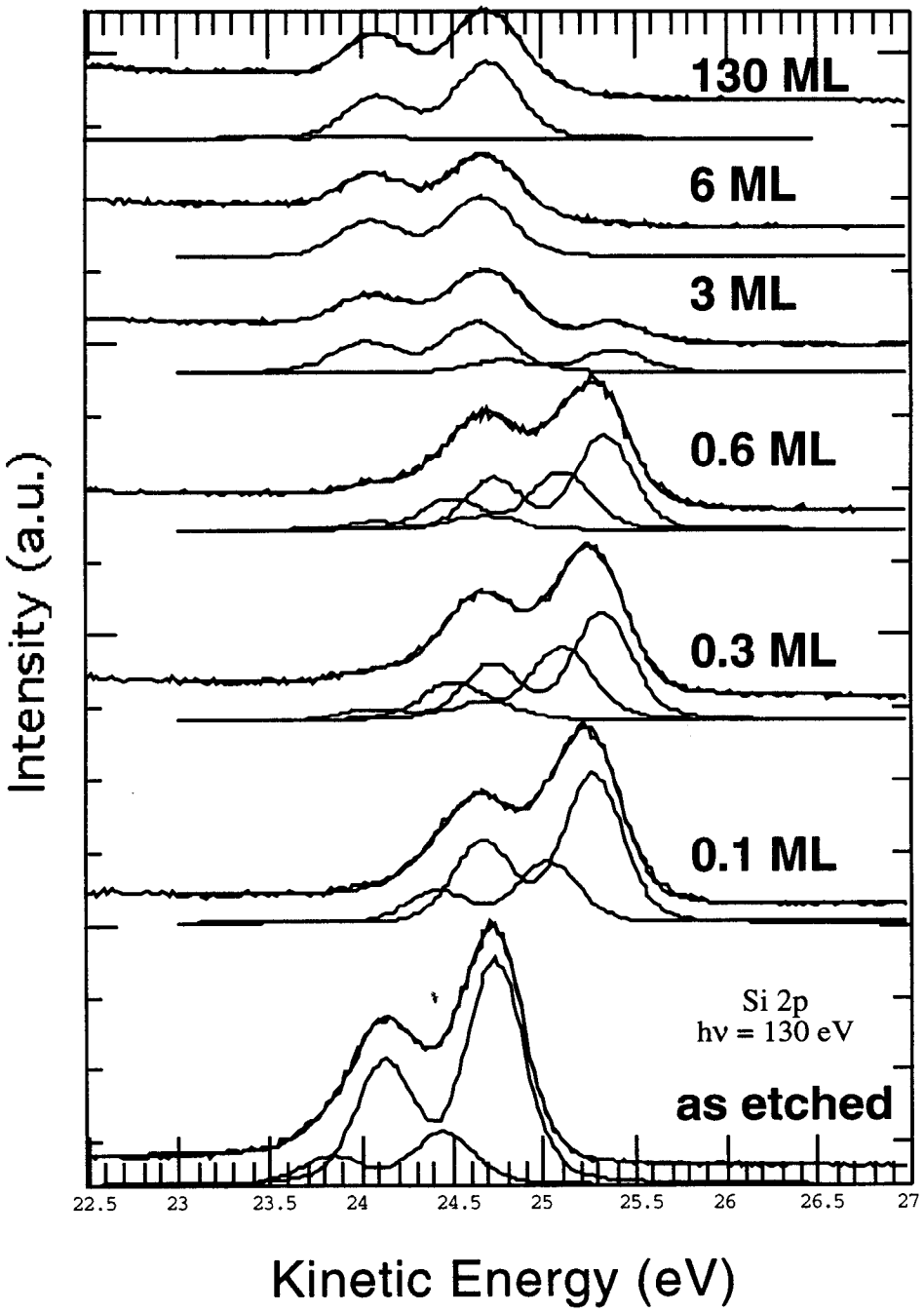

Figure III.5: Au 4f core level spectra from p–type Au/H–Si(111) taken with a photon energy of 130 eV.

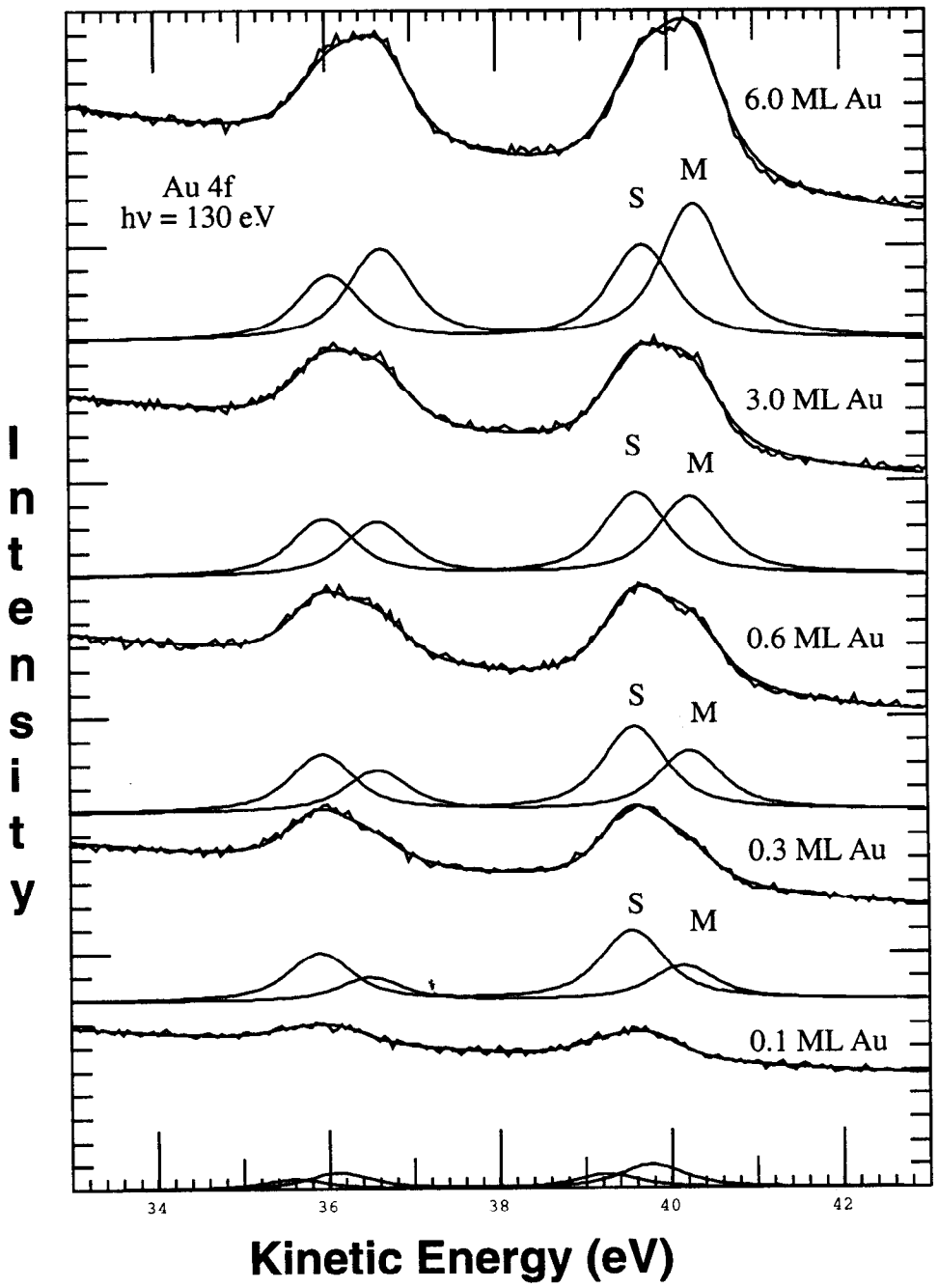

Figure III.6: Valence Band spectra taken at normal emission with a photon energy of 27 eV with different Au coverages are shown.

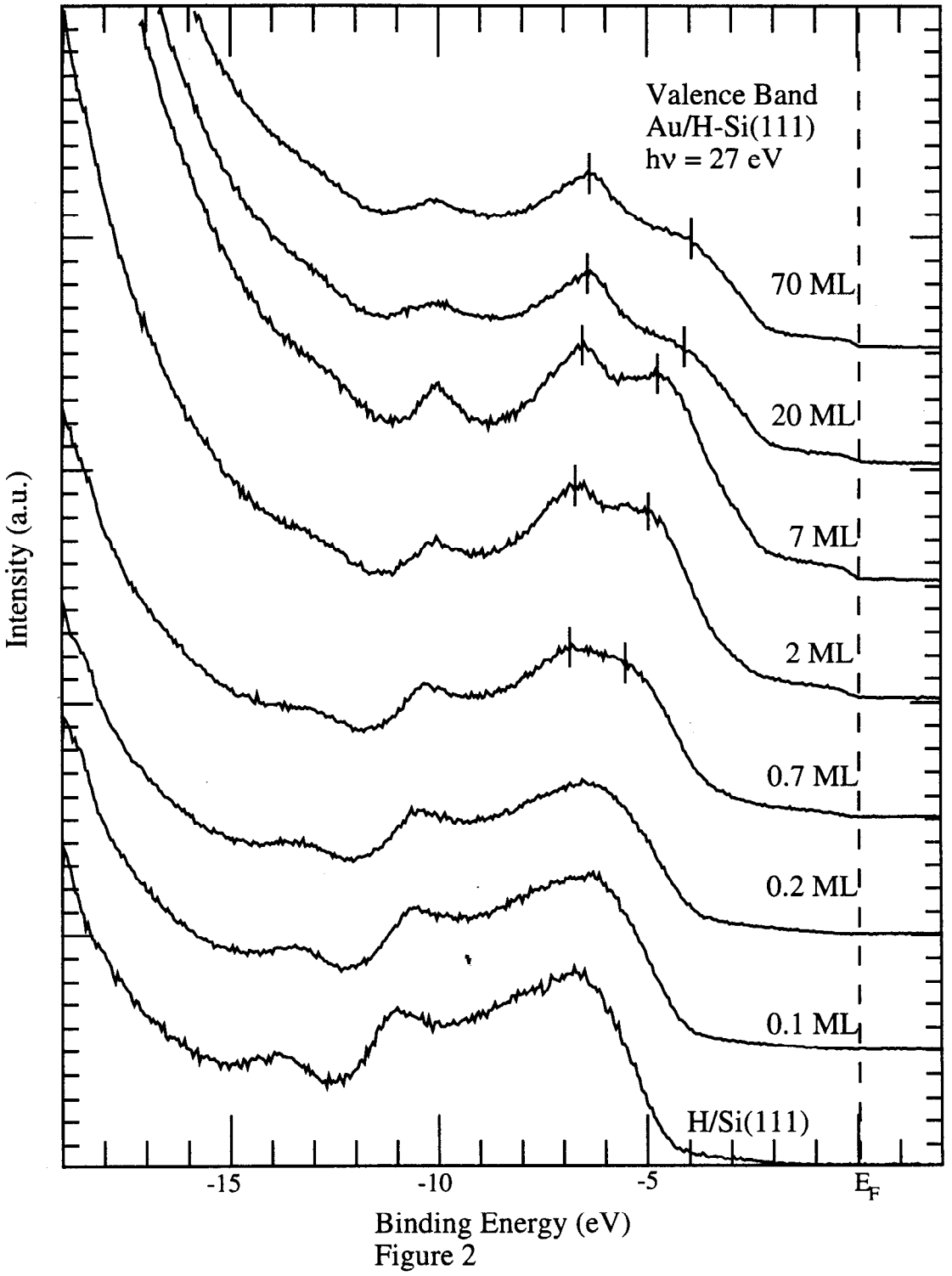

Figure 2

Figure III.7: Silicon 2p core level spectra taken at a photon energy of 130 eV with different Ge coverages are shown.

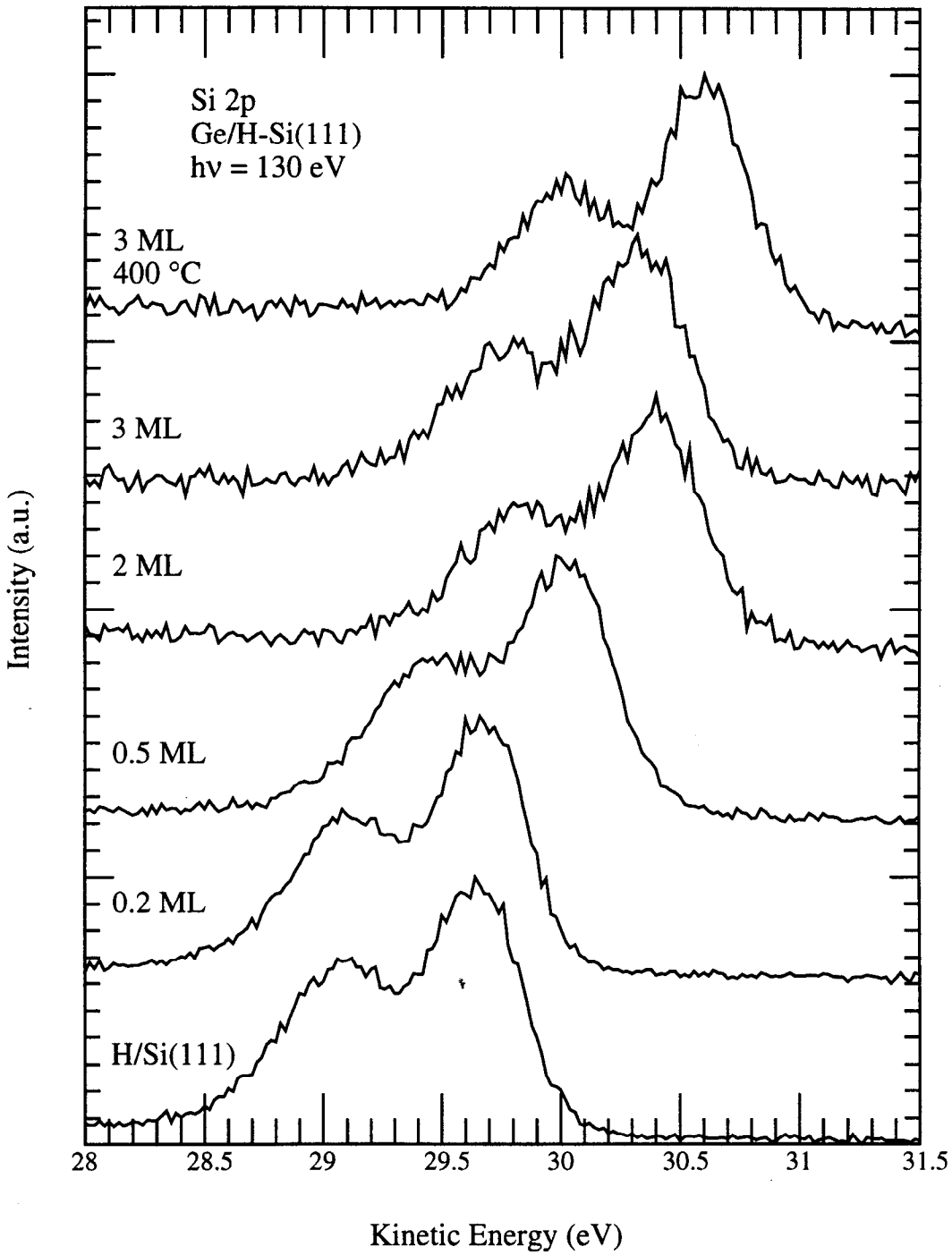

Figure 3

Figure III.8: Silicon 2p core level spectra taken at a photon energy of 110 eV with different Ge coverages are shown.

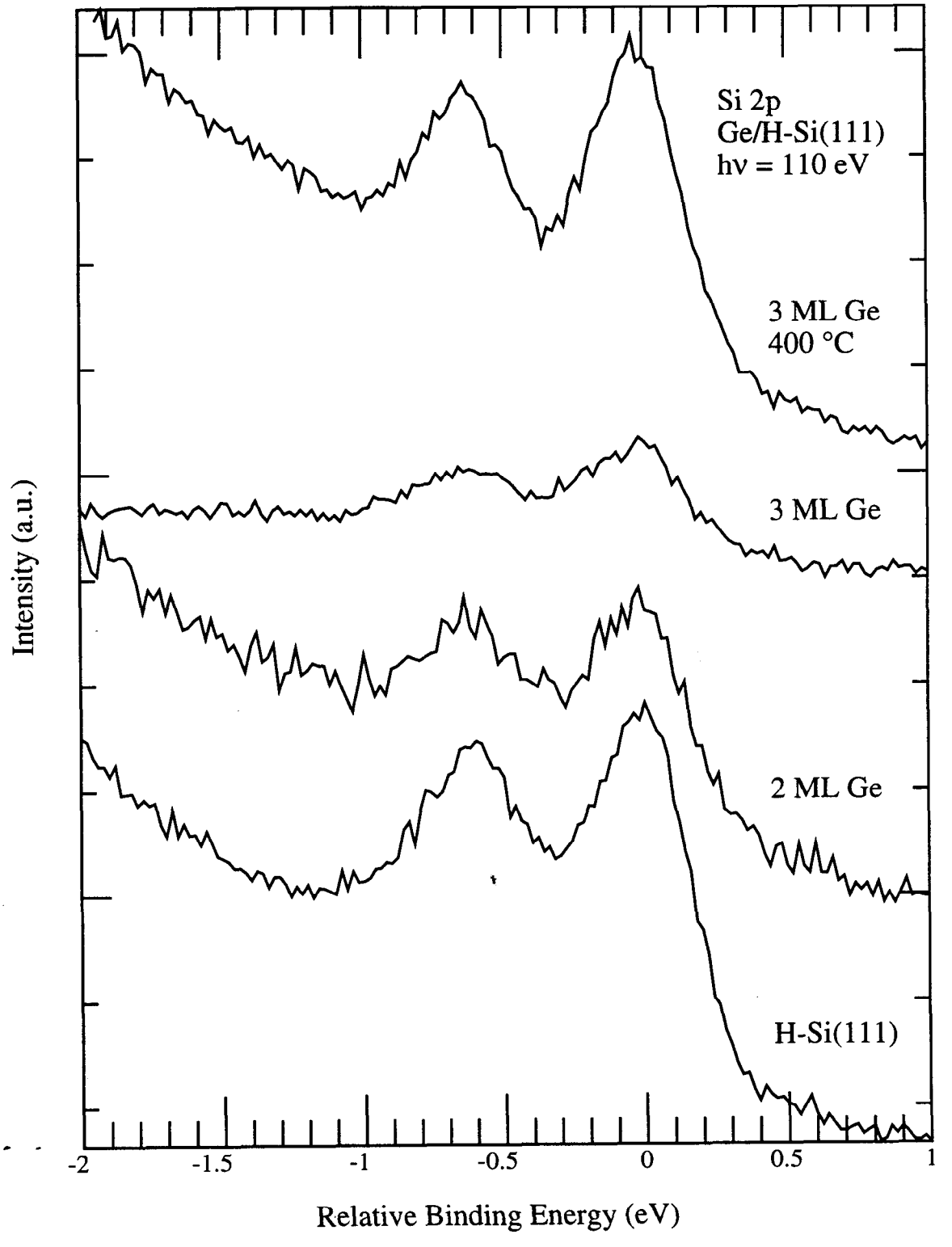

Figure III.9: Germanium 3d core level spectrum from Ge/H–Si(111) before and after annealing is shown. A reference spectrum from a 3 ML Ge film after surfactant growth with antimony on a Si(111) substrate.

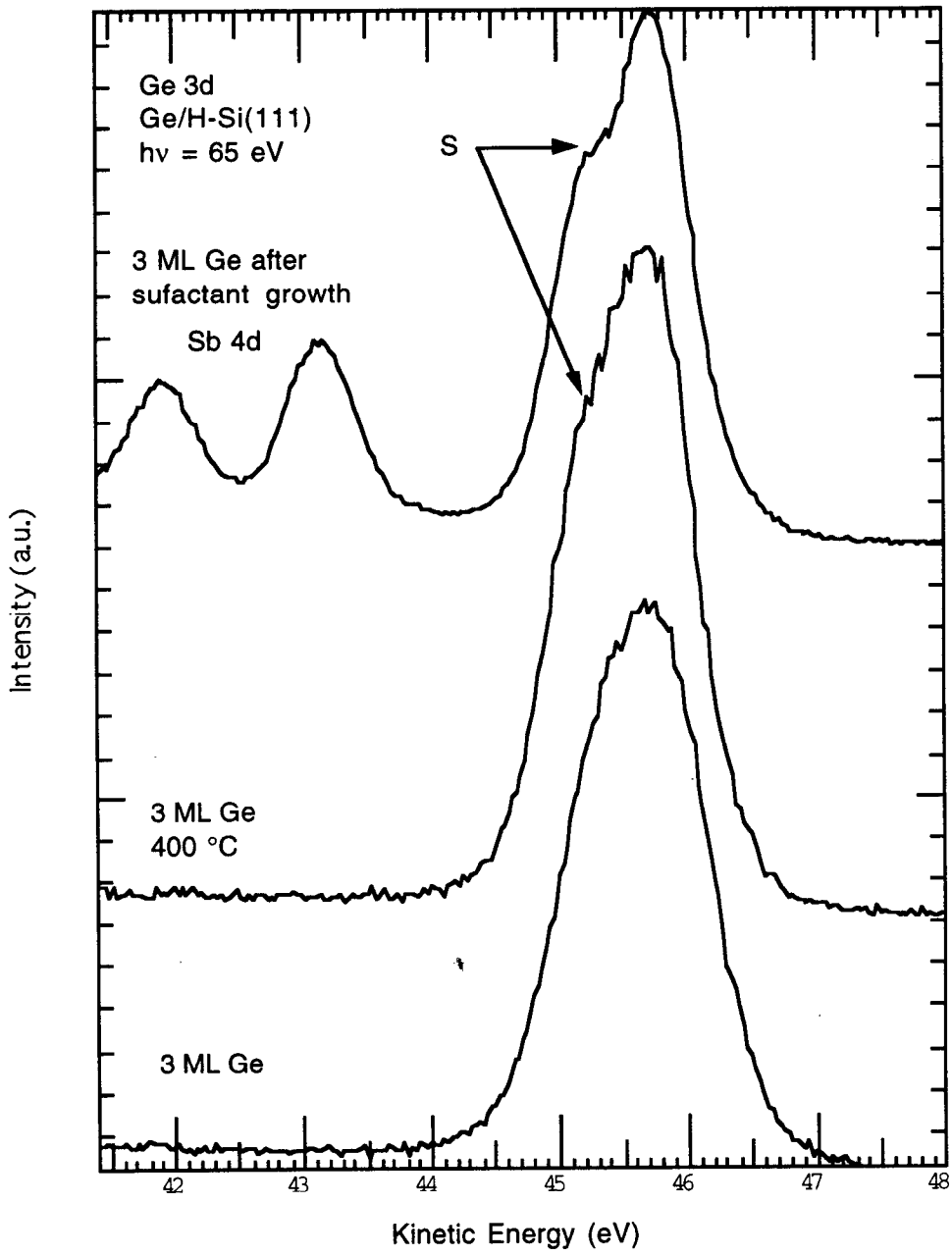

Figure III.10: Silicon 2p core level spectra from HF etched Si(111) exposed to O_2 in vacuum are shown. These spectra were taken at a photon energy of 130 eV.

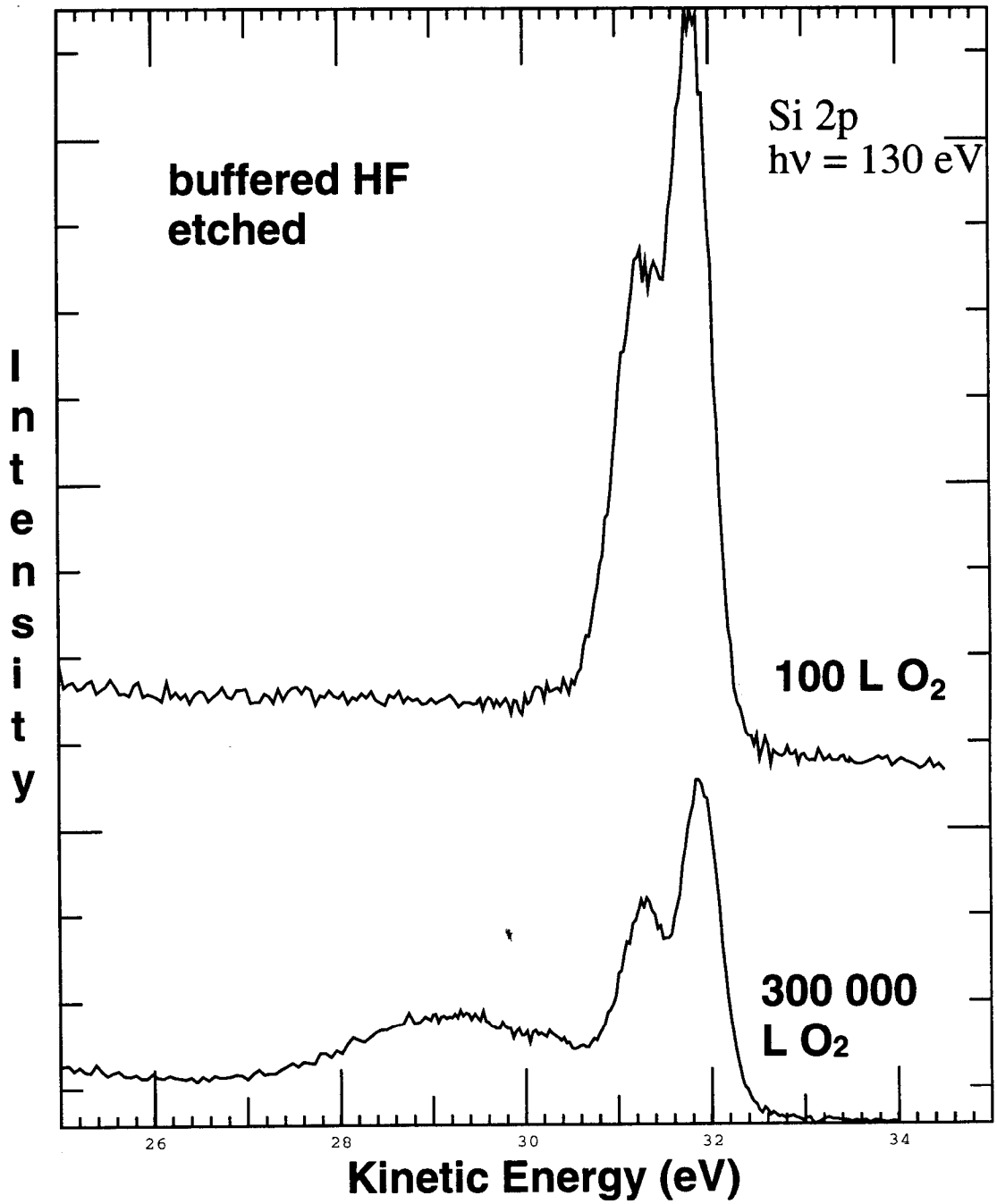

Figure III.11: Same as Figure III.10 except the samples were etched with NH_4F instead of HF.

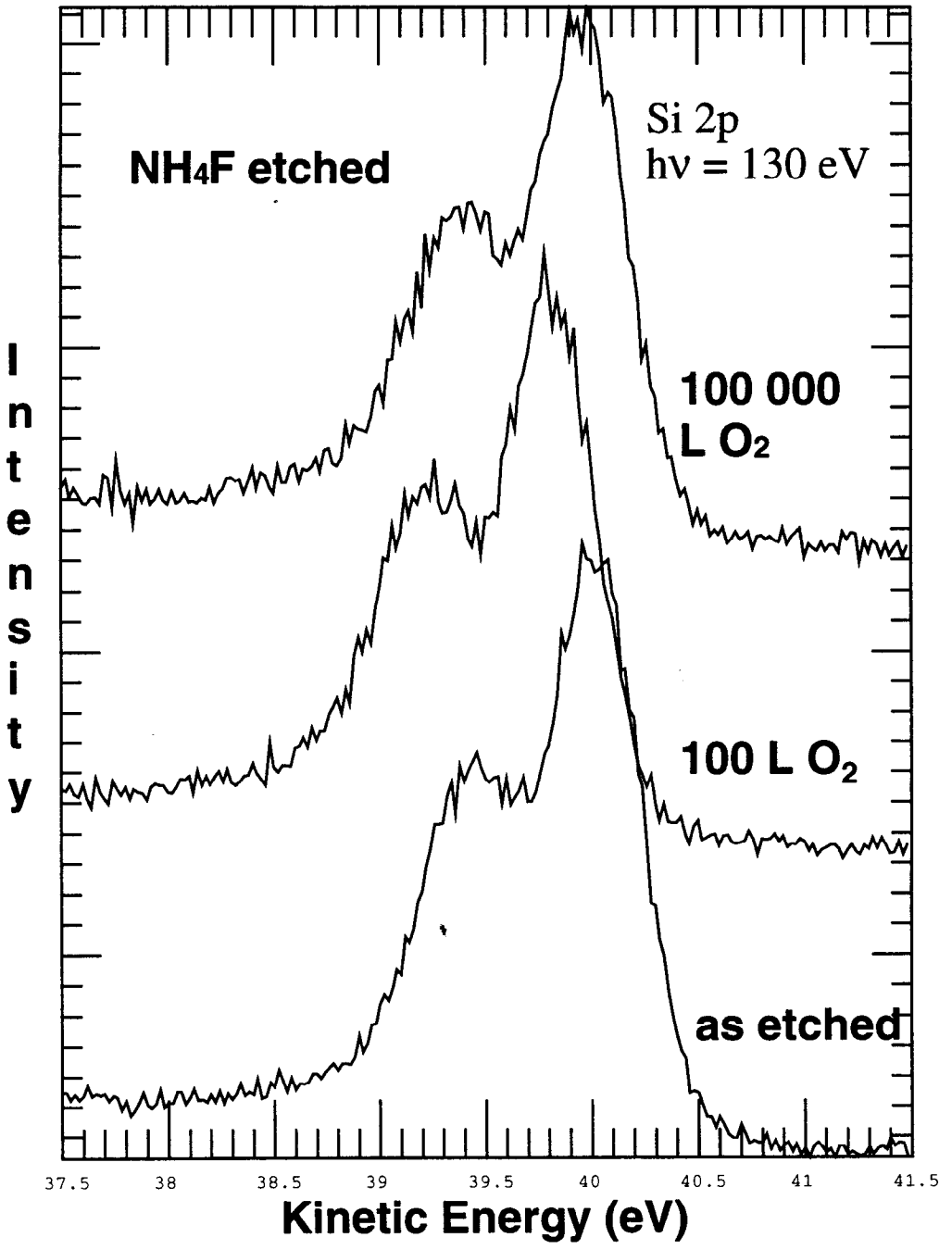

Figure III.12: Si 2p core level spectra for H–Si(111), Cl_2 exposed H–Si(111), and Br_2 exposed H–Si(111) taken at a photon energy of 130 eV. These spectra have been decomposed into two spin–orbit doublets. Clearly, replacement of H by the halogens was observed.

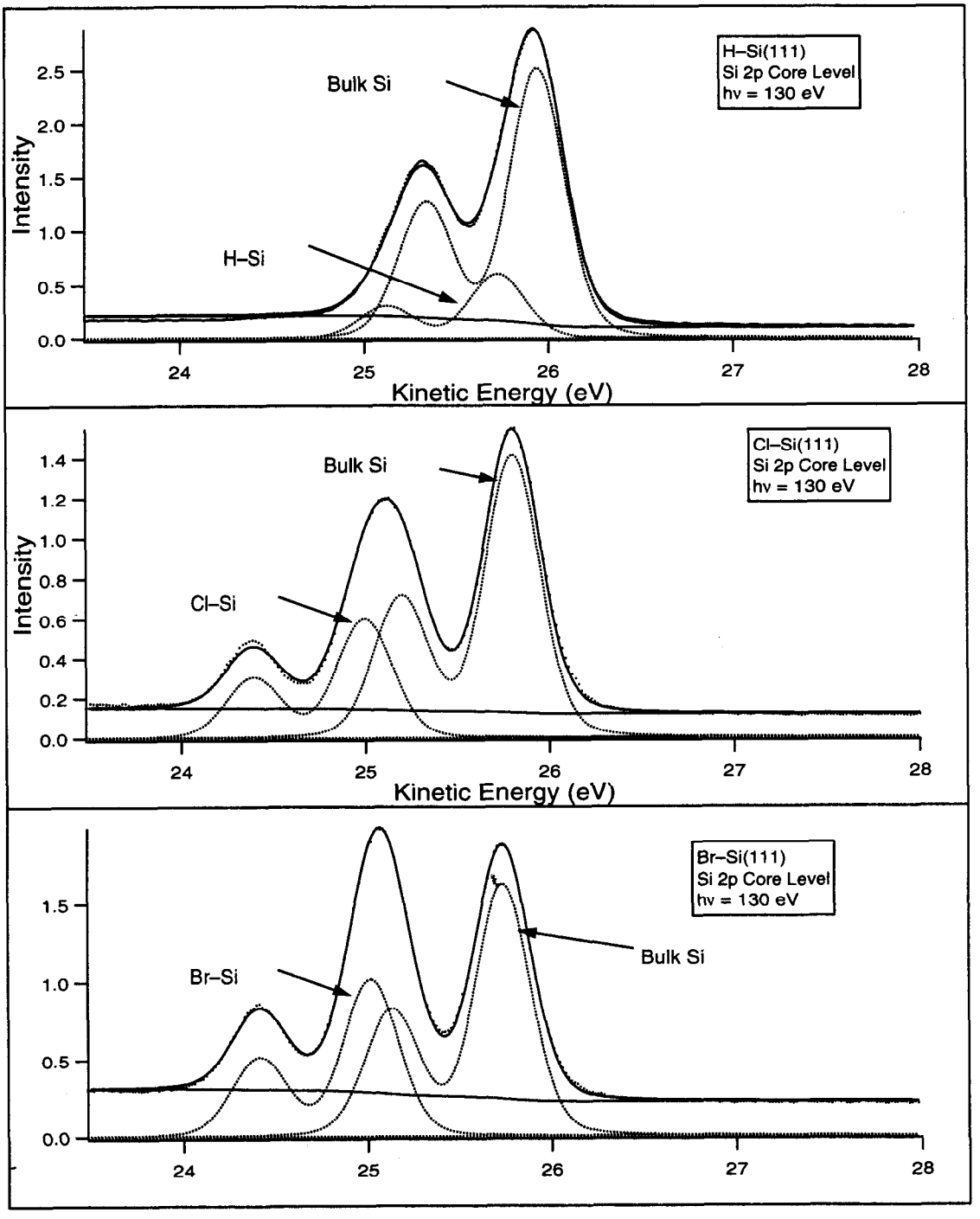

Figure III.13: Comparison of the Si 2p core level from a H–Si(111) surface exposed to Cl_2 in vacuum in total darkness and from one exposed to Cl_2 under UV illumination and transferred through air into the vacuum chamber.

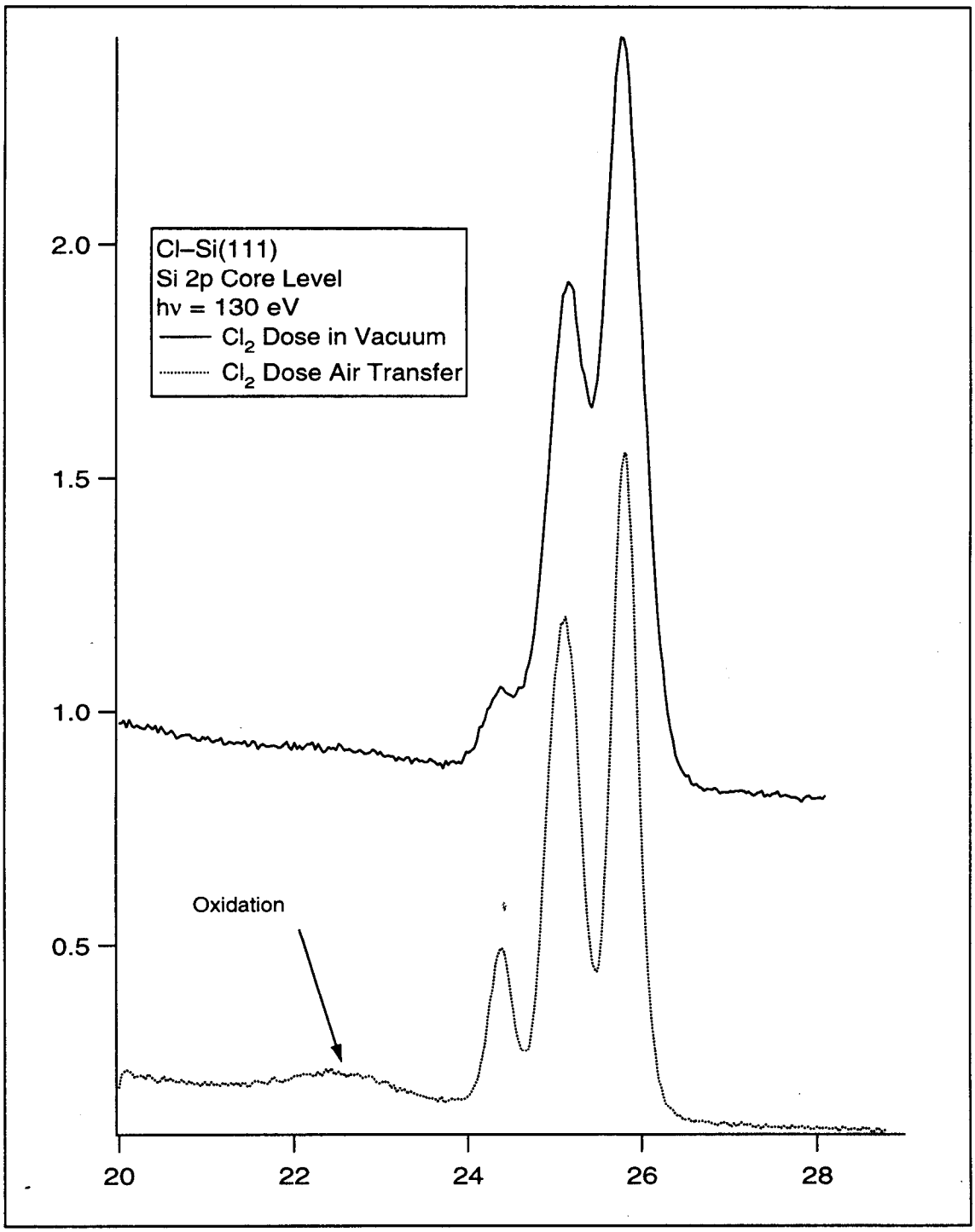

Figure III.14: A valence band spectrum from H–Si(111) exposed to 1–pentene is shown. Note that the C 2s region (-12 to -22 eV) provides a means of identifying the surface species because the number of components observed is equal to the number of C atoms in the chain. The solid vertical lines are referenced gas phase binding energies of the C 2s based molecular orbitals in n–pentane(Potts and Streets 1974) See text for an explanation of the referencing procedure.

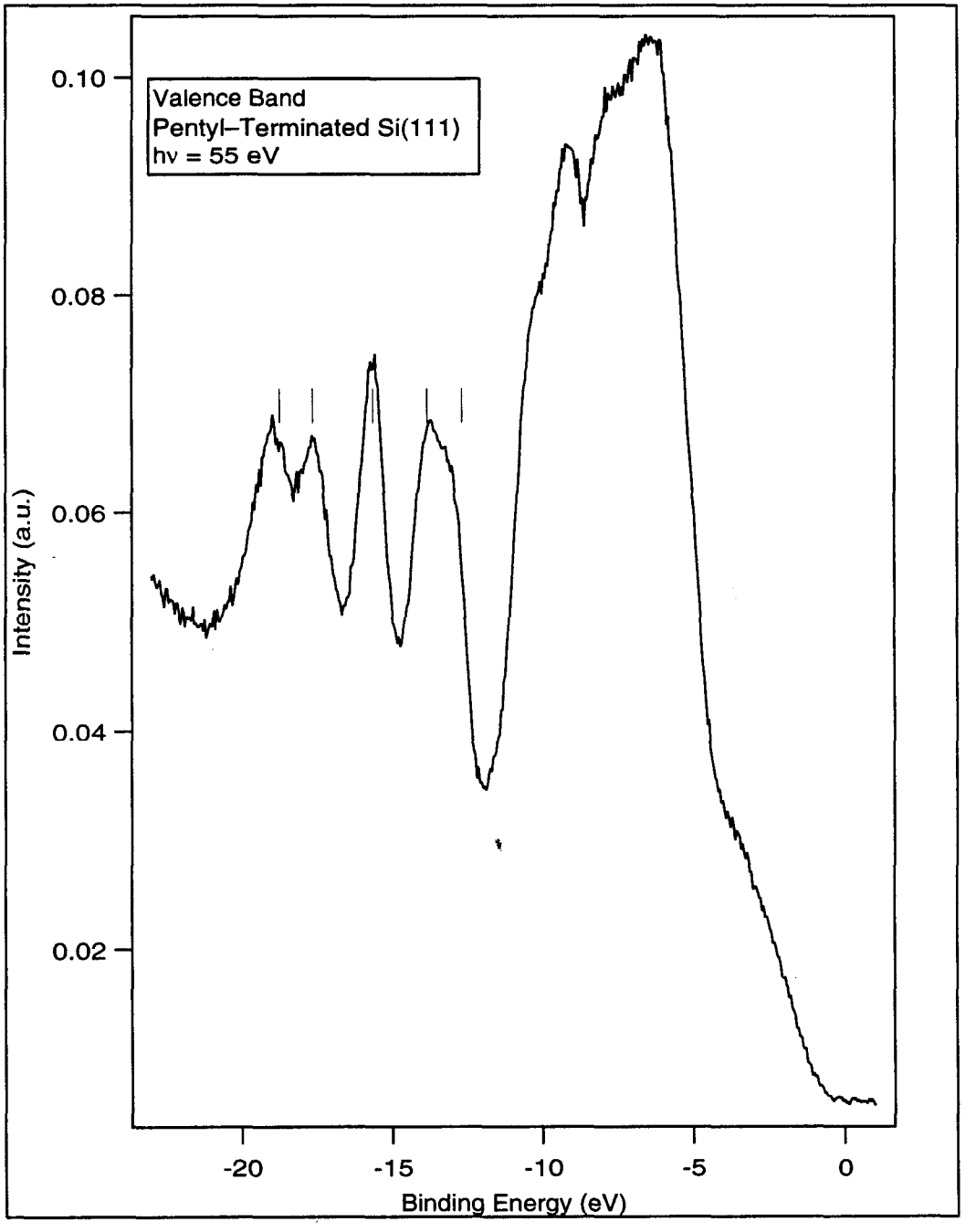

Figure III.15: Surface sensitive Si 2p core level spectra from methyl–terminated Si(111) and H–Si(111) surfaces exposed to 1–pentene and 1–decene taken at a photon energy of 130 eV. **The spectrum from a H–Si(111) sample exposed to 1–octadecene was taken with a photon energy of 120 eV because a larger electron escape depth was necessary in order to increase the signal strength of the Si 2p core level. This spectrum was then aligned with those of the short chains.

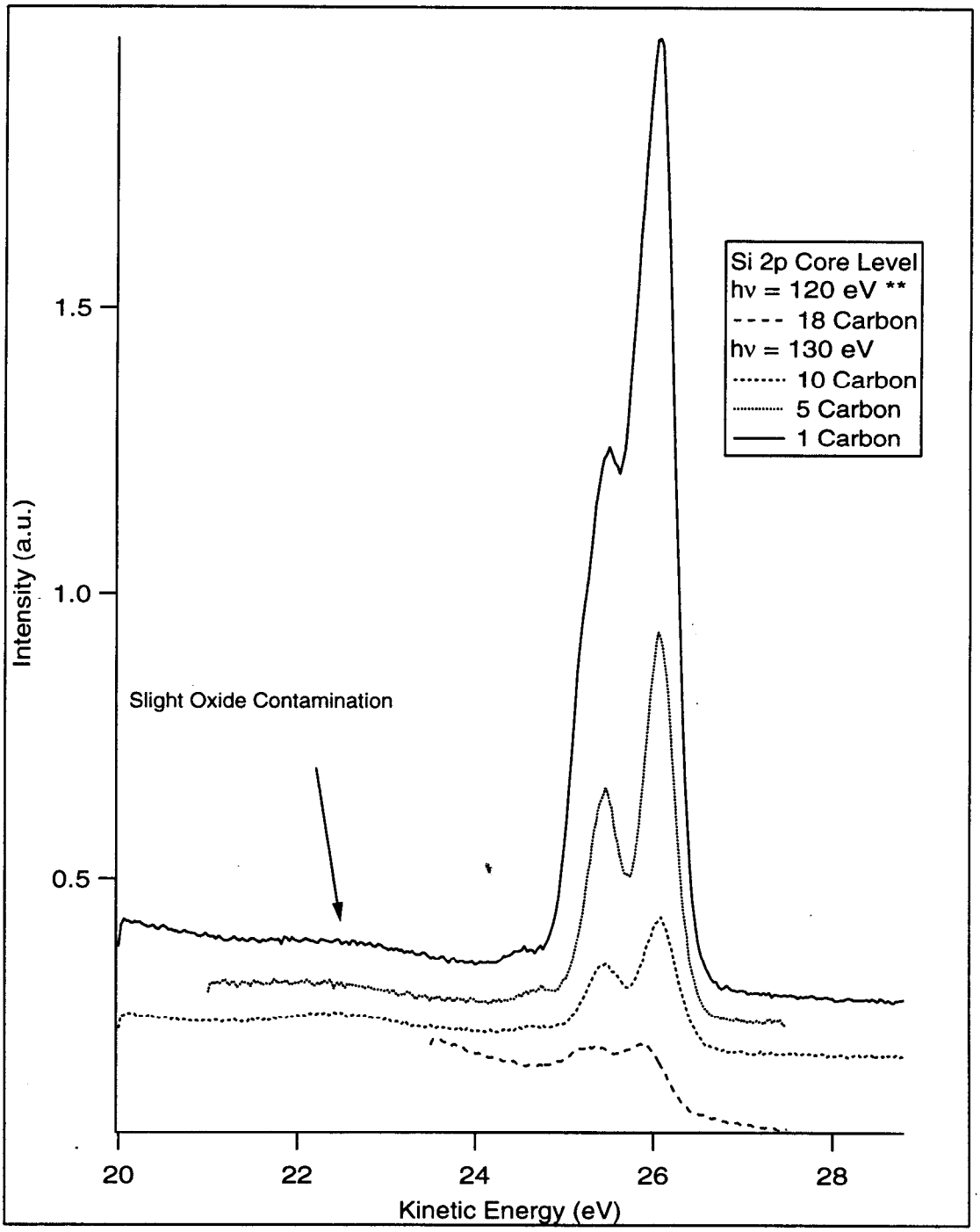

CHAPTER IV. ALKYL–TERMINATED Si(111) SURFACES

IV.1. ABSTRACT

This chapter describes the characterization of the first alkyl–terminated Si(111) surfaces prepared using methods of synthetic chemical synthesis based upon standard organic functional group reactions proposed by Linford and Chidsey(Linford and Chidsey 1993; Linford et al. 1995). Semiconductor surfaces terminated with organic functional groups are of great interest in gas and biochemical sensor development and as passivation layers for semiconductors were an oxide film cannot be used. The alkyl–terminated silicon surfaces were characterized using both valence band and core level photoelectron spectroscopy (PES), scanned–energy, chemical–shift photoelectron diffraction (PED), and near–edge x–ray absorption spectroscopy (NEXAFS). The valence band spectra from these surfaces have a fingerprint region characteristic of alkanes from which the alkyl group on the silicon surface can be identified. C 1s and Si 2p core level spectra consisted of two components. By using the intensity changes of the two components as the alkyl chain length was varied, it was possible to assign the components to emission from bulk–like Si atoms, Si atoms bonded to C, C bonded to Si, and bulk–like C atoms in the alkyl chain. The direction of the chemical shifts of these components indicated charge transfer from the Si to C. Therefore, the alkyl chains are bound to the silicon surface. Scanned–energy, chemical–shift photoelectron diffraction data from the component of the C 1s core level spectrum assigned to the C atom bound to the Si surface was analyzed to determine a Si–C bond length of 1.85 Å. The C K–Edge NEXAFS data consisted of three main features, assigned to σ^*(C–H) and σ^*(C–C) absorption. The position of the σ^*(C–C) orbitals was used to determine the C–C bond length of 1.53 Å in the alkyl chain. Using polarization dependent C K–edge NEXAFS data, it was determined that the alkyl chains were tilted 33° with respect to the surface normal. It was then possible to combining these individual pieces of the puzzle in order to arrive at a complete picture of the local bonding geometry of the

alkyl chains at the Si(111) surface. Finally, the decomposition of the alkyl chains upon annealing was studied. The alkyl chains did not fragment upon annealing, desorption of the chains occurred along with the formation of a silicon–carbon alloy.

IV.2. INTRODUCTION

This work describes the characterization of the first alkyl–terminated Si(111) surfaces prepared using standard organic functional group chemical methods proposed by Linford and Chidsey(Linford and Chidsey 1993; Linford et al. 1995). The placement of organic functional groups on semiconductor surfaces is of great interest in gas and biochemical sensor development and as passivation layers for semiconductors were an oxide film cannot be used. Historically, Langmuir–Blodgett (LB) methods(Blodgett 1934; Blodgett 1935; Langmuir 1920) have been used to prepare thin organic films on semiconductor surfaces. These Langmuir–Blodgett films have been the subject of much recent inquiry(Petty 1996). The application of LB techniques to silicon surfaces deserves special mention due to the promise of placing reactive organic functional groups on a surface that can be married to conventional semiconductor device technology. Recent studies reporting on the modification of silicon surfaces using LB techniques(Krull, Brown, and Safarzadeh-Amiri 1988; Larkins, Fung, and Rickert 1989; Outka et al. 1988; Outka et al. 1987; Schedel-Niedrig et al. 1991) have shown possible applications as biosensors(Krull, Brown, and Safarzadeh-Amiri 1988) and as field effect transistors (FET's)(Larkins, Fung, and Rickert 1989). The general orientation of certain LB films on silicon have even been obtained(Outka et al. 1988; Outka et al. 1987; Schedel-Niedrig et al. 1991). Unfortunately, the organic thin films made using LB techniques have an oxide layer at the interface which can influence device characteristics. However, it will be shown that a monolayer of an organic functional group can be directly attached to Si(111) surfaces without the need of LB techniques and thus without an intervening oxide layer by using the methodology of Linford and Chidsey(Chidsey and Linford 1995; Linford and Chidsey 1993; Linford et al. 1995).

Preliminary evidence of monolayer formation had been gained from infrared absorption spectroscopy, low–resolution X–ray photoelectron spectroscopy, ellipsometry, X–ray reflectivity, and contact angle measurements(Linford and Chidsey 1993; Linford et al.

1995). These preliminary studies have indicated that the monolayers are extraordinarily stable in atmosphere and under harsh conditions such as boiling solvents and boiling aqueous acids, but had provided no direct evidence of surface bonding. The fundamental questions about the orientation and bonding of the alkyl chains to the silicon surface were probed using the techniques of valence band (VB) and core level photoelectron spectroscopy to determine the electronic structure of the interface, using scanned–energy, chemical–shift photoelectron diffraction (PED) on the C 1s core level to determine the local bonding geometry at the interface, and using polarization dependent C K–Edge Near–edge x–ray absorption spectroscopy (NEXAFS) to determine the orientation of the alkyl chain.

VB photoemission spectra of alkanes possess a fingerprint region due to the formation of bonding and antibonding molecular orbitals in the alkane. As n carbon atoms are brought together to form the alkane, the n C 2s orbitals form bonding and anti–bonding combinations (molecular orbitals). The number of molecular orbitals formed is equal to the original number of C 2s orbitals (i.e. the number of C atoms) as has been observed in valence band spectra obtained from gas phase alkanes(Hamrin et al. 1968; Pireaux et al. 1986; Potts and Streets 1974), condensed alkanes(Pireaux et al. 1986), and from ethyl–terminated silicon surfaces(Lapiano-Smith, Himpsel, and Terminello 1993). This fingerprint region was observed in the valence band spectra from the samples prepared using the methodology of Linford and Chidsey(Chidsey and Linford 1995; Linford and Chidsey 1993; Linford et al. 1995). Therefore, it was certain that alkyl chains were present on the silicon surface. However, were the alkyl chains strongly bound to the silicon atoms or were they weakly physisorbed?

Core level photoemission spectra(Hufner 1995) have been shown to be very sensitive to the local chemical environment of the emitting atom. The C 1s and Si 2p photoemission spectra from these samples were decomposed into two components. It was possible to use the intensity behavior. In both cases, it was possible to assign a component to bulk–like emission from silicon atoms deep in the crystal (Si 2p spectra) or to carbon atoms in the alkyl chain (C 1s spectra). For reasons to be discussed in detail later in this Chapter, the other components were then attributed to emission from the C or Si atoms at the interface

between the alkyl monolayer and the silicon crystal. The presence of interfacial components in the spectra from these samples strongly suggests that strong chemical bonding occurred between the alkyl group and the silicon surface. However, what is the local bonding geometry of the C–Si interface?

Recently, photoelectron diffraction (PED) has been used to determine the geometric structure of many surface adsorbates(Fadley 1988; Fadley et al. 1994). In a PED measurement, the photoemission process creates a free electron that propagates away from the emitting atom as a spherical wave which undergoes scattering from neighboring atoms. At the detector, the scattered waves interfere with the unscattered, primary wave. This interference is observed as variation in emitted electron intensity as a function of electron wave vector (**k**). As long as the initial state is localized in space, the photoelectron diffraction pattern is highly site specific. Weiss, *et. al.*(Weiss et al. 1992; Weiss et al. 1993)have demonstrated the ability of chemical–shift, scanned–energy, photoelectron diffraction to determine the local geometric structure of adsorbate atoms in chemically different environments. This technique was used to determine the local geometric structure of the alkyl chains at the interface. C 1s core level spectra were collected at different photon energies, the observed core level spectra were decomposed into chemically–shifted components at each photon energy. The observed intensity modulations of the C 1s component attributed to the interfacial C atom was then used to determine the local bonding geometry of the surface species. It was determined that this C atom was located in an atop site with a Si–C bond length of 1.85±0.05 Å. Assuming sp^3 hybridization, one would then expect the alkyl chain to be tilted ~30° with respect to the surface normal, could the geometry of the alkyl chain be determined?

The NEXAFS spectra from oriented hydrocarbons(Outka et al. 1988; Outka et al. 1987; Schedel-Niedrig et al. 1991) consist of three major features, one assigned to transitions to σ^*(C–H) states and two assigned to transitions to σ^*(C–C) states. Using the polarization dependence of these features, it was possible to determine the tilt angle of the alkyl chains relative to that of known standard compounds. The standard compounds used to determine the tilt angle of the alkyl monolayers were Ca Arachidate and Cd Arachidate(Outka et al.

1988; Outka et al. 1987) with known tilt angles of 33° and 0° with respect to the surface normal, respectively. By comparison to the published standards, it was determined that the alkyl chains tilt 33° with respect to the surface normal. Furthermore, it was possible to determine the C–C bond length in the alkyl chain by determining the distance of the peak position of the σ^*(C–C) orbitals from the C 1s ionization potential using a technique dubbed "bond length with a ruler"(Stohr, Sette, and Johnson 1984). The C–C bond length in the alkyl monolayers was determined to be 1.53 Å. Since the fundamental questions about the interfacial structure had been determined, the questions turned to practical applications of the alkyl monolayers. Could the monolayers be removed by annealing and what were the intermediary products?

The alkyl monolayers were annealed to various incremental temperatures, after the samples cooled to room temperature, photoemission spectra were collected. It was determined that the alkyl monolayers did not fragment into smaller chains. Most of the chains desorbed by a temperature of 350°C, however, evidence of silicon carbon alloying was observed. The alloy disappeared when the annealing temperature reached 700°C. Therefore, the alkyl chains may be useful as a carbon source in silicon carbide thin film growth or by providing sp^3 hybridized C nucleation sites for diamond growth.

Therefore, by assembling all of the above information, it can be reported that densely packed monolayers of alkyl groups, $H_{2n+1}C_n$, with chain lengths (n) of 1 to 18, on Si(111) surfaces with no intervening oxide have been prepared using the methods of Linford and Chidsey(Chidsey and Linford 1995; Linford and Chidsey 1993; Linford et al. 1995).

IV.3. EXPERIMENTAL

IV.3.1. Sample Preparation and Transportation

The preparation of the alkyl–terminated Si(111) surfaces was described in great detail in the Ph.D. thesis of Matt Linford(Linford 1996). Therefore, only a brief summary of the sample preparations will be given here.

First, the silicon wafer was cleaned and a chemical oxide film was grown. The oxide film

was grown using the following procedure(Linford et al. 1995): immersion in a 50/50 solution of conc. H_2SO_4 and 30% H_2O_2 at 100°C for 1 hour. The wafer was then removed from this solution and rinsed in deionized H_2O to remove all traces of the previous solution. After this step the H_20 was observed to spread out in a thin layer across the surface, indicative of the formation of a hydrophillic oxide layer. The wafer was then placed in a 50/50 mixture of 30% H_20_2 and conc. NH_4OH for 30 minutes, followed by another deionized H_2O rinse. The wafer was again immersed in a 50/50 solution of conc. H_2SO_4 and 30% H_2O_2 at 100°C for 1 hour. After which the surface was rinsed in deionized H_2O to remove all traces of the previous solution and then blown dry with dry nitrogen leaving a uniform oxide film on the silicon wafer.

Second, the oxide film was removed by etching in 40% aqueous NH_4F for 10 minutes producing a uniform H–terminated Si(111) surface. This procedure was first described by Higashi, Chabal, and coworkers(Higashi et al. 1990). This preparation was chosen because the resultant surface has been shown to have a low step density along with large, uniform terraces, i.e. a nearly ideal starting surface for chemical synthesis.

At this point, the method of preparation of the alkyl–terminated Si(111) surface diverged depending upon the length of the desired alkyl chain. For alkyl chains, $H_{2n+1}C_n$, with chain lengths, n, greater than 4, the preparation was as follows: the H–Si(111) surface was placed into a glass manifold vacuum system and evacuated to a base pressure below 5 x 10^{-5} torr. Five to six grams of the corresponding 1–alkene, $H_{2n}C_n$, were placed into a flask located elsewhere on the vacuum line. The alkene was pumped below the base pressure for three hours while being constantly stirred to remove dissolved oxygen. The H–Si(111) surface was then exposed to the deoxygenated 1–alkene, for 12–24 hours to form the alkyl–terminated surface.

For alkyl chains, $H_{2n+1}C_n$, with chain lengths, n, less than or equal to 4, the preparation was slightly more complicated. First, the H on the H–Si(111) surface was replaced with Cl. This was accomplished by exposing the H–Si(111) surface to Chlorine gas (Matheson, 99.999%). The residual Cl was pumped away. Finally, using a metal cannula described

elsewhere(Linford 1996), the Cl–Si(111) surface was immersed in the corresponding alkyl lithium, $H_{2n+1}C_nLi$, reagent (methyllithium 1.4 M solution in diethyl ether, Aldrich; and butyllithium 2.5 M solution in hexanes, Aldrich). After exposures of 12–24 hours, excess alkyl lithium reagent was removed using cannula transfer. The alkyl–terminated silicon was then rinsed with a 50:1 mixture of tetrahydrofuran (THF) and conc. HCl, followed by a deionized H_2O rinse. The surface was then dried with an inert gas (Ar).

After preparation the alkyl–terminated silicon samples were transported to the Stanford Synchrotron Radiation Laboratory for analysis. The wafers were placed in vials sealed with a viton septum. The septum was puncture with two needles, one used as an Ar inlet and the other acted as a purge. After the vial was filled with Ar, the sample was transported to the Synchrotron, mounted on a sample holder, and placed into the analysis chamber. Exposure to atmosphere was limited in order to reduce the risk of sample contamination.

IV.3.2. Photoemission Measurements

All measurements were performed at the Stanford Synchrotron Radiation Laboratory. The VB and Si 2p core level photoemission spectra were collected at BL 8–1. BL 8–1 uses a Toroidal Grating Monochromator (TGM). At this beam line, photons with energies between 10 and 200 eV were available for use, therefore, only valence band and low binding energy core levels could be studied. It was not possible to observe the C 1s core level (binding energy of 290 eV) at this beam line, necessitating the use of different samples for the respective studies. The analysis chamber used for these measurements consisted of a load–lock sample transfer system, a low energy electron diffraction analyzer (LEED), and a double pass Cylindrical Mirror Analyzer (CMA). Valence band spectra were obtained using a photon energy of 55 eV and an analyzer pass energy of 10 eV. Silicon 2p core level spectra were obtained using photon energies of 130 eV, 115 eV and 110 eV to observe relative intensity changes as the electron escape depth varied(Eastman, Himpsel, and van der Veen 1982; Hricovini et al. 1993). This aids in the assignment of the observed components. The total energy resolution (monochromator and analyzer) was determined to be 200 meV at a photon energy of 130 eV. Valence band and Si 2p core level spectra were collected from methyl–, butyl–, pentyl–, decyl–, and octadecyl–terminated

Si(111) surfaces.

The C 1s core level photoemission spectra were collected at BL 10–1. BL 10–1 uses a Spherical Grating Monochromator (SGM). This beam line has photons selectable within the energy range of 180 eV to 1000 eV. However, the usable energy range had an upper limit of 650 eV because of the use of a Ni refocusing mirror. This beam line was well suited for the study of the C 1s core level., but not acceptable for either valence band studies due to low cross sections at these energies or Si 2p core level studies due to large electron escape depths. The analysis chamber for the C 1s core level measurements consisted of a load–lock sample transfer system, a reverse–view LEED, and a 100 mm VSW hemispherical electron energy analyzer. The photon beam and the analyzer were fixed at an angle of 30°. Carbon 1s spectra were collected at a photon energy of 350 eV. The total energy resolution (monochromator and analyzer) was determined to be 150 meV at a photon energy of 350 eV. Carbon 1s core level spectra were collected from methyl–, pentyl–, decyl–, and octadecyl–terminated Si(111) surfaces.

All core level spectra were decomposed using the least–squared fitting procedure described in Chapter I. The Si 2p core level spectra were fit using spin–orbit split doublets with Voight lineshapes with a branching ration of 0.5, spin–orbit splitting of 0.605 eV and a Lorentzian linewidth of 0.053 eV FWHM. The C 1s spectra taken at Beam line 10–1 were fit using singlet Voight lineshapes with a Lorentzian linewidth of 0.342 eV FWHM.

IV.3.3. Chemical–Shift, Scanned–Energy Photoelectron Diffraction

Chemical–shift, scanned–energy photoelectron diffraction measurements were conducted on the C 1s core level at BL 10-1 system described above. Two main components are needed in a system capable of photoelectron diffraction measurements. A system designed to perform photoelectron diffraction measurements must be equipped with, first, a sample manipulator with sample motion with accurate 360° polar rotation and 360° azimuthal rotation; and second, an angle–resolving analyzer with small cone of angular acceptance. The angular reproducibility of the manipulator in this system was better than 0.25° and the angular acceptance of the hemispherical analyzer was ±1.5°.

The measurements were carried out on a pentyl–terminated Si(111) surface prepared using a 1–alkene and on a methyl–terminated Si(111) surface prepared using methyllithium. Carbon 1s photoemission spectra were collected at photon energies ranging from 300 eV to 650 eV. The processing of the C 1s spectra into a photoelectron diffraction spectrum will be described in detail later in this Chapter.

IV.3.4. Near–Edge X–Ray Absorption Spectroscopy

NEXAFS measurements were also performed at BL 10–1 using the above described system. The absorption spectra were measured simultaneously in Total Yield Mode, by measuring the sample refresh current which is proportional to absorption(Stohr 1992), and in Auger Yield Mode, by measuring the intensity of the C KLL Auger line, again which is proportional to the absorbtion(Stohr 1992). The sample refresh current was measured using a Keithley current amplifier placed between electrical ground and the sample. The Auger Yield was measured by setting the hemispherical analyzer at a kinetic energy of 239 eV with a pass energy of 50 V. Polarization depend studies were performed by varying the angle between the surface normal and the polarization vector of the light, which was in the plane of the synchrotron. The spectra were normalized using the photocurrent from a gold grid in order to compensate for beam decay and the transmission function of the monochromator. Polarization dependent NEXAFS data were collected from methyl–, pentyl–, decyl–, and octadecyl–terminated silicon.

IV.3.5. Thermal Annealing

Annealing studies were performed at BL 8-1 using the CMA system described above. This system was equipped with a sample manipulator capable of electron bombardment heating. Annealing temperatures below 500° C were reached by radiant heating by a nude filament located behind the sample. Temperatures above 500° C were obtained by electron bombardment heating. E–beam heating entails biasing the sample positively so that electrons emitted from the nude filament are accelerated into the sample. Once the desired temperature was reached, the sample was allowed to equilibrate and was then held at temperature for 15 minutes. The sample was then cooled to room temperature before further analysis was performed.

As the annealing data was collected using BL 8-1, it was only possible to monitor the Si 2p core level and valence band structure. These measurements were performed for the methyl–, pentyl–, decyl–, and octadecyl–terminated Si(111) samples. One expected problem was observed in the spectra that should be noted. These experiments were not the typical surface science measurements where all sample preparation was performed under ultra–high vacuum conditions. Therefore, it was not possible to perform standard outgassing procedures. Normally, the sample holder would be outgassed prior to performing measurements of this nature to prevent possible cross–contamination of the sample. However, this was not possible as annealing the sample holder would necessarily entail heating the sample which would have destroyed the interface that was to be studied. Therefore, slight oxidation of the sample was observed, most notably in the valence band structure, upon annealing. However, it does not appear to significantly alter the results of the annealing studies.

IV.4. RESULTS

IV.4.1. Valence Band

Figure IV.1 shows valence band (VB) spectra collected from a clean Si(111) 7x surface and four different alkyl–terminated Si(111) surfaces, methyl–, pentyl–, decyl–, and octadecyl–terminated. The spectra were all taken with a photon energy of 55 eV. These spectra can be divided into four regions of different origin. The first region occurs from kinetic energies of 48 to 50 eV (Region I). Intensity in this region is characteristic of emission from surface states arising from the presence of dangling bonds (partially–filled orbitals)(Eastman et al. 1978). These states are normally observed on clean, unterminated surfaces. The second region occurs from kinetic energies of 45 to 48 eV (Region II). Intensity in this region is characteristic of emission from the bulk valence states of the silicon crystal(Eastman et al. 1978). The remainder of the spectral region can be divided into two regions with kinetic energies from 38 to 45 eV (Region III) and with kinetic energies of 28 to 38 eV (Region IV). As can be seen from the spectra in Figure IV.1, emission in the latter two regions only occurred in the alkyl–terminated samples. The four spectral regions will be discussed in detail below.

Qualitatively, only the spectrum from the reconstructed Si(111) 7x7 surface exhibited intensity in Region I, 48 to 50 eV, which was attributed to dangling bond states. The presence of the dangling bond states at the Fermi level causes the Si(111) 7x7 surface to be metallic, i.e. no band gap exists. The lack of any observed states in Region I of the valence band spectra from the methyl– and pentyl–terminated surfaces indicated that significant numbers of dangling bonds do not occur at the interface between the alkyl monolayer and the silicon substrate. In other words, the partially–filled Si orbitals become involved in bonding with the alkyl chains. This bonding interaction lowers the energy of the now filled molecular orbitals moving them away from the Fermi level. As a result the methyl– and ethyl–terminated surfaces are no longer metallic. The above statements cannot be made for the decyl– and octadecyl–terminated surfaces because of loss of signal due to inelastic scattering of the silicon photoelectrons by the alkyl chains (Evidence of inelastic loss was not found in the data of Region I but becomes clear in Region II). Even though the intensity of the Si VB features are too low to state with confidence that no dangling bonds exist on these surfaces; and a comparison of the VanDerWall's radii of the alkyl chains and the Si(111) surface unit cell area would suggest that significant numbers of sites could not be terminated by alkyl chains(Linford 1996), it was likely that the sites that not involved in bonding to alkyl groups were terminated with hydrogen and few dangling bonds existed at these interfaces(Linford 1996).

Region II, 45 to 48 eV, contains emission from the bulk silicon valence band states and as such will not be discussed in detail. Two reasons for this assignment are given. First, the spectrum from the clean Si(111) 7x7, clearly showed spectral features in this region. Second, loss of intensity in this region as the size of the alkyl chain increased was observed in the alkyl–terminated spectra. Attenuation of signal from the a substrate is expected as the thickness of an overlayer is increased; it is caused by inelastic scattering of the photoelectrons in the overlayer(Hufner 1995). As only Region II shows this type of attenuation. It was clear that the origin of valence band features in this region was below the alkyl group (i.e. the silicon substrate).

The only obvious change in this region can be seen by comparing the methyl–terminated

and the clean Si(111) 7x7 spectra. Intensity from the surface states of Region I was pushed deeper into the silicon valence band as is evidenced by the lack of surface states in Region I and the increased intensity at 47 eV kinetic energy in the methyl–terminated spectrum. Similar behavior was reported for H/Si(111) 1x1 surfaces(Himpsel et al. 1991) and was attributed to the formation of a bulk–like, unreconstructed surface with no dangling bonds. Therefore, it appears that the methyl groups bond to the silicon substrate with a density of dangling bonds to low to be observed.

Shown in Figure IV.2 are the valence band spectra from the alkyl–terminated surfaces taken with a photon energy of 55 eV along with photoemission spectra from the corresponding alkane(Pireaux et al. 1986) taken using an X–ray tube (photon energy >1000 eV). The similarities of spectral shape between these spectra are obvious. The intensity differences between the features of Region III and IV of the spectra are due to changes in the photoemission cross section at the different photon energies. Therefore, the spectra features in Region III, 38 to 45 eV, and Region IV, 28 to 38 eV, of the valence band spectra were attributed to emission from the alkyl group.

Region III, 38 to 45 eV, was attributed to the C 2p based molecular orbitals of the alkyl group as similar features were reported in valence band spectra obtained from gas phase alkanes(Hamrin et al. 1968; Pireaux et al. 1986; Potts and Streets 1974), condensed alkanes(Pireaux et al. 1986), and from ethyl–terminated silicon surfaces(Lapiano-Smith, Himpsel, and Terminello 1993). Unfortunately, this region had a high density of states due to the three C 2p orbitals from each carbon atom in the alkyl chain and even on the methyl–terminated surface, the simplest system, individual components could not be resolved.

However, Region IV, 28 to 38 eV, did exhibit well resolved components. As Figure IV.2 shows, the methyl spectrum has one peak and the pentyl spectrum five. Spectra from butyl–terminated surfaces (not shown here) had four components. The larger chains exhibited band–like behavior and the observed double–humped density of states agreed well with theoretical calculations of long chain alkanes(Pireaux et al. 1986). In fact, this region behaved as a fingerprint for identifying the surface species. This fingerprint region of the

VB arises due to the formation of bonding and antibonding molecular orbitals in the alkane. As n carbon atoms are brought together to form an alkane, the n C 2s orbitals form bonding and anti–bonding combinations (molecular orbitals). The number of molecular orbitals formed is equal to the original number of C 2s orbitals (i.e. the number of C atoms) as has been observed in valence band spectra obtained from gas phase alkanes(Hamrin et al. 1968; Pireaux et al. 1986; Potts and Streets 1974), condensed alkanes(Pireaux et al. 1986), and from alkyl–terminated silicon surfaces(Lapiano-Smith, Himpsel, and Terminello 1993; Terry et al. 1997).

Figure IV.3 shows the valence band spectrum of the pentyl–terminated Si(111) surface and the positions of the corresponding features from gas phase pentane(Potts and Streets 1974). For n <6, the splitting of these molecular orbitals is large, greater than or equal to 1 eV, and as shown in Figure IV.3, the components are well resolved. This spectral region thus provides an excellent method for determining the chemical species present at the interface and it is obvious from Figure IV.3 that pentyl chains are present on the surface that was believed to be pentyl–terminated. This spectrum unlike those in the previous two figures was referenced to the position of the Fermi Level, so that peaks have negative binding energies. Region IV, which corresponds to binding energies from -12 to -21 eV, had five components that were resolved in the pentyl–terminated spectrum. The observed binding energies were -19.1 eV, -17.6 eV, -15.6 eV, -13.7 eV, and -12.8 eV with respect to E_F. Potts et al. reported gas phase binding energies of the $1a_1$, $1b_2$, $2a_1$, $2b_2$(-19.9, and $2b_u$ molecular orbitals of n-pentane with assumed C_{2v} symmetry(Potts and Streets 1974) to be -24.8 eV, -23.7 eV, -21.7 eV, -19.9 eV, and -18.74 eV, respectively. Gas phase spectra and condensed or crystalline spectra have different reference levels (Fermi Level in solid and Vacuum Level in gas phase) which partially account for the difference in binding energies. Shifting the gas phase data by 6 eV brought the reported gas phase data (-18.8 eV, -17.7 eV, -15.7 eV, -13.9 eV, and -12.74 eV) from n–pentane(Pireaux et al. 1986; Potts and Streets 1974) into excellent agreement with the pentyl–terminated spectrum. The features are all within the experimental error of ±0.1 eV except for the $1a_1$(-18.8 eV) molecular orbital of pentane and the associated feature of the pentyl–terminated surface (-19.1 eV). The pentyl group molecular orbital is shifted 0.3 eV to higher binding energy relative to

the gas phase feature. The energy lowering of this molecular orbital could indicate that this molecular orbital was involved to a greater extent than the other C 2s based molecular orbitals in bonding to the silicon substrate.

The observed shift of 6 eV appears to be characteristic of alkyl–terminated silicon surfaces as the gas phase spectra from ethane(Potts and Streets 1974) must be shifted by 6 eV to align with the observed valence band features from ethyl–terminated Si(111) and Si(100) surfaces prepared by decomposition of diethylsilane(Lapiano-Smith, Himpsel, and Terminello 1993). This shift (ΔE) must account for the different reference levels (Fermi Level in solid and Vacuum Level in gas phase) of the measurements. The difference between the Fermi Level and the Vacuum level is defined as the work function (Φ) of the material. For alkanes, the work function, Φ, can be approximated as 4.5 eV(Pireaux et al. 1986). This leaves a difference of 1.5 eV which must still be accounted for. This final difference must be due to extramolecular relaxation, i.e. a charge redistribution in neighboring alkyl groups and the silicon substrate. Therefore, the difference, ΔE, can be written as:

$$\Delta E = \Phi + P_{alkane} + P_{Si} \qquad \text{(IV.1)}$$

where P_{alkane} is the relaxation energy of a condensed alkane and P_{Si} is the relaxation energy due to the presence of the silicon substrate. For a valence level in a condensed alkane, P_{alkane} is approximately 0.5 to 0.8 eV(Pireaux et al. 1986). The relaxation due to the substrate, P_{Si}, then must be between 0.7 and 1.0 eV. P_{Si} would not be expected to vary with alkyl chain length, thereby explaining the constant shift, ΔE, of 6 eV of the different alkyl–terminated Si surfaces. It was obvious that the alkyl spectra and the gas phase spectra were readily shifted by a reasonable value into excellent agreement. Therefore, the valence band spectrum from an alkyl–terminated surface could be used to identify the presence of an alkyl group.

Finally, Figure IV.4 shows a valence band spectrum from a pentyl–terminated Si(111)

surface and a valence band spectrum from a penteyl–terminated Si(111) surface. The penteyl surface was prepared exactly as described above except that the H/Si(111) surface was exposed to pentyne instead of pentene. The valence band was sensitive to the presence of a carbon–carbon double bond as was evidenced by the chemical shifts of two of the C 2s based molecular orbitals. This strong sensitivity to different chemical environments will undoubtedly be useful in determining the success of future synthesis procedures using other organic functional groups.

IV.4.2. Si 2p Core Level Photoemission

Silicon 2p core level spectra were collected at two different photon energies from methyl–, pentyl–, decyl–, and octadecyl–terminated Si(111) samples. By taking spectra where the emitted photoelectrons had different escape depths(Eastman, Himpsel, and van der Veen 1982; Hricovini et al. 1993), the intensity of the measured photopeaks changed based upon their depth from the vacuum interface. The intensity of deeper peaks increased as the escape depth increased, i.e. fewer electrons were inelastically scattered. Therefore, if photopeaks originate in different layers, they can be identified by varying the photon energy. Surface sensitive Si 2p core level spectra from methyl– ($h\nu$=130 eV), pentyl– ($h\nu$=130 eV), decyl– ($h\nu$=130 eV), and octadecyl– ($h\nu$=120 eV) terminated Si(111) samples are shown in Figure IV.5. The octadecyl spectrum was taken at a lower photon energy to increase the escape depth of the photoemitted electrons in order to enhance the signal of the Si 2p photopeak. Bulk sensitive spectra, $h\nu$=115 eV, from the same samples are shown in Figure IV.6. Three elements were qualitatively obvious from the data. First, in the Si 2p core level spectra shown in Figure IV.5, the presence of a Si^{4+} peak at 22.6 eV kinetic energy due to slight surface oxidation was observed. Second, the Si 2p photopeak was strongly attenuated as the carbon chain length increased. Finally, the lineshape changed as the carbon chain length increased.These three elements will be discussed below in the above order.

First, a Si^{4+} peak was observed in all spectra taken at a surface–sensitive photon energy of 130 eV (Figure IV.5). This peak arises from SiO_2 contamination. Thus, a fraction of the silicon surface has been oxidized. However, this peak was noticeably absent in the spectra

taken at the bulk–sensitive photon energy of 115 eV (Figure IV.6) which indicates that it is not a thick oxide film. To quantitatively determine the amount of oxide present, it is necessary to fit the measured photopeaks which will be described below.

Second, the attenuation behavior of the Si 2p photopeak indicated that a thin film of some type of carbon was deposited on top of the silicon substrate. It is obvious from Figure IV.5 that as the number of carbon atoms in the alkyl chains was increased, the intensity of the Si 2p photopeak decreased. As shown in Eq. IV.2 the amount of attenuation is exponentially related to the thickness

$$I = I_0 e^{-\frac{d}{\lambda}} \qquad \text{(IV.2)}$$

of the alkyl film (d) and the escape depth of the photoelectrons in the carbon film (λ), with I being the measured intensity of the Si 2p core level and I_0 the intensity from an unattenuated sample. If one assumes that the escape depth of the photoelectrons did not change significantly as the chain length was increased, then the increasing attenuation of the Si 2p photopeak could only be caused by a corresponding increase in the film thickness (d). The structural model of the alkyl group–silicon interface that best accounts for this behavior would have the alkyl groups oriented nearly vertical to the surface so that by adding additional (-CH_2-) groups the film thickness would be increased. By further assuming a geometrical model based on sp^3 hybridization of the carbon and silicon atoms it was possible to calculate the escape depth of the alkyl groups using the measured Si 2p core level intensities and Eq. IV.2. At a photon energy of 130 eV, (photoelectron kinetic energy of 26 eV) the escape depth in the alkyl monolayer was 4.64 Å. Thus, by qualitatively studying the Si 2p core level photopeak, it was possible to determine a reasonable model of the interfacial geometry.

Finally, the Si 2p core level spectra changed lineshape as the number of carbon atoms in the alkyl chain was increased. It is clear from the spectra in Figure IV.5 that a valley

becomes apparent between the main spin–orbit doublet. This suggests that the observed photopeak consists of multiple spin–orbit doublets that have a variation in intensity that is dependent upon chain length. To further investigate this lineshape change, the Si 2p core level spectra taken with hν=130 eV from the from methyl–, pentyl–, and decyl–terminated Si(111) samples shown in Figure IV.5 were decomposed into multiple spin–orbit doublets using a least squares fitting procedure with Voight lineshapes (convolution of a Gaussian and Lorentzian) as described in Chapter I. The best fits of these spectra are shown in Figure IV.7 with the peak positions listed in Table IV.1 and the peak intensities listed in Table IV.2. In all cases, a Gaussian linewidth (FWHM) of 320 meV and a Lorentzian linewidth (FWHM) of 54 meV along with a spin–orbit splitting of -0.605 eV and a branching ratio of 0.5 were used as fitting parameters. These values are in reasonable agreement with the values of Hricovini, et al. for the ideal H–terminated Si(111) surface(Hricovini et al. 1993).

Two strong peaks were observed in all the Si 2p spectra. The highest kinetic energy (lower binding energy) peak was attributed to emission from the bulk silicon substrate. This assignment was made by comparing spectra taken at both bulk and surface sensitive photon energies (Figure IV.5 and Figure IV.6). It was obvious from the data that this component strongly increased in intensity as the photon energy was made more bulk sensitive. Table IV.1 shows that this peak shifted to higher kinetic energy as the alkyl chain length increased. This peak position shift was attributed to different Fermi Level pinning positions of the different alkyl–terminated surfaces. More interesting is the second component that was shifted to lower kinetic energy (higher binding energy) relative to the bulk peak.

A core level shift to higher binding energy is indicative of charge transfer from the emitting atom to a more electronegative neighbor(Eastman, Himpsel, and van der Veen 1982). Because carbon is more electronegative than silicon, the shifted component observed in the Si 2p core level spectra from the alkyl monolayers is consistent with photoemission from top layer silicon atom that is donating charge to an alkyl group. On this basis, the low kinetic energy peak in the Si 2p core level spectra has been assigned to photoemission from a silicon atom bound to the terminal carbon atom of the alkyl group. SiC formation

can be ruled out because the reported chemical–shifts in Si 2p core level spectra have been reported to be between 1.2 and 1.4 eV(Kusunoki and Igari 1992; Stinespring and Wormhoudt 1989; Taylor et al. 1989) to higher binding energy with respect to the bulk position. This is significantly greater than the measured shifts (0.21 – 0.27 eV) in the Si 2p core level spectra from alkyl–terminated Si(111).

From Table IV.1, it can immediately be seen that the chemical shifts (methyl 0.27 eV, pentyl 0.21 eV, decyl 0.21 eV) from the different surfaces are not identical. These chemical shifts came directly from the curve fitting routine. The differences in the observed chemical shift can be explained by either, a true variation in charge transfer between the Si and C atoms involved in bonding, or due to the presence of hydrogen termination of the surface. The calculated surface coverages strongly suggest that the observed motion of the Si 2p component from Si bonded to C was not due to variation in charge transfer but was in fact due to the presence of H at the interface.

The surface coverages of the alkyl group were calculated using the method described by Himpsel, *et al*(Himpsel et al. 1988). In this method, coverages are determined using the ratio of the chemically–shifted surface component to the total core level intensity. For the Si 2p core level, a ratio of 0.35 corresponds to 1.0 ML of Si atoms on the Si(111) surface. Here, 1 ML is defined as 7.8×10^{14} atoms/cm^2, the number of top layer Si surface atoms. A further assumption that the alkyl group attenuates the photoelectrons from both the surface and bulk Si atoms equally has been made. The calculated coverages for the methyl–, pentyl–, and decyl–terminated Si(111) surfaces are listed in Table IV.2.

The methyl coverage was calculated to be 1.0 ± 0.1 ML. This surface was prepared from the Cl–Si(111) surface as described above. As a comparison, Figure IV.8 shows the Si 2p core level spectrum from a methyl–Si(111) surface along with those from the H–Si(111) and Cl–Si(111) surfaces. Clearly, the Si $2p_{1/2}$ component at 24.4 eV, indicative of the presence of a Si–Cl bond in the spectrum from the Cl–Si(111) surface(Terry et al. 1996a) was absent in the spectrum from the methyl–Si(111) surface. Therefore, the Si 2p core level spectra from the methyl–Si(111) surface showed no residual Cl. This was in excellent agreement with the calculated coverage of 1 ML. The methyl group is small and one could

imagine that a methyl group could fit at each Si surface lattice site.

The pentyl coverage was calculated to be 0.6 ± 0.1 ML. One would expect to obtain a lower surface coverage than from the methyl–terminated surface as the pentyl–groups are bulkier than the methyl groups and steric effects might suggest that not all Si surface sites would bonded to pentyl groups. The pentyl–terminated surface, unlike the methyl–terminated surface, was prepared from the H–Si(111) as described above. Unfortunately, the Si 2p core level shifts from the H–Si(111) surface are presently the subject of great debate(Hricovini et al. 1993; Terry et al. 1994), and the presence or absence of H can not be determined as accurately as Cl was on the methyl–terminated surface.

The decyl coverage was calculated to be 0.9 ± 0.5 ML. This was a very surprising result as it was predicted from steric hindrance that the surface coverage would be less than that observed from the pentyl–Si(111) surface. In fact, the decyl coverage must be less than 0.5 ML due to steric hindrance. However, this surface was also prepared using the H–Si(111) surface. Unfortunately, the weak intensity of this core level due to strong attenuation by the organic film which made the fitting uncertain. Furthermore, the presence of silicon atoms bonded to H at the silicon–decyl group interface acted to broaden the peaks. These coupled features most likely account for the inflated coverages calculated for the decyl–Si(111) surface.

Finally, the extent of surface oxidation can be determined in a similar fashion. Comparison of the ratios of the chemically–shifted Si 2p components related to oxidation to the total intensity yields oxide coverages. The methyl–terminated surface had an oxide coverage of less than 0.1 ML, which is smaller than can accurately be determined experimentally. The calculated oxide coverages from the pentyl–terminated and decyl–terminated surfaces were between 0.5 – 0.7 ML. When combined with the calculated alkyl group coverages, the total surface coverage is well over 1ML. Unfortunately, this method of determining coverage can only be used for coverages of 1 ML or less. Therefore, what appears to be happening is that domains of oxidized and alkylated silicon exist at the surface. The high oxidation coverages then likely are the result of subsurface oxidation in the oxidized domains.

Even though the exact coverages of the longer alkyl groups are not accurately known. It cannot be disputed that the chemically–shifted component existed and was shifted in a direction consistent with Si bonded to C. This behavior strongly indicated that a bond was formed between the top layer Si atoms and the terminal C atom of the alkyl group. Further evidence for bond formation was obtained from the C 1s core level spectra described below.

IV.4.3. C 1s Core Level Photoemission

Carbon 1s core level spectra were collected from methyl–, pentyl–, decyl–, and octadecyl–terminated Si(111) samples. Representative spectra are shown in Figure IV.9. Two components were observed in the C 1s spectra until the chain length exceeded 10 carbon atoms(Terry et al. 1997). The low binding energy component (58.6 eV Kinetic Energy)was attributed to photoelectrons from carbon atoms bonded to the silicon substrate. The high binding energy component (57.5 eV Kinetic Energy) was attributed to photoelectrons from the carbon atoms in the chain. A C 1s core level spectra showing the fits to these two spectral features from the pentyl–Si(111) surface is shown in Figure IV.10. These assignments were made because of 1.) intensity arguments; 2.) electronegativity arguments; and 3.) observed photoelectron diffraction effects.

First, the intensity of the high binding energy component increased as the size of the alkyl group increased. This main difference between alkyl groups was an increase in the number of $-CH_2-$ or $-CH_3$ groups present. The chemical shift between a $-CH_2-$ group and a $-CH_3$ group was expected to be to small to be observed. Therefore, this component of the C 1s spectra was attributed to photoelectrons from C bonded only to other C and H atoms in the alkyl chain. This assignment was further supported by the observation that after the length of the alkyl group exceeded 10 carbon atoms, this component was the only one observed in the C 1s core level spectra.

The low binding energy component was observed to have the opposite behavior. As the chain length increased, this component was severely attenuated. Varying the chain length increased the distance from the monolayer–substrate interface to the vacuum monolayer–

vacuum interface because of the increased number of $-CH_2-$ units which acted as spacer layers. A photoelectron originating near the monolayer–substrate interface would be more likely to undergo inelastic scattering before reaching the vacuum in thicker films (i.e. monolayers with larger chain lengths), assuming that the escape depth of an electron is a constant independent of the length of the alkyl group. Therefore, any component that originated beneath the organic film near the monolayer–substrate interface would be expected to show attenuation as the chain length (thickness of the organic thin film was increased). Thus, the observed behavior of the low binding energy component showed that this component originated from C atoms physically located near the silicon–alkyl group interface. However, this interfacial component cannot simply be attributed to C–Si bonding without further evidence.

Second, the observed chemical shifts of the components in the respective C 1s core level spectra were consistent with C–Si bond formation. The high binding energy component labeled C–C in Figure IV.10 was immediately attributed to bulk–like C in the alkyl chain as described above. Therefore, the other component was shifted to lower binding energy with respect to the bulk–like position. If C–Si bond formation occurred, one would prediction that charge would be transferred from the silicon atom to the carbon atom based upon the relative electronegativities of carbon and silicon. Charge transfer of this nature would manifest itself in a C 1s peak that originated from the C atom bonded to Si shifted to lower binding energy with respect to the bulk–like position. This was the exact behavior observed in the C 1s core level spectra from the alkyl–terminated surfaces. Therefore, the low binding energy component, labeled C–Si in Figure IV.10, was attributed to photoemission from the terminal carbon atom of the alkyl group which was bonded to the silicon substrate.

This assignment corroborated the previously assigned behavior in the Si 2p core level spectra, where an interfacial component was shifted to higher binding energy. The chemical shifts in the Si 2p core level and the C 1s core level were in the opposite directions indicating that charge transfer between surface Si atoms and interfacial C atoms was occurring. Since charge transfer from the silicon atoms at the interface to a carbon atom in

the alkyl chain was observed, it can be inferred that the alkyl chains are chemically bonded to the silicon surface. This is in agreement with a previous study(Lapiano-Smith, Himpsel, and Terminello 1993) of ethyl–terminated surfaces formed by the decomposition of diethylsilane, were a broad C 1s spectrum approximately 2 eV wide was observed. In their study, the observed spectra were not decomposed so but it is speculated that the 2 eV wide peak in fact consisted of two components of approximately equal intensity, one C–C feature and one C–Si feature, as one would expect from that surface according to our model.

Note that the high binding energy component was observed in the C 1s spectrum from the methyl–terminated Si(111) surface (Figure IV.9). One would expect to observe only a single peak at the low binding energy position (58.6 eV Kinetic Energy) in the C 1s spectrum from the methyl–Si(111) surface due to the presence of only a C atom bonded to the Si substrate. The high binding energy component was then attributed to contamination associated with the methyllithium reaction and workup. X–ray Photoelectron Spectroscopy has shown that the magnitude of this feature was dependent on the immersion time of the silicon in the methyllithium solution and on the type of rinse employed after removing that solution(Terry et al. 1996b). Short immersion times and rinsing with an HCl solution both contributed to the relatively low level of adventitious contamination observed on this surface.

Finally, variation of the intensity ratios between the two components was observed as the photon energy was varied. This intensity variation was evident through a comparison of the spectrum in Figure IV.11A taken with $h\nu \neq 350$ eV with that in Figure IV.11B taken with $h\nu = 370$ eV. The observed intensity ratio between the two components (C–C/C–Si) was approximately 20 to 1 in the first spectrum while the observed intensity ratio was approximately 10 to 1 in the second. The observed intensity variations were believed to be photoelectron diffraction oscillations due to a fixed experimental geometry at the interface. The observation of photoelectron diffraction effects indicated that C atoms were bonding to the silicon surface in similar bonding sites as disordered C atoms should have contributed little, if at all, to the measured diffraction oscillations.

Unfortunately, these photoelectron diffraction oscillations made it impossible to determine

the size of the alkyl group from the ratio of the C–C peak to the C–Si peak. However, similar measurements were performed using an XPS on a pentyl–Si(111) surface(Terry et al. 1996b). XPS spectra were obtained on a Surface Science Model 150 XPS spectrometer with an Al Kα (1486 eV) source, quartz monochromator, hemispherical analyzer, and a multichannel detector. The pressure during analysis was less than $5x10^{-8}$ torr. The energy resolution was approximately 1 eV. The take off–angle was 35° from the surface with an angular acceptance of approximately 30°. Under these conditions, photoelectron diffraction effects should be negligible in the C 1s core level. Core level fits using various C 1s lineshapes gave ratios of the areas of the components ranging from 90%:10% to 84%:16%. The two components described above were observed. The ratio of the areas of the two components was somewhat less than the ideal ratio of 80%:20% predicted for a pentyl–chain bonded to silicon. The bulk of the discrepancy was probably due to adventitious hydrocarbon contamination of the sample surface similar to that observed on the methyl–Si(111) surface.

These intensity oscillations due to photoelectron diffraction were used to determine the bonding geometry of the C atom bonded to the Si substrate. These measurements were carried out on both the pentyl–Si(111) and methyl–Si(111) surface in order to characterized the samples made using the different preparation techniques. These results are described below.

IV.4.4. Chemical–Shift, Scanned–Energy Photoelectron Diffraction

Photoelectron diffraction measurements were performed on the C 1s core level spectra from both pentyl–terminated and methyl–terminated Si(111) surfaces in order to determine the surface geometry of the alkyl groups because a chemically–shifted component assigned to carbon bonded to silicon was observed and the intensity of the components varied with photon energy. Scanned–energy photoelectron diffraction was performed as the bond length was the most important geometrical parameter to determine. The scanned–energy photoelectron diffraction measurements required a tunable radiation source and an angle–resolved analyzer with a small angular acceptance cone ($<\pm 3°$). The synchrotron radiation source was continuously tunable between photon energies of 300 eV

and 650 eV. By tuning the photon energy, it is possible to vary the magnitude of the wave vector (k) of the photoelectron as detailed in Chapter I. The hemispherical electron energy analyzer had an angular acceptance of ±1.5°. The additional constraint imposed by chemical–shift photoelectron diffraction required that the combined resolution of the analyzer and monochromator be small enough to resolve the chemically–shifted component of the core level under study. The total energy resolution (monochromator and analyzer) of the system used in the photoelectron diffraction measurements of the C 1s core level was determined to be 150 meV at a photon energy of 350 eV. Therefore, the experimental system met all the requirements for collecting photoemission spectra that could be used to extract photoelectron diffraction data.

The C 1s core level spectra were collected with a single experimental geometry. The incident photon beam made an angle of 30° with respect to the collection cone of the analyzer. Furthermore, these photoemission spectra were acquired with the hemispherical analyzer oriented along the surface normal of the sample. This geometry was chosen because one would expect the terminal C atom of the alkyl group to be perpendicular to the surface, assuming sp^3 hybridization of both the Si and C. Therefore, the intensity modulations in the C 1s core level should have been dominated by the interference with the backscattered wave from the nearest–neighbor Si atom in this geometry.

Extraction of the photoelectron diffraction oscillations from the individual C 1s core level spectra was done in four parts. First, each C 1s core level spectrum collected at different photon energies was decomposed into two singlet components using the least squares fitting. Second, the intensities of the two components was determined. Third, these intensities were normalized to the photon flux and the analyzer transmission. Finally, the contribution from the atomic partial cross section, I_0, was removed. The atomic partial cross section is the intensity distribution that would be measured in the absence of any photoelectron diffraction effects.

C 1s core level spectra were collected at different kinetic energies over a range from 50 to 350 eV. They were decomposed into two components using Voight lineshapes (convolution of Gaussian and Lorentzian) and Shirley backgrounds according to the least–squares

minimization fitting procedure described in Chapter I. The Lorentzian half–width at half–maximum (HWHM) was fixed at 0.172 eV. The Gaussian component was allowed to vary in order to account for the decreased resolution of the monochromator at high photon energies. The intensity of the two components was then determined by numerical integration of the two component over the complete spectral region collected. Figure IV.11A ($h\nu$ = 350 eV) and Figure IV.11B ($h\nu$ = 370 eV) show the decomposed C 1s spectra from a pentyl–Si(111) surface. Figure IV.12A and Figure IV.12B show the corresponding spectra from a methyl–Si(111) surface. The low kinetic energy component observed in the C 1s spectra from the methyl–Si(111) surface was due to hydrocarbon contamination as described above.

These measured intensities were then corrected for differences in photon flux. The photon flux at a synchrotron depends upon both the electron current in the storage ring and the transmission function of the monochromator. The photon flux was determined by measuring the sample refresh current of a gold grid located in front of the sample but behind the monochromator. The intensities derived from curve fitting were normalized to the measured sample refresh current. At this point, the measured intensities of the components of the C 1s core level spectra were still dependent upon the transmission function of the electron energy analyzer.

The transmission function of the electron energy analyzer is the most difficult correction for which to account. This correction required making assumptions about the background due to inelastically scattered electrons. The transmission function of the analyzer was corrected for by normalizing the intensities from the pentyl–terminated surface to the ratio of the background 2 eV to higher kinetic energy than the C 1s spectrum to the value (545 counts) of the background spectra at 151 eV Kinetic Energy at a photon energy of 440 eV. The corresponding data from the methyl–terminated surface was normalized using a similar ratio with the value (36 counts) of the background spectra at 151 eV Kinetic Energy at a photon energy of 440 eV. This correction assumed that the background due to inelastically scattered electrons was constant in the sample and that the measured variations in the background were due to a decrease in the transmission function of the analyzer at high

kinetic energies. In fact, the background depends upon the absorption cross sections of any elements that contribute to it. Crossing a threshold can impart large changes to the measured background. In the C 1s data, the background at low kinetic energies was strongly affected by the presence of a Si LVV Auger line at approximately 88 eV Kinetic Energy. Deconvolution of this Auger Line was responsible for the underestimation of the intensities of the C 1s components near 88 eV. However, the intensities at this point have been corrected for the external factors that affect the intensity measurements using the best available methods(Barton 1985a; Barton 1985b; Barton, Robey, and Shirley 1986; Barton and Shirley 1985b; Barton and Shirley 1985a).

The crosses in Figure IV.11C show the intensities of the chemically–shifted component of the C 1s core level spectra from the pentyl–Si(111) surface assigned to the C atom bonded to the silicon substrate. The data is plotted as a function of the magnitude of the wave vector of the photoelectron in the direction along the sample normal. Note that the intensity oscillates strongly as it decays toward zero at high wave vector. The decay is due to the universal decrease in photoemission cross section as the photoexcitation energy is increased above the core level absorption edge. The oscillations were assigned to constructive and destructive interference of the photoelectron waves that go directly to the detector from the emitting atom and those that scatter off neighboring atoms. The corresponding data from the methyl–Si(111) surface is shown in Figure IV.12C.

The intensity from the low kinetic energy component of the C 1s spectra from the pentyl–Si(111) surface, which was assigned to aliphatic carbon bonded to only carbon and hydrogen, was observed to decay without significant oscillations. This was unexpected because with assumed sp^3 hybridization some C–C bonds should have been oriented in this direction and oscillations should have been observed from the backscattered wave from the C atom located closer to the interface. The absence of diffraction in this component could be due to either a range of conformational isomers in the chain, dynamic fluctuations of the chain, or the presence of an adventitious overlayer of carbon. A similar decay was observed in the low kinetic energy component from the methyl–Si(111) surface indicating that the adventitious carbon does not show significant diffraction oscillations.

To isolate the intensity oscillations of the partial atomic cross sections from the pentyl–Si(111) surface in Figure IV.11C and the methyl–Si(111) surface in Figure IV.12C, a function, $\chi(k)$, was determined as in Eq. IV.3

$$\chi(k) = \frac{(I - I_0)}{I_0}. \qquad \text{(IV.3)}$$

where, I is the measured intensity of the C–Si component and I_0 is the partial atomic cross section. I_0 was approximated by fitting a decaying exponential to the measured intensity as shown in both Figure IV.11C (pentyl) and Figure IV.12C (methyl). This is an adequate approximation because calculations of the atomic cross sections from free atoms have been shown to contain only low frequency oscillations, whereas the oscillations that are important for determining geometric structure are of much higher frequency(Barton 1985a; Barton 1985b; Barton, Robey, and Shirley 1986; Barton and Shirley 1985b; Barton and Shirley 1985a).

The resulting χ function from the pentyl–terminated Si(111) surface is shown in Figure IV.13A. That from the methyl–terminated Si(111) surface is shown in Figure IV.13B. These χ functions represent the interference between the primary and scattered photoelectron waves. In order to determine the bonding geometry of the alkyl monolayer, the experimental χ functions were compared with calculated χ functions from various adsorption geometries.

The calculation of the χ functions proceeded in two parts. First, the partial–wave phase shifts form sp^3 hybridized Si and C were calculated. Second, these values along with the adsorption geometries were then input into the curved–wave multiple–scattering calculation. The Si–C bond length was varied in the following adsorption sites on the Si(111) surface: atop, bridge, three–fold hollow, and three–fold atop sites.

The partial–wave phase shifts were calculated using Roothan–Hartree–Fock atomic

wavefunctions(Clementi and Roetti 1974) as input to the program Mufpot(Note). Mufpot used the atomic wavefunctions to calculate solid–state wavefunctions using the augmented plane–wave method (APW)(Loucks 1967).

The partial–wave phase shifts were input into the full curved–wave multiple–scattering program NEWCHP(Moler and Barton ; Note) which calculates χ functions from the input model structures using the Taylor Series–Magnetic Quantum Number Expansion(Barton 1985b; Barton, Robey, and Shirley 1986; Barton and Shirley 1985b; Barton and Shirley 1985a; Terminello et al. 1988; Zheng, Hussain, and Shirley 1993; Zheng et al. 1993). This program performs the scattering calculations on a four layer thick slab of infinite length and width. The quality of the theoretical models was determined using the five R-factors (Reliability factors) of Van Hove, *et al.*(Van Hove, Tong, and Elconin 1977).

The best theoretical χ functions along with the values of the first R–factor(Van Hove, Tong, and Elconin 1977) as a function of C–Si bond length (inset) are also shown in Figure IV.13A (pentyl) and Figure IV.13(methyl). Due to the limits of the computer program used to calculate the scattering, the calculations from two slabs, one with 1 C layer and three Si layers (Figure IV.14), the other with 2 C layers and 2 Si layers (Figure IV.15) were performed to simulate the pentyl–terminated surface. The theoretical χ functions from the two slabs in each model geometry were identical. The best model structure from the pentyl–terminated Si(111) surface as determined using the above method (solid line Figure IV.13A) had the bonding C atom of the pentyl group sitting directly above the top layer silicon atoms (atop site). The C–Si bond length was found to be 1.85 ± 0.05 Å. This value is in excellent agreement with the C–Si bond length of 1.88 Å observed in SiC(Sumakeris et al. 1993), and C–Si bond lengths of 1.86 Å observed in alkylsilanes(Bowen et al. 1958). Unfortunately, the theoretical calculations of the atop site were not very sensitive to the position of the second silicon layer so no information about subsurface relaxation was obtained. The next best fit (R–factor of 0.127) placed the alkyl chain in a three–fold atop site (three–fold site with a second layer Si atom directly beneath the C atom) with three C–Si bond lengths of 2.46 Å. It is not surprising that this site gave a low R–factor, as in this position, the C atom is 1.85 Å directly above the second layer Si

atom. However, such a dense packing is sterically unreasonable.

In the case of the methyl–terminated surface, only the slab containing 1 C layer and three Si layers (Figure IV.14) was used in each structural model. The best model structure from the methyl–terminated Si(111) surface as determined using the above method had the bonding C atom of the methyl group sitting directly above the top layer silicon atoms (atop site). The C–Si bond length was 1.85 ± 0.05 Å. The C–Si bond lengths and bonding sites determined from the methyl– and pentyl–terminated surfaces are in excellent agreement even though the surfaces were prepared using two entirely different synthetic methods.

IV.4.5. Near–Edge X–Ray Absorption Spectroscopy

C K-edge absorption spectra were collected from methyl–, pentyl–, decyl–, and octadecyl–terminated Si(111) surfaces. The synchrotron radiation was polarized in the plane of the electron's orbit. Therefore, it was possible to collect the absorption data at different incident polarizations by rotating the sample. Two geometries were very important, glancing incidence and normal incidence. At glancing incidence, the polarization vector made an angle of approximately 20° with the surface normal, out of surface plane. At normal incidence, the polarization vector made an angle of 90° with the surface normal, in surface plane. Changes in the measured NEXAFS spectra with different incident polarizations indicated that the alkyl groups were oriented. Furthermore, comparisons of the polarization dependent C K–edge Absorption spectra have been made between the NEXAFS spectra from the monolayers and spectra taken from both Langmuir–Blodgett monolayers(Outka et al. 1988; Outka et al. 1987) and from oriented hydrocarbons(Stohr et al. 1987). Spectral normalization was performed according to the procedures outlined by Outka, *et al*(Outka et al. 1988; Outka et al. 1987).

Figure IV.16 shows the polarization dependent C K–edge absorption spectra from the octadecyl–Si(111) surface. These spectra were in remarkable agreement with those measured by Outka, *et al.*(Outka et al. 1988; Outka et al. 1987) and Stohr, *et al.*(Stohr et al. 1987). First, the there were obvious changes as the polarization vector was varied indicating that the alkyl groups were oriented. Second, the three features characteristic of the

NEXAFS spectra from alkyl chains were present in the data from the octadecyl–Si(111) system. The three main features of the C K–edge NEXAFS spectrum are strongly polarization dependent in oriented samples. Therefore, a difference spectrum was obtained by subtracting the normal incidence spectrum from the glancing incidence spectrum to highlight these features. The feature at 292 eV was identified as a σ^*(C–H) resonance. The features at 297 and 303 eV were identified as σ^*(C–C) resonances. From the presence of these three resonances and the observed polarization dependent spectra, it is concluded that the octadecyl groups were oriented on the Si substrate.

The ionization potential (IP) of 296 eV is also marked in Figure IV.16. Stohr(Stohr 1992) has measured an empirical correlation between C–C bond lengths in hydrocarbons and the position of the σ^*(C–C) resonance with respect to the IP. This empirical relation ship was used to determine the C–C distances in the octadecyl group. The approximately 1 V difference between the position of the ionization potential and the σ^*(C–C) resonance corresponds to a C–C bond length of 1.53 ± 0.05 Å.

Figure IV.17 shows the polarization dependent C K–edge NEXAFS spectra from the octadecyl–, decyl–, pentyl–, and methyl–terminated Si(111) surfaces. Large variations in the difference spectra were observed as the length of the alkyl group decreased. As described above, the NEXAFS spectra from the octadecyl–Si(111) surface was remarkably similar to those from other alkanes. However, as the chain length decreased, the negative intensity peak at 292 eV corresponding to the σ^*(C–H) resonance disappeared. The intensity loss could not be attributed to loss of alkyl groups as their presence was confirmed using other methods(Terry et al. 1997). In fact as the number of C atoms in the alkyl chain was reduced, the signal from the C atom bonded to the Si substrate contributes a greater percentage to the measured spectrum. Therefore, it was believed that the spectral differences were due to the presence of a fourth component in the C K–edge NEXAFS region. By looking at the methyl–terminated spectrum, it appeared that a strongly polarization dependent component was present in the glancing incidence data. This feature so dominated the spectrum that it was impossible to normalize the spectra from the two different polarization dependences in order to calculate a

difference spectrum. This large feature was attributed on this basis to a σ*(C–Si) resonance.

Finally, it is possible to determine the relative orientation of a sample by comparing the difference spectra of two similar systems(Outka et al. 1988; Outka et al. 1987). The polarization dependent C K–edge spectra were compared to the published spectra from Cd Arachidate (tilt angle 0°), Ca Arachidate spectra (tilt angle 33°)(Outka et al. 1988; Outka et al. 1987) and adsorbed polyethylene (tilt angle 90°)(Stohr et al. 1987). Figure IV.18 shows the C K–edge spectra from each standard and the octadecyl–terminated Si(111) surface.

By first comparing the difference spectra from the octadecyl sample and polyethylene, it can immediately be seen that the three hydrocarbon features discussed above exhibited the opposite polarization dependences (i.e. the peaks have opposite sign). Therefore, it can be concluded that the octadecyl group did not lie in the plane of the silicon surface. However, the polarization dependences were very similar to those of the two arachidate samples indicating that the tilt angle of the octadecyl group was less than 45° from the sample normal. In fact, the intensities of the σ* features in the difference spectra from the octadecyl–Si(111) surface were almost identical to those measured from Ca arachidate, suggesting that the tilt angle of the octadecyl groups was likely near 33°. In order to quantify this tilt angle, the intensity of the σ*(C–H) peak at 292 eV and the first σ*(C–C) peak at 296 eV were used to calculate tilt angles using the difference spectra methodology proposed by Outka, *et al*(Outka et al. 1988; Outka et al. 1987).

A brief discussion as outline by Outka, *et al*(Outka et al. 1988; Outka et al. 1987) of this methodology will follow. The intensity from the component of the polarization vector parallel to a single vector type orbital, i.e. an isolated σ*(C–C) orbital on a surface with three–fold symmetry or higher is given by Eq. IV.4.

$$I^{\parallel} = A[\cos^2(\theta)\cos^2(\alpha) + \tfrac{1}{2}\sin^2(\theta)\sin^2(\alpha)] \qquad \text{(IV.4)}$$

θ is the angle between the polarization vector and the surface normal, α is the angle between the p component of the σ* orbital and the surface normal, and A is a constant that depends on the sample and experimental detection geometry. It has been found through algebraic manipulation of Eq. IV.4 that the intensity of a peak in the difference spectra divided by the difference of the squares of the cosines of the two polarization angles, θ, is a constant (S) as shown in Eq. IV.5.

$$\frac{I(\theta_{glancing}) - I(\theta_{normal})}{\cos^2\left(\theta_{glancing}\right) - \cos^2\left(\theta_{glancing}\right)} = S = constant \qquad \text{(IV.5)}$$

The constant S is composed of the afore mentioned, A, and a geometrical factor, f, according to S = A x f. The geometric factor, f, can not be directly determined from the difference spectra without knowing A. However, by comparing the difference spectra from two similar systems with similar experimental setups where A is expected to be constant, a ratio of the S from the respective systems will cancel the factor A. This ratio, $R = S_{unknow}/S_{known} = f_{unknow}/f_{known}$ relates the geometries of the two systems. As the arachidate chains are similar to the octadecyl groups and the spectra were all collected in Total–Yield mode, it was assumed that the values of A will cancel as the ratios are calculated. The following ratios were determined from the experimental data: $R_{Cd}(C–C) = 0.66$, $R_{Ca}(C–C) = 1.01$, $R_{Cd}(C–H) = 0.71$, and $R_{Ca}(C–H) = 1.05$. The term in brackets notes which resonance the ratio applied to and the subscript notes which arachidate was used to form the ratio.

In order to determine the tilt angle of the octadecyl chain, a model for description of the geometrical factor, f, must be postulated. Outka, *et al*(Outka et al. 1988; Outka et al. 1987) demonstrated that a tilted chain model best described the polarization dependence of the C K–edge NEXAFS spectra from the arachidates. This tilted chain model assumes that all the C atoms have a trans geometry and that the only tilting occurs in the plane of the C–C bonds. The tilted chain model was used to determine the tilt angle of the octadecyl groups on the Si(111) surface.

Outka, *et al*(Outka et al. 1988; Outka et al. 1987) demonstrated that the geometric factor, f, for the C–C bonds is given by Eq. IV.6.

$$f_{tilt}^{C-C} = 1 - \frac{3}{4}(1 + \cos(\partial)\cos(2\tau) \qquad \text{(IV.6)}$$

In this equation, δ is the C–C–C bond angle and τ is the tilt angle with respect to the surface normal. Utilizing Eq. IV.6, the tilt angle of the octadecyl groups was calculated to be 35° using R_{Cd}(C–C) and 33° using R_{Ca}(C–C) assuming a bond angle of 109.5°.

Futhermore, these calculated values can be checked using the σ^*(C–H) resonances. Outka, *et al*(Outka et al. 1988; Outka et al. 1987) demonstrated that the geometric factor, f, for the C–H bonds is given by Eq. IV.7.

$$f_{tilt}^{C-C} = 1 - \frac{3}{4}(1 - \cos(2\tau) + \cos(\phi) - \cos(\phi)\cos(2\tau)) \qquad \text{(IV.7)}$$

In this equation, ϕ is the C–C–C bond angle and τ is the tilt angle with respect to the surface normal. Utilizing Eq. IV.7, the tilt angle of the octadecyl groups was calculated to be 32° using R_{Cd}(C–C) and 31° using R_{Ca}(C–C) assuming a bond angle of 109.5°.

The calculated tilt angles from the octadecyl–terminated Si(111) surface were all within 4° of each other well within the experimental error of ±10° for this technique. Therefore, the tilt angle of the octadecyl chains with respect to the surface normal was determined to be 33° ± 10°. This is in excellent agreement with our structural model of an sp3 hybridized alkyl group bonded to the Si(111) substrate.

IV.4.6. Thermal Annealing

The decomposition behavior of the alkyl–terminated surfaces was investigated to

determine both the stability of the organic film and the utility of these surfaces as possible starting points for thin film growth (SiC or diamond). Valence band spectra and Si 2p core level spectra were collected from the methyl–, pentyl–, decyl–, and octadecyl–terminated Si(111) samples as a function of annealing temperature. The valence band spectra are shown in Figure IV.19 (pentyl), Figure IV.21 (methyl), Figure IV.23 (decyl), and Figure IV.25 (octadecyl). The surface–sensitive Si 2p core level spectra are shown in Figure IV.20 (pentyl), Figure IV.22 (methyl), Figure IV.24 (decyl), and Figure IV.26 (octadecyl). Due to the similar decomposition behavior of all the alkyl–terminated surfaces, the decomposition behavior will be discussed in terms of the pentyl–terminated Si(111) surface.

The pentyl–Si(111) surface was annealed to temperatures between 25° C and 700° C. The valence band spectra were collected using a photon energy of 55 eV and are shown in Figure IV.19. Three distinct temperature regions were noted in these spectra. Below 300° C, the valence band spectra was characteristic of the presence of the pentyl–group. Between 300° C and 600° C, the spectra had indicated that a Si–C alloy had been formed. Above 500° C, the valence band spectra were identical to that expected from the clean Si(111) 7x7 surface reconstruction.

Below 300° C, a comparison of the valence band intensity in the spectral region between 30 and 40 eV kinetic energy, that was attributed to the five C 2s based molecular orbitals in the pentyl group, and in the region near 47 eV kinetic energy showed that the intensity of the C 2s based peaks had diminished. This intensity loss in the C 2s region suggested that the pentyl–groups were desorbing from the surface through this temperature range. However, even though the intensity of these features decreased, the characteristic pattern of the five C 2s based molecular orbitals remained. This indicated that the main decomposition pathway was through desorption rather than through dissociation of the pentyl group into carbon chains of shorter length. This statement can be made with certainty, because if smaller alkyl groups formed on the surface, the valence band spectra would have shown different peak patterns in this region due to the presence of peaks from the four C 2s based molecular orbitals from butyl groups, the three molecular orbitals from propyl groups, etc.

After, the annealing temperature reached 300° C, the valence band had been change dramatically. No evidence of pentyl groups was seen in the valence band as the signal from the five C 2s based molecular orbitals had decayed to the background. Furthermore, a strong feature at 43.5 eV kinetic energy was present. This feature has been previously observed in valence band spectra from annealed silicon surfaces that had previously been exposed to diethylsilane(Lapiano-Smith, Himpsel, and Terminello 1993) and from α–SiC surfaces that had been irradiated with 50 eV photons(Didziulis et al. 1991). These studies attributed this valence band feature to a strong C 2p valence level from a SiC alloy. As the annealing temperature was increased, the intensity of the feature attributed to a SiC alloy decreased. Indicating that this carbon species was desorbing or diffusing into the silicon substrate.

Annealing above 600° C, resulted in the appearance of valence band spectra that resembled those from the reconstructed Si(111) 7x7 surface. In fact, the two surface states characteristic of the 7x7 surface reconstruction were present in the valence band at 49 and 50 eV Kinetic Energy. Bozso, *et al.*(Bozso et al. 1985) have reported that silicon out diffuses from the bulk covering surface carbon at these temperatures and the C forms SiC clusters beneath the top silicon layers. Thus, while the surface appeared to be clean, SiC clusters likely existed just below a thin film of reconstructed Si surface atoms.

As noted above, the behavior of the valence band spectra from the different alkyl–terminated surfaces was identical to that of the pentyl–terminated surface, with the exception of the octadecyl–Si(111) surface (Figure IV.25). The octadecyl groups were still present on the surface at 400° C and where not completely removed until the annealing temperature reached 500° C. It is possible that intermolecular attraction between neighboring octadecyl groups contributed to the higher desorption temperature observed for these long alkyl chains.

The Si 2p core level spectra core level spectra were collected with a photon energy of 130 eV. The Si 2p spectra from the pentyl–Si(111) surface are shown in Figure IV.20. The observed changes in this core level upon annealing were not as dramatic as those observed in the valence band spectra. At annealing temperatures below 300° C, the only observed

change in the Si 2p core level spectra was a slight increase in intensity. This, as with the valence band spectra, indicated that some of the alkyl groups were desorbing from the surface. Between 300° C and 600° C, the Si 2p core level continued to increase in intensity, but also showed linewidth broadening. It was impossible to accurately decompose these spectra due to the presence of a multitude of surface species. In this range, the valence band showed the existence of a SiC alloy. Almost certainly, domains of crystalline Si were also present on the surface. Finally, as these temperatures were below the desorption temperature of H(Coon et al. 1992), it was also likely the Si–H was present at the surface. As the annealing temperature went above 600° C, the Si 2p core level spectra were identical to those from the reconstructed Si(111) 7x7 surface. Again, as with the valence band data, indicating that a thin film of reconstructed silicon diffused out from the bulk and covered the SiC alloy.

Again, as noted above, the behavior of the Si 2p core level spectra from the different alkyl–terminated surfaces was identical to that observed from the pentyl–terminated surface. However, the extent of the recovery of the intensity of the Si 2p core level upon annealing due to desorption of the alkyl group and outdiffusion of silicon is clear in the Si 2p core level spectra from the octadecyl–terminated Si(111) surface (Figure IV.26). Here an order of magnitude increase in the Si 2p core level was observed upon annealing.

It has clearly been shown that at low temperatures, below 300°C that the alkyl groups desorbed as intact groups. Between 300° C and 600° C, elemental carbon was formed which reacted with the silicon substrate forming a SiC alloy. Finally, above 600° C, outdiffusion of silicon from the bulk covered the SiC alloy, and the Si film that covered the alloy reconstructed into the well know Si(111) 7x7 surface. It may be possible that the SiC alloy may in fact be useful as a precursor to either SiC or diamond growth.

IV.5. DISCUSSION

IV.5.1. Alkyl Monolayers

The goal of this work was to unequivocally show that the synthetic methodology proposed by Linford and Chidsey(Linford 1996) resulted in the formation of organic thin films with

a direct bond between the terminal C atom of the alkyl group and the Si substrate. In order to make this determination, it was necessary to identify the dominant C species, to determine if a chemical bond was formed, to determine the interfacial structure, and to determine the overlayer structure. High–resolution photoelectron spectroscopy, photoelectron diffraction, and near–edge X–ray absorption spectroscopy were used to determine the pieces to this puzzle.

Identification of the dominant C species was accomplished using valence band photoelectron spectroscopy. The C 2s region of the valence band indicated that the dominant C species was in the form of alkyl groups. The exact alkyl group was even be determined for the smaller alkyl groups by counting the number of peaks observed in this region. No evidence of multiple C surface species was observed.

Determination of C–Si bond formation was obtained using high–resolution photoelectron spectroscopy on the C 1s and Si 2p core levels. A chemically–shifted component in addition to the expected bulk–like peak were observed in both core level spectra. The Si 2p component was shifted to higher binding energy, while the C 1s component was shifted to lower binding energy. The Si component was indicative of charge transfer to a more electronegative atom. The C 1s component was indicative of charge transfer from a less electronegative atom. Combined they provide direct evidence of bond formation through charge sharing between the Si surface atoms and terminal C atom of the alkyl group.

Determination of the interfacial structure of the C–Si bond was provided by chemical–shift, scanned–energy photoelectron diffraction. The C 1s core level component attributed to the C–Si bond showed intensity oscillations as the photon energy was varied. These photoelectron diffraction oscillations were isolated and compared with theoretical models in order to determine that the C–Si bond length was 1.85 Å and that the alkyl groups were located in atop sites on the Si(111) surface.

Finally, determination of the thin film structure was provided by near–edge X–ray absorption spectroscopy. The polarization dependence of the C K–edge absorption spectra demonstrated that the alkyl groups were ordered above the silicon substrate. Utilizing the

difference spectra, it was determined that the alkyl groups were tilted 33° with respect to the sample normal.

Thermal annealing of these monolayers showed that they were stable below 200° C. The alkyl groups desorbed as intact units until the annealing temperature reached 300° C. Above this temperature, elemental carbon was formed and it reacted with the silicon substrate to form a SiC alloy. This surface may find utility as a starting surface for both diamond and silicon carbide thin film growth.

Therefore, it has been proven that the synthetic methods proposed by Linford and Chidsey(Linford 1996) result in the formation of a thin alkyl monolayer with direct bond formation to the underlying silicon substrate. Figure IV.27 shows the graphical representations of the pentyl–terminated surface (A) and the methyl–terminated surface (B) that result from the two synthetic methods described above.

IV.5.2. Applications of Chemical–Shift Photoelectron Diffraction

Novel techniques in materials chemistry may open exciting technological opportunities in the electronic sensing and control of complex molecular processes by providing durable bonds directly between organic materials, with their tailored chemical and biological specificities, and single–crystal semiconductors, with their excellent electronic properties. Unfortunately, determining the nature of the chemical bonds that hold a surface species to a substrate is often a difficult task. The problem is particularly acute for large molecular adsorbates such as those that comprise self–assembled monolayers. In fact, the exact nature of the substrate bonding remains controversial in the two most studied self–assembled monolayer systems: alkane thiols adsorbed on gold(Fenter, Eberhardt, and Eisenberger 1994) and trichloroalkylsilanes adsorbed on silica(Ulman 1991). By providing both direct experimental evidence of C–Si bonding and an accurate determination of bonding geometry, it has been demonstrated that the technique of chemical–shift, photoelectron diffraction can be used to determine the local geometric structure of the products of these novel *ex situ* synthetic surface chemical reactions. This technique should allow synthetic surface chemists to experiment with chemical

preparations derived from well–known solution chemistry knowing that they will have the ability to accurately determine the bonding and structure of the resulting adsorbate/ substrate interface.

IV.6. CONCLUSION

The novel passivation layers, alkyl–terminated silicon(111) surfaces, have been characterized using high–resolution photoelectron spectroscopy (PES), scanned–energy photoelectron diffraction (PED), and near–edge x–ray absorption spectroscopy (NEXAFS). Using high–resolution photoelectron spectroscopy, direct spectroscopic evidence of C–Si bond formation at the interface of the alkyl monolayers and the silicon substrate has been obtained. Scanned–energy PED measurements on the chemically–shifted C 1s core level components from pentyl– and methyl–terminated Si(111) surfaces over the energy range, $h\nu = 340$ eV to $h\nu = 600$ eV to determined that both monolayers reside in atop sites with a C–Si bond length of 1.85 ± 0.05 Å. NEXAFS spectra proved that the alkyl groups were oriented on the surface with a tilt angle of approximately 30°. As direct evidence of the formation of these monolayers as now been acquired, the preparation techniques can directly be extended to more complex monolayers containing electroactive and photoactive molecules.

By providing direct experimental evidence of C–Si bonding; the utility of chemical–shift photoelectron diffraction to determine the local geometric structure of the end products of multi–step, *ex situ* synthetic surface chemical reactions has been shown. This technique should allow synthetic surface chemists to experiment with chemical preparations derived from well–known solution chemistry surfaces knowing that they will have the ability to simply and accurately determine the resultant end products.

IV.7. ACKNOWLEDGEMENTS

This work was performed at the Stanford Synchrotron Radiation Laboratory, which is supported by the Department of Energy, Office of Basic Energy Science, Division of Chemical Sciences. The authors would also like to thank that Office's Division of Materials

Research. Further support was provided by the NSF–MRSEC program through the Center for Materials Research at Stanford University. Dr. M. R. Linford and Prof. C. E. D. Chidsey must be acknowledged for providing the samples and the XPS measurements used in this study. The XPS work benefited from the facilities and equipment made available to Stanford University by the NSF–MRSEC program through the Center for Materials Research at Stanford University. Also, Dr. E. J. Moler, Professor D. A. Shirley, and Professor C. S. Fadley provided the computer code used in the analysis of our data. Finally, Dr. L. J. Terminello provided thoughtful insight in the analysis of the photoelectron diffraction data.

IV.8. REFERENCES

Barton, J. J. 1985a. *Angle–Resolved Photoemission Extended Fine Structure*, Ph. D. Dissertation, University of California, Berkeley.

Barton, J. J. 1985b. *Angle–Resolved Photoemission Extended Fine Structure*: LBNL Report Number 19215, Lawrence Berkeley National Laboratory, University of California Berkeley, Berkeley.

Barton, J. J., S. W. Robey, and D. A. Shirley. 1986. *Physical Review B* 34:778.

Barton, J. J., and D. A. Shirley. 1985b. *Physical Review B* 32:1906.

Barton, J. J., and D. A. Shirley. 1985a. *Physical Review B* 32:1892.

Blodgett, K. B. 1934. *Journal of the American Chemical Society* 56:495.

Blodgett, K. B. 1935. *Journal of the American Chemical Society* 57:1007-22.

Bowen, H. J. M., J. Donohue, D. G. Jenkin, O. Kennard, P. J. Wheatley, and D. H. Whiffen. 1958. *Tables of Interatomic Distances and Configuration in Molecules and Ions.* London: The Chemical Society.

Bozso, F., J. T. Yates Jr., W. J. Choyke, and L. Muchlhoff. 1985. *Journal of Applied Physics* 57:2771.

Chidsey, C. E. D., and M. R. Linford. 1995. in the proceedings of the *Fourth International Symposium on Cleaning Technology in Semiconductor Device Manufacturing.*

Clementi, E., and C. Roetti. 1974. *Atomic Data and Nuclear Data Tables* 14:177.

Coon, P. A., M. L. Wise, A. C. Dillon, M. B. Robinson, and S. M. George. 1992. *Journal*

of Vacuum Science and Technology B 10:221.

Didziulis, S. V., J. R. Lince, P. D. Fleischauer, and J. A. Yarmoff. 1991. *Inorganic Chemistry* 30:672.

Eastman, D. E., F. J. Himpsel, J. A. Knapp, and K. C. Pandey. 1978. In *Physics of Semiconductors*, edited by B. L. H. Wilson. London: Institute of Physics.

Eastman, D. E., F. J. Himpsel, and J. F. van der Veen. 1982. *Journal of Vacuum Science and Technology* 20:609.

Fadley, C.S. 1988. in *Core-Level Spectroscopy in Condensed Systems. Proceedings of the Tenth Taniguchi International Symposium*, edited by J. Kanamori and A. Kotani. Berlin, West Germany: Springer-Verlag.

Fadley, C.S., S. Thevuthasan, A.P. Kaduwela, C. Westphal, Y.J. Kim, R. Ynzunza, P. Len, E. Tober, F. Zhang, Z. Wang, S. Ruebush, A. Budge, and M.A. Van Hove. 1994. *Journal of Electron Spectroscopy and Related Phenomena* 68:19.

Fenter, P., A. Eberhardt, and P. Eisenberger. 1994. *Science* 266:1216.

Hamrin, K., G. Johansson, U. Gelius, A. Fahlman, C. Nordling, and K. Siegbahn. 1968. *Chemical Physics Letters* 11:613.

Higashi, G.S., Y.J. Chabal, G.W. Trucks, and K. Raghavachari. 1990. *Applied Physics Letters* 56:656.

Himpsel, F. J., U. O. Karlsson, A. B. McLean, L. J. Terminello, F. M. F. de Groot, M. Abbate, J. C. Fuggle, J. A. Yarmoff, B. T. Thole, and G. A. Sawatzky. 1991. *Physical Review B* 43:6899.

Himpsel, F. J., F. R. McFeely, A. Taleb–Ibrahimi, J. A. Yarmoff, and G. Hollinger. 1988. *Physical Review B* 38:6084.

Hricovini, K., R. Gunther, P. Thiry, A. Taleb-Ibrahimi, G. Indlekofer, J.E. Bonnet, P. Dumas, Y. Petroff, X. Blase, X. Zhu, S. G. Louie, Y. J. Chabal, and P. A. Thiry. 1993. *Physical Review Letters* 70:1992.

Hufner, Stefan. 1995. *Photoelectron Spectroscopy.* Edited by M. Cardona. Vol. 82, *Solid–State Sciences*. Berlin: Springer–Verlag.

Krull, U.J., R.S. Brown, and A. Safarzadeh-Amiri. 1988. *Proceedings of the SPIE - The International Society for Optical Engineering* 906:49.

Kusunoki, I., and Y. Igari. 1992. *Applied Surface Science* 59:95.

Langmuir, I. 1920. *Transactions of the Faraday Society* 15:62-74.

Lapiano-Smith, D. A., F. J. Himpsel, and L. J. Terminello. 1993. *Journal of Applied Physics* 74:5842.

Larkins, G. L., C. D. Fung, and S. E. Rickert. 1989. *Thin Solid Films* 180:217-25.

Linford, M. R. 1996. *Chemical Functionalization of Hydrogen–Terminated Silicon Surfaces: The First Self–Assembled Monolayers on Silicon*, Ph. D. Dissertation, Stanford University, Stanford, CA.

Linford, M. R., and C. E. D. Chidsey. 1993. *Journal of the American Chemical Society* 115:12631.

Linford, M. R., P. Fenter, P. M. Eisenberger, and C. E. D. Chidsey. 1995. *Journal of the American Chemical Society* 117:3145.

Loucks, T. L. 1967. *Augmented Plane Wave Method.* New York: W. A. Benjamin, Inc.

NEWCHP. Moler, E. J., and J. J. Barton. 1994, University of California, Berkeley.

Note. 1. The program Mufpot was obtained from Prof. C. S. Fadley at the University of California, Davis.

Note. 2. The program NEWCHP was obtained from E. J. Moler at LBNL in Berkeley, California.

Outka, D. A., J. Stohr, J. P. Rabe, and J. D. Swalen. 1988. *Journal of Chemical Physics* 88:4076.

Outka, D. A., J. Stohr, J. P. Rabe, J. D. Swalen, and H. H. Rotermund. 1987. *Physical Review Letters* 59:1321.

Petty, M. C. 1996. *Langmuir–Blodgett films An Introduction.* Cambridge: Cambridge University Press.

Pireaux, I. J., J. Riga, P. A. Thiry, R. Caudano, and J. J. Verbist. 1986. *Physica Scripta* T13:78.

Potts, A. W., and D. G. Streets. 1974. *Journal of the Chemical Society Faraday Transactions II* 70:875.

Schedel-Niedrig, Th., M. Keil, H. Sotobayashi, T. Schilling, B. Tesche, and A.M. Bradshaw. 1991. *Journal of Physics: Condensed Matter* 3:S23.

Stinespring, C. D., and J. C. Wormhoudt. 1989. *Journal of Applied Physics* 65:1733.

Stohr, J. 1992. *NEXAFS Spectroscopy.* Edited by R. Gomer. Vol. 25, *Springer Series in*

Surface Sciences. Berlin: Springer–Verlag.

Stohr, J., D. A. Outka, K. Baberschke, D. Arvanitis, and J. A. Horsley. 1987. *Physical Review B* 36:2976.

Stohr, J., F. Sette, and Allen L. Johnson. 1984. *Physical Review Letters* 53:1684.

Sumakeris, J.J., L.B. Rowland, R.S. Kern, S. Tanaka, and R.F. Davis. 1993. *Thin Solid Films* 225:219.

Taylor, P. A., M. Bozack, W. J. Choyke, and J. T. Yates Jr. 1989. *Journal of Applied Physics* 65:1099.

Terminello, L.J., X.S. Zhang, Z.Q. Huang, S. Kim, A.E. Schach von Wittenau, K.T. Leung, and D.A. Shirley. 1988. *Physical Review B* 38:3879.

Terry, J., R. Cao, C. Wigren, and P. Pianetta. 1994. *Journal of Vacuum Science & Technology A* 12:1869.

Terry, J., M. R. Linford, R. Cao, J. Terry, P. Pianetta, and C. E. D. Chidsey. 1996a. in the proceedings of *The First International Conference on Synchrotron Radiation in Materials Science*. Chicago, IL., submitted.

Terry, J., M. R. Linford, C. Wigren, R. Cao, P. Pianetta, and C. E. D. Chidsey. 1996b. *Applied Physics Letters* in press.

Terry, J., C. Wigren, R. Cao, P. Pianetta, M. R. Linford, and C. E. D. Chidsey. 1997. in prep.

Ulman, A. 1991. *An Introduction to Ultrathin Organic Films: from Langmuir–Blodgett to Self–Assembly*. Boston: Academic Press.

Van Hove, M. A., S. Y. Tong, and M. H. Elconin. 1977. *Surface Science* 4:85.

Weiss, K.–U., R. Dippel, K.–M. Schindler, P. Gardner, V. Fritzsche, A. M. Bradshaw, A. L. D. Kilcoyne, and D. P. Woodruff. 1992. *Physical Review Letters* 69:3196.

Weiss, K.–U., R. Dippel, K.–M. Schindler, P. Gardner, V. Fritzsche, A. M. Bradshaw, D. P. Woodruff, M. C. Asensio, and A. R. Gonzalez–Elipe. 1993. *Physical Review Letters* 71:581.

Zheng, Y., Z. Hussain, and D.A. Shirley. 1993. *Chemical Physics Letters* 206:161.

Zheng, Y., E. Moler, E. Hudson, Z. Hussain, and D.A. Shirley. 1993. *Physical Review B* 48:4760.

Table IV.1: Si 2p core level peak positions from the spectra in Figure IV.7 taken at a photon energy of 130 eV.

Sample Termination	Bulk Position (eV)	C–Si Position (eV)	Chemical Shift (eV)
Methyl	26.09	25.82	-0.27
Pentyl	26.10	25.89	-0.21
Decyl	26.16	25.95	-0.21

Table IV.2: Si 2p core level intensities from the spectra in Figure IV.7 taken at a photon energy of 130 eV.

Sample Termination	Bulk Intensity	C–Si Intensity	Total Si 2p Intensity	Ratio C–Si to Total Intensity	Calculated Coverage (See text) (ML)
Methyl	0.849	0.500	1.360	0.368	1.05
Pentyl	0.338	0.108	0.551	0.196	0.56
Decyl	0.0937	0.0713	0.226	0.315	0.90

Figure IV.1: Valence band spectra from methyl–, pentyl–, decyl–, and octadecyl–terminated Si(111) surfaces are shown. These spectra were collected at a photon energy of 55 eV. A valence band spectrum from a Si(111) 7x7 surface is shown as a reference.

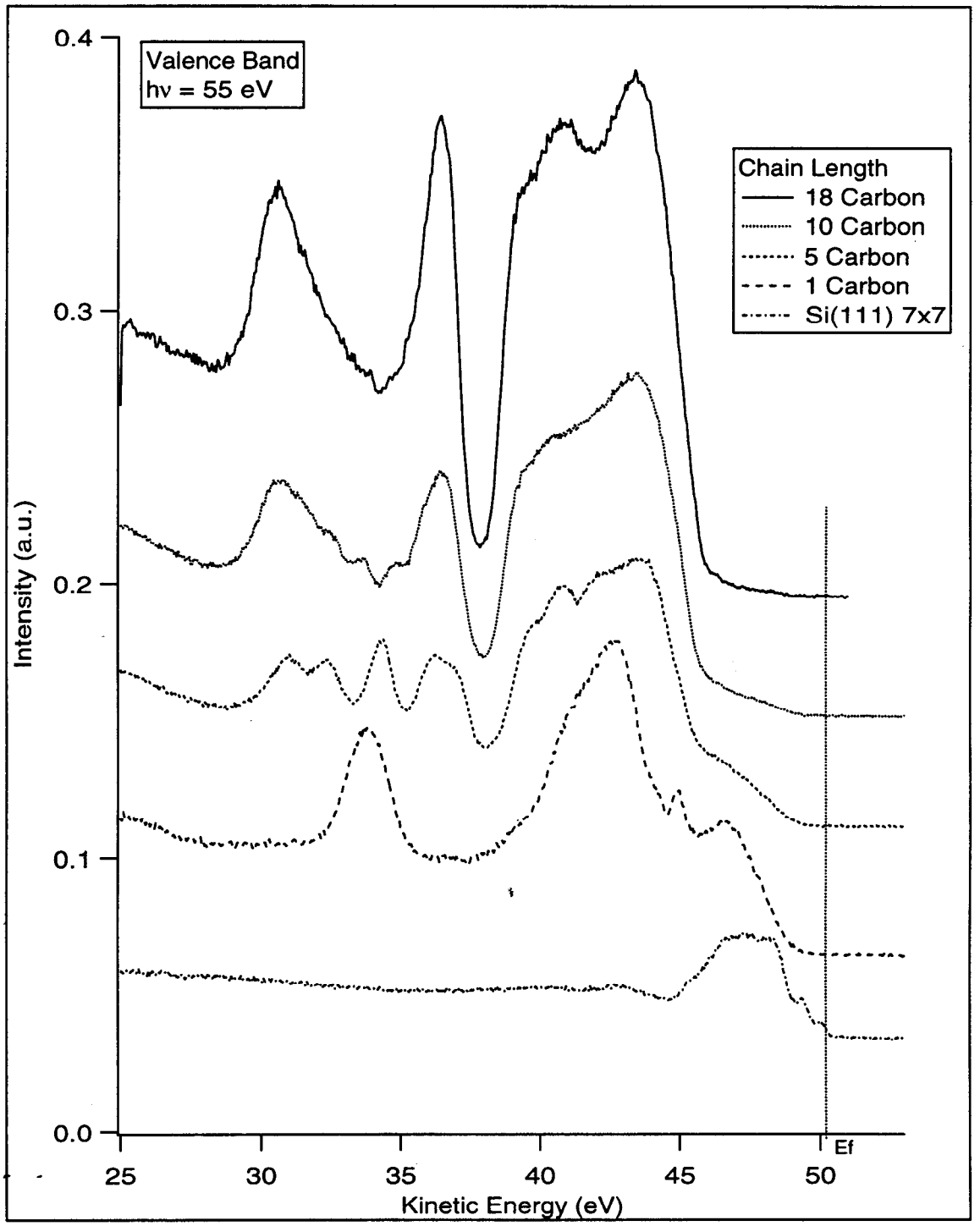

Figure IV.2: The valence band spectra from the alkyl–terminated surfaces are shown along with spectra from the corresponding alkane. It is evident that alkyl chains are present on the silicon surfaces and that the valence band can be used a fingerprint to identify the alkyl species. The alkane spectra(Pireaux et al. 1986) were collected with an XPS source and were aligned with the data from the present study.

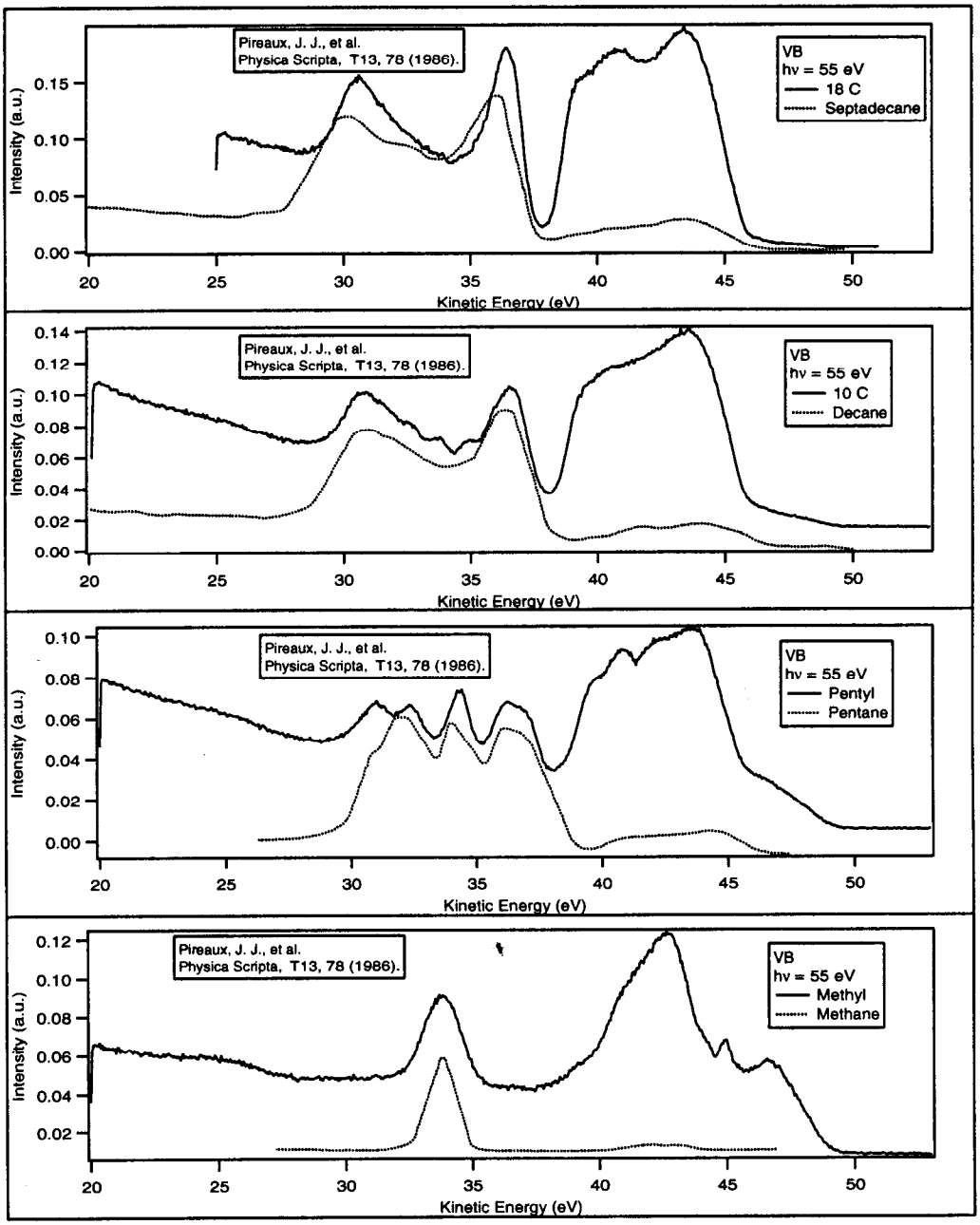

Figure IV.3: A valence band spectrum from pentyl–terminated Si(111) is shown. Note that the C 2s region provides a means of identifying the surface species because the number of components observed is equal to the number of C atoms in the chain. The solid vertical lines are referenced gas phase binding energies of the C 2s based molecular orbitals in n–pentane(Potts and Streets 1974) See text for an explanation of the referencing procedure.

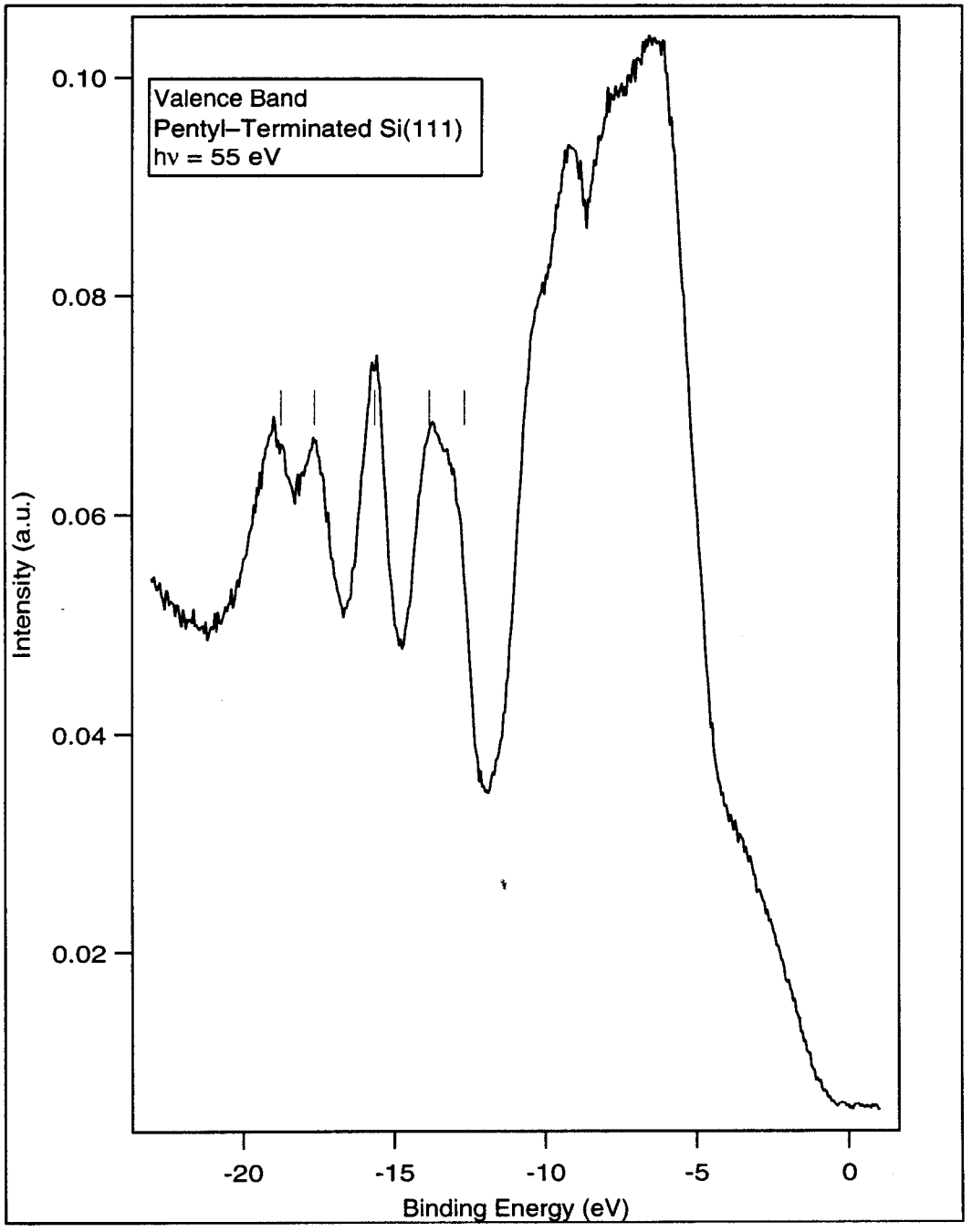

Figure IV.4: Valence band spectra from pentyl– and penteyl–terminated Si(111) are shown. Clearly evident is the sensitivity of the C 2s based molecular orbitals to chemical state, i.e. sp^3 vs. sp^2 hybridization in the chain. These spectra were taken with a photon energy of 55 eV.

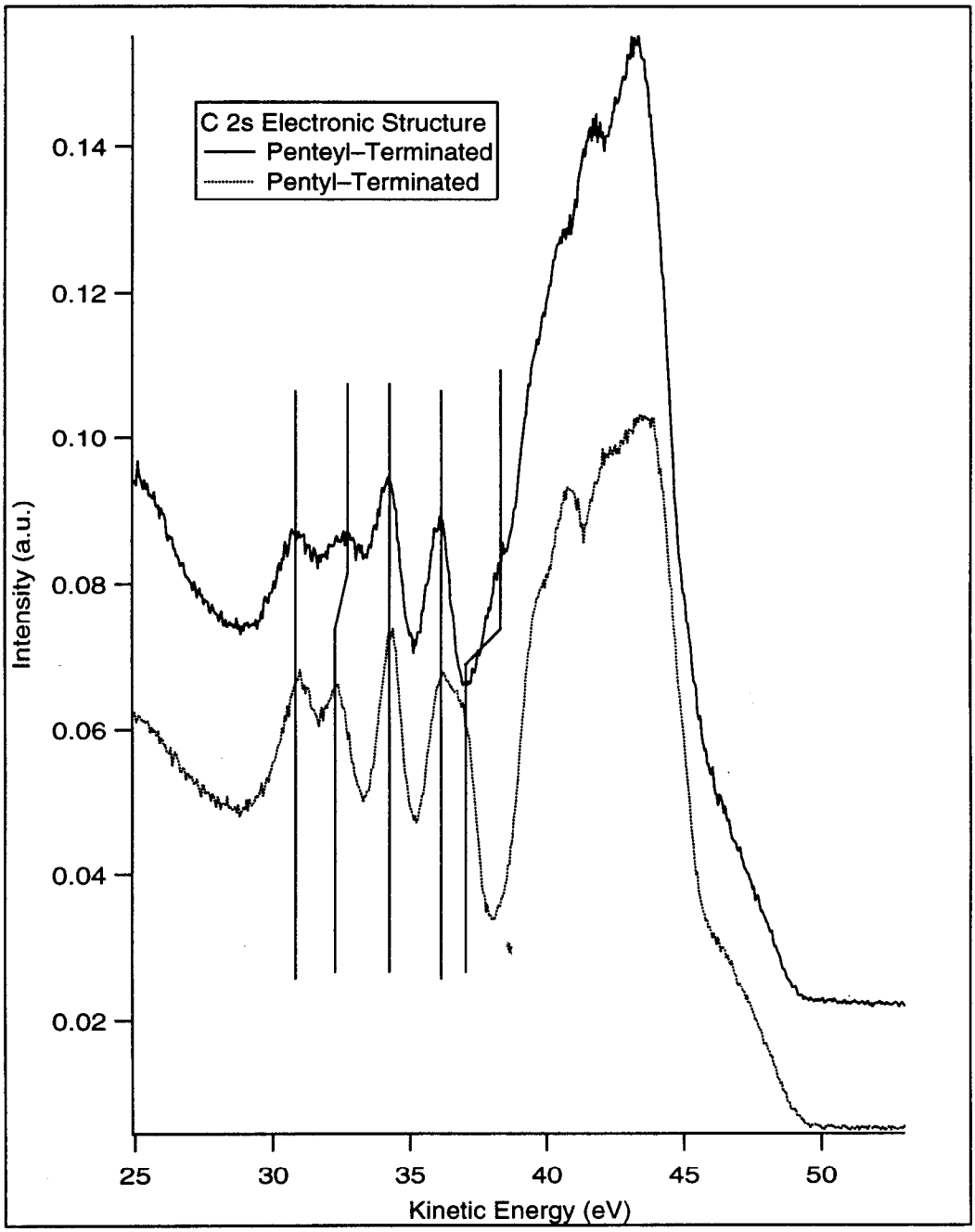

Figure IV.5: Surface sensitive Si 2p core level spectra from methyl–, pentyl–, and decyl–terminated Si(111) samples taken at a photon energy of 130 eV. **The spectrum from an octadecyl–terminated sample was taken with a photon energy of 120 eV because a larger electron escape depth was necessary in order to increase the signal strength of the Si 2p core level. This spectrum was then aligned with those of the short chains.

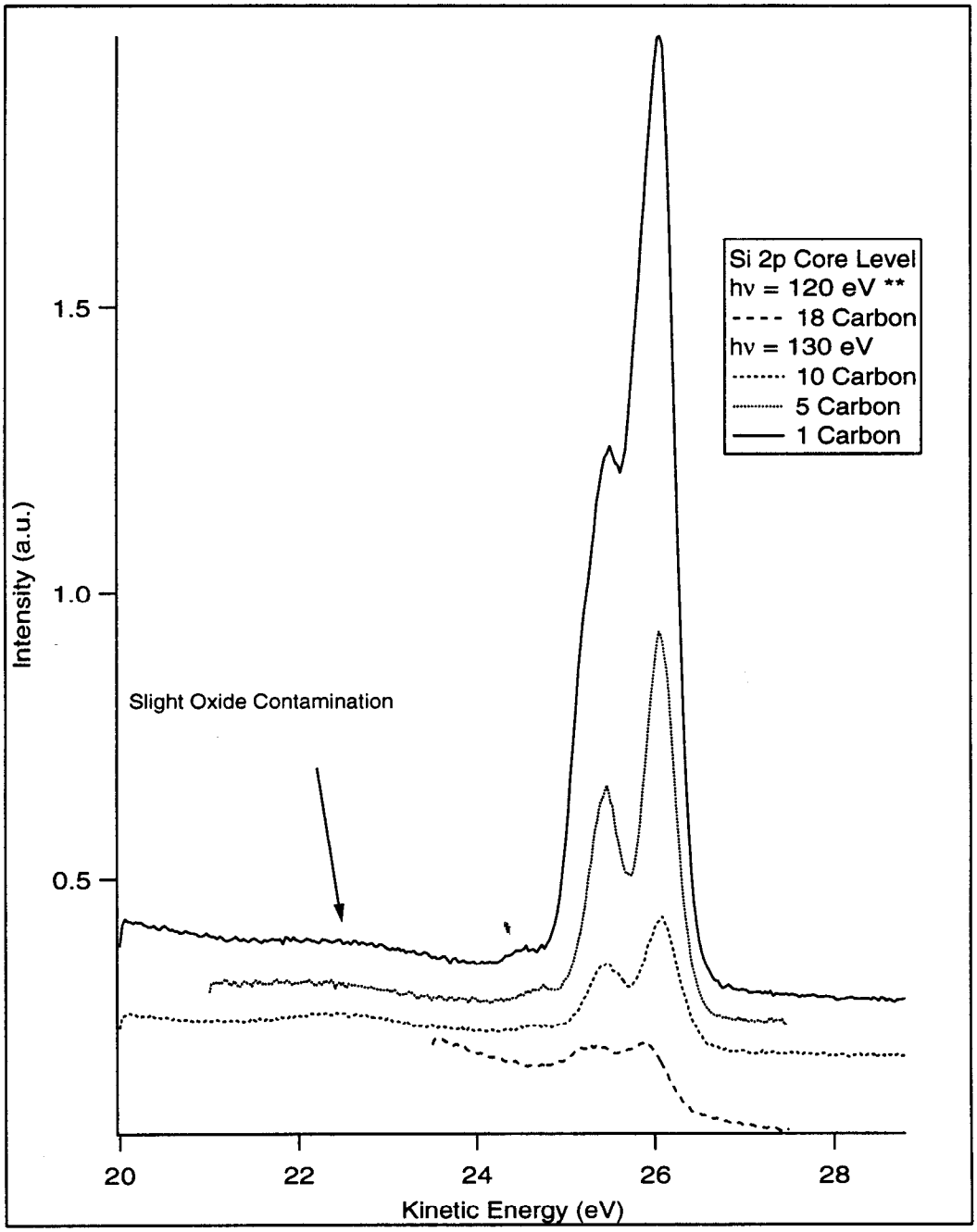

Figure IV.6: Same as Figure IV.5 except the spectra were taken with a photon energy of 115 eV. These spectra are more bulk sensitive than those in Figure IV.5 due to a larger escape depth of the photoelectrons.

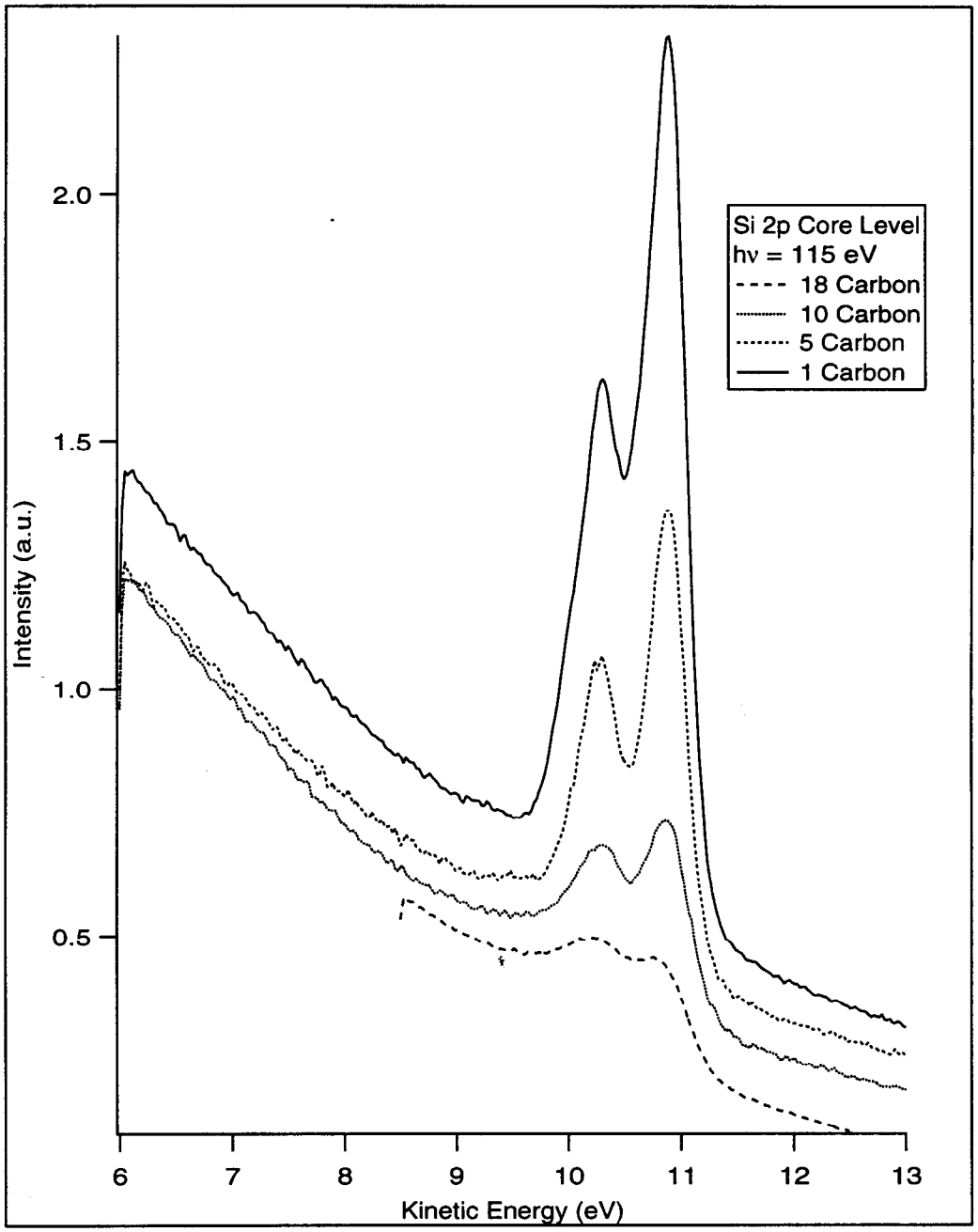

Figure IV.7: Shown are the Si 2p core level spectra from Figure IV.5 decomposed into multiple components. Three main features were observed and were attributed to emission from bulk–like Si, Si bound to C, and SiO_x species.

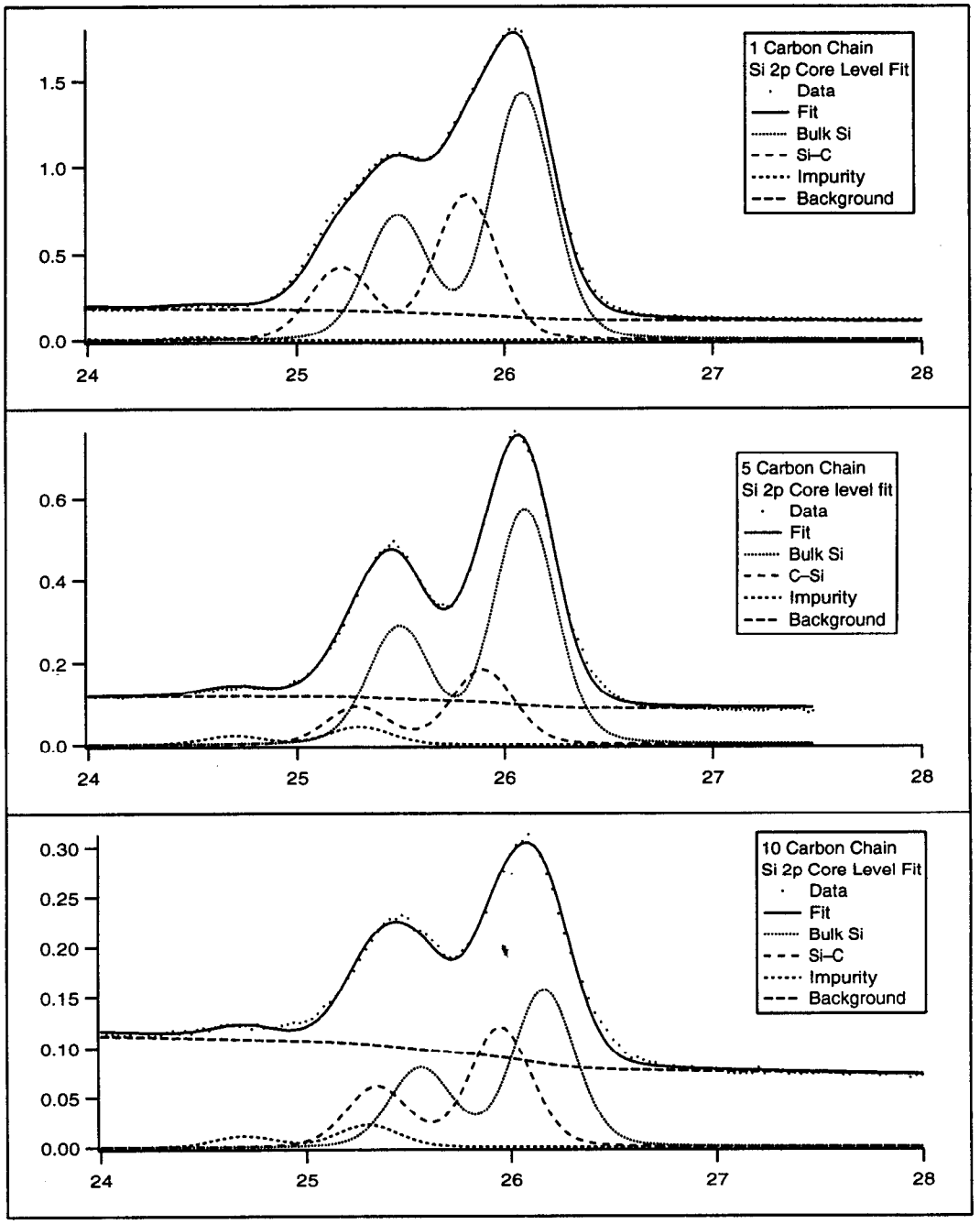

Figure IV.8: Si 2p core level spectra from hydrogen–, chlorine–, and methyl–terminated Si(111) surfaces are shown. These spectra have been decomposed into spin–orbit split doublets as described in the text. In each spectrum, a component is labeled as bulk silicon emission. The other component is attributed to the adsorbed species.

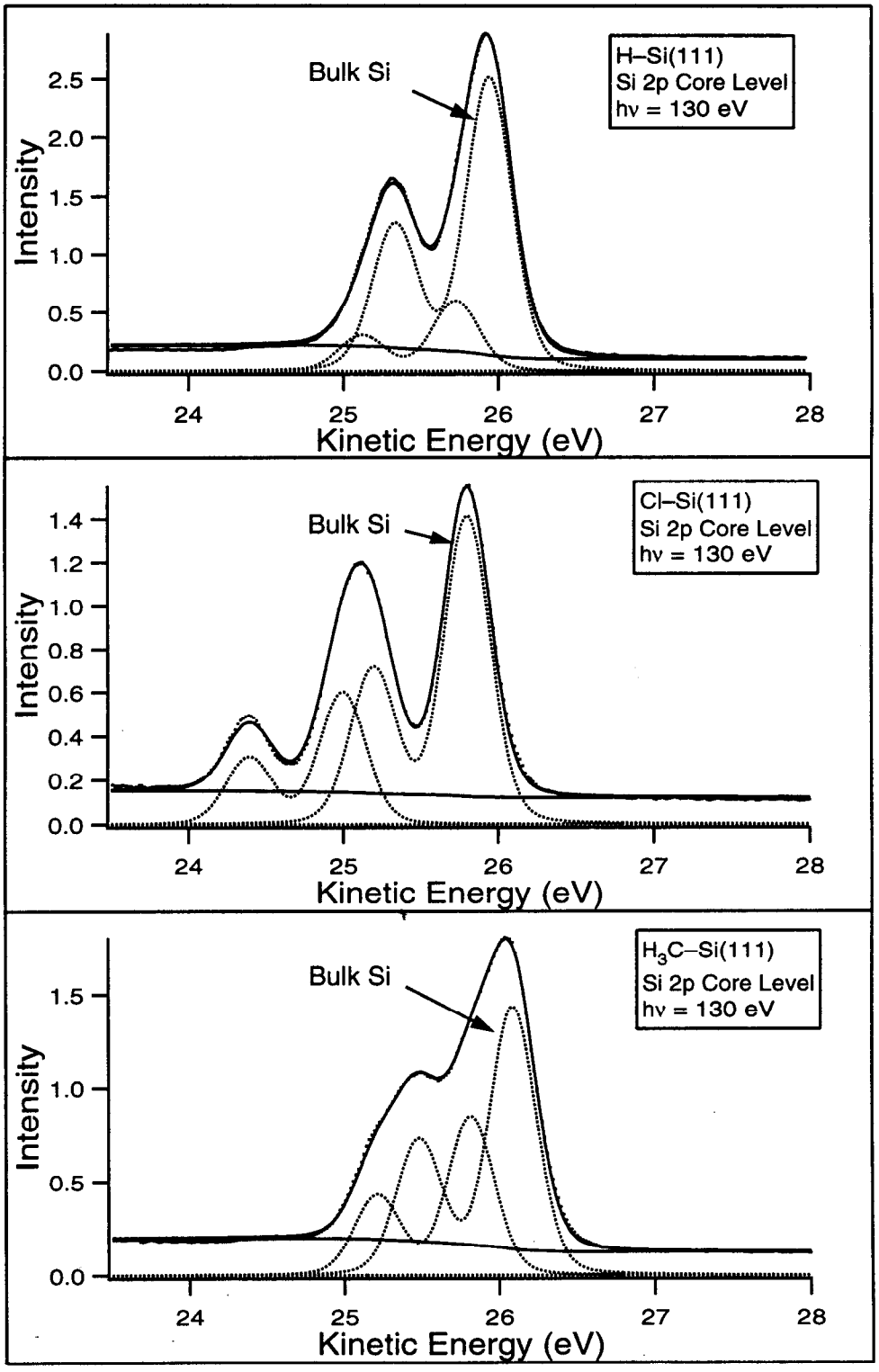

Figure IV.9: Carbon 1s core level spectra from methyl–, pentyl–, decyl–, and an octadecyl–terminated Si(111) samples taken at a photon energy of 350 eV are shown. Two components were observed in all spectra. The intensity of the peak at a kinetic energy of 57.5 eV increased markedly from samples terminated with longer C chains. A corresponding decrease in intensity was observed for the higher kinetic energy component.

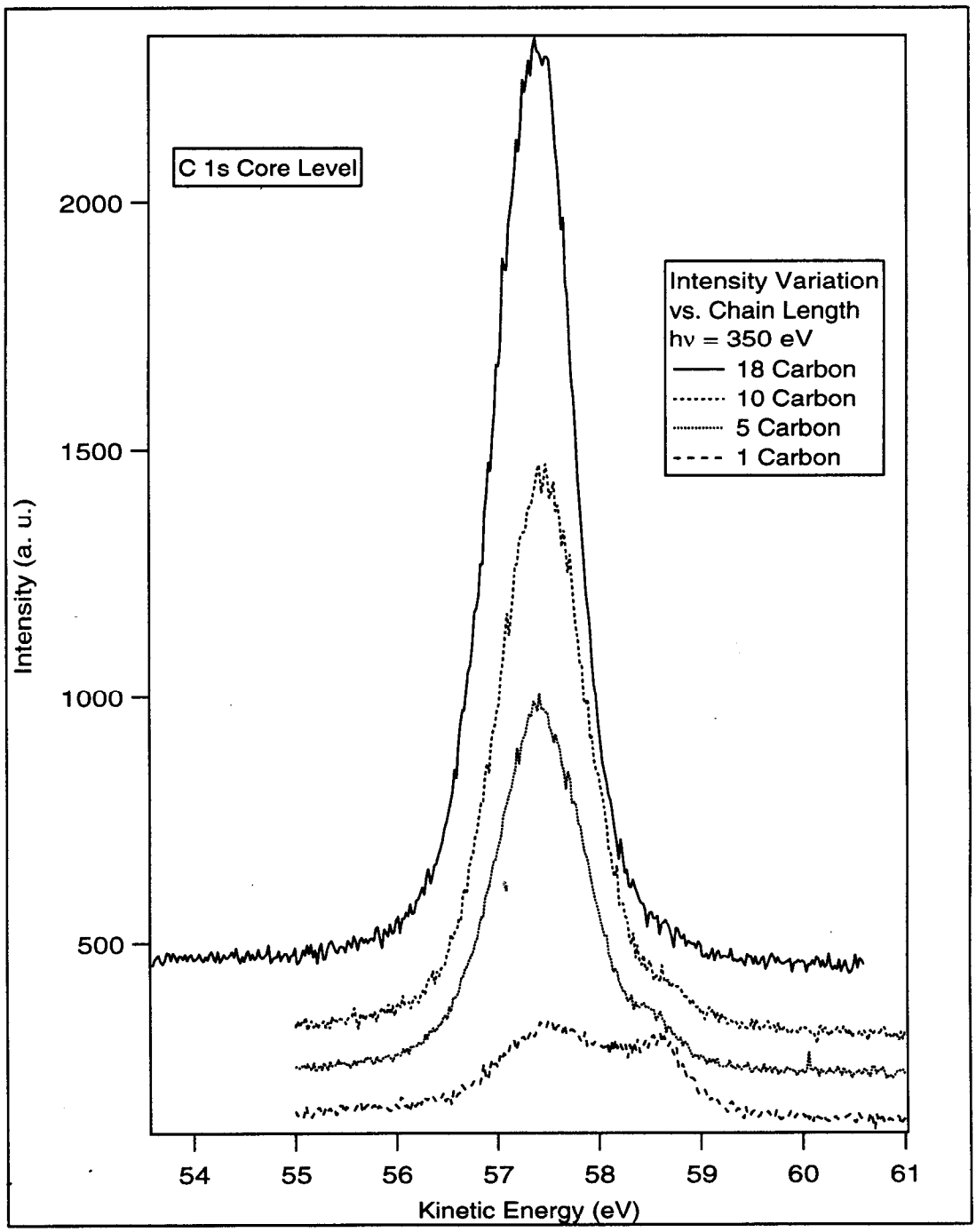

Figure IV.10: The C 1s core level spectra taken at a photon energy of 350 eV from the pentyl–terminated Si(111) sample of Figure IV.9 is shown decomposed into two singlet components. For reasons described in the text the components are attributed to emission from the bulk–like C atoms in the alkyl chain (C–C) and to emission from the C atom bound to the Si surface (C–Si).

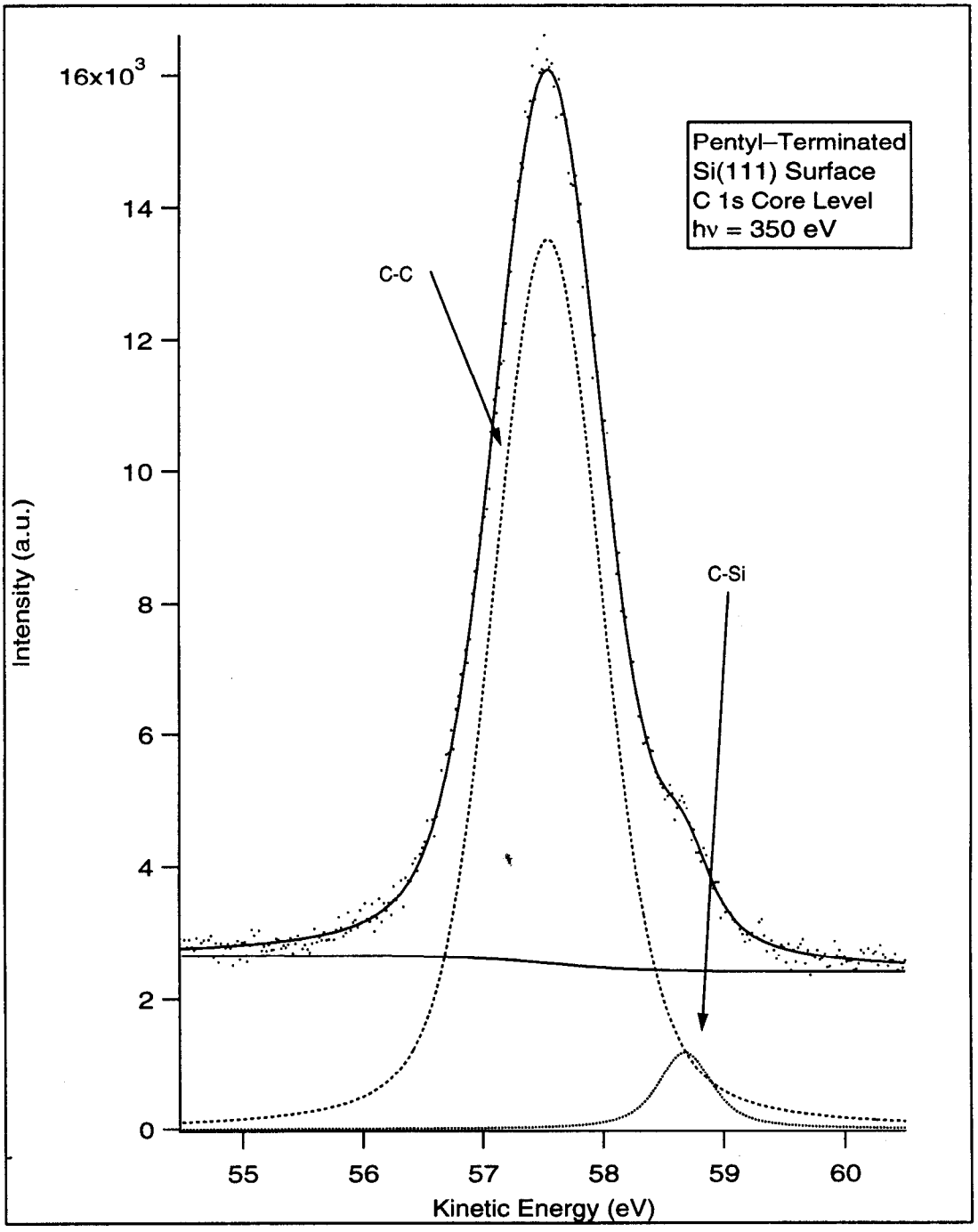

Figure IV.11: A.) A C 1s spectra from a pentyl–terminated Si(111) surface taken with a photon energy of 350 eV is shown. It has been decomposed into two singlet components which for reasons described in the text have been labeled C–C and C–Si. B.) Same as in A.) except the photon energy was 370 eV. Note the difference in intensity of the C–Si component. C.) Experimental partial cross section determined by decomposing the C 1s core level as above is shown. The atomic partial cross section (0 order) was obtained by fitting a smooth function to the experimental data.

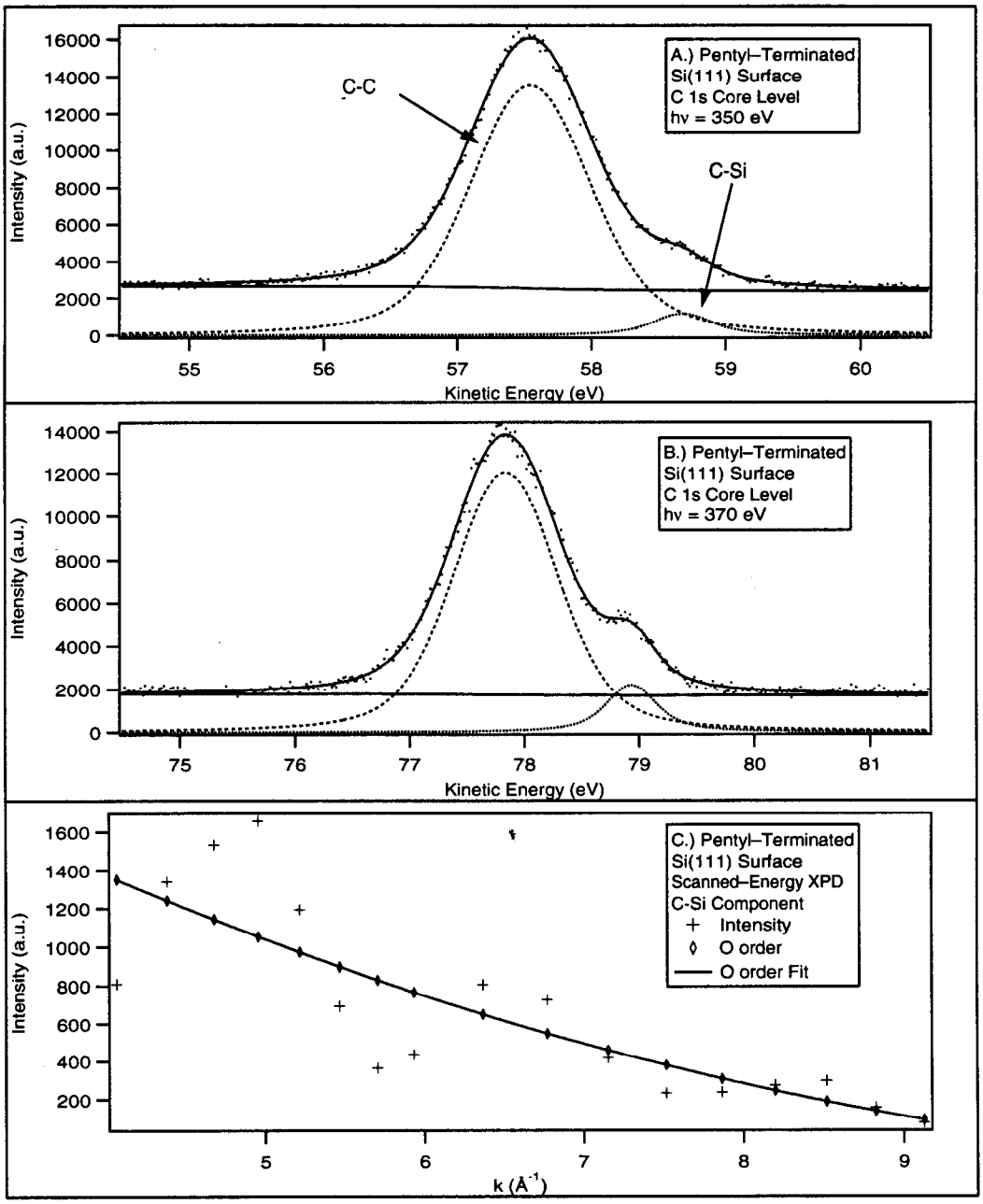

Figure IV.12: A.) A C 1s spectra from a methyl–terminated Si(111) surface taken with a photon energy of 350 eV is shown. It has been decomposed into two singlet components which for reasons described in the text have been labeled C–C and C–Si. B.) Same as in A.) except the photon energy was 370 eV. Note the difference in intensity of the C–Si component. C.) Experimental partial cross section determined by decomposing the C 1s core level as above is shown. The atomic partial cross section (0 order) was obtained by fitting a smooth function to the experimental data.

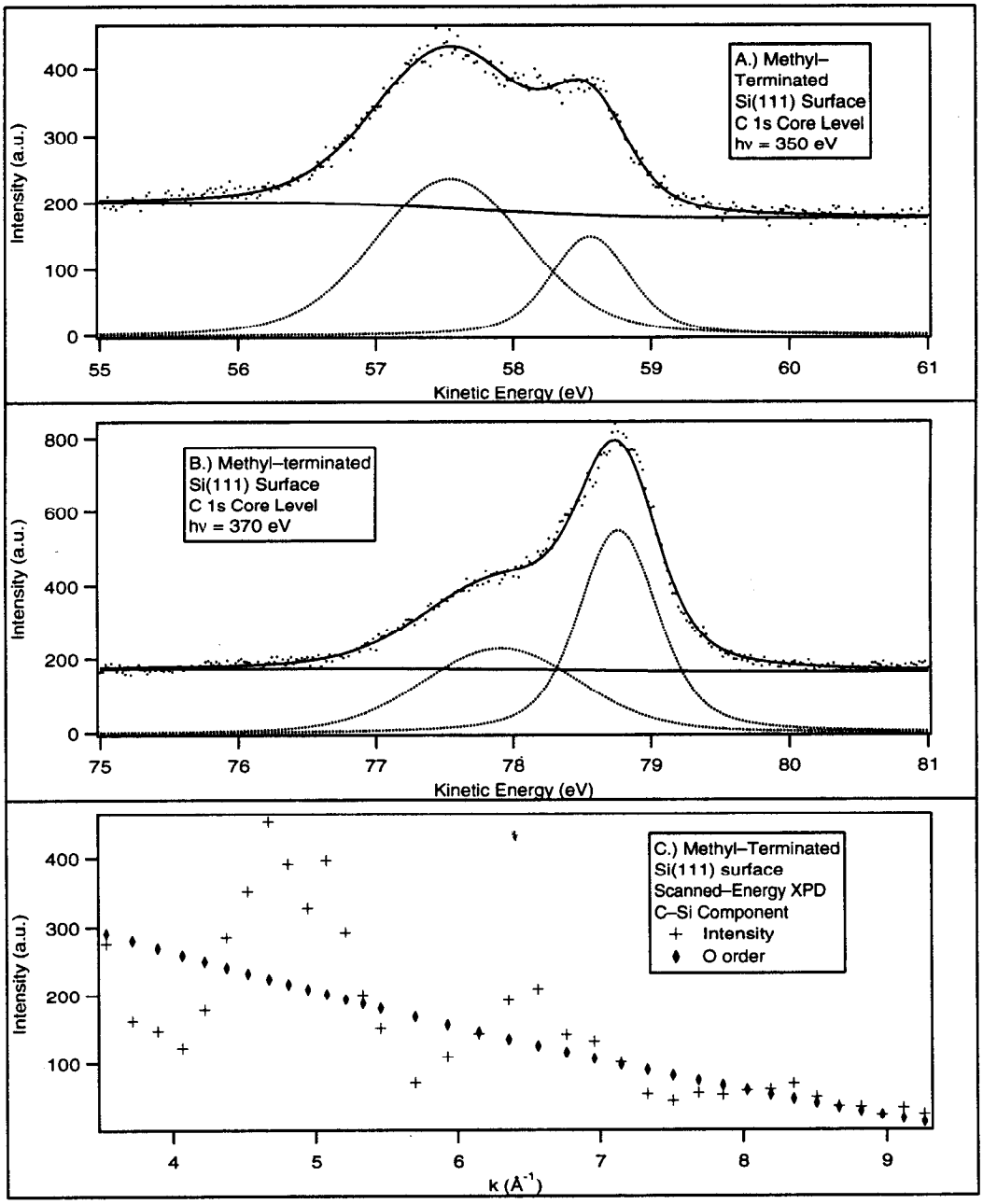

Figure IV.13: A.) The experimental modulation function, $\chi(k)$, and that from the best theoretical model is shown from the pentyl–terminated surface. The inset shows the R–factor analysis as a function of modeled Si–C bond length. The C–Si bond length was determined to be 1.85 ± 0.05 Å. B.) The experimental modulation function, $\chi(k)$, and that from the best theoretical model is shown from the methyl–terminated surface. The inset shows the R–factor analysis as a function of modeled Si–C bond length. The C–Si bond length was again determined to be 1.85 ± 0.05 Å.

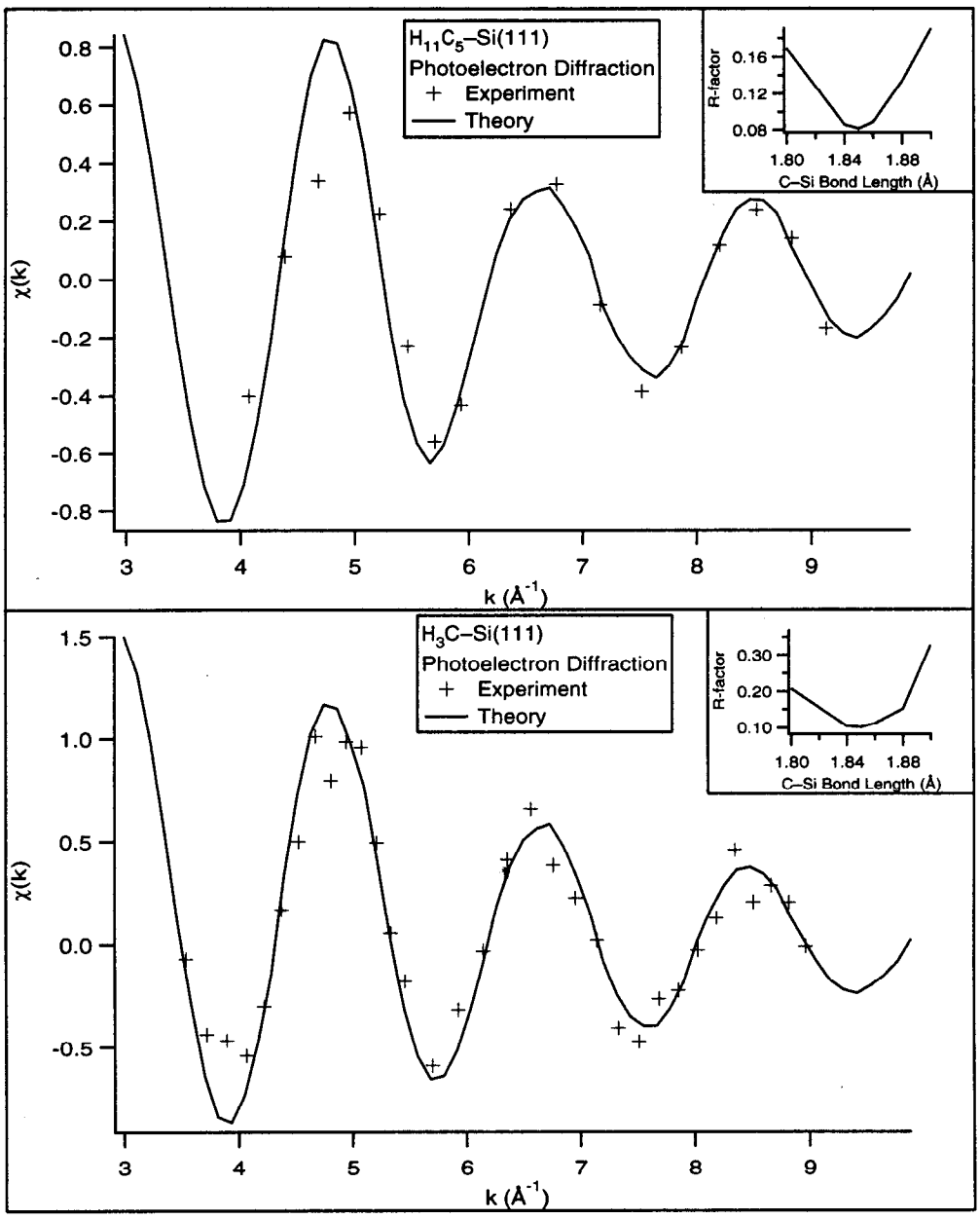

Figure IV.14: The four layer slab used in the photoelectron diffraction calculations of both the methyl– and pentyl–terminated Si(111) surfaces. This slab depicts the alkyl group in an atop site which had the best fitting calculated χ function. In the case of the pentyl–terminated surface, this model includes scattering from the third layer silicon atoms, but neglects scattering from the neighboring C atom.

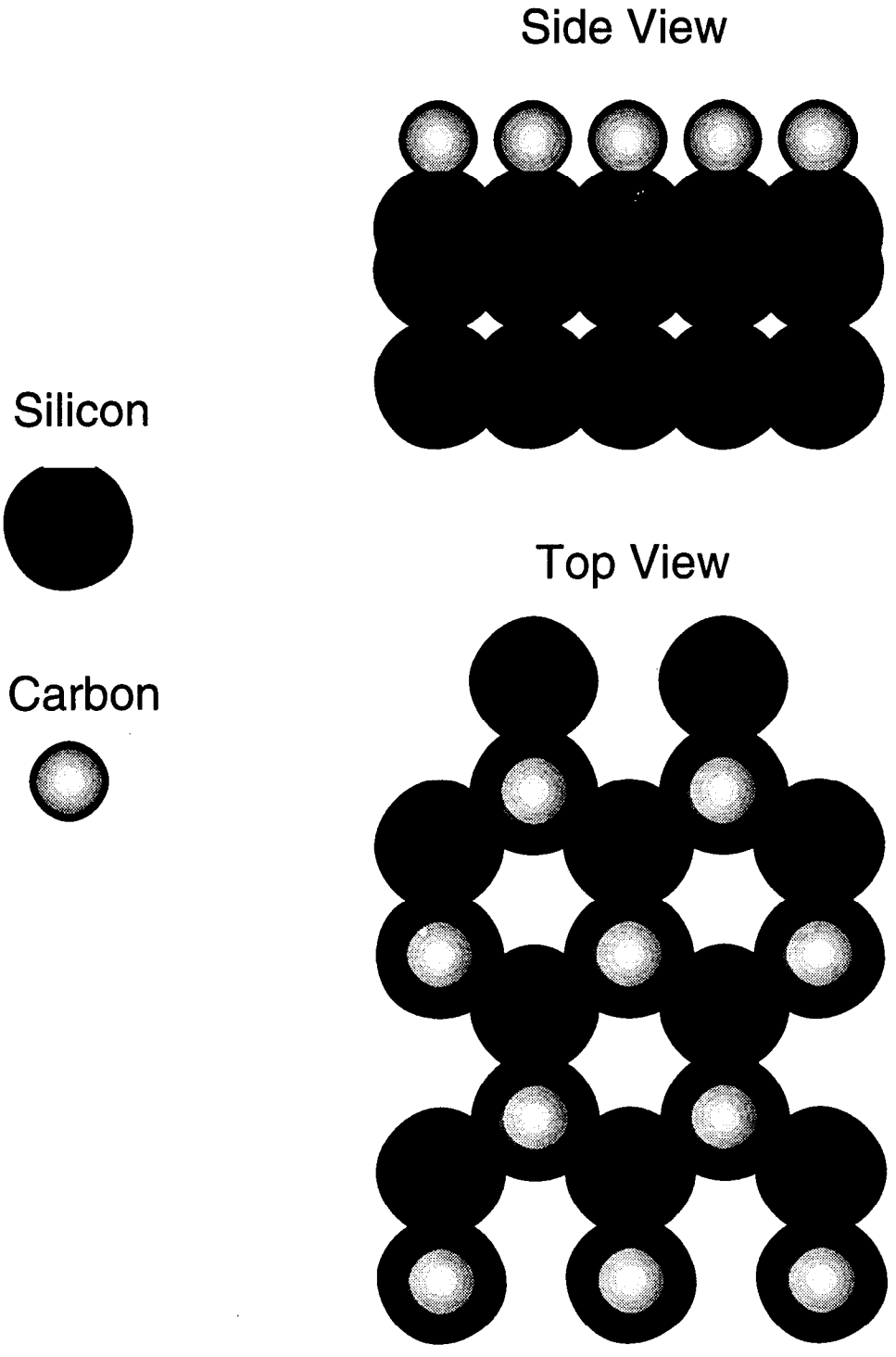

Figure IV.15: The four layer slab used in the photoelectron diffraction calculations from the pentyl–terminated Si(111) surface. This slab depicts the alkyl group in an atop site which had the best fitting calculated χ function. This model includes scattering from the neighboring C atom, but neglects scattering from the third layer silicon atoms.

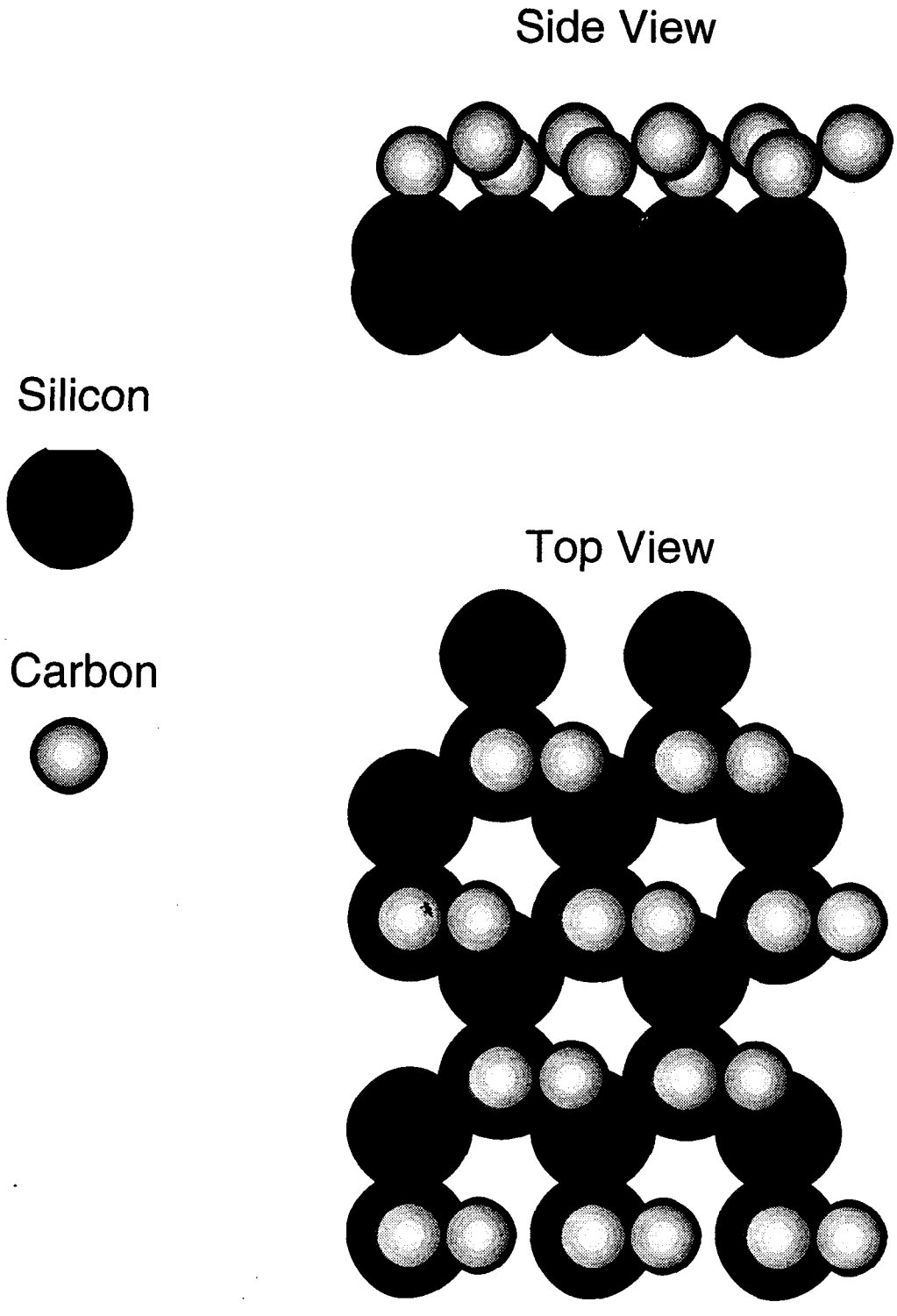

Figure IV.16: NEXAFS spectra from an octadecyl–terminated sample collected using the C KLL Auger line with the photon beam at glancing and grazing incidence are shown. The difference spectra which will be used to determine the orientation of alkyl chain is also shown. The main features are identified along with the position of the ionization potential. The C–C bond length in the chain was determined to be 1.53 Å by using the position of the σ*(C–C) features as described in the text.

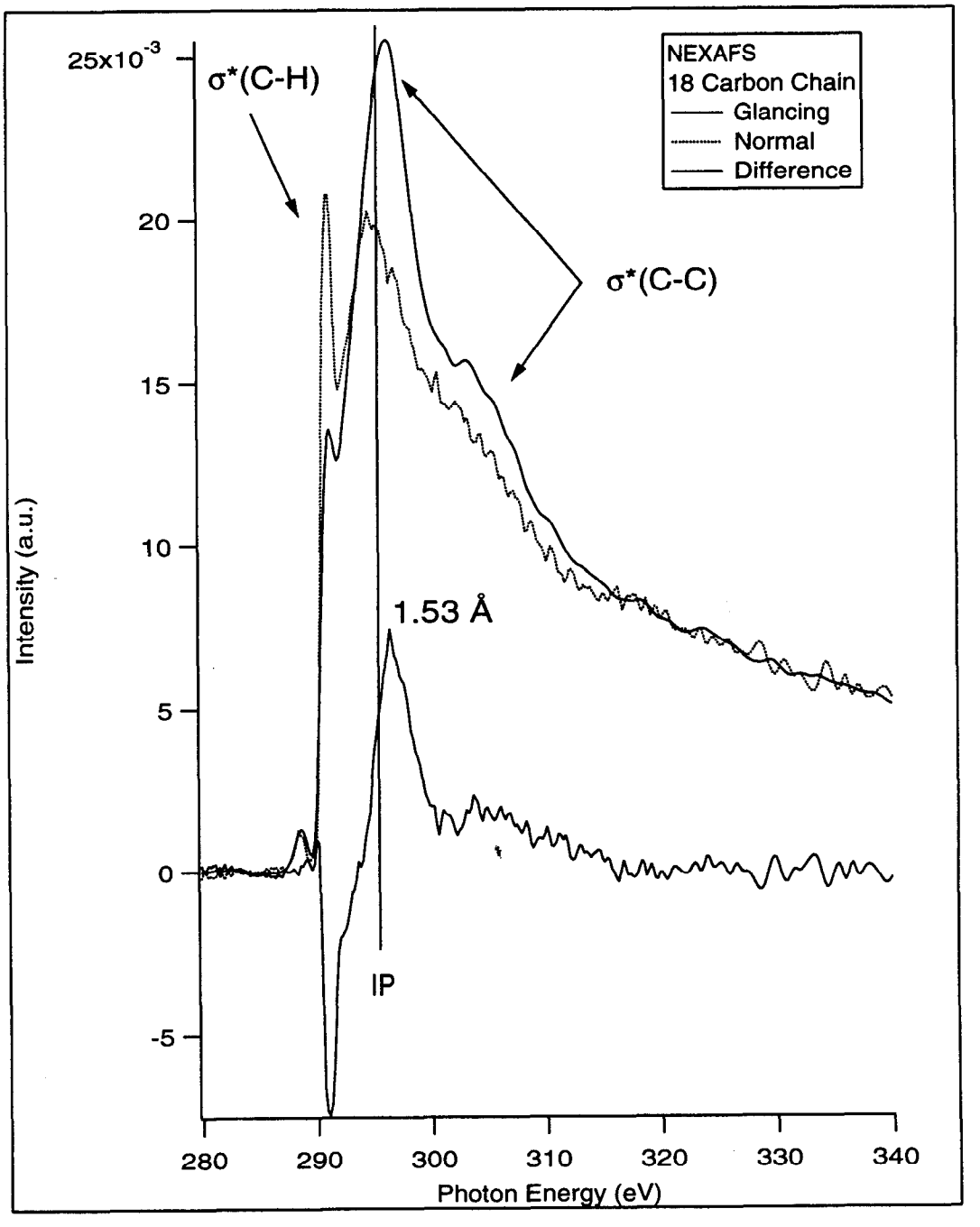

Figure IV.17: NEXAFS spectra collected as in Figure IV.16 from methyl–, pentyl–, decyl–, and octadecyl–terminated Si(111) samples are shown. Note that as the length of the alkyl chain decreased, the spectra show strong contribution from the absorption of the C atom bound to the Si substrate. This clearly shows up in the differences observed in the difference spectra from the different samples.

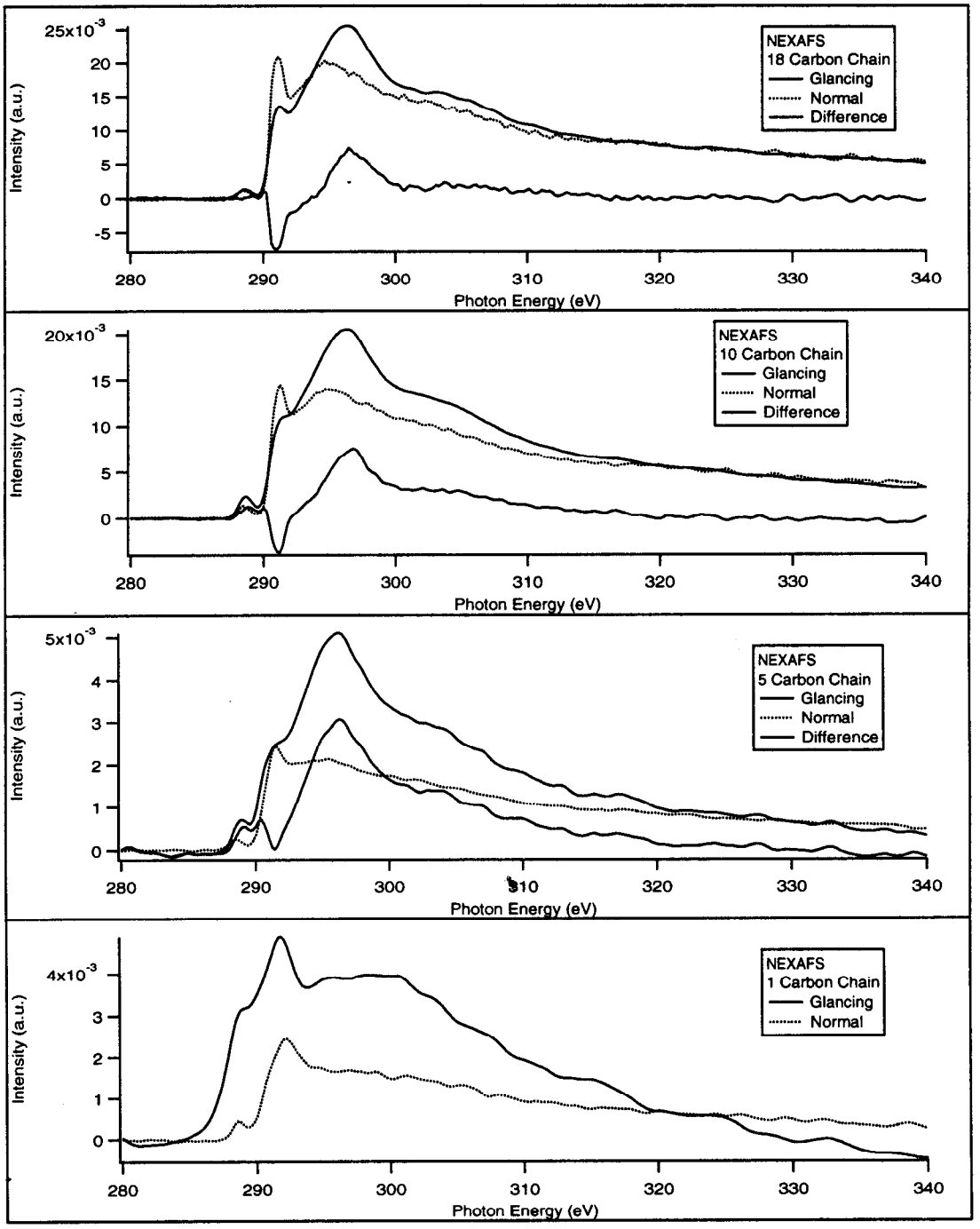

Figure IV.18: In order to obtain an accurate tilt angle of the alkyl chains with respect to the surface normal, the difference spectrum from the octadecyl–terminated sample (least contribution from the C atom bound to the surface) were compared to difference spectra from standard compounds with known tilt angles. This figure shows the NEXAFS spectra from Polyethylene (tilt angle 90°)(Stohr et al. 1987), Ca Arachidate (tilt angle 33°)(Outka et al. 1988; Outka et al. 1987), Cd Arachidate (tilt angle 0°)(Outka et al. 1988; Outka et al. 1987), and octadecyl–terminated Si(111). Note the similarity of the difference spectra of Ca Arachidate.

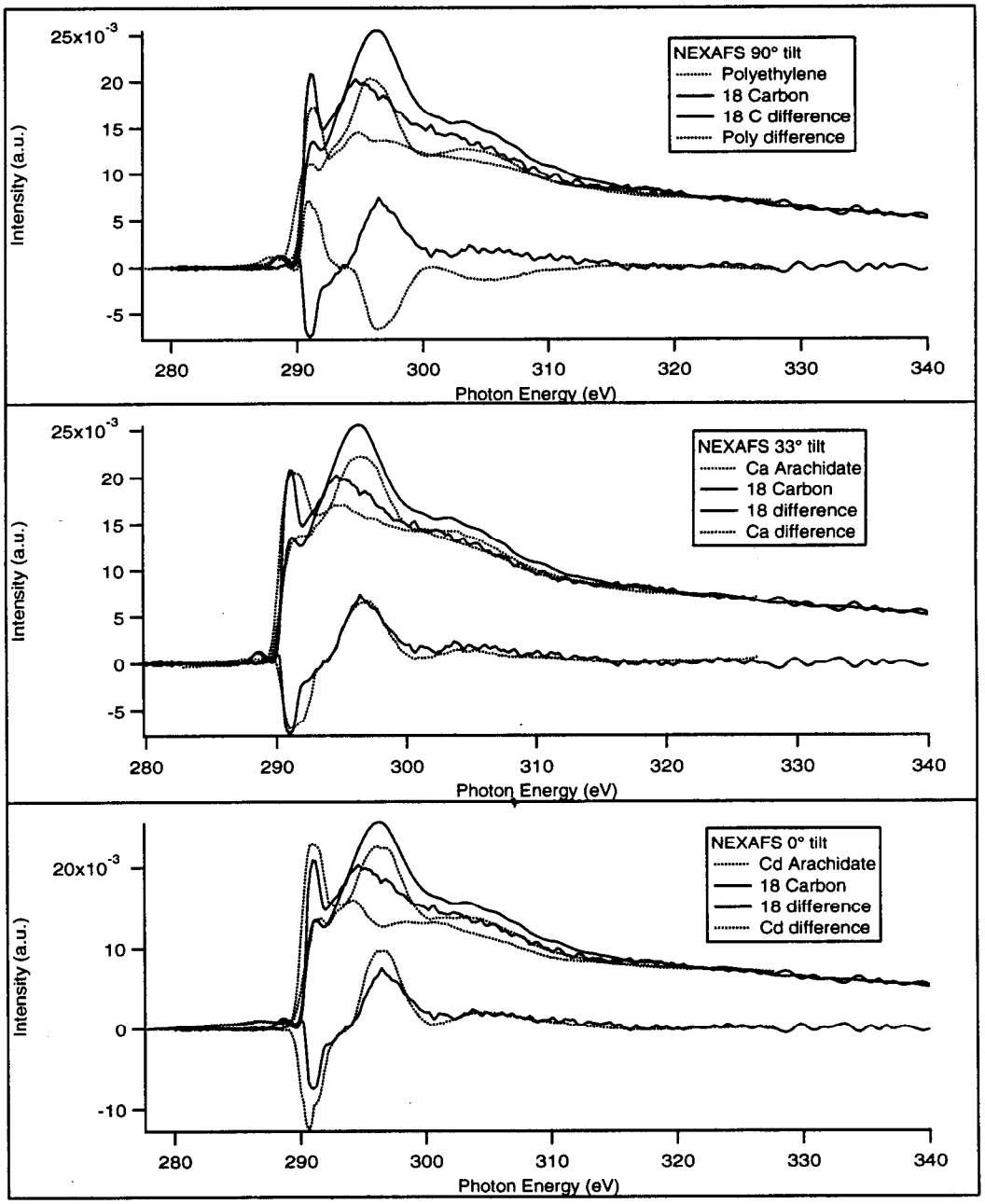

Figure IV.19: Valence band spectra taken from a pentyl–terminated Si(111) surface with a photon energy of 55 eV after annealing to the listed temperature are shown. Note that the pentyl chain did not break apart into smaller alkane units as was evidenced by the presence of only the 5 molecular orbitals on the pentyl–terminated surface. Silicon carbon alloying occurred at temperatures above 250° C (growth of peak at 44 eV). Above 600° C the surface reconstructed into the clean Si(111) 7x7 surface indicating that the alloy desorbed or diffused into the bulk.

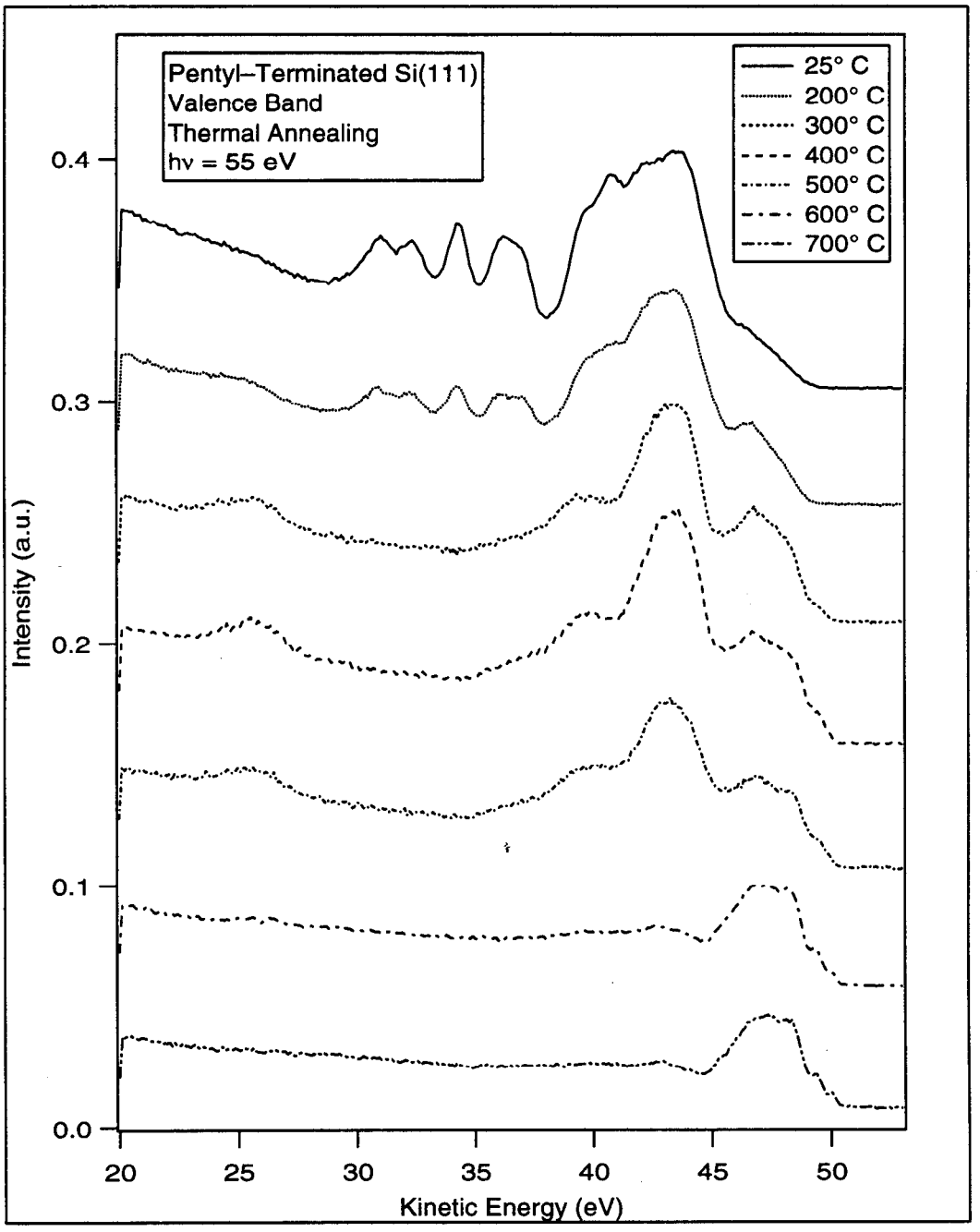

Figure IV.20: Silicon 2p core level spectra from a pentyl–terminated Si(111) surface with a photon energy of 130 eV (surface sensitive) after annealing to the listed temperature are shown. The transition from an alkyl–terminated surface to a clean Si(111) 7x7 surface is evident.

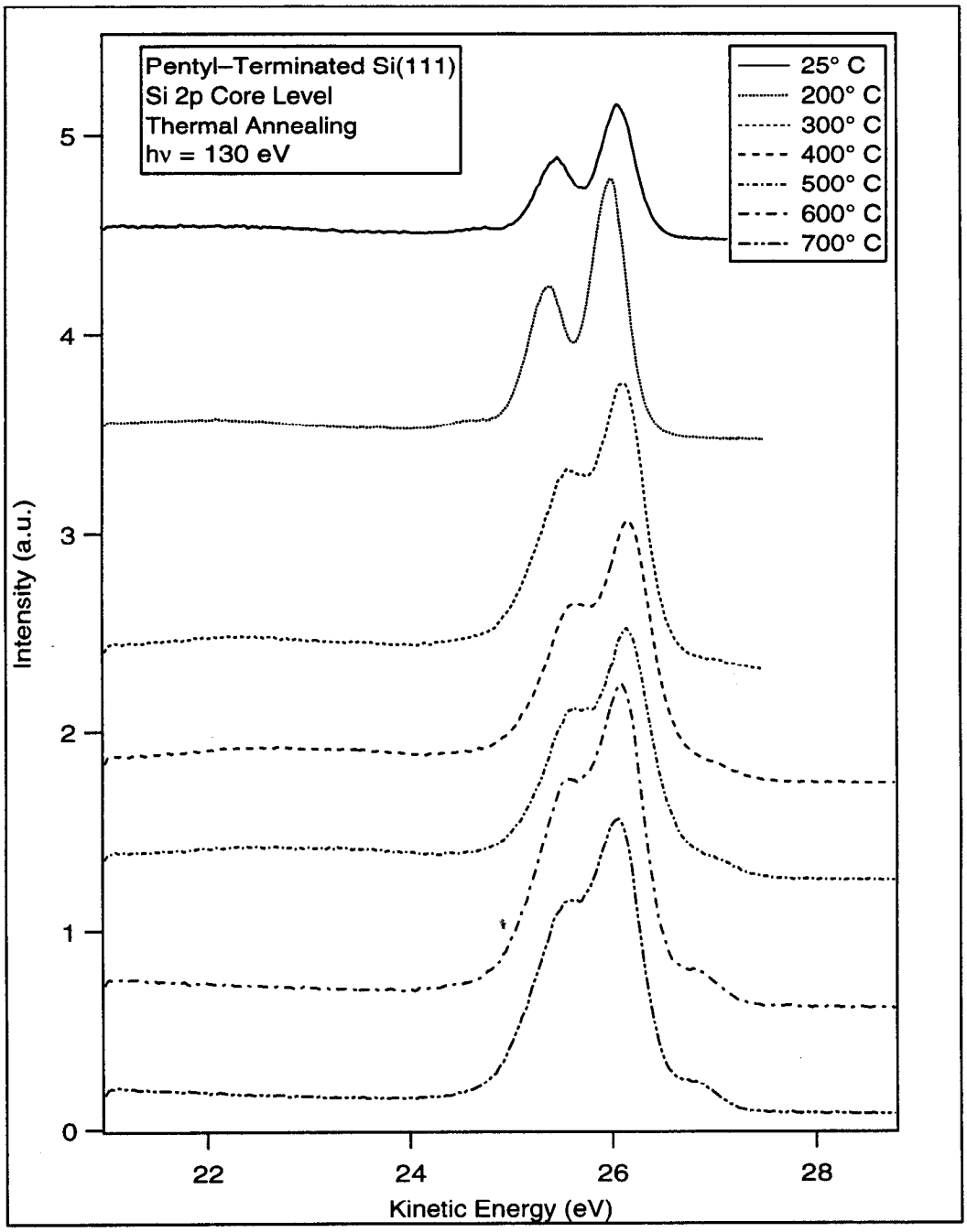

Figure IV.21: As in Figure IV.19 except the spectra are from a methyl–terminated surface.

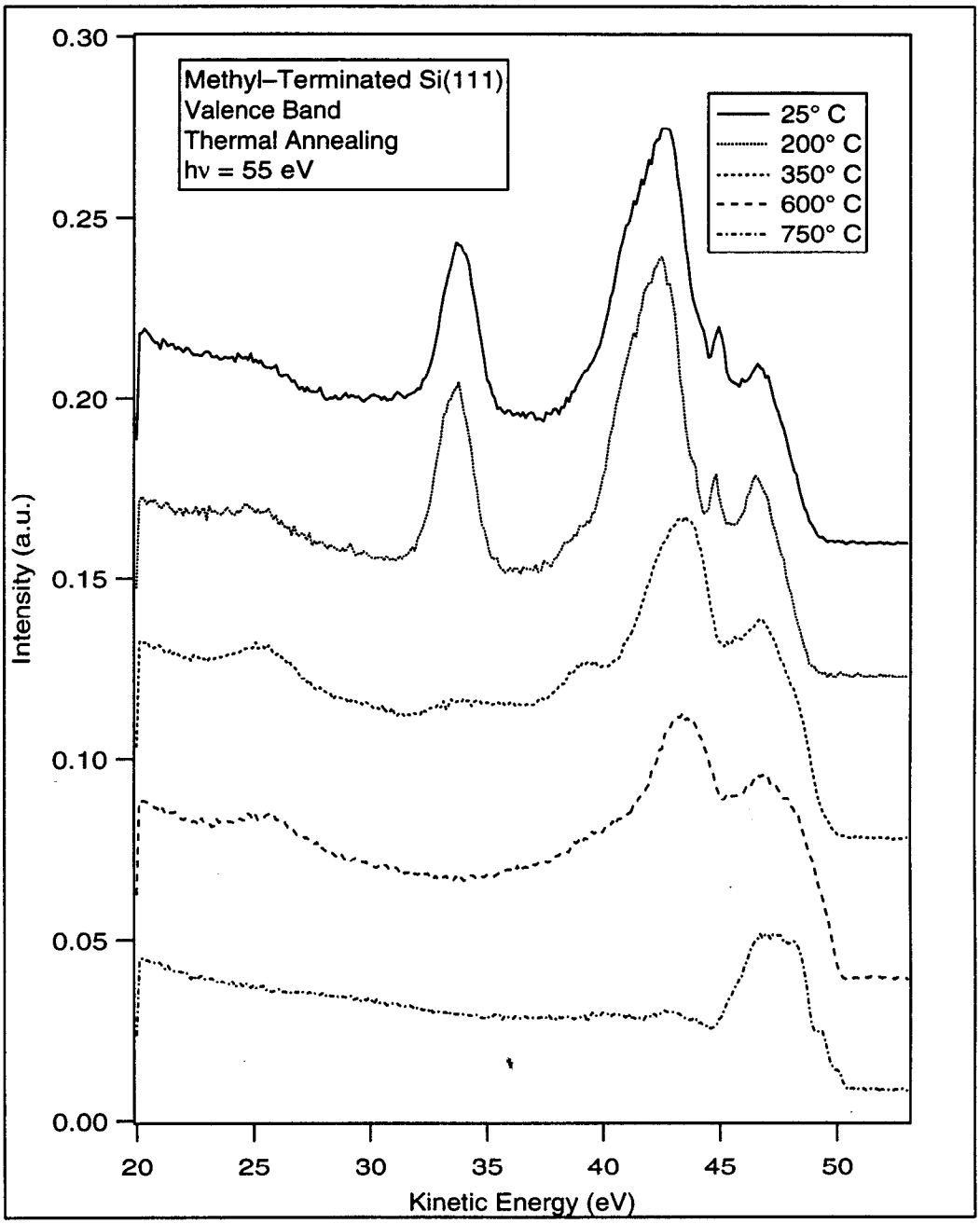

Figure IV.22: As in Figure IV.20 except the spectra are from a methyl–terminated surface.

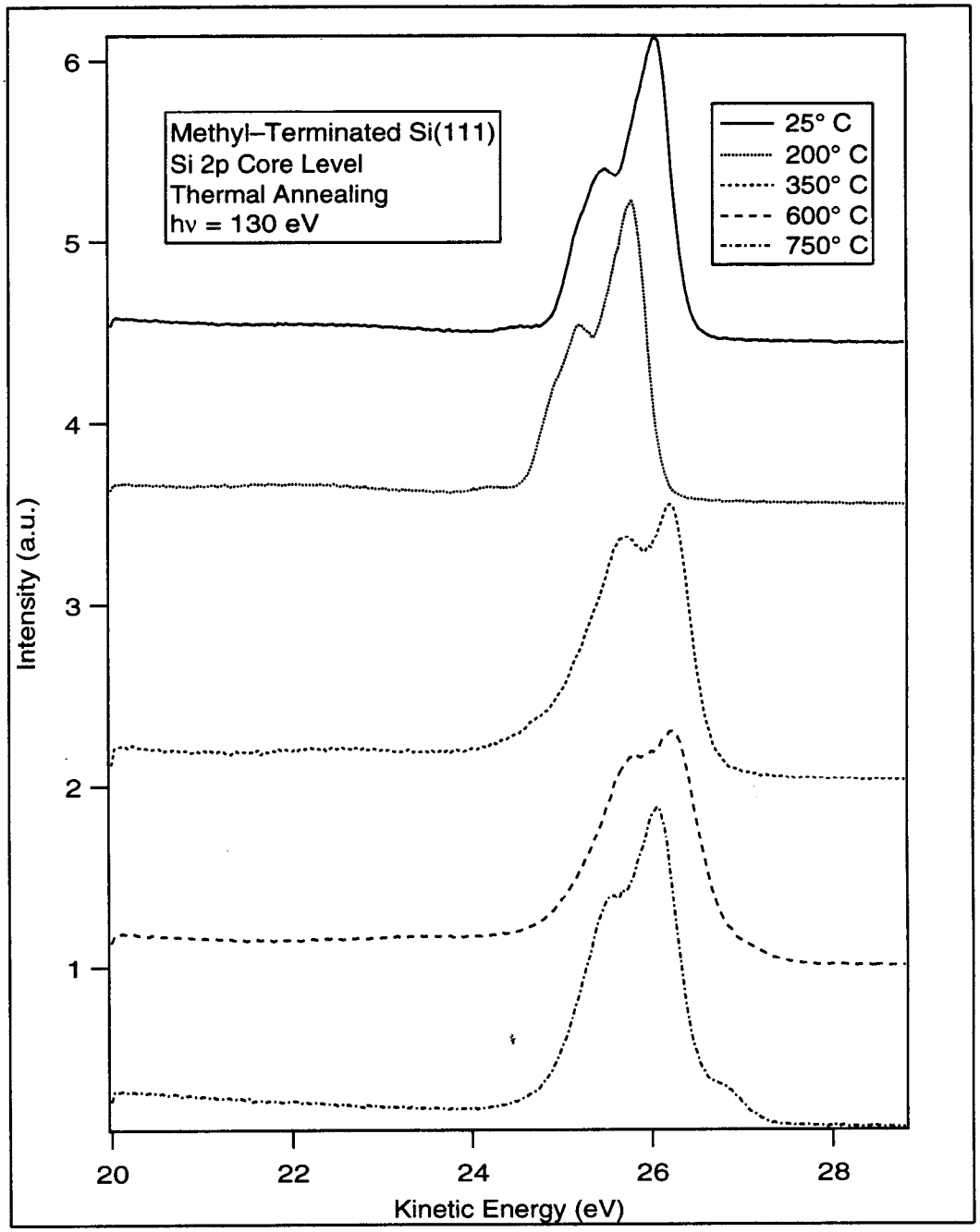

Figure IV.23: As in Figure IV.19 except the spectra are from a decyl–terminated surface.

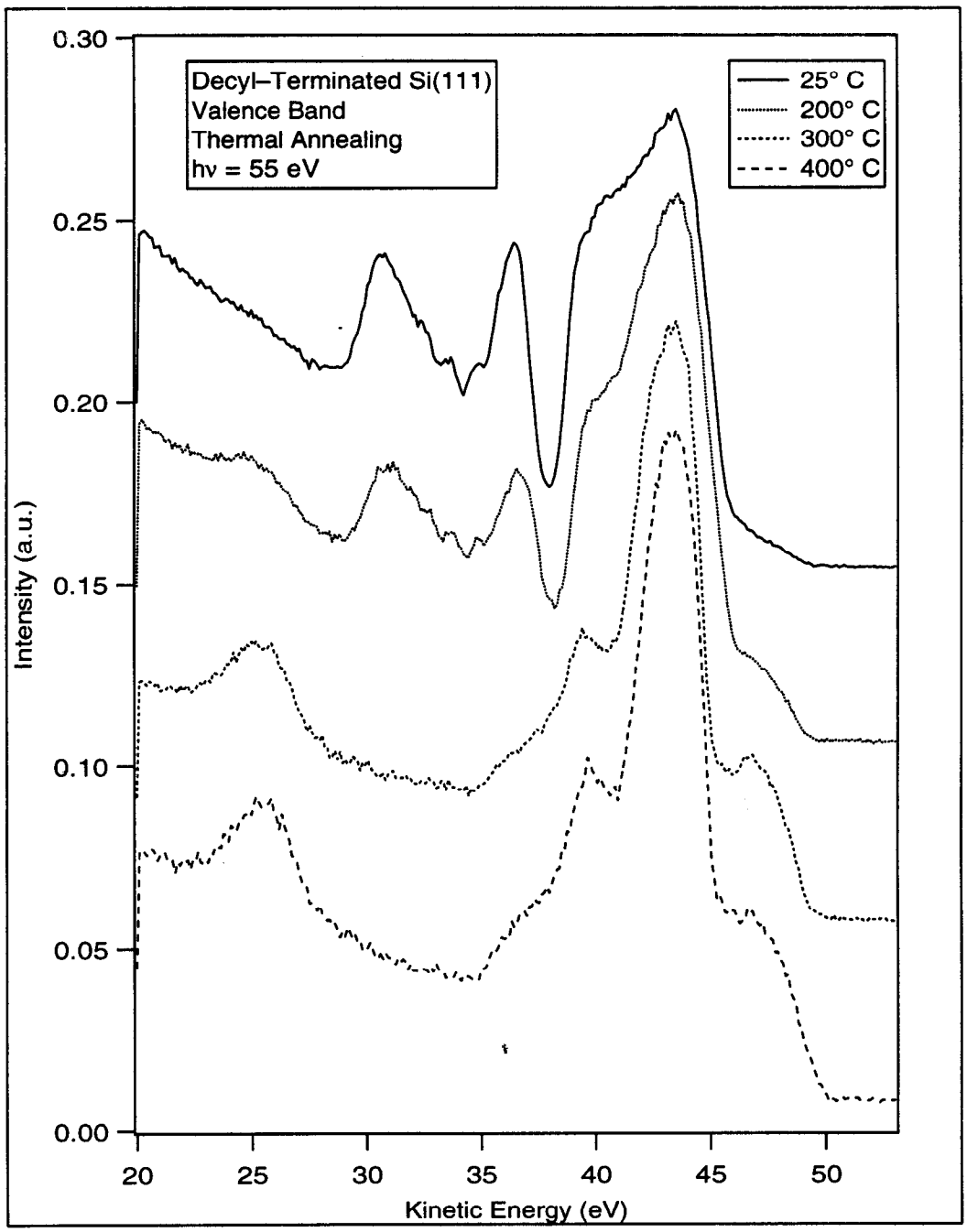

Figure IV.24: As in Figure IV.20 except the spectra are from a decyl–terminated surface.

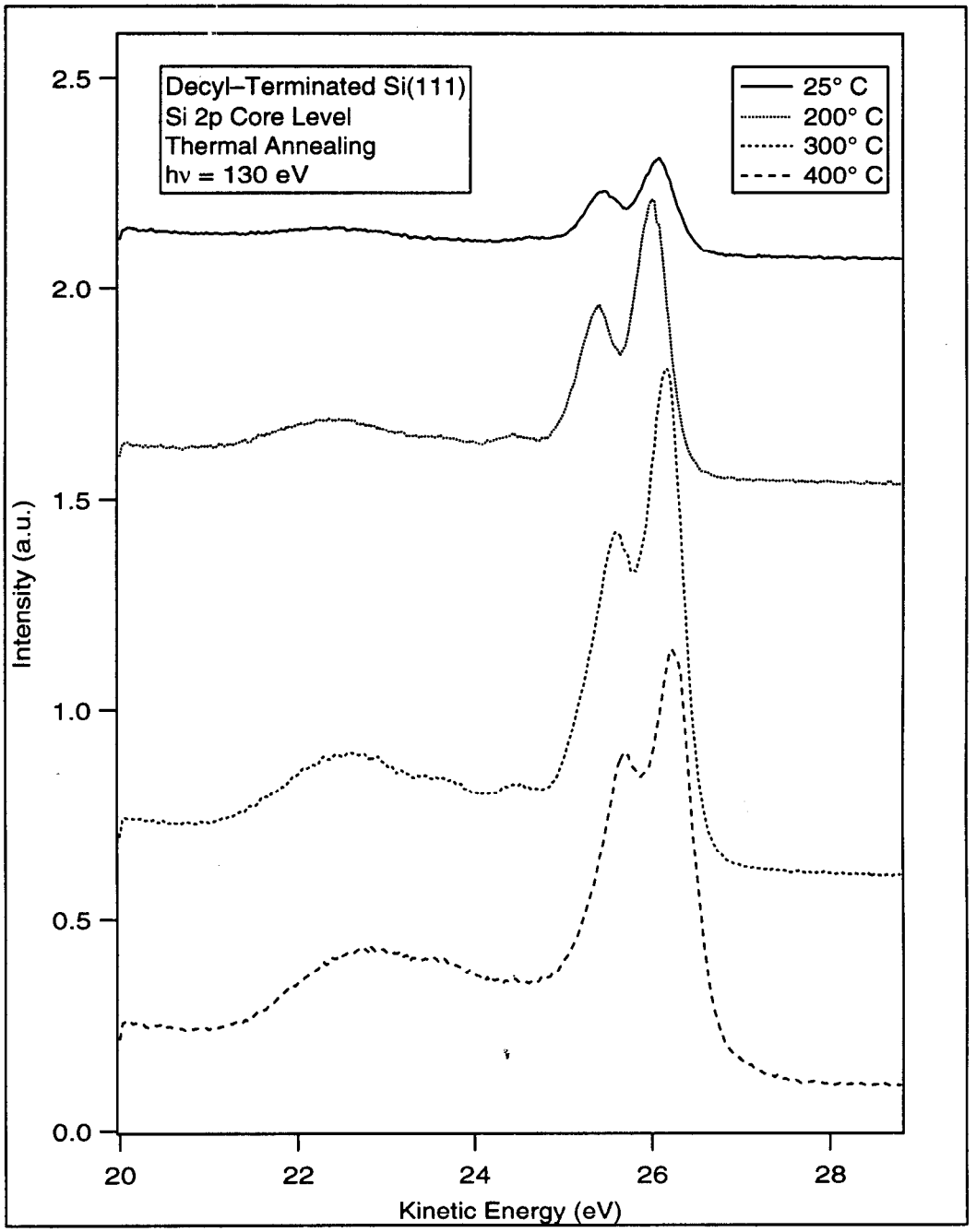

Figure IV.25: As in Figure IV.19 except the spectra are from an octadecyl–terminated surface.

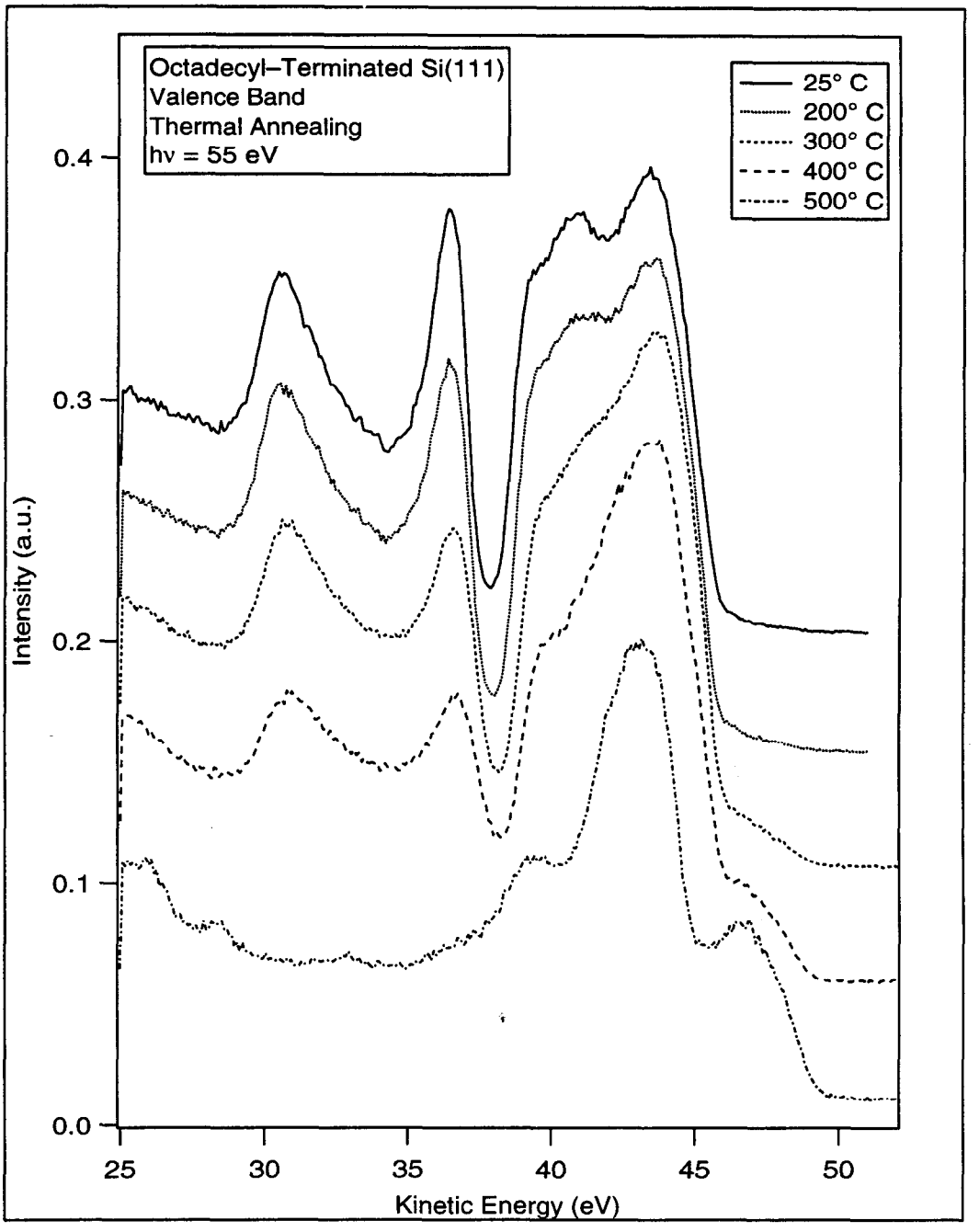

Figure IV.26: As in Figure IV.20 except the spectra are from an octadecyl–terminated surface.

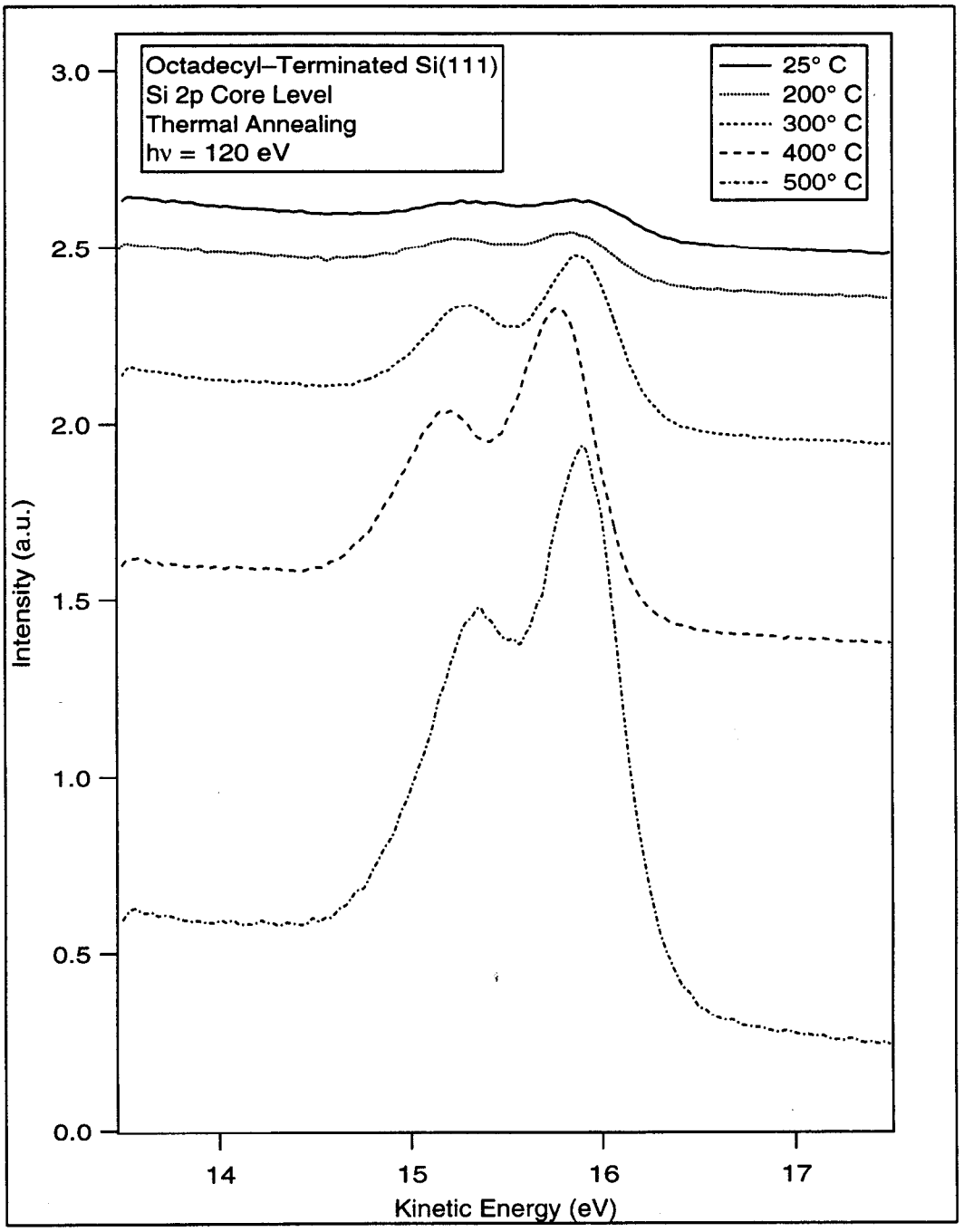

Figure IV.27: Representations of the surface structure consistent with the scanned–energy photoelectron measurements are shown. A.) The pentyl–terminated surface has a Si–C bond length of 1.85Å and the chain tilt angle must be less than 45° from the surface normal. B.) The methyl–terminated surface has a Si–C bond length of 1.85 Å and is directed along the surface normal.

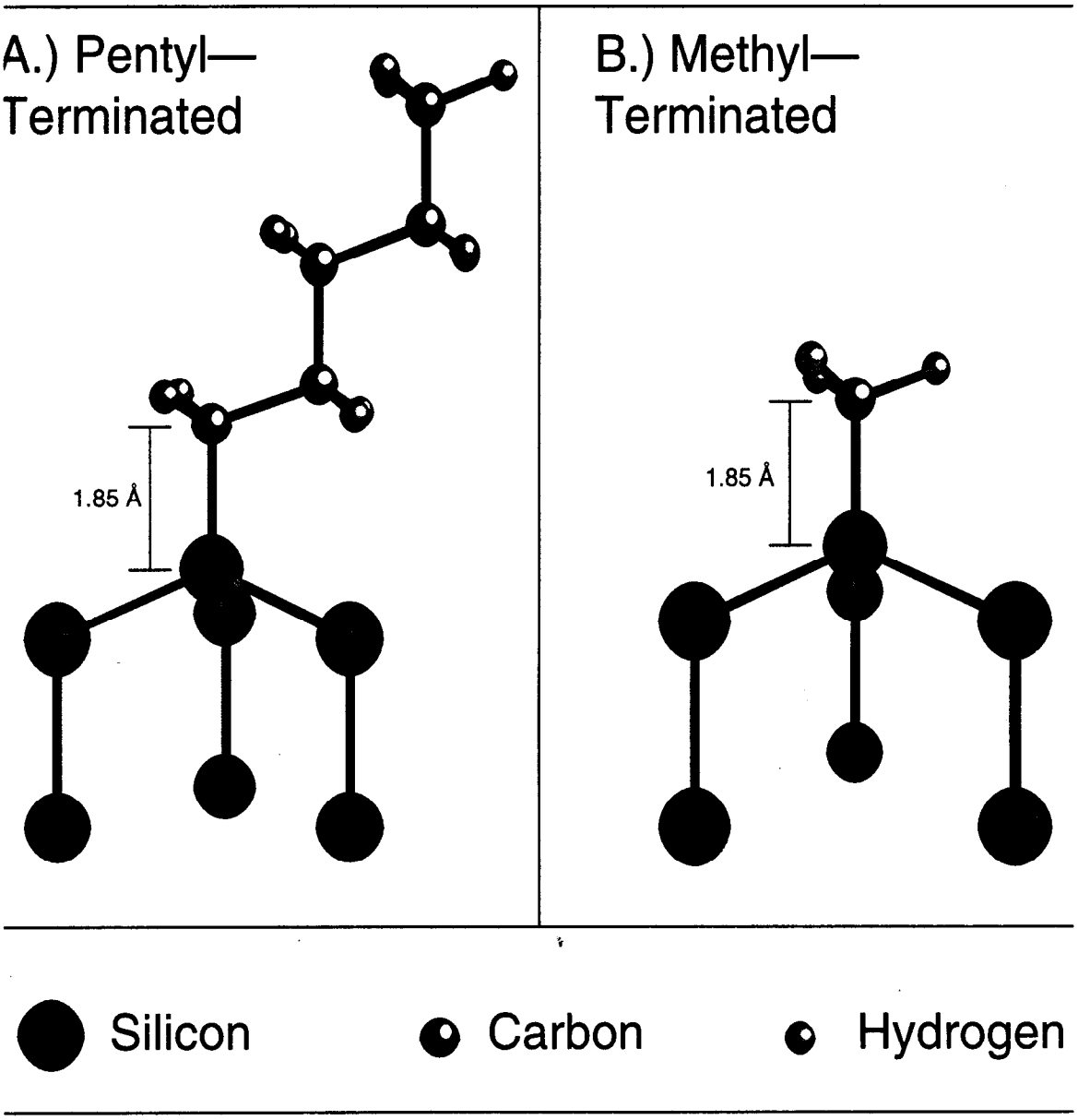

CHAPTER V.
ZINC OXIDE

V.1. ABSTRACT

The geometric structure of ZnO($10\bar{1}0$) surface is the source of much controversy. Theoretical studies(Jaffe, Harrison, and Hess 1994; Schroer, Kruger, and Pollman 1994; Wang and Duke 1987a; Wang and Duke 1987b; Wang and Duke 1988; Wang, Duke, and Mailhoit 1987) suggest that ZnO dimers are formed on the surface. However, there is a wide discrepancy in the calculated tilt angle with respect to the surface. Tight binding calculations(Wang and Duke 1987a; Wang and Duke 1987b; Wang and Duke 1988; Wang, Duke, and Mailhoit 1987) predict the tilt to be 18°,while *ab initio* Hartree–Fock(Jaffe, Harrison, and Hess 1994) and density–functional(Schroer, Kruger, and Pollman 1994) calculations predict a value between 2° and 4°. To date the only experimental determination of the geometric structure of the surface reconstruction has been a low energy electron diffraction (LEED) study(Duke et al. 1978) were the tilt angle was determined to be 11.5° ± 5°. The high experimental uncertainty of this measurement did not help to select the correct model of the ZnO($10\bar{1}0$) surface. Therefore, photoelectron diffraction was used to attempt to determine the surface reconstruction of the ZnO($10\bar{1}0$) surface.

V.2. INTRODUCTION

X–ray photoelectron diffraction (PED) has been under development for a number of years as a tool for the determination of surface geometry(Barton and Himpsel 1990). One of the attractive properties of PED is that it has the same sensitivity to chemical state as photoelectron spectroscopy (PES). Diffraction data from chemically shifted components can be used to determine the local bonding geometries of the surface atoms of interest without any interference from neighboring atoms. In PED, the photoemission process creates a free electron that propagates away from the emitting atom as a spherical wave which undergoes scattering from neighboring atoms. The scattered waves interfere with

the primary wave. This interference is observed as variations in emitted electron intensity as a function of electron wave vector (**k**). As long as the initial state is localized in space, the photoelectron diffraction pattern is highly site specific. Furthermore, if high photon energies are used, the photoelectron intensity is observed to peak along the directions connecting the emitter and its neighbors(Chambers 1992; Fadley 1987). This phenomenon, called forward focussing, often allows a straight forward determination of the bonding geometries even without detailed analysis of the data. This can be of great help in studies of overlayer geometries, surface segregation and interdiffusion. When more detailed information, i.e. bond lengths, is needed, single and multiple scattering calculations can be performed. In recent years, progress has been made in this area including the ability to treat the photoelectron distributions as holograms which can be Fourier transformed to reconstruct the real space configuration of the suface(Barton and Himpsel 1990; Terminello, Barton, and Lapiano–Smith 1993; Tonner, Zhang, and Han 1993; Tran et al. 1993; Wu et al. 1993).

The ionic large band gap semiconductors, ZnO and Fe_2O_3, have many technologically important applications (i.e. catalysis, sensors, etc.) In recent years these semiconductors have been well studied. However, at present the surface geometric structure of ZnO($10\bar{1}0$) is the source of much controversy. Recent, theoretical studies(Jaffe, Harrison, and Hess 1994; Schroer, Kruger, and Pollman 1994; Wang and Duke 1987a; Wang and Duke 1987b; Wang and Duke 1988; Wang, Duke, and Mailhoit 1987) agreed that the ZnO surface dimers are tilted with respect to the surface but are widely discrepant in the reported values of the tilt angle. Tight binding calculations(Wang and Duke 1987a; Wang and Duke 1987b; Wang and Duke 1988; Wang, Duke, and Mailhoit 1987) predict the tilt to be 18° with little change in bond lengths, while *ab initio* Hartree–Fock(Jaffe, Harrison, and Hess 1994) and density–functional(Schroer, Kruger, and Pollman 1994) calculations predict a value between 2° and 4°. A low energy electron diffraction (LEED) study(Duke et al. 1978) of this surface measured the tilt angle of 11.5° ± 5°. The high experimental uncertainty of this measurement does not help to select the correct model of the ZnO($10\bar{1}0$) surface. PED curves were measured from the reconstructed ZnO($10\bar{1}0$) surface at many

photon energies and angles in order to determine the tilt angle of the reconstructed dimers by comparing the experimental PED curves to spherical–wave single (SW–SSC) and multiple (SW–MSC) scattering cluster calculations to determine which model best describes the ZnO($10\bar{1}0$) surface.

V.3. EXPERIMENTAL

All experiments were performed at Beam Line 10–1 at the Stanford Synchrotron Radiation Laboratory, Stanford Linear Accelerator Center. Beam Line 10–1 is a Wiggler beam line with a spherical grating monochromator with a photon energy range of 180 – 1200 eV. These experiments were performed in our PED system which consists of a 100 mm VSW hemispherical analyzer, a reverse view LEED, and a motorized sample manipulator. The angular resolution of the VSW hemispherical analyzer is approximately ±1.5°. The clean ZnO($10\bar{1}0$) surface was prepared by repeated sputter and annealing cycles until no contaminates were observed and the LEED was a strong 1x1. Anneals up to 650 °C were performed at a pressure of $1x10^{-5}$ torr of O_2. Surface segregation of potassium was observed at temperatures above 650 °C.

V.4. RESULTS

Figure V.1 shows a representative Zn 3p core level spectrum from a clean ZnO($10\bar{1}0$) surface. No surface shifted components are visible in this spectrum. The absence of a surface shifted component made the goal of determining the tilt angle of the dimers more difficult as the signal from the Zn atoms in the dimers could not be separated from emission from bulk Zn atoms. It follows that the diffraction effects also could not be separated. Figure V.1, also, shows an O 1s core level from a clean ZnO($10\bar{1}0$) surface. In this case, two components are clearly visible in the spectrum. However, based on spectra taken under different preparation conditions, this component is likely due to surface defects rather than due to a chemical shift of the dimer O atom. These two core levels were used for polar PED scans. PED scans at higher photon energies were dominated by bulk fea-

tures due to the larger escape depths of high kinetic energy photoelectrons. This factor along with the previously described absence of a surface core level shift made directly observing forward scattering along the dimer infeasible. Therefore, surface sensitive PED scans were collected at a kinetic energy of 261 eV and compared the observed spectra with single and multiple scattering calculations using the scattering code developed by the Fadley Research Group at the University of California, Davis(Kaduwela, Friedman, and Fadley 1995), and based upon the Green's function scattering matrix approach of J.J. Rehr and R.C. Albers(Rehr and Albers 1990). The two model structures used were based on a bulk–like surface with no reconstruction (Figure V.2) and a tilted dimer surface based upon the LEED measurement(Wang and Duke 1987a; Wang and Duke 1987b; Wang and Duke 1988; Wang, Duke, and Mailhoit 1987) (Figure V.3). The experimental curve and multiple–scattering curves from the two model structures are shown in Figure V.4. Modified R–factor analysis(VanHove, Tong, and Elconin 1977) of the data indicated that the experimental curve lies between the two model structures.

V.5. DISCUSSION

Unfortunately, a surface reconstruction for the ZnO($10\bar{1}0$) surface has yet to be accurately determined. After analyzing the preliminary PED measurements, it appears that this method will in fact be able to determine whether or not the surface dimers reconstruct. However, in order to make this determination it will be necessary to carry out much more detailed measurements. Polar PED scans are very accurate in determining forward scattering peaks but they limited in the breadth of data that they contain. To increase the amount of PED information that can be compared to the theoretical calculations, 360° azimuthal scans must be measured at 1° polar angle intervals throughout the region shown in Figure V.4. These spectra will then be compared to the multiple scattering calculations on the model structures. The breadth of this data will certainly allow a determination of the tilt angle of the dimers on the ZnO($10\bar{1}0$) surface to be made.

V.6. CONCLUSION

It was not possible to accurately determine the tilt angle of the surface dimers on the ZnO($10\bar{1}0$) surface. However, the PED data suggested that the dimers were tilted in a range between 0° and 11.5° ± 5° determined by the LEED study(Duke et al. 1978). Furthermore, the PED data shows that by performing more detailed PED measurements, particularly, azimuthal scans through polar angles less than 30°, it should be possible to accurately determine the surface reconstruction of the ZnO($10\bar{1}0$) surface.

V.7. ACKNOWLEDGEMENTS

This work was performed at the Stanford Synchrotron Radiation Laboratory, which is supported by the Department of Energy, Office of Basic Energy Science, Division of Chemical Sciences. The authors would also like to thank that Office's Division of Materials Research. J. T. was supported by the NSF–MRSEC program through the Center for Materials Research at Stanford University. We thank Professor C. S. Fadley for providing the computer code used in the analysis of our data. Finally, J. T. gratefully acknowledges Dr. L. J. Terminello for many helpful discussions. Finally, Dr. S. Thevuthasan, Dr. Y. J. Kim, and Dr. G. S. Herman must be recognized for their help with the multiple–scattering data analysis.

V.8. REFERENCES

Barton, J. J., and F. J. Himpsel. 1990. . In *Photoelectron Spectroscopy in Photoemission and Absorption Spectroscopy of Solids and Interfaces with Synchrotron Radiation*, edited by M. Campagna and R. Rosei. Amsterdam: Elsevier.

Chambers, S. A. 1992. *Surface Science Reports* 16:251.

Duke, C. B., R. J. Meyer, A. Paton, and P. Mark. 1978. *Physical Review B* 18:5225.

Fadley, C. S. 1987. *Physica Scripta* T17:39.

Jaffe, J. E., N. M. Harrison, and A. C. Hess. 1994. *Physical Review B* 49:11153.

XPD Code. Kaduwela, A. P., D. J. Friedman, and C. S. Fadley. 1995. , Davis, California.

Rehr, J. J., and R. C. Albers. 1990. *Physical Review B* 41:8139.

Schroer, P., P. Kruger, and J. Pollman. 1994. . Edited by B. Langeler, H. Luth, W. Monch and J. Pollmann. , *Proceedings of the 4th International Conference on the Formation of Semiconductor Interfaces*: World Scientific, 85.

Terminello, L. J., J. J. Barton, and D. A. Lapiano–Smith. 1993. *Physical Review Letters* 70:599.

Tonner, B. P., J. Zhang, and Z.–L. Han. 1993. *Applied Surface Science* 70:378.

Tran, T. T., S. Thevuthasan, Y. J. Kim, D. J. Friedman, A. P. Kaduwela, G. S. Herman, and C. S. Fadley. 1993. *Surface Science* 281:270.

VanHove, M. A., S. Y. Tong, and M. H. Elconin. 1977. *Surface Science* 4:85.

Wang, Y. R., and C. B. Duke. 1987a. *Surface Science* 192:307.

Wang, Y. R., and C. B. Duke. 1987b. *Physical Review B* 36:2763.

Wang, Y. R., and C. B. Duke. 1988. *Physical Review B* 37:6417.

Wang, Y. R., C. B. Duke, and C. Mailhoit. 1987. *Surface Science* 188:L708.

Wu, H., G. J. Lapeyre, H. Huang, and S. Y. Tong. 1993. *Physical Review Letters* 71:251.

Figure V.1: A Zn 3p core level spectrum taken at a photon energy of 350 eV and an O 1s core level spectrum taken at a photon energy of 650 eV.

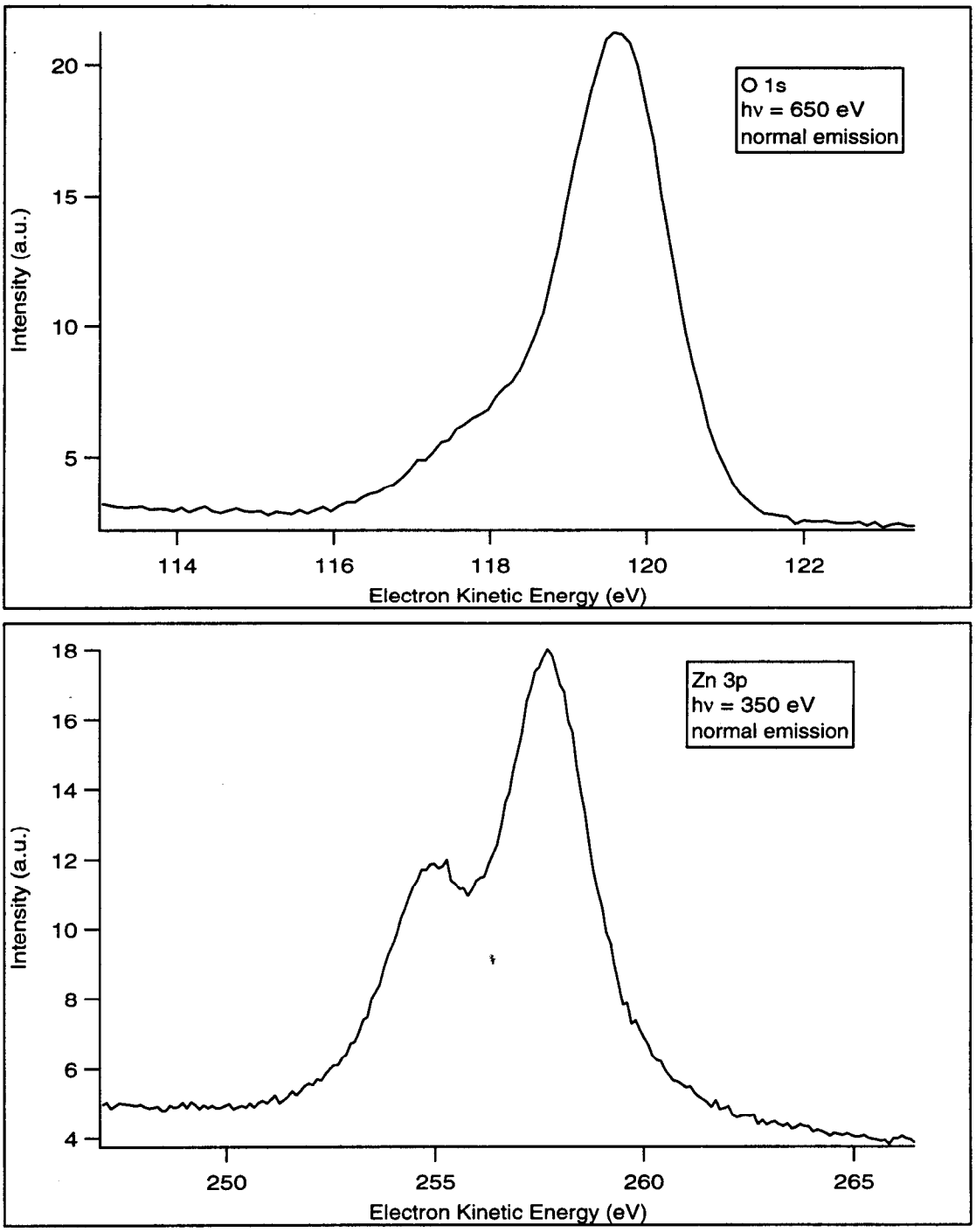

Figure V.2: Bulk terminated ZnO($10\bar{1}0$) surface used in calculations.

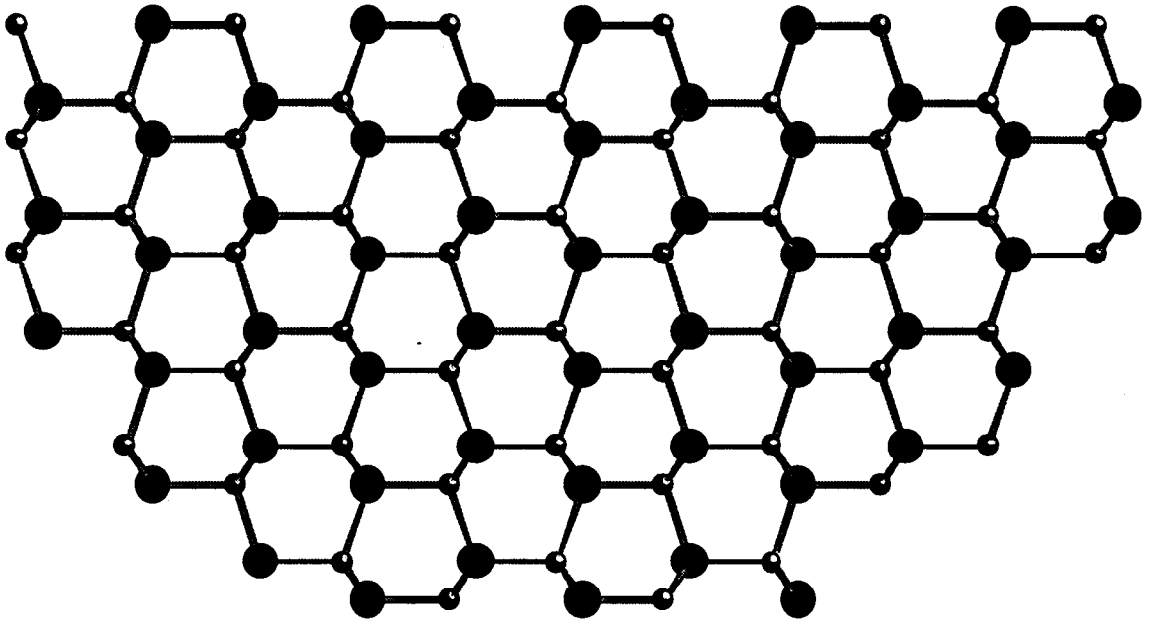

Figure V.3: LEED reconstructed ZnO($10\bar{1}0$) surface used in calculations.

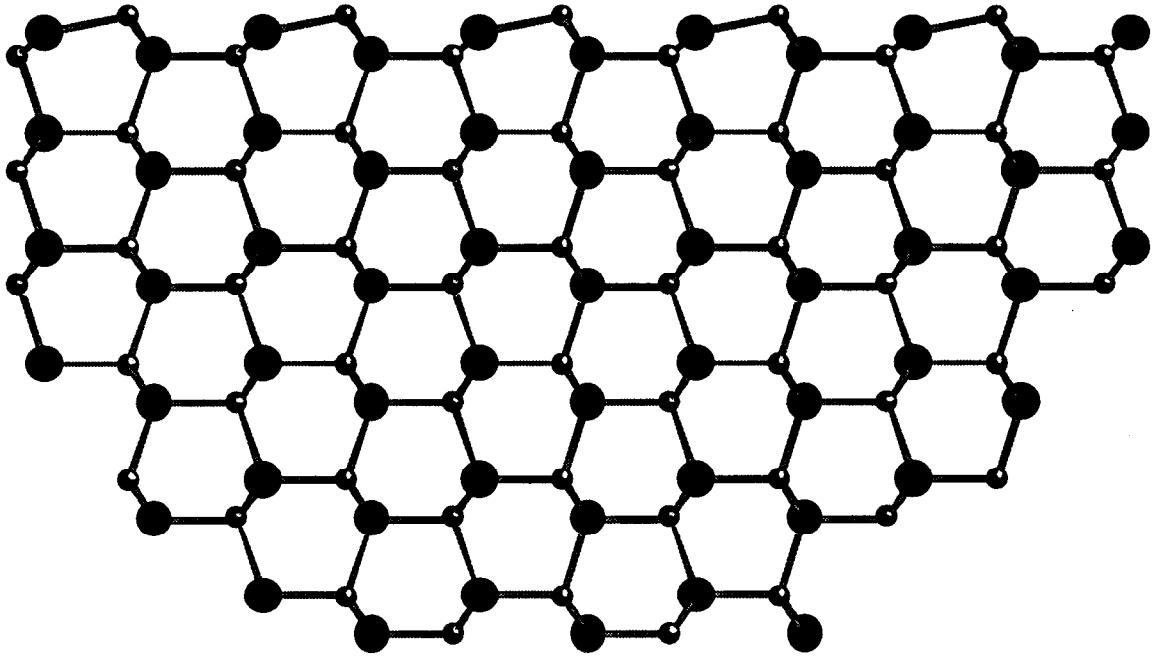

Figure V.4: The experimental PED data is shown along with multiple–scattering calculations using both the Bulk and LEED clusters.

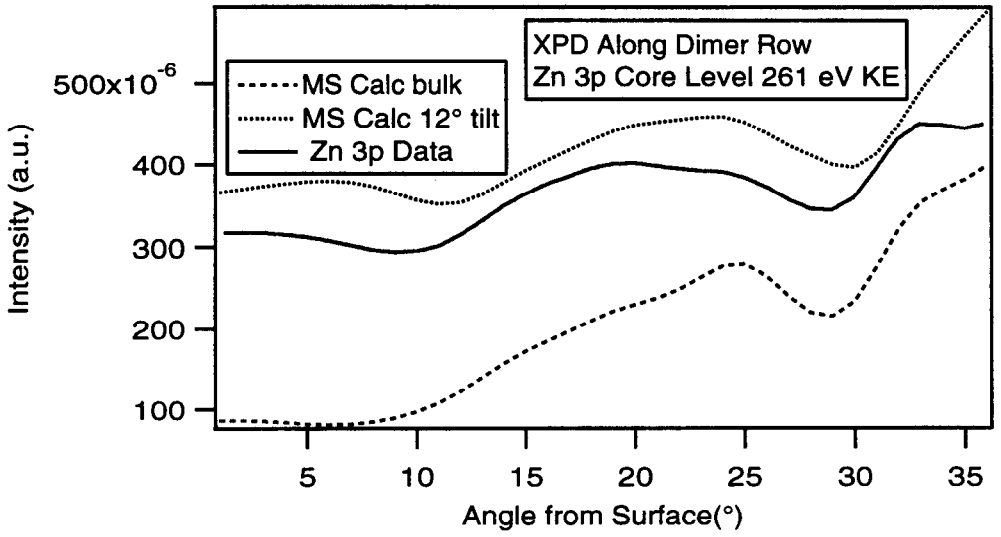

CHAPTER VI.
CONCLUSION

In this work, the light–emitting porous silicon, H–Si(111), Cl–Si(111), and Alkyl–Si(111) surfaces have been characterized in order to determine the fundamental properties of surface geometry and electronic structure using synchrotron radiation–based techniques. The light–emitting porous silicon was shown to be crystalline with only low concentrations of impurity species. Therefore, luminescence from amorphous silicon and from impurity based molecular species on electrochemically etched porous silicon was ruled out. The H–Si(111) surface was found to be non–reactive with both atomic and molecular oxygen. However, metal and semiconductor depositions were nearly identical to those on the clean surface. However, surface oxidation was observed when the H–Si(111) surface was exposed to molecular and atomic halogens. The Si 2p core level spectra from the halogen–exposed surfaces showed two components, from bulk silicon and from silicon bonded to a single halogen atom. This result was unlike halogen exposure of the Si(111) 7x7 surface where halogen exposure results in mono–, di–, and trihalogenated Si atoms. EXAFS spectroscopy showed that the Si–Cl bond length of the Cl–Si(111) surface was 2.03 ± 0.02 Å.

The alkyl–terminated silicon surfaces was found to contain a direct chemical bond between the top layer Si atoms and the terminal C atom of the alkyl group. The alkyl groups present was identified using the C $2s_{\pi}$–based molecular orbitals as a fingerprint. Scanned–energy, chemical shift PED was used to determine that the that the alkyl chains sat in atop sites with a Si–C bond length of 1.85 ± 0.05 Å. NEXAFS spectroscopy showed that the alkyl chains were oriented on the surface.

Finally, it has been shown that the traditional ultra–high vacuum based surface science techniques have the ability to characterize the products of surface synthetic chemical reactions. Therefore, it is hoped that these techniques will be used in the future to accurately determine bond lengths and geometries of novel compounds prepared using standard wet

chemical techniques.